

Utilization of Long Columns Packed with Sub-2 μm Particles Operated at High Pressures and Elevated Temperatures for High-Efficiency One-Dimensional Liquid Chromatographic Separations

Edward Gordon Franklin

A dissertation submitted to the faculty of the University of North Carolina at Chapel Hill in partial fulfillment of the requirements for the degree of Doctor of Philosophy in the Department of Chemistry.

Chapel Hill
2012

Approved by:

Dr. James W. Jorgenson

Dr. Mark H. Schoenfish

Dr. Gary L. Glush

Dr. Michel R. Gagné

Dr. Marcey L. Waters

© 2012
Edward Gordon Franklin
ALL RIGHTS RESERVED

ABSTRACT

EDWARD GORDON FRANKLIN: Utilization of Long Columns Packed with Sub-2 μm Particles Operated at High Pressures and Elevated Temperatures for High-Efficiency One-Dimensional Liquid Chromatographic Separations
(Under the direction of James W. Jorgenson)

As Ultrahigh Pressure Liquid Chromatography (UHPLC) techniques have become increasingly popular across a number of scientific disciplines, the strongest emphasis has remained on its ability to yield moderately high separation efficiencies on much faster timescales than were previously achievable. This has been accomplished through the use of commercial instrumentation capable of generating maximum pressures of 18,000 psi and 15 – 25 cm columns packed with 1.8 – 2.0 μm particles, providing theoretical plate counts upwards of 60,000. While this represents a major step forward when compared to typical HPLC approaches, many applications involving highly complex samples, such as those encountered in “-omics” settings, stand to benefit from even higher efficiency separations.

The work presented in this dissertation explores the combined benefits of using ultrahigh pressures (up to 50,000 psi), small particles (sub-2 μm) and elevated temperatures (up to 85°C). Efforts were made to improve microcapillary column packing procedures by investigating the individual and synergistic effects of experimental packing parameters on ultimate column performance. Findings were used to pursue two of the most enduring objectives in the separation sciences: faster speeds and higher efficiencies. By packing 20 – 30 cm columns with fully porous 1.0 μm particles, plate counts in excess of 100,000 were achieved with column dead times of approximately 1 minute. Alternatively, 1.9 μm particles

were used to pack columns several meters in length to achieve very high separation efficiencies. A 360 cm x 50 μ m ID column produced over 10^6 plates with a column dead time of just over 100 minutes at 25°C. Likewise, ~ 200 cm columns were used in the analyses of proteomic samples under gradient elution conditions to generate peak capacities approaching 1000 in just over three hours at 65°. These results suggest a real applicability of high-efficiency one-dimensional approaches to proteomics and similar fields of study.

ACKNOWLEDGEMENTS

I would first like to thank my advisor, Dr. Jorgenson, under whom I have had the privilege of working and studying for the past five years. His intellectual brilliance and enthusiasm for research are truly remarkable. Through his guidance I have found much encouragement for the completion of the work contained in this dissertation. Funding, materials, and instrumentation for this work were provided by Waters Corporation. Also with regard to this work, I must thank fellow graduate students Jordan Stobaugh and Kaitie Fague. Without them, Chapter 5 would not exist. Thanks must also be given to many other former and current Jorgenson Group members. They made the lab a great place to work, and I am happy and blessed to call so many of them friends. Finally, I must thank my mother and father... for everything.

TABLE OF CONTENTS

LIST OF FIGURES.....	xi
LIST OF ABBREVIATIONS.....	xxii
LIST OF SYMBOLS.....	xxiv
CHAPTER 1: THEORY AND BACKGROUND	1
1.1 Overview.....	1
1.2 Chromatographic Theory	3
1.2.1 Chromatographic Separations	3
1.2.2 Separation Efficiency	4
1.2.3 Van Deemter Theory.....	6
1.2.3.1 A-term	8
1.2.3.2 B-term.....	13
1.2.3.3 C-term.....	14
1.2.4 Corrected Interstitial Velocities	17
1.2.5 Ultrahigh Pressure Liquid Chromatography (UHPLC)	18
1.2.5.1 UHPLC Pressures, Mobile Phase Viscosities, and Diffusion Coefficients	19
1.2.7 Kinetic Plots	20
1.3 References	22
1.4 Figures.....	23
CHAPTER 2: INVESTIGATIONS AND IMPROVEMENTS OF MICROCAPILLARY COLUMN PACKING AND PERFORMANCE	30
2.1 Introduction.....	30
2.1.1 Slurry Packing	30

2.1.2 Bed Morphology and Its Influence on Chromatographic Performance	31
2.1.3 Experimental Packing Conditions for Producing Desired Bed Morphologies.....	33
2.2 Experimental	37
2.2.1 Chemicals	37
2.2.2 General Capillary Column Packing Procedure.....	38
2.2.3 Column Evaluation	39
2.2.4 Segmented Column Performance	40
2.2.5 Column Outlet Effect	45
2.2.6 Slurry Concentration Effects	47
2.2.7 The Effect of Packing and Flushing Pressure.....	52
2.2.8 Effect of Slurry Solvent	56
2.3 Conclusions	58
2.4 References	60
2.5 Figures.....	62
CHAPTER 3: USE OF 1.0 MICRON-SIZED PACKING FOR FAST ANALYSES IN ULTRA HIGH PRESSURE CAPILLARY LIQUID CHROMATOGRAPHY	92
3.1 Introduction	92
3.1.1 Alternative Approaches to Fast, Efficient Liquid Chromatographic Separations	92
3.1.2 Theoretical Utility of 1.0 μm Porous Particle Supports.....	94
3.1.3 Previous Efforts with 1.0 μm Porous Particles.....	97
3.2 Experimental	99
3.2.1 Chemicals	99
3.2.2 Initial Efforts to Pack Capillary Columns With 1.0 μm Porous Particles.....	99

3.2.3 Effect of Slurry Concentration in Packing 1.5 and 1.0 μm Porous Particles	102
3.2.4 Effect of Column ID on Performance of Columns Packed with 1.5 and 1.0 μm Particles.....	103
3.2.5 Effect of Packing Pressure on Performance of Columns Packed with 1.0 μm Particles.....	104
3.2.5 Evaluation of 10 μm ID Columns Packed with 1.9, 1.5, and 1.0 μm Porous Particles.....	105
3.3 Conclusions	108
3.4 References	111
3.5 Figures.....	112
CHAPTER 4: LONG MICROCAPILLARY COLUMNS AT ELEVATED TEMPERATURE AND PRESSURE FOR HIGH-EFFICIENCY ONE-DIMENSIONAL SEPARATIONS	129
4.1 Introduction	129
4.1.1 Survey of High-Efficiency Packed-Column Liquid Chromatography Separations	129
4.1.2 Alternative Means of Achieving High Separation Efficiency in Liquid Chromatography	131
4.1.2.1 Multidimensional Separations	131
4.1.2.2 Superficially Porous Particles.....	131
4.1.2.3 Porous Layer Open Tubular (PLOT) Columns.....	132
4.1.2.4 Monolithic Columns.....	133
4.1.2.5 Micropillar Array Columns (PACs).....	133
4.1.3 Temperature as a Parameter in Liquid Chromatography	134
4.1.3.1 The Effect of Elevated Temperature on Column Efficiency	135
4.1.3.2 The Effect of Elevated Temperature on Retention	136

4.1.4 Kinetic Plots: The Combined Effects of Small Particles, High Pressures, and Elevated Temperatures	137
4.1.5 Peak Capacity in Gradient Elution of Peptides	138
4.2 Experimental	141
4.2.1 Chemicals	141
4.2.2 Isocratic Characterization at Elevated Temperatures	142
4.2.3 100 cm Microcapillary Columns	144
4.2.3.1 Column ID Effects	145
4.2.3.2 Gradient Elution Characterization of 100 cm Microcapillary Columns	146
4.2.3.3 Slurry Concentration Effects	150
4.2.4 200 cm Microcapillary Columns	151
4.2.5 > 200 cm Microcapillary Columns	153
4.3 Conclusions	159
4.4 References	160
4.5 Figures.....	162
CHAPTER 5: CONSTANT PRESSURE GRADIENT-CAPABLE PLATFORM FOR HIGH-EFFICIENCY ONE-DIMENSIONAL UHPLC SEPARATIONS	199
5.1 Introduction.....	199
5.1.1 Previous UHPLC Gradient System.....	199
5.1.2 Conceptual Features of New Gradient UHPLC System	201
5.2 System Design and General Operation	203
5.3 Chromatographic Performance of Constant-Pressure UHPLC System.....	207
5.3.1 Utilized Microcapillary Columns	207
5.3.2 Results with Sample Trapping.....	207

5.3.3 Results with Direct Injection	210
5.4 Conclusions	213
5.5 Figures.....	215
5.6 References	238

LIST OF FIGURES

Figure 1-1: Theoretical relationship between the a-, b-, and c-terms of the van Deemter equation, and the resultant overall plate height (h)	23
Figure 1-2: Categorical distances of the five contributors to eddy diffusion identified by Giddings. Figure adapted from Ref. 6.	24
Figure 1-3: Overlay of the reduced forms of the van Deemter, Giddings, and Knox equations with typical values for the coefficients.	25
Figure 1-4: Mobile phase velocities experimentally determined from a dead time marker can be corrected to account for intraparticle stagnant mobile phase to find approximate interstitial velocities. The corrected interstitial velocities should be used in constructing van Deemter curves.	26
Figure 1-5: The mechanism of hydrodynamic flow chromatography (HDC) in a channel. Large particles cannot adequately sample the slowest flow regimes at the walls, and measuring their elution times results in overestimating the actual interstitial velocity.	27
Figure 1-6: The effect of decreasing particle diameter on column performance.	28
Figure 1-7: Kinetic plots for 1, 3, and 5 μm particles. $\Delta P = 400$ bar (~ 5800 psi); viscosity, $\eta = 1$ cP; interparticle porosity, $\varepsilon_i = 0.4$; diffusion coefficient, $D_m = 1 \times 10^{-5}$ cm/s; reduced van Deemter coefficients $A = 1.0$, $B = 1.0$, and $C = 0.1$	29
Figure 2-1: van Deemter curves of inlet and outlet halves of a bisected 100 cm x 50 μm ID column packed with ~ 10 mg/mL slurry of 1.9 μm BEH particles in acetone. Data points are for the intact 100 cm column.	62
Figure 2-2: Overlaid van Deemter curves for all four ~ 25 cm segments of an originally 100 cm x 50 μm ID column packed with ~ 10 mg/mL slurry of 1.9 μm BEH particles in acetone.	63
Figure 2-3: Resistance to flow data for all four ~ 25 cm segments of an originally 100 cm x 50 μm ID column packed with ~ 10 mg/mL slurry of 1.9 μm BEH particles in acetone.	64
Figure 2-4: Retention data for all four ~ 25 cm segments of an originally 100 cm x 50 μm ID column packed with ~ 10 mg/mL slurry of 1.9 μm BEH particles in acetone.	65
Figure 2-5: Replicate data of overlaid van Deemter curves for all four ~ 25 cm segments of an originally 100 cm x 50 μm ID column packed with ~ 10 mg/mL slurry of 1.9 μm BEH particles in acetone.	66

Figure 2-6: Replicate data of resistance to flow for all four ~ 25 cm segments of an originally 100 cm x 50 μ m ID column packed with ~ 10 mg/mL slurry of 1.9 μ m BEH particles in acetone.	67
Figure 2-7: Replicate retention data for all four ~ 25 cm segments of an originally 100 cm x 50 μ m ID column packed with ~ 10 mg/mL slurry of 1.9 μ m BEH particles in acetone.	68
Figure 2-8: Overlaid van Deemter curves from column where increasing lengths of column were clipped from the outlet end. A ~ 3 mg/mL slurry of BEH particles in acetone was used to pack the original 50 cm x 50 μ m ID column.	69
Figure 2-9: Overlaid van Deemter curves from column where increasing lengths of column were clipped from the outlet end. A ~ 100 mg/mL slurry of BEH particles in acetone was used to pack the original 49 cm x 50 μ m ID column.	70
Figure 2-10: Rates of packing with 5, 10, and 20 mg/mL slurries of 1.9 μ m BEH particles in acetone.	71
Figure 2-11: Performances of columns packed with 5, 10, and 20 mg/mL slurries of 1.9 μ m BEH particles slurried in acetone.	72
Figure 2-12: Rates of packing with 100, 20, 10, and 5 mg/mL slurries of 1.9 μ m BEH particles in acetone. The 100 mg/mL slurry packing rate is highlighted in red.	73
Figure 2-13: Overlaid van Deemter curves for consecutively packed 50 μ m ID columns.	74
Figure 2-14: Comparison of performances for ~ 25 cm x 75 μ m ID columns packed with 3 and 100 mg/mL slurries of 1.9 μ m BEH particles.	75
Figure 2-15: Comparison of column retention for ~ 25 cm x 75 μ m ID columns packed with 3 and 100 mg/mL slurries of 1.9 μ m BEH particles.	76
Figure 2-16: Comparison of column resistance to flow for ~ 25 cm x 75 μ m ID columns packed with 3 and 100 mg/mL slurries of 1.9 μ m BEH particles.	77
Figure 2-17: Overlaid van Deemter curves for all four ~ 25 cm segments of an originally 100 cm x 50 μ m ID column packed with ~ 100 mg/mL slurry of 1.9 μ m BEH particles in acetone.	78
Figure 2-18: Retention data for all four ~ 25 cm segments of an originally 100 cm x 50 μ m ID column packed with ~ 100 mg/mL slurry of 1.9 μ m BEH particles in acetone.	79

Figure 2-19: Resistance to flow data for all four ~ 25 cm segments of an originally 100 cm x 50 μ m ID column packed with ~ 100 mg/mL slurry of 1.9 μ m BEH particles in acetone.	80
Figure 2-20: Overlaid van Deemter curves for permutations of ~ 25 cm columns packed at 10,000 or 30,000 psi and subsequently flushed at 23,000 or 46,000 psi. Columns were packed with ~ 100 mg/mL of 1.9 μ m BEH particles in acetone.	81
Figure 2-21: Retention data for permutations of ~ 25 cm columns packed at 10,000 or 30,000 psi and subsequently flushed at 23,000 or 46,000 psi. Columns were packed with ~ 100 mg/mL of 1.9 μ m BEH particles in acetone.	82
Figure 2-22: Resistance to flow data for permutations of ~ 25 cm columns packed at 10,000 or 30,000 psi and subsequently flushed at 23,000 or 46,000 psi. Columns were packed with ~ 100 mg/mL of 1.9 μ m BEH particles in acetone.	83
Figure 2-23: Overlaid van Deemter curves of ~ 25 cm column packed at 10,000 psi and flushed at 23,000 psi with a second column packed at 30,000 psi and flushed at 46,000 psi.	84
Figure 2-24: Retention data of ~ 25 cm column packed at 10,000 psi and flushed at 23,000 psi with a second ~ 25 cm column packed at 30,000 psi and flushed at 46,000 psi.	85
Figure 2-25: Resistance to flow data of ~ 25 cm column packed at 10,000 psi and flushed at 23,000 psi with a second column packed at 30,000 psi and flushed at 46,000 psi.	86
Figure 2-26: Performances of 50 μ m ID columns packed with 3, 10, and 50, and 100 mg/mL slurries of 1.9 μ m BEH particles in methanol.	87
Figure 2-27: Performances of 75 μ m ID column packed with 50 mg/mL slurry of 1.9 μ m BEH particles in methanol.	88
Figure 2-28: Performances of 75 μ m ID column packed with 100 mg/mL slurry of 1.9 μ m BEH particles in methanol.	89
Figure 2-29: Performances of 150 μ m ID column packed with 100 mg/mL slurry of 1.9 μ m BEH particles in methanol.	90
Figure 2-30: Performances of 150 μ m ID column packed with 100 mg/mL slurry of 1.9 μ m BEH particles in acetone.	91
Figure 3-1: Kinetic plots showing the performance of 1 vs. 2 μ m particles with pressure limitations of 15,000 psi (solid lines) and 40,000 psi (dashed lines). Plots are constructed assuming viscosity, η = 1 cP; interparticle porosity, ϵ_i = 0.4; analyte	

diffusion coefficient, $D_m = 1 \times 10^{-5} \text{ cm}^2/\text{s}$; reduced van Deemter coefficients $A = 1.5$, $B = 1.0$, and $C = 0.17$	112
Figure 3-2: Expected performance of columns of various lengths packed with $1 \text{ }\mu\text{m}$ particles operated at 15,000 psi (blue trace) and 40,000 psi (red trace) Plots are constructed assuming viscosity, $\eta = 1 \text{ cP}$; interparticle porosity, $\varepsilon_i = 0.4$; analyte diffusion coefficient, $D_m = 1 \times 10^{-5} \text{ cm}^2/\text{s}$; reduced van Deemter coefficients $A = 1.5$, $B = 1.0$, and $C = 0.17$	113
Figure 3-3: h vs. v plots for $19 \text{ cm} \times 30 \text{ }\mu\text{m}$ ID column packed with $1.0 \text{ }\mu\text{m}$ BEH particles run in 50/50 acetonitrile/water and 0.5% TFA. The sudden deterioration in performance at higher linear velocities was caused by bed collapse.	114
Figure 3-4: Chromatogram of $20 \text{ cm} \times 30 \text{ }\mu\text{m}$ ID column packed with $1.0 \text{ }\mu\text{m}$ BEH operated at 40,000 psi in 50/50 acetonitrile/water and 0.1% TFA.....	115
Figure 3-5: van Deemter performance of a $20 \text{ cm} \times 30 \text{ }\mu\text{m}$ ID column packed with $1.0 \text{ }\mu\text{m}$ BEH particles run in 50/50 acetonitrile/water and 0.5% TFA.	116
Figure 3-6: Comparison of performances of $30 \text{ }\mu\text{m}$ ID columns packed with 2 mg/mL (14.6 cm) and 20 mg/mL (15.1 cm) slurries of $1.0 \text{ }\mu\text{m}$ BEH particles.	117
Figure 3-7: Comparison of column retention for $\sim 15 \text{ cm} \times 30 \text{ }\mu\text{m}$ ID columns packed with 2 (dashed lines) and 20 mg/mL (solid lines) slurries of $1.0 \text{ }\mu\text{m}$ BEH particles.....	118
Figure 3-8: Comparison of column resistance to flow for $\sim 15 \text{ cm} \times 30 \text{ }\mu\text{m}$ ID columns packed with 2 (dashed line) and 20 (solid line) mg/mL slurries of $1.0 \text{ }\mu\text{m}$ BEH particles.	119
Figure 3-9: Comparison of performances of $25.4 \text{ cm} \times 50 \text{ }\mu\text{m}$ ID columns packed with 3 mg/mL and 30 mg/mL slurries of $1.5 \text{ }\mu\text{m}$ BEH particles.	120
Figure 3-10: Comparison of column retention for $25.4 \text{ cm} \times 50 \text{ }\mu\text{m}$ ID columns packed with 3 (dashed lines) and 30 mg/mL (solid lines) slurries of $1.5 \text{ }\mu\text{m}$ BEH particles.....	121
Figure 3-11: Comparison of column resistance to flow for $25.4 \text{ cm} \times 30 \text{ }\mu\text{m}$ ID columns packed with 3 (dashed line) and 30 (solid line) mg/mL slurries of $1.5 \text{ }\mu\text{m}$ BEH particles.	122
Figure 3-12: Effect of column inner diameter on chromatographic performance for columns packed with $1.5 \text{ }\mu\text{m}$ BEH particles. Columns dimensions were $25.7 \text{ cm} \times 30 \text{ }\mu\text{m}$ ID, $25.4 \times 50 \text{ }\mu\text{m}$ ID; $25.8 \times 75 \text{ }\mu\text{m}$	123

Figure 3-13: Effect of column inner diameter on chromatographic performance for columns packed with 1.0 μm BEH particles. Columns dimensions were 28 cm x 15 μm ID; 20 cm x 30 μm ID; 30.2 x 50 μm	124
Figure 3-14: Effect of maximum packing pressure on chromatographic performance for columns packed with 1.0 μm BEH particles. Columns dimensions were 19.8 cm x 30 μm ID (10,000 psi); 20 cm x 30 μm ID (20,000 psi); and 20 x 30 μm (30,000 psi).	125
Figure 3-15: Performance of 10 μm ID columns packed with 1.0 μm BEH (14.3 cm), 1.5 μm BEH (26.3 cm), and 1.9 μm BEH (25.8 cm).	126
Figure 3-16: Kinetic plots showing the performance of 1.0 vs. 1.9 μm particles with pressure limitations of 40,000 psi. Reduced van Deemter coefficients of $A=0.30$, $B=2.06$, and $C=0.15$ are used in the construction of the 1.9 μm curve (blue trace) and the theoretical 1.0 μm curve (dashed red trace). Reduced van Deemter coefficients of $A=0.15$, $B=2.26$, and $C=0.27$ are used in the construction of the 1.0 μm curve (red trace). Plots are constructed assuming viscosity, $\eta = 1$ cP; interparticle porosity, $\epsilon_i = 0.4$; analyte diffusion coefficient, $D_m = 1 \times 10^{-5} \text{ cm}^2/\text{s}$	127
Figure 3-17: Kinetic plots showing the performance of 1.0 μm particles with pressure limitations of 40,000 psi packed in 10 μm and 30 μm ID capillary. Reduced van Deemter coefficients of $A=0.15$, $B=2.26$, and $C=0.27$ are used in the construction of the 10 μm ID curve (red trace). Reduced van Deemter coefficients of $A=0.03$, $B=2.41$, and $C=0.30$ are used in the construction of the 30 μm ID curve (blue trace). Plots are constructed assuming viscosity, $\eta = 1$ cP; interparticle porosity, $\epsilon_i = 0.4$; analyte diffusion coefficient, $D_m = 1 \times 10^{-5} \text{ cm}^2/\text{s}$	128
Figure 4-1: Theoretical H vs. U curves for 1.9 μm particles at 25, 45, 65, and 85°C, using reduced A-, B-, and C- terms of 1.5, 1.0, and 0.1, respectively. Mobile phase viscosities are calculated according to the Chen-Horvath equation, and diffusion coefficients are scaled accordingly.	162
Figure 4-2: Series of theoretical curves representing the performance of 25 cm – 1000 cm columns. Curves are constructed using reduced van Deemter coefficients of 1.0, 1.0, and 0.1 for A-, B-, and C-, respectively. Mobile phase viscosities of 0.89 cP and diffusion coefficients of $8.0 \times 10^{-6} \text{ cm}^2/\text{s}$ are assumed. Each dead-time corresponds to an operating pressure. The intersection of the red trace with the curves shows expected performance when operating at 40,000 psi.	163
Figure 4-3: Theoretical plates vs. column dead times for 25 cm – 400 cm columns. The separation speeds and efficiencies that become newly accessible upon increasing maximum operating pressure from 15,000 psi to 40,000 psi are represented in the shaded region.	164
Figure 4-4: Maximum number of theoretical plates vs. column dead times for columns packed with 1.9 μm particles given a limiting operating pressure. The black	

curve represents columns run at 25°C and 15,000 psi. The red trace highlights the increase in accessible efficiencies that become available when operating at 85°C and 40,000 psi. Each dead-time corresponds to a column length..... 165

Figure 4-5: Peak capacity as a function of gradient time using Equation 4-10 for a 15 cm x 4.6 mm column with 5 μ m particles and a fixed flow rate of 1.0 mL/min. Theoretical plates are estimated using $A=5d_p$, $B=1D_m$, and $C=d_p^2/(6D_m)$. A diffusion coefficient of 8.0×10^{-6} cm²/s is assumed. 166

Figure 4-6: Peak capacity as a function of flow rate for a 15 cm x 4.6 mm column packed with 5 μ m particles. Gradient time is fixed at 1 hour. Maximum N as determined by the van Deemter coefficients $A=5d_p$, $B=1D_m$, and $C=d_p^2/(6D_m)$ occurs at a flow rate 8x slower than that which yields the highest peak capacity. 167

Figure 4-7: Peak capacity as a function of column flow rate for 15 cm x 4.6 mm columns. The solid trace is for 5 μ m particles; the dashed trace is for 1.9 μ m particles. Gradient time is fixed at 1 hour. 168

Figure 4-8: Experimental set-up for performing isocratic characterization at elevated temperatures. The majority of the column is housed within an aluminum heating block, held at temperature through feedback control of two heating cartridges. The first ~6 cm of column is unthermostatted within the column injector. 0.5 cm of column outlet protrudes from the heating block and is butt-connected to an open capillary for electrochemical detection. 169

Figure 4-9: Chromatograms collected near optimum linear velocity for a 66 cm x 50 μ m ID column packed with 1.9 μ m BEH particles at 23, 45, 65, and 85°C in 50/50 acetonitrile/water and 0.1% TFA. 170

Figure 4-10: Overlaid reduced van Deemter curves for hydroquinone collected at 23, 45, 65, and 85°C for a 66 cm x 50 μ m ID column packed with 1.9 μ m BEH particles. 171

Figure 4-11: Modified experimental set-up for performing isocratic characterization at elevated temperatures. The majority of the column is housed within an aluminum heating block, held at temperature through feedback control of two heating cartridges. The injector is held at matching temperature using four heating cartridges. Approximately 2 cm of column resides between the injector and heating block. 0.5 cm of column outlet protrudes from the heating block and is butt-connected to an open capillary for electrochemical detection. 172

Figure 4-12: Chromatograms collected near optimum linear velocity for a 60 cm x 50 μ m ID column packed with 1.9 μ m BEH particles at 23, 45, 65, and 85°C using 30/70 acetonitrile/water and 0.1% TFA. 173

Figure 4-13: Retention as a function of operating pressure at 23, 45, 65, and 85°C for a 60 cm x 50 µm ID column packed with 1.9 µm BEH in 30/70 acetonitrile/water and 0.1% TFA.	174
Figure 4-14: Van't Hoff plot of the retained test analytes at 23, 45, 65, and 85°C in 30/70 acetonitrile/water and 0.1% TFA.	175
Figure 4-15: H vs. U plots for hydroquinone at 23, 45, 65, and 85°C. Comparison with theoretical predictions in Figure 4-1 reveals the expected increase in U_{opt} at elevated temperatures and preserved column efficiency.	176
Figure 4-16: Overlay of reduced van Deemter plot for each analyte at 23, 45, 65, and 85°C. Reduced parameters at elevated temperatures are calculated from estimated pressure-dependent mobile phase viscosities and corresponding increases in analyte diffusion coefficients.	177
Figure 4-17: Chromatograms highlighting the on-column oxidation of 4-methyl catechol. With longer analysis times, the peak is rendered electrochemically undetectable. a) 33,000 psi; b) 18,000 psi; c) 12,000 psi.	178
Figure 4-18: Overlay of van Deemter performances for five ~100 cm x µm ID columns packed over a three month period. Experimental packing conditions were virtually identical with particle slurry concentrations ranging between 5-10 mg/mL.	179
Figure 4-19: Effect of column inner diameter on performance of ~100 cm columns. As observed in the past, performance improves dramatically with decreasing ID.	180
Figure 4-20: Schematic view of UHPLC gradient system. The gradient is generated by a Waters CapLC pump and loaded onto an external storage loop, followed by the sample. Flow resistances of the packed analytical column and small-ID flow splitter ensure that the vast majority of flow reaches the loop. Once the sample is loaded, both pin valves are closed, and the hydraulic amplifier is engaged to push the sample and gradient into the micro-volume cross. Much of the sample and gradient is diverted to waste through the flow splitter, while a small volume makes it onto the analytical column for analysis.	181
Figure 4-21: Representative chromatograms of a tryptic digest of bovine serum albumin run in 1-50% acetonitrile gradients corresponding to total run times of 60, 120, 180, and 240 minutes. Runs were performed on a 100 cm x 50 µm ID column packed with 1.9 µm BEH particles. Operating pressure was ~ 24,000 psi, but varied throughout the runs with changing mobile phase viscosities. Mass spectrometric detection was accomplished using a Waters LCT-TOF.	182
Figure 4-22: Peak capacities vs. gradient time for 100 cm columns with different inner diameters. Isocratic performance was best for the 30 µm ID column and worst for the 75 µm ID column. Peak capacities were calculated by determining 4σ base	

widths of representative peaks in 1-50% acetonitrile gradients for a BSA tryptic digest sample.	183
Figure 4-23: Peak capacity vs. retention window for a 100 cm x 30 μ m ID column packed with 1.9 μ m particles. 1-50% acetonitrile gradients for a BSA tryptic digest sample were run and peak capacities determined from 4σ base widths of representative peaks. Retention windows were determined from the elution times of two characteristic peaks, and peak capacities calculated by dividing the retention window by the average peak width.	184
Figure 4-24: Peak capacity vs. mobile phase linear velocity as determined by the column dead time for four gradient steepnesses, represented by % change of mobile phase composition per column volume.	185
Figure 4-25: Representative chromatograms of a) 105 cm and b) 103 cm x 50 μ m ID columns packed with a 100 mg/mL slurry of 1.9 μ m BEH particles.	186
Figure 4-26: Reduced van Deemter curves of the consecutively packed 105 cm and 103 cm x 50 μ m ID columns packed with 100 mg/mL slurries of 1.9 μ m BEH.	187
Figure 4-27: Retention data for the consecutively packed 105 (solid trace) cm and 103 cm (dashed trace) columns, highlighting the similarity of column permeability.	188
Figure 4-28: Flow resistances of the consecutively packed 105 cm (solid trace) and 103 cm (dashed trace) columns.	189
Figure 4-29: Chromatograms collected at 25°C and 65°C for a 180 cm x 50 μ m ID column operated at 45,000 psi.	190
Figure 4-30: h vs. v plots of the 180 cm x 50 μ m ID column. 4-methyl catechol is oxidized on-column at 65 °C.	191
Figure 4-31: Representative chromatogram of a 214 cm x 50 μ m ID column packed with a 100 mg/mL slurry of 1.9 μ m BEH particles, operated at 38,500 psi. The improved performance when packing with concentrated slurries is reflected in the number of theoretical plates.	192
Figure 4-32: Chromatograms and determined peak capacities for a 216 cm x 50 μ m ID column packed with 1.9 μ m BEH. 1-50% acetonitrile gradients of 120, 240, and 360 minutes for a BSA tryptic digest sample were run and peak capacities determined from 4σ base widths of representative peaks.	193
Figure 4-33: Peak capacity vs. retention window for a 216 cm x 50 μ m ID column packed with 1.9 μ m BEH particles. 1-50% acetonitrile gradients for a BSA tryptic digest sample were run and peak capacities determined from 4σ base widths of representative peaks. Retention windows were determined from the elution times of	

two characteristic peaks, and peak capacities calculated by dividing the retention window by the average peak width.	194
Figure 4-34: Overlaid h vs. v data for the first (closed markers) and last packed (open markers) ~ 100 cm segments of a originally 330 cm x 50 μm ID column packed with 1.9 μm BEH particles. Data highlighted in the red circle shows deteriorated performance subsequent to collected data at the highest operating pressures, signaling packed bed instability.	195
Figure 4-35: Overlaid reduced van Deemter plots of 100 cm x 50 μm ID columns packed at 30,000 psi and subsequently flushed at either 23,000 psi or 50,000 psi. The column flushed at 50,000 psi performs superiorly.	196
Figure 4-36: Modified UHPLC compression fitting to allow for the zero dead-volume connection of two microcapillary columns in series. The body is machined from 17-4 PH stainless steel, the compression bolt from 316 stainless steel, and the stem from D-2 air hardened tool steel. Capillary columns are abutted in the center of the PEEK ferrule and compression serves to grip the columns axially without twisting the silica faces over one another, thereby preventing breakage.	197
Figure 4-37: Chromatograms collected at a) 40,000 psi and b) 45,000 psi of a 360 cm x 50 μm ID column packed with 1.9 μm BEH particles. Total column length was achieved by the series connection of a 190 cm and 170 cm column in the compression fitting shown in Figure 4-36.	198
Figure 5-1: Chromatograms of a yeast cell lysate digest. a) A 90 minute 5-40% acetonitrile gradient performed on a commercial 25 cm x 75 μm ID packed with 1.9 μm BEH particles at 40°C; b) A 6 hour 1-50% acetonitrile gradient performed on a 200 cm x 50 μm ID column packed with 1.9 μm BEH at 25°C; c) An ~ 100 minute expanded view of the separation in (b); d) The same gradient utilized in (b) played back at 65°C.	215
Figure 5-2: Viscosity as a function of acetonitrile/water composition according to the Chen-Horvath equation shown in Equation 5-1 at 25, 45, 65, and 85°C.	216
Figure 5-3: Viscosity as a function of acetonitrile/water composition according to the Chen-Horvath equation shown in Equation 5-1 at 25, 45, 65, and 85°C. The data is normalized to the highest viscosity at each temperature to highlight the % change through 0-50% acetonitrile.	217
Figure 5-4: Schematic of the modified instrumentation to perform constant pressure gradient UHPLC separations with sample trapping.	218
Figure 5-5: Gradient loading scheme: Pin valves 1 and 5 are closed. Pin valves 2, 3, and 4 are open to allow flow from the nanoAcquity to the gradient storage loop.	219

Figure 5-6: Sample trapping scheme: Pin valves 1, 3, and 4 are closed. Pin valves 2 and 5 are open to allow flow from the nanoAcquity through the trap column to waste. 220

Figure 5-7: Gradient playback at UHPLC pressures: Pin valves 2, 4, and 5 are closed. Pin valve 3 is open, and engagement of the Haskel pump pushes the gradient from the storage loop onto the trap and analytical columns. Pin valve 1 is open to allow flow from the nanoAcquity to ramp down and to divert flow away from the commercial instrument should Pin valve 2 fail during operation. 221

Figure 5-8: Theoretical plates vs. dead times for 50 – 400 cm columns packed with 1.9 μm particles, operated at 65°C. The intersection of the red trace with the curves shows expected performance when operating at 30,000 psi. Curves are constructed using reduced van Deemter coefficients of 1.0, 1.0, and 0.1 for A-, B-, and C-, respectively. Mobile phase viscosities of 0.48 cP and diffusion coefficients of $1.7 \times 10^{-5} \text{ cm}^2/\text{s}$ are assumed. 222

Figure 5-9: Theoretical plates vs. dead times for 25 – 200 cm columns packed with 1.5 μm particles, operated at 65°C. The intersection of the red trace with the curves shows expected performance when operating at 30,000 psi. Curves are constructed using reduced van Deemter coefficients of 1.0, 1.0, and 0.1 for A-, B-, and C-, respectively. Mobile phase viscosities of 0.48 cP and diffusion coefficients of $1.7 \times 10^{-5} \text{ cm}^2/\text{s}$ are assumed. 223

Figure 5-10: Theoretical plates vs. dead times for 25 – 200 cm columns packed with 1.0 μm particles, operated at 65°C. The intersection of the red trace with the curves shows expected performance when operating at 30,000 psi. Curves are constructed using reduced van Deemter coefficients of 1.0, 1.0, and 0.1 for A-, B-, and C-, respectively. Mobile phase viscosities of 0.48 cP and diffusion coefficients of $1.7 \times 10^{-5} \text{ cm}^2/\text{s}$ are assumed. 224

Figure 5-11: Separation of a yeast cell lysate on a 200 cm x 75 μm ID column packed with 1.9 μm BEH particles at 30,000 psi and 65°C using a 35 μL gradient of 4-40% acetonitrile. 225

Figure 5-12: Peak tailing as evidenced by five single ion chromatograms from 139-144 minutes for the separation of a yeast cell lysate on a 200 cm x 75 μm ID column packed with 1.9 μm BEH particles at 30,000 psi and 65°C using a 35 μL gradient of 4-40% acetonitrile. 226

Figure 5-13: Separations of a yeast cell lysate on 75 μm ID columns packed with 1.5 μm BEH particles at 30,000 psi and 65°C. a) 117 cm column, 25 μL gradient of 3-40% acetonitrile; b) 117 cm column, 45 μL gradient of 3-40% acetonitrile; c) 100 cm column, 85 μL gradient of 1-40% acetonitrile. 227

Figure 5-14: Peak tailing as evidenced by three single ion chromatograms from 140-145 minutes for the separation of a yeast cell lysate on a 100 cm x 75 μm ID column

packed with 1.5 μm BEH particles at 30,000 psi and 65°C using a 85 μL gradient of 1-40% acetonitrile.	228
Figure 5-15: Separations of a yeast cell lysate on a 25 cm x 75 μm ID column packed with 1.0 μm BEH particles at 30,000 psi and 65°C using 1-40% acetonitrile gradients. a) 15 μL gradient; b) 25 μL gradient; c) 35 μL gradient.	229
Figure 5-16: Peak capacity vs. retention window plot comparing the performances of a commercial 25 cm x 75 μm ID column packed with 1.9 μm BEH particles (black) and a 25 cm x 75 μm ID column packed with 1.0 μm BEH particles (red).	230
Figure 5-17: Schematic of the modified instrumentation to perform constant pressure gradient UHPLC separations with direct sample injections.	231
Figure 5-18: Gradient and sample loading scheme in direct injection mode: Pin valve 1 is closed. Pin valves 2 and 4 are open to allow flow from the nanoAcquity to the gradient storage loop.	232
Figure 5-19: Gradient playback at UHPLC pressures in direction mode: Pin valves 2 and 4 are closed. Engagement of the Haskel pump pushes the sample and gradient from the storage loop onto the analytical column. Pin valve 1 is open to allow flow from the nanoAcquity to ramp down and to divert flow away from the commercial instrument should Pin valve 2 fail during operation.	233
Figure 5-20: Separations of an E.coli digestion standard using a 100 cm x 75 μm ID column packed with 1.5 μm BEH particles in direct injection mode at 30,000 psi and 65°C with 1-40% acetonitrile gradients with total volumes of: a) 25 μL ; b) 50 μL ; c) 100 μL ; d) 150 μL ; e) 200 μL	234
Figure 5-21: Peak capacity vs. retention window plot showing the performance of a 100 cm x 75 μm ID column packed with 1.5 μm BEH particles operated at 30,000 psi and 65°C in direct injection mode.	235
Figure 5-22: Improved peak shape as evidenced by five single ion chromatograms from 57-60 minutes for the separation of an E.coli digestion standard on a 100 cm x 75 μm ID column packed with 1.5 μm BEH particles at 30,000 psi and 65°C using a 100 μL gradient of 1-40% acetonitrile in direct injection mode.	236
Figure 5-23: Theoretical plates vs. dead time plot highlighting the similarity in performances of columns packed with 1.9 μm (black) and 1.5 μm (red) particles, operated 30,000 psi and 65°C. Curves are constructed using reduced van Deemter coefficients of 1.0, 1.0, and 0.1 for A-, B-, and C-, respectively. Mobile phase viscosities of 0.48 cP and diffusion coefficients of $1.7 \times 10^{-5} \text{ cm}^2/\text{s}$ are assumed.	237

LIST OF ABBREVIATIONS

2D-LC	two-dimensional liquid chromatography
BEH	ethylene Bridged Hybrid
BSA	bovine serum albumin
C18	n-octadecyl
CEC	capillary electrochromatography
CLSM	confocal laser scanning microscopy
EMT	effective medium theory
ESI	electrospray ionization
HDC	hydrodynamic chromatography
HETP	height equivalent of a theoretical plate
HPLC	high performance liquid chromatography
ID	inner diameter
ISEC	inverse size exclusion chromatography
LC	liquid chromatography
MEK	methyl ethyl ketone
MS	mass spectrometry
MS/MS	tandem mass spectrometry
PAC	micropillar array column
PEEK	polyether ether ketone
PLOT	porous-layer open tubular
PSD	particle size distribution
QTOF	quadrupole time-of-flight

RSD	relative standard deviation
TFA	trifluoroacetic acid
THF	Tetrahydrofuran
TOF	time-of-flight
UHPLC	ultrahigh pressure liquid chromatography

LIST OF SYMBOLS

ϕ	Fraction of mobile phase contained inside pores
ϕ_p	Volume fraction of particles
\overline{w}	Average peak width
Δc	Change in solvent composition over the course of the gradient
ΔH_0	System enthalpy
ΔP	Change in pressure
ΔP_{opt}	Pressure needed to obtain optimum flow rate/mobile phase linear velocity
ΔS_0	System entropy
A	Eddy dispersion van Deemter coefficient
A_{SP}	Specific surface area
B	Longitudinal diffusion van Deemter coefficient
C	Resistance to mass transfer van Deemter coefficient
C_M	Concentration of analyte in mobile phase
C_S	Concentration of analyte in stationary phase
$D_{A,B}$	Diffusion coefficient of solute A infinitely diluted in solvent B
d_c	Column diameter
D_{eff}	Effective diffusion coefficient
D_M	Diffusion coefficient of analyte in mobile phase
D_{ms}	Diffusion coefficient inside porous particle
d_p	Particle diameter
D_s	Diffusion coefficient in the stationary phase
d_s	Thickness of the stationary phase

F	Flow
g	Gravitational constant
G	Gradient steepness factor
H	Height equivalent of a theoretical plate
h	Reduced plate height
H_A	Height equivalent to a theoretical plate due to eddy dispersion
H_B	Height equivalent to a theoretical plate due to longitudinal diffusion
H_C	Height equivalent to a theoretical plate due to resistance to mass Transfer
H_{CM}	Contribution to H_C occurring in the mobile phase
H_{CS}	Contribution to H_C occurring in the stationary phase
H_{CSM}	Contribution to H_C occurring in stagnant mobile phase
H_{heat}	Heat of friction contribution to theoretical plate height
h_{min}	Minimum reduced plate height
K	Partition coefficient
k	Boltzman constant
k'	Retention factor
K_2	Particle-solvent dependent constant
L	Column length
M_B	Molecular weight of solvent B
N	Number of theoretical plates
n_c	Peak capacity
n_D	number of exchanges between flow paths due to diffusion mechanism
n_f	number of exchanges between flow paths due to flow mechanism

n_M	Number of moles in mobile phase
n_S	Number of moles in stationary phase
r	Radius of packed bed
R	Universal gas constant
r_H	Hydrodynamic radius of solute
R_s	Specific resolution
S	Distance traveled by analyte molecule in a given flow path
S_k'	Slope of the plot of the natural logarithm of the retention factor versus solvent composition
T	Absolute temperature
t_e	Time to transfer analyte molecule from one velocity extreme to another
t_g	Gradient run time
t_M	Time analyte spends in mobile phase
t_m	Column dead time
t_R	Retention time
t_S	Time analyte spends in stationary phase
u	Mobile phase linear velocity
u_i	Interstitial velocity
v	Reduced velocity
V_A	Molecular volume of solute A at normal boiling temperature
V_M	Volume of mobile phase
v_{opt}	Optimum reduced velocity
V_P	Peak volume at elution from column

$V_{P,0}$	Peak volume with very small injection volume
V_R	Retention volume
V_S	Volume of stationary phase
v_s	Sedimentation velocity
V_S	Sample injection volume
V_{SP}	Specific pore volume
x	Mole fraction
α	Selectivity factor
β	Phase ratio
γ	Tortuosity factor
ϵ_f	Particle porosity filled with mobile phase
ϵ_i	Volume fraction of interstitial spaces
ϵ_p	Particle porosity
ϵ_t	Volume fraction of column occupied by mobile phase
η	Mobile phase viscosity
λ	Scaling factor associated with the structure of the packed bed
ρ_l	Solvent density
ρ_{skel}	Particle skeleton density
σ_L^2	Spatial variance
σ_t^2	Temporal variance
ϕ	Intraparticle tortuosity factor
Φ_B	Association factor of solvent B
χ	Dimesionless parameter associated with the structure of the packed bed

ω	Flow resistance factor
ω_α	Fractional value of the particle diameter traveled to get from one velocity extreme to another
ω_β	Velocity ratio defined by $\Delta u/u$, where Δu is the difference between the velocity extreme and the mean velocity

CHAPTER 1: THEORY AND BACKGROUND

1.1 Overview

In attempting to improve the majority of liquid chromatographic separations, it is generally regarded that selectivity factor (α) plays a more significant role than the column efficiency parameter (N), as illustrated by Equation 1-1, an approximate expression for peak resolution (R_s)¹.

$$R_s = \left(\frac{1}{4} \right) \left[\frac{k'}{(1+k')} \right] \left(\frac{\alpha-1}{\alpha} \right) \sqrt{N} \quad (1-1)$$

where k' is the retention factor of the first peak. A notable exception to this rule is in the analysis of complex samples containing many components. In such instances, high-efficiency use of the entire separation space is often more important than the critical resolution of any two specific peaks. The two principal means of achieving higher efficiencies in liquid chromatography are reducing particle size (d_p) and increasing column length (L). In either of these approaches, the efficiency limit that can be achieved is dictated by the pressure drop across the column. Thus, instrumentation (i.e. pumping capabilities) becomes a key limiting factor in the maximization of separation efficiency.

Typical High Performance Liquid Chromatography (HPLC) instrumentation is capable of generating pressures up to 6,000 psi. As such, researchers are generally restricted to using short columns (≤ 25 cm) packed with 3 to 5 μm particles with maximum efficiencies of approximately 25,000 theoretical plates. The Jorgenson group noted that significant advantages could be had in terms of both speed and efficiency by using smaller

particles at higher pressures, and by the late 1990s, they had demonstrated these improvements with what was termed Ultrahigh Pressure Liquid Chromatography (UHPLC). The technique utilized fused silica capillary columns packed with sub-2 μm nonporous silica particles and operating pressures as high as 100,000 psi to generate plate numbers upwards of 300,000 in under 6 minutes^{2,3}.

More than a decade later, commercialization of technologies commensurable with UHPLC performances has not been realized. Nonetheless, significant strides were taken when Waters Corporation (Milford, MA) began marketing instrumentation (Acquity) capable of operating at 15,000 psi for use with 15 cm columns packed with 1.7 μm particles. Other manufacturers quickly followed suit with high pressure hardware: Agilent (the 1200 series) Thermo Fisher (Accela), Jasco (Xtreme-LC), Shimadzu (UFLC-XR), Hitachi (LaChrom Ultra), Scientific Systems (Ultra HP), Dionex (RSLC), Knauer (Platin Blue), and PerkinElmer (Flexar). The general marketing strategy for these higher pressure systems has emphasized the speed of analysis and the long-term cost savings as it relates to decreased solvent consumption. However, using the technology to push the limits of high-efficiency one-dimensional separations remains a relatively under-sampled endeavor.

The work presented in this thesis focuses on harnessing the combined benefits provided by ultrahigh pressures, small particle diameters, and elevated temperatures to achieve very high efficiency separations on time-scales that are much more manageable than those previously reported. The remainder of this introductory chapter will lay the theoretical groundwork needed to understand chromatographic theory and the relevant aspects of UHPLC toward this goal. Chapter 2 discusses general features of the microcapillary column packing process and improvements thereof with occasional reference to long columns and the

insights gained through investigating them. Chapter 3 specifically discusses the use of 1 μm fully porous particles in UHPLC, their utility, and strides made with regard to improving the efficiencies of columns packed with these materials. Chapter 4 describes the performance characteristics of capillary columns packed in excess of 1 meter under both isocratic and gradient elution conditions. Finally, Chapter 5 describes a new UHPLC gradient-capable platform designed specifically for use with long microcapillary columns for high-resolution applications.

1.2 Chromatographic Theory

1.2.1 Chromatographic Separations

Successful chromatographic separations work by exploiting the differences in the relative affinities of analytes for the stationary phase over the mobile phase or vice versa. An analyte's relative affinity for the station phase over the mobile phase is described by the partition coefficient, K :

$$K = \frac{C_S}{C_M} \quad (1-2)$$

where C_S is the equilibrium concentration of the analyte in the stationary phase and C_M is the concentration in the mobile phase. An analyte with a larger K will partition into the stationary phase for longer periods of time and elute later than an analyte with a smaller K .

The retention factor, k' , can also be used to describe the distribution of analyte molecules between the two phases.

$$k' = \frac{n_S}{n_M} \quad (1-3)$$

where n_S is the number of moles of analyte in the stationary phase and n_M is the number of moles in the mobile phase. Equations 1-2 and 1-3 can be related through the phase ratio, β , a column descriptor:

$$\beta = \frac{V_S}{V_M} \quad (1-4)$$

where V_S and V_M are the volumes of stationary phase and mobile phase, respectively, to give

$$k' = K\beta \quad (1-5)$$

Retention factor can also be written in terms relative to the times an analyte spends in the stationary phase (t_S) versus the mobile phase (t_M):

$$k' = \frac{t_S}{t_M} \quad (1-6)$$

By defining an analyte's retention time (t_R) as the time spent in both the stationary and mobile phases, equation 1-6 can be written:

$$k' = \frac{t_R - t_M}{t_M} \quad (1-7)$$

1.2.2 Separation Efficiency

The discussion of analyte retention presented in the previous section describes only one of the mechanisms relevant to practical liquid chromatographic separations. If it provided a complete picture in its own right, successful resolution of analytes with even very small differences in k' would be relatively easy. However, when a mixture of analytes is injected onto a column, it enters not in an infinitely narrow band, but in a spatially finite zone. As each of the analyte zones migrate the length of the column, the analytes will separate based upon their retention factors. At the same time, however, each of the zones will be broadened in accordance with several random processes resulting in Gaussian

distributions for each analyte, which can be defined in terms of spatial variance (σ_L^2). As each zone broadens, it becomes increasingly difficult to resolve a given pair of analytes. Characterization of these broadening phenomena as a function of migration distance or time is described as a column's separation efficiency.

The height equivalent of a theoretical plate (HETP or H) is defined as:

$$H = \frac{\sigma_L^2}{L} \quad (1-8)$$

where L is the length of the column, the distance traveled by the analyte zone. The efficiency of a separation is defined by the number of theoretical plates (N):

$$N = \frac{L}{H} = \frac{L^2}{\sigma_L^2} \quad (1-9)$$

N, a dimensionless parameter, can also be calculated from a peak's retention time and temporal variance.

$$N = \frac{t_R^2}{\sigma_t^2} \quad (1-10)$$

Equation 1-10 is often the most convenient to use when calculating column efficiency from a chromatogram.

Whereas N provides a rather generic description of separation quality, critical resolution, R_S , is an appropriate descriptor to express the specific extent of the separation of two given peaks.

$$R_S = \frac{2(t_2 - t_1)}{w_1 + w_2} \quad (1-11)$$

where t and w are the elution times and base widths (4σ) of the peaks under consideration.

When many components are present in a separation, peak capacity, n_c , can be used to assess

the separation power. This term refers to the total number of peaks that can fit within the chromatogram when every peak is separated from adjacent peaks with $R_s = 1$, where there is approximately 2% cross contamination between peaks of equal height. Under isocratic elution, peak capacity is calculated by

$$n_c = 1 + \frac{\sqrt{N}}{4} \ln(1 + k'_{last}) \quad (1-12)$$

where k'_{last} is the retention factor of the last eluting peak. It should be noted that the determination of peak capacity is of limited value for isocratic elution because the upper end of the retention window is unbounded. Peak capacity with respect to gradient elution chromatography will be discussed in greater detail in Chapter 4.

1.2.3 Van Deemter Theory

As mentioned in the previous section, chromatographic peak broadening is the result of several random processes. If these processes are considered to be independent of one another, their individual contributions toward overall peak broadening can be written:

$$H = \frac{\sigma_1^2 + \sigma_2^2 + \sigma_3^2 + \dots}{L} \quad (1-13)$$

The various contributions can be grouped according to their dependence on the mobile phase linear velocity (u) and written as the van Deemter equation:

$$H = H_A + H_B + H_C \quad (1-14)$$

This equation can be rewritten such that each term's dependence on linear velocity is made explicit:

$$H = A + \frac{B}{u} + Cu \quad (1-15)$$

where A, B, and C are known as the van Deemter coefficients and describe chromatographic band broadening contributions from eddy dispersion, longitudinal diffusion, and resistance to mass transfer, respectively. An additional contributor to H is due to the heat of friction caused as eluent percolates through the packed bed (H_{heat}). This term becomes most significant when considering highly retained analytes and wide-bore columns at high flow rates. In the present work, this term is ignored due to the use of microcapillary columns which efficiently dissipate the heat generated at high flow rates, and the use of lightly retained analytes during column characterization⁴.

In the following discussion, dependence of band broadening on both particle diameter and diffusion coefficients will be noted. It becomes advantageous to use reduced parameters as a means of comparing column performance independent of these variables. Reduced plate height, h , is defined below in Equation 1-16, and reduced velocity, v , in Equation 1-17.

$$h \equiv \frac{H}{d_p} \quad (1-16)$$

$$v \equiv \frac{ud_p}{D_M} \quad (1-17)$$

Substituting Equations 1-16 and 1-17 into the van Deemter equation gives the reduced form:

$$h = a + \frac{b}{v} + cv \quad (1-18)$$

The dimensionless a, b, and c-terms allow for meaningful performance comparisons of columns regardless of particle size and analyte properties. Typically, well-packed columns are expected to have a, b, and c-terms of 1.5, 1, and 0.17, respectively, resulting in minimum reduced plate heights (h_{min}) of approximately 2.0 and optimum linear velocities (v_{opt}) of 3.0⁵.

Figure 1-1 illustrates the effects of the three individual contributors to band broadening as a function of reduced velocity and the resultant van Deemter behavior when considered in sum.

1.2.3.1 A-term

The A-term, or the multiple flow path term, is velocity independent and describes band broadening which occurs as a result of the multifarious flow paths that analytes can sample as they navigate the length of a packed bed.

$$A = \lambda d_p \quad (1-19)$$

where λ is a dimensionless parameter associated with the structure of the packed bed, with typical values ranging between 1.5 and 2 for well-packed columns⁵. This equation assumes that all effective A-term broadening is due to interstitial volume alone, although other contributions exist. For example, the distribution of the sample over the column inlet cross section can play a significant role in the nature of the band when collected at the outlet.

Equation 1-19 is based upon the assumption that each analyte molecule samples only one particular flow stream path. Analytes, however, diffuse quite rapidly between regions of mobile phase where flow velocities are significantly different. This rapid exchange, an interaction between flow and diffusive mechanisms, serves to reduce the velocity persistence span, or the longitudinal distance traveled in a particular flow stream, and to increase the number of displacement steps taken in traveling a fixed distance. Since plate height increases with the square of the step length, but only with the first power of the number of steps, the increase in H will be less than predicted by flow or diffusion alone. Giddings considered this coupled relationship with respect to five categorical distances over which diffusive exchange between velocity extremes occur⁶. These distances are shown in Figure 1-2, and will be discussed in turn below.

Before considering the coupling of the diffusive and flow mechanism described above, consider the contribution to plate height from diffusive exchange alone. The time needed to exchange, or transfer, an analyte molecule from one velocity extreme to another is defined as t_e . The distance over which the analyte diffuses depends on which of the five categories is being considered and is defined as $\omega_\alpha d_p$. ω_α can be considered as a fractional value of the particle diameter traveled to get from one velocity extreme to another. The exchange time can thus be written

$$t_e = \frac{\omega_\alpha^2 d_p^2}{2D_m} \quad (1-20)$$

where D_m is the diffusion coefficient of the analyte in the mobile phase. The molecule will be carried a certain distance, S , in a given flow path with velocity u . Thus

$$S_{\text{Diffusion}} = ut_e \quad (1-21)$$

The distance, l , gained or lost by an analyte with respect to the mean can be defined as

$$l = \omega_\beta S \quad (1-22)$$

where ω_β is the velocity ratio defined by $\Delta u/u$, where Δu is the difference between the velocity extreme and the mean velocity. The number of random steps, n , taken in migrating a total distance, L , is thus

$$n = \frac{L}{S} \quad (1-23)$$

Allowing $\sigma^2 = l^2 n$, and combining the previous expressions with Equation 1-8 leads to

$$H_{\text{Diffusion}} = \omega_\beta^2 S = \frac{\omega_\alpha^2 \omega_\beta^2 d_p^2 u}{2 D_m} \quad (1-24)$$

Each of the five exchange distances, i , will be considered under the parameter ω_i , which is substituted for the constant $\omega_\alpha^2\omega_\beta^2/2$ to give

$$H_{\text{Diffusion}} = \frac{\omega_i d_p^2 u}{D_m} \quad (1-25)$$

In considering the contribution to plate height for the flow mechanism, consider again the distance traveled in any particular step of the random walk.

$$S_{\text{Flow}} = \omega_\lambda d_p \quad (1-26)$$

where ω_λ is a structural parameter near unity. Taking the same approach as demonstrated above for diffusive exchange, the plate height contribution from flow exchange can be written as

$$H_{\text{Flow}} = \omega_\beta^2 \omega_\lambda d_p \quad (1-27)$$

Again, by substituting a parameter λ_i for the constant $\omega_\beta^2\omega_\lambda^2/2$, the contribution to H can be considered for each of the categorical distances illustrated in Figure 1-2.

$$H_{\text{Flow}} = 2\lambda_i d_p \quad (1-28)$$

Considering the diffusive and flow exchange mechanisms in concert, a total migration distance, L , is traversed with n exchanges between flow paths.

$$S_{\text{Total}} = \frac{L}{n_f + n_D} \quad (1-29)$$

where n_f is the number of exchanges that occur due to the flow mechanism and n_D is the number of exchanges which occur due to diffusion. The total plate height expression is found in combining the above equations.

$$H_{A,i} = \frac{1}{\frac{1}{H_{\text{Flow}}} + \frac{1}{H_{\text{Diffusion}}}} = \frac{1}{\frac{1}{2\lambda_i d_p} + \frac{D_m}{\omega_i u d_p^2}} \quad (1-30)$$

The categorical distances considered by Giddings in developing his model, and shown in Figure 1-2, are empirical in nature. The transparticle contribution which exists in beds packed with porous media should not be included as an eddy dispersion term because the intraparticle mobile phase velocity is zero, and transfer occurs only via diffusion⁷. Additionally, the transcolumn and transchannel distances are intrinsic to bed morphologies in cylindrically confined packings, but the short- and long-range interchannel distances are somewhat arbitrarily defined. In the subsequent discussion, long-range interchannel contributions to the plate height are ignored.

Velocity inequalities exist in the interstitial channels of the packed bed with the highest velocity at the center of the channel and the lowest velocities occurring at the walls of the particle interfaces. The contribution to plate height due to analyte exchange between these regions is described by the transchannel term, $H_{A,Transchannel}$. Giddings estimated ω and λ values for this term to be approximately 0.01 and 0.5, respectively. The Tallarek group theoretically determined values for these parameters by numerical analysis of flow and mass-transport through computer-generated packings of monodisperse, nonporous, incompressible spheres⁸. Values were calculated for both bulk packings and cylindrically confined packings with $d_{column}/d_p=20$. In the confined packing, ω and λ were calculated as 0.0038 and 0.41, respectively.

$$H_{A,Transchannel} = \frac{1}{\frac{1}{0.82d_p} + \frac{D_m}{0.0038ud_p^2}} \quad (1-31)$$

Short-range interchannel effects describe flow inequalities resulting over distances of a few particle diameters due to differences in relative packing densities. Theoretically

determined values for ω and λ in randomly packed beds were found to be 0.436 and 0.86, respectively⁸.

$$H_{A,SR} = \frac{1}{\frac{1}{1.72d_p} + \frac{D_m}{0.436ud_p^2}} \quad (1-32)$$

The final contributor to multi-path dispersion is a transcolumn term, $H_{transcolumn}$, arising from radial inhomogeneities in the packed bed thereby creating flow velocity variations from the center of the column to the column walls. Wall effects are a significant contributor in this case, as determined interparticle porosities were calculated to be 0.378 and 0.4 for bulk packings and confined packings with $d_{column}/d_p=20$, respectively. Giddings estimated the magnitude of the contribution by this effect as

$$\omega_{transcolumn} \cong \frac{1}{2} \left(\frac{\Delta u}{u} \right)^2 \left(\frac{m}{2} \right)^2 \sim 0.001m^2 \quad (1-33)$$

where m is the number of particle diameters across the column diameter⁶. The contribution is therefore larger with wider bore columns, and relaxation of the effect requires longer time-scales. Calculations reveal this to be true as the longitudinal dispersion in confined packings is significantly larger than for bulk packings. The transverse dispersion length in confined packings, $\langle l_T \rangle_{confinedL}$, was found to be

$$\langle l_T \rangle_{confinedL} = \sqrt{2D_T(v)t} \approx 10d_p \equiv \frac{d_{column}}{2} \quad (1-34)$$

where $D_T(v)$ is the transverse diffusion coefficient. This value was significantly lower in the bulk packing experiments ($\langle l_T \rangle_{bulk} \approx \sqrt{2}d_p$), thus demonstrating the macroscopic flow heterogeneity present in a confined packed bed, which requires a relaxation time relative to

the radius of the column. Theoretically determined values for ω and λ were found to be 0.23 and 2.61, respectively.

$$H_{A,Transcolumn} = \frac{1}{\frac{1}{5.22d_p} + \frac{D_m}{0.23ud_p^2}} \quad (1-35)$$

The large value for $\lambda_{Transcolumn}$ shows that wall effects to have an extremely significant influence on bed morphology and the resultant macroscopic flow heterogeneity. In comparing the theoretical performances of bulk and confined packings, the bulk packing was found to exhibit a 2.5 times lower minimum plate height at a linear velocity 4 times faster than the confined packings⁸.

1.2.3.2 B-term

The B-term describes the longitudinal diffusion of the molecules in the analyte band and is defined as:

$$\frac{B}{u} = \frac{2\gamma D_m}{u} \quad (1-36)$$

where γ is a tortuosity factor, typically ranging between 0.5 and 1.0, which accounts for the obstruction of simple diffusion by the packed bed. The B-term, however, depends not only upon molecular diffusion, but also upon the equilibrium between the mobile and stationary phases, thus leading to the expanded expression below⁹.

$$H_B = \frac{2\gamma_m D_m}{u} + \frac{2k'\gamma_s D_s}{u} \quad (1-37)$$

The distinction between mobile and stationary phase diffusion coefficients is difficult to make, and the B-term is consequently thus written as

$$H_B = \frac{2D_{eff}}{u} (1 + k') \quad (1-38)$$

where D_{eff} is an effective diffusion coefficient defined as

$$D_{\text{eff}} = \frac{t_{\text{me}} \gamma_{\text{me}} D_{\text{m}} + t_{\text{ms}} \gamma_{\text{ms}} D_{\text{ms}} + t_{\text{s}} \gamma_{\text{s}} D_{\text{s}}}{t_{\text{me}} + t_{\text{ms}} + t_{\text{s}}} \quad (1-39)$$

Where subscripts *me*, *ms*, and *s* denote terms descriptive of diffusion processes occurring outside the particles in the mobile phase, inside the pores of the particles, and in the stationary phase. Recent work suggests that the above model is physically unsound because it violates Maxwell's basic law of diffusion. However, attempts to employ more rigorous models, such as the effective medium theory (EMT), have proven insufficient in rectifying all of the associated errors⁹.

1.2.3.3 C-term

The C-term describes resistance to mass transfer, and its simplest deconvolutions typically result in three distinct contributions: resistance to mass transfer in the mobile phase (H_{CM}), in the stationary phase (H_{CS}), and in the stagnant mobile phase located inside the pores of porous materials (H_{CSM}).

Resistance to mass transfer in the mobile phase is described by the following equation⁵:

$$H_{\text{CM}} = \frac{(1 + 6k' + 11k'^2) d_p^2 u}{(1 + k')^2 D_M \chi} \quad (1-40)$$

where χ is a dimensionless parameter associated with the structure of the packed bed. The physical nature of resistance to mass transfer in the mobile phase can be considered in two ways. The first is due to the parabolic flow profiles which occur in the interstitial spaces between the particles. Flow is faster at the center of these profiles than at the walls, or particle interfaces, due to friction, and analyte molecules at the centers will migrate the length of the column faster. The second cause is that molecules at the center of these profiles

must diffuse a greater distance than those at the particle interfaces in order to experience a partitioning event. Such explains the dependence of H_{CM} on d_p and k' . Interstitial spaces will be larger with larger particle diameters, thus causing longer diffusion distances from the centers of the parabolic flow profiles to the particle interfaces.

In the stationary phase, resistance to mass transfer occurs as a result of the time it takes for the analyte to diffuse out of the thin film and is described by⁵:

$$H_{CS} = \frac{2}{3} \frac{d_s^2}{D_s} \frac{k'}{(k'+1)^2} u \quad (1-41)$$

where d_s is the thickness of the stationary phase and D_s is the analyte diffusion coefficient in the stationary phase. This contribution is zero for unretained analytes ($k'=0$), and approaches zero for highly retained analytes ($k'/(k'+1)^2 \rightarrow 0$).

The third contributor to C-term band broadening is due to the stagnant mobile phase contained within the pores of the particles comprising the packed bed. Resistance to mass transfer in these regions are described by⁵

$$H_{CSM} = \frac{(1-\phi + k')^2 d_p^2}{30(1-\phi)(1+k')^2 \phi D_M} u \quad (1-42)$$

where ϕ is the fraction of mobile phase contained inside the pores and ϕ is the intraparticle tortuosity factor, both of which are estimated to be 0.5 for fully porous particles. The physical interpretation of the band broadening described in Equation 1-42 is the frequency and depth with which analyte molecules enter the pore regions. Upon entrance into regions of stagnant mobile phase, the analyte has essentially experienced a partitioning event similar to that undergone when partitioning into the stationary phase. In effect, more obstructed pore structures will tend to lessen the contribution of this term to C-term broadening.

The generalized Giddings equation, which accounts for the flow and diffusive coupling discussed above, can thus be written as

$$h = \frac{H}{d_p} = \frac{b}{v} + \sum_{i=1}^3 \frac{2\lambda_i}{1 + (2\lambda_i/\omega_i)v^{-1}} + cv \quad (1-43)$$

where the middle term accounts for the transchannel, short-range interchannel, and transcolumn coupling terms. The long-range interchannel effects, which cannot be decoupled from the short-range effects, and the transparticle effects, which are not proper contributors to eddy diffusion broadening, are ignored. The same type of equation was derived by Berdichevsky and Neue¹⁰, and for well-packed columns, the reduced form with typical coefficients is found to be

$$h = \frac{1.8}{v} + \frac{v}{1 + 0.4v} + \frac{v}{8} \quad (1-44)$$

Finally, the Knox equation represents an attempt to find a simple equivalent to the Giddings equation wherein the different contributions to eddy dispersion are condensed to a single empirical term, based upon a number of experimental data sets¹¹.

$$h = \frac{b}{v} + av^n + cv \quad (1-45)$$

where n is between 0.2 and 0.35, most often taken as one-third. The van Deemter equation, identical in form, assumes $n = 0$. Figure 1-3 is an overlay of the van Deemter equation, the Giddings equation, and the Knox equation with typical values for the coefficients. The curves are practically indistinguishable over the range of reduced velocities typical of practical HPLC. While the Giddings equation is certainly the most correct descriptor of column performance, the van Deemter equation provides the most practical representation,

and is therefore used to compare column performances throughout the remainder of this thesis.

1.2.4 Corrected Interstitial Velocities

A particular remark must be made at this point with regard to the performance data presented within this thesis. Linear velocities have been determined from the elution times of an unretained analyte using the following equation:

$$u = \frac{L}{t_M} \quad (1-46)$$

Linear velocity can be related to flow, F , by dividing by the cross section of the column that is occupied by the mobile phase.

$$u = \frac{F}{\varepsilon_t \pi r^2} \quad (1-47)$$

where ε_t is the volume fraction of the column occupied by mobile phase and r is the radius of the packed bed. The interstitial velocity, u_i , describes the velocity of the mobile phase in the interstitial regions between particles. It is written as:

$$u_i = \frac{F}{\varepsilon_i \pi r^2} \quad (1-48)$$

where ε_i is the volume fraction of the interstitial spaces. For nonporous materials, u_i , as determined by Equation 1-48 is the same as u from Equation 1-46, but will be higher when considering columns packed with porous particles, where the measured t_m includes time spent by the analyte in both the interstitial mobile phase and the stagnant mobile phase. Because interstitial velocity, u_i , is the only real velocity that exists in the packed bed, it should be used when performing van Deemter analysis of column performance¹². Assuming that the intraparticle mobile phase comprises approximately half of the total mobile phase

volume for columns packed with fully porous particles, the linear velocity as determined from a dead time marker can be roughly doubled in order to estimate the actual interstitial velocity.

Correcting the measured linear velocities in this way to obtain more accurate estimations of interstitial velocity would have no effect upon the a-terms, b-terms would be doubled, and c-terms halved. This effect is illustrated in Figure 1-4. Methods for determining actual interstitial velocities exist, but not without drawbacks. For example, inverse size exclusion chromatography (ISEC) utilizes probes which are too large to access the pore regions of particles in a packed bed in order to directly measure interstitial velocity¹³. However, probes of this size are significantly affected by the same mechanisms which govern hydrodynamic chromatography (HDC), as illustrated in Figure 1-5¹⁴. In considering the parabolic flow profiles in the interstitial channels of packed beds, large probes are unable to adequately sample the slowest flow regimes, and their respective elution times may significantly overestimate the actual interstitial velocities. Another method, total pore blocking, uses hydrophobic solvents to block the pores of the packed particles¹⁵. Small molecular weight tracers, which are completely excluded from the pore blocking solvent, are then eluted from the column to determine the true interstitial velocity. The difficulty with this technique lies in the assurance that all pores have been effectively blocked. Because of the inconvenience of employing these techniques for every column packed, the data based upon measured linear velocities in this thesis are left uncorrected.

1.2.5 Ultrahigh Pressure Liquid Chromatography (UHPLC)

The discussion in the previous section highlights the dependence of both the A and C-term band broadening on particle diameter. By decreasing particle diameter, h_{\min} is reduced,

and the slope of the high linear velocity region dictated by mass transfer in the van Deemter curve is lowered. The benefits appear manifold in terms of both maximum achievable plate counts and in the ability to run columns well beyond u_{opt} without sacrificing these efficiency gains, as illustrated in Figure 1-6.

The pressure requirements, however, become increasingly prohibitive as smaller particle are used, as illustrated by the following equation:

$$\Delta P = \frac{\omega \eta L u}{d_p^2} \quad (1-49)$$

where ω is a flow resistance factor associated with the structure of the packed bed and η is the mobile phase viscosity. Combining this with Equation 1-17 and the knowledge that $v_{opt} \approx 3$ for well-packed columns, it can be seen that

$$\Delta P_{opt} \propto \frac{1}{d_p^3} \quad (1-50)$$

where ΔP_{opt} is the pressure required to operate the column at u_{opt} . That is to say, for every halving of particle diameter, an 8-fold increase in pressure is required to operate a given column length at its maximum efficiency. As such, the current state for the routine use of smaller particles in liquid chromatography has emphasized speed of analysis rather than the pursuit of very high-efficiencies.

1.2.5.1 UHPLC Pressures, Mobile Phase Viscosities, and Diffusion Coefficients

Accurate assessment of chromatographic performance requires a thorough understanding of relevant analyte diffusion processes. Noting that the determination of reduced velocities require knowledge of the analyte diffusion coefficient (Equation 1-17), it is therefore necessary to measure analyte diffusion coefficients directly in the mobile phases being used without neglecting the effects of ultrahigh pressures. Because solvents compress

under high pressures, their viscosities tend to increase and an analyte's corresponding diffusion coefficient decreases, as indicated by the Stoke-Einstein equation¹⁶.

$$D_m = \frac{kT}{6\pi\eta r_H} \quad (1-51)$$

where k is the Boltzman constant, T is temperature, and r_H is the hydrodynamic radius of the solute. Diffusion coefficients for analytes commonly used to assess the chromatographic performance of columns packed in the Jorgenson lab have been determined in various acetonitrile-water mixtures from atmospheric pressure to 2000 bar (~30,000 psi) at 25°C. These pressure dependent diffusion coefficients are used to determine the reduced van Deemter parameters presented in this thesis¹⁷.

1.2.7 Kinetic Plots

Typical characterization of LC columns examines zone broadening as a function of linear velocity (van Deemter analysis), but neglects column permeability (i.e. the pressure drop over column length). Poppe developed a series of theoretical plots (kinetic plots) that allowed speed and efficiency analyses to be considered with respect to pressure limitations¹⁸. Such plots describe the plate time versus the plate number (N). The plate time characterizes the number of theoretical plates obtained per unit time and is commonly represented by H/u or t_m/N . These plots are especially helpful when considering how to achieve the highest efficiency in the shortest time given a set of limiting parameters.

Given that the maximum obtainable efficiency depends solely upon the maximum pressure that is available, the following equation can serve as a basis for constructing a theoretical kinetic plot.

$$u = \frac{\Delta P d_p^2 \varepsilon_i^2}{180\eta L(1 - \varepsilon_i)^2} \quad (1-52)$$

where ΔP , d_p , ε_i , and η are held constant. Linear velocity, u , is adjusted stepwise, and resultant column lengths, L , which correspond to the other given parameters, are determined. An approximate, or experimentally determined, diffusion coefficient can then be used to find the reduced velocity, v , and substituted into Equation 1-18 with appropriate values for a , b , and c to give corresponding reduced plate heights, h . Figure 1-7 shows the theoretical kinetic plots for three different particle sizes (1, 3, and 5 μm). The following values were used in constructing the plot: maximum pressure, $\Delta P = 400$ bar (~ 5800 psi); viscosity, $\eta = 1$ cP; interparticle porosity, $\varepsilon_i = 0.4$; diffusion coefficient, $D_m = 1 \times 10^{-5}$ cm^2/s ; reduced van Deemter coefficients $A = 1.0$, $B = 1.0$, and $C = 0.1$.

Each curve in Figure 1-7 represents the most efficient analysis for the given particle size when operating at 400 bar. Points in the lower left region of the plot represent fast, low-efficiency analyses. These analyses tend toward horizontal asymptotes because at high linear velocities, the C-term is efficiency limiting. Points in the upper right region represent slower, high-efficiency runs with vertical asymptotes where analyte diffusion (B-term) becomes efficiency limiting. The dashed diagonal lines represent the dead times for various types of analyses. As demonstrated by these theoretical curves, for lower required efficiencies, smaller particles provide for faster analyses. Higher efficiencies come only at the price of longer analyses times and can be reached with larger particle sizes. Kinetic plots will be examined in greater detail throughout this thesis, with specific consideration of smaller particles and UHPLC pressures as well the role temperature plays in expanding the available analysis space.

1.3 References

- ¹ Snyder, L.R.; Kirkland, J.J.; Dolan, J. *Introduction to Modern Liquid Chromatography*. 3rd Ed., Wiley: New York, **2010**.
- ² MacNair, J.E.; Lewis, K.C.; Jorgenson, J.W. *Analytical Chemistry* **1997**, 69, 983-989.
- ³ MacNair, J.E.; Patel, K.D.; Jorgenson, J.W. *Analytical Chemistry* **1999**, 71, 700-708.
- ⁴ Gritti, F.; Guiochon, G. *Journal of Chromatography A* **2007**, 1176, 107-122.
- ⁵ Neue, U.D. *HPLC Columns: Theory, Technology, and Practice*; Wiley-VCH, Inc.: New York, NY, **1997**.
- ⁶ Giddings, J.C. *Dynamics of Chromatography: Principles and Theory*, Marcel Dekker Inc.: New York, **1965**.
- ⁷ Gritti, F.; Guiochon, G. *Analytical Chemistry* **2006**, 78, 5329-5347.
- ⁸ Khirevich, S.; Höltzel, A.; Seidel-Morgenstern, A.; Tallarek, U. *Analytical Chemistry* **2009**, 81, 7057-7066.
- ⁹ Desmet, G.; Broekhoven, K.; De Smet, J.; Deridder, S.; Baron, G.V.; Gzil, P. *Journal of Chromatography A* **2008**, 1188, 171-188.
- ¹⁰ Berdichevsky, A.L.; Neue, U.D.; *Journal of Chromatography* **1990**, 535, 189-198.
- ¹¹ Kennedy, G.J.; Knox, J.H. *Journal of Chromatographic Science* **1975**, 13, 25
- ¹² Neue, U.D. *HPLC Columns: Theory, Technology, and Practice*; Wiley-VCH, Inc.: New York, NY, **1997**.
- ¹³ Yao, Y.; Lenhoff, A.M. *Journal of Chromatography A* **2004**, 1037, 273-282.
- ¹⁴ Small, H.; Langhorst, M.A. *Analytical Chemistry* **1982**, 54, 892A-898A.
- ¹⁵ Cabooter, D.; Lynen, F.; Sandra, P.; Desmet, G. *Journal of Chromatography A* **2007**, 1157, 131-141.
- ¹⁶ Ueno, M.; Ueyama, S.; Hashimoto, S.; Tsuchihashi, N.; Ibuki, K. *Journal of Solution Chemistry* **2004**, 33, 827-846.
- ¹⁷ Kaiser, T.J.; Thompson, J.W.; Mellors, J.S.; Jorgenson, J.W. *Analytical Chemistry* **2009**, 81, 2860-2868
- ¹⁸ Poppe, H. *Journal of Chromatography A* **1997**, 778, 3-21.

1.4 Figures

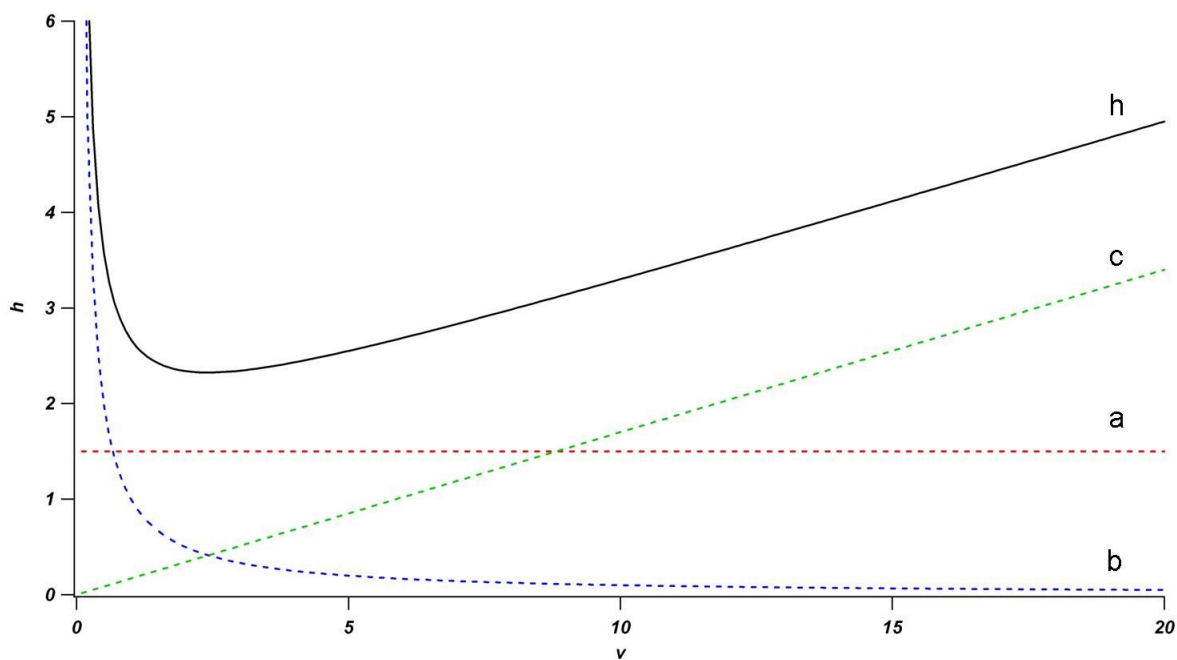


Figure 2-1: Theoretical relationship between the a-, b-, and c-terms of the van Deemter equation, and the resultant overall plate height (h)

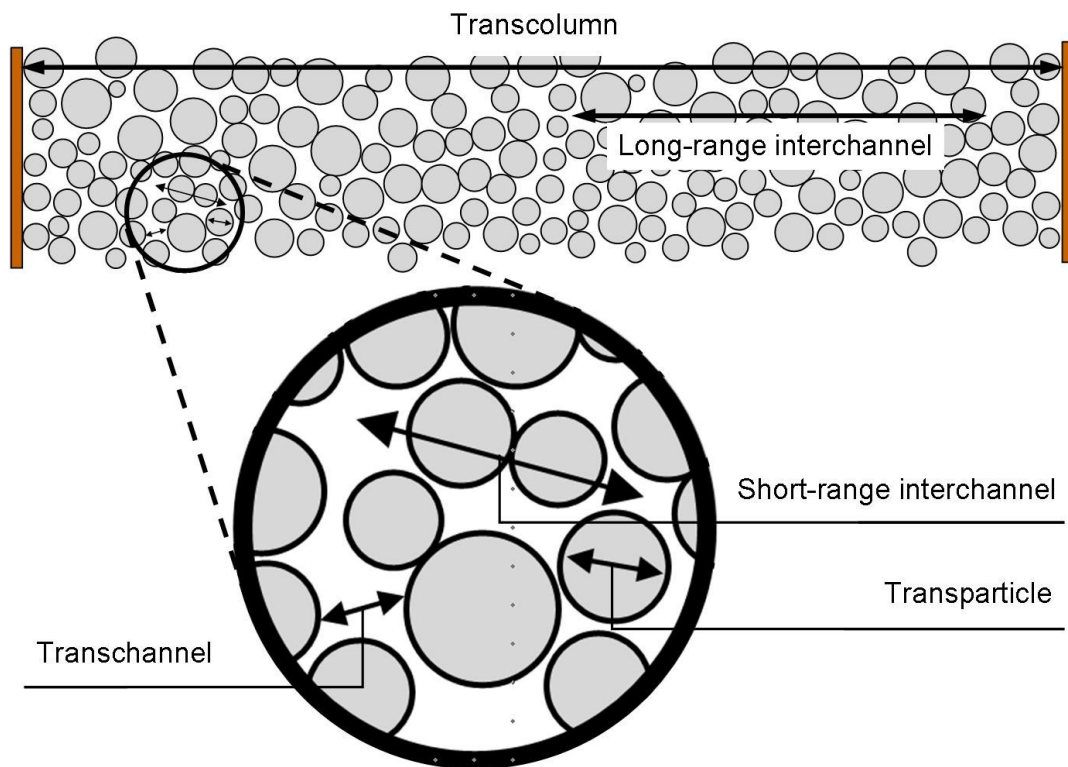


Figure 1-2: Categorical distances of the five contributors to eddy diffusion identified by Giddings. Figure adapted from Ref. 6.

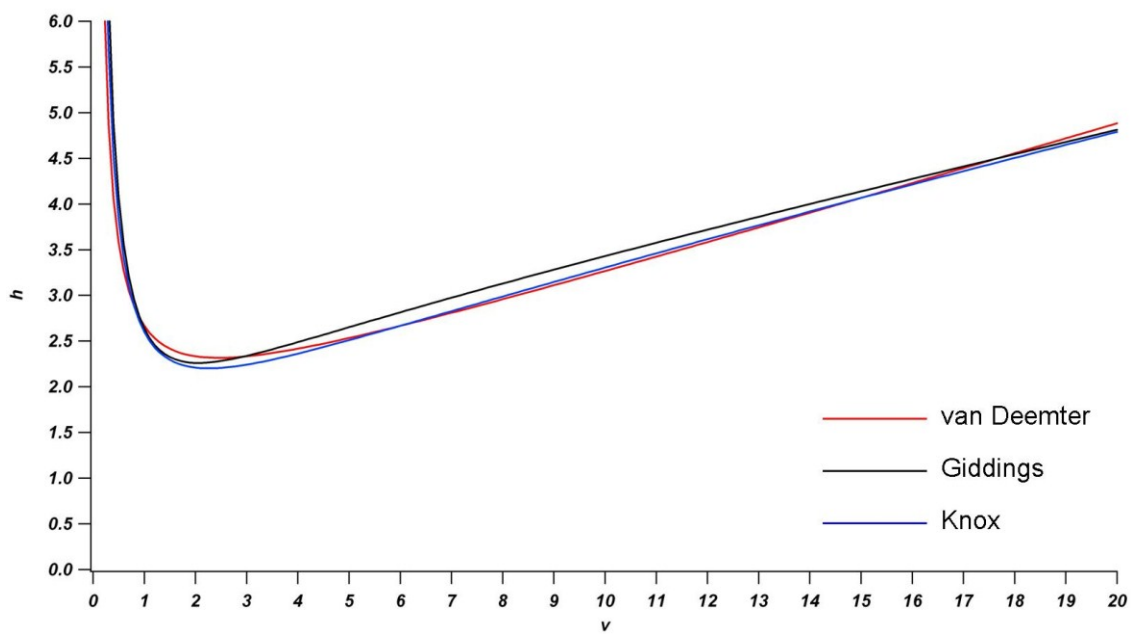


Figure 1-3: Overlay of the reduced forms of the van Deemter, Giddings, and Knox equations with typical values for the coefficients.

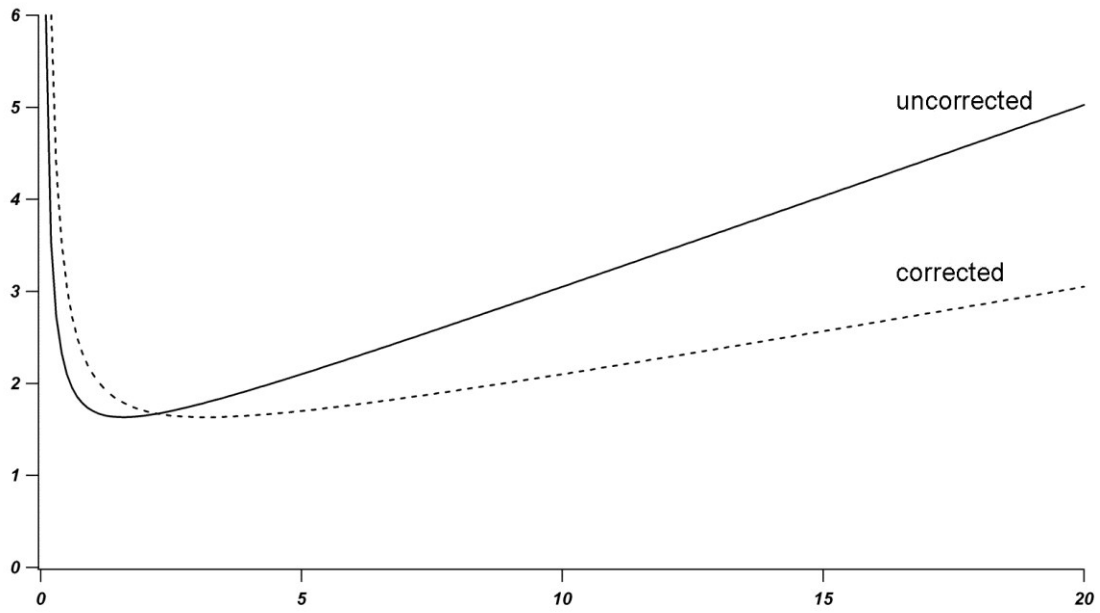


Figure 1-4: Mobile phase velocities experimentally determined from a dead time marker can be corrected to account for intraparticle stagnant mobile phase to find approximate interstitial velocities. The corrected interstitial velocities should be used in constructing van Deemter curves.

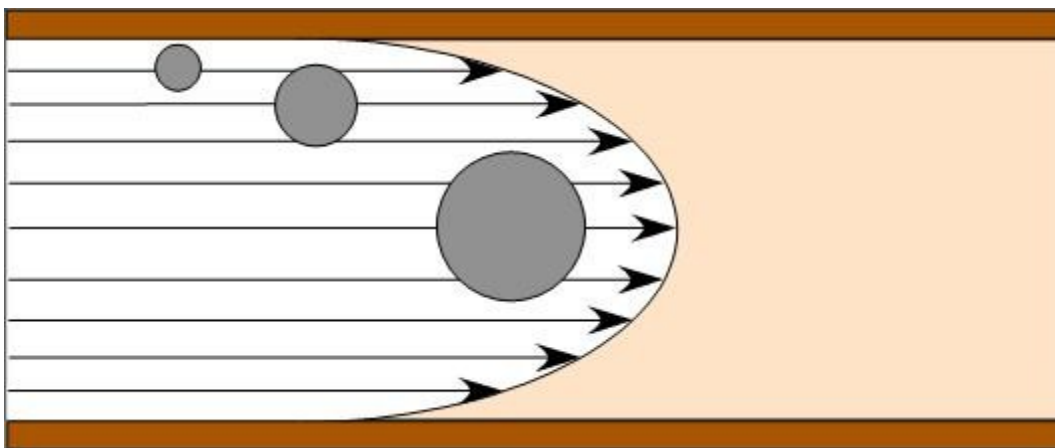


Figure 1-5: The mechanism of hydrodynamic flow chromatography (HDC) in a channel. Large particles cannot adequately sample the slowest flow regimes at the walls, and measuring their elution times results in overestimating the actual interstitial velocity.

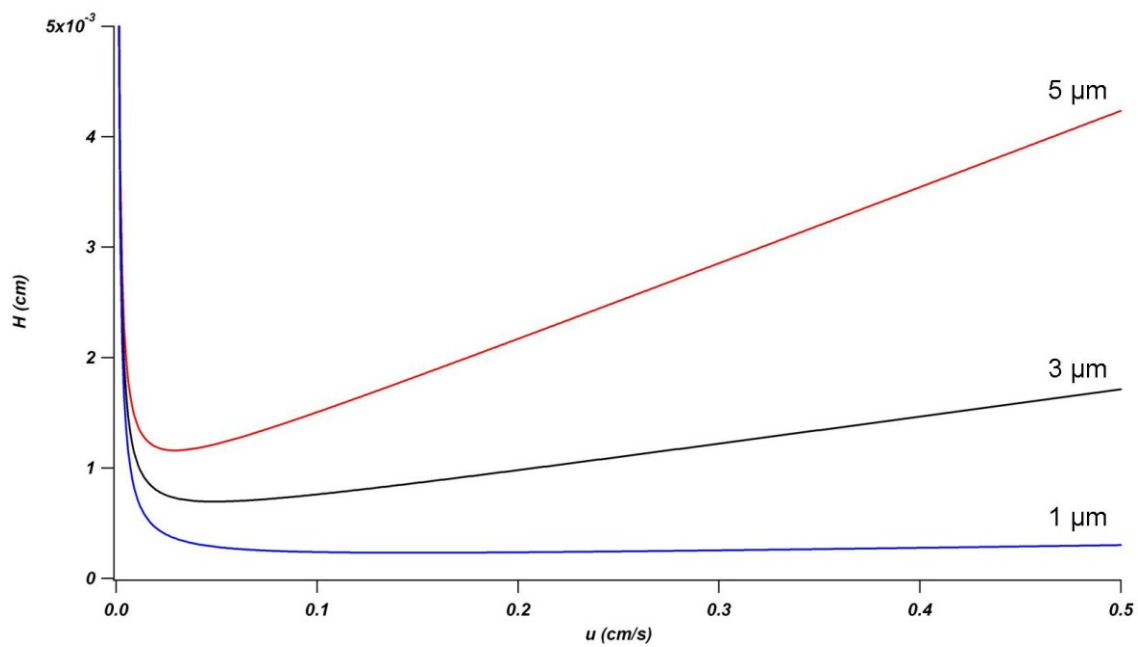


Figure 1-6: The effect of decreasing particle diameter on column performance.

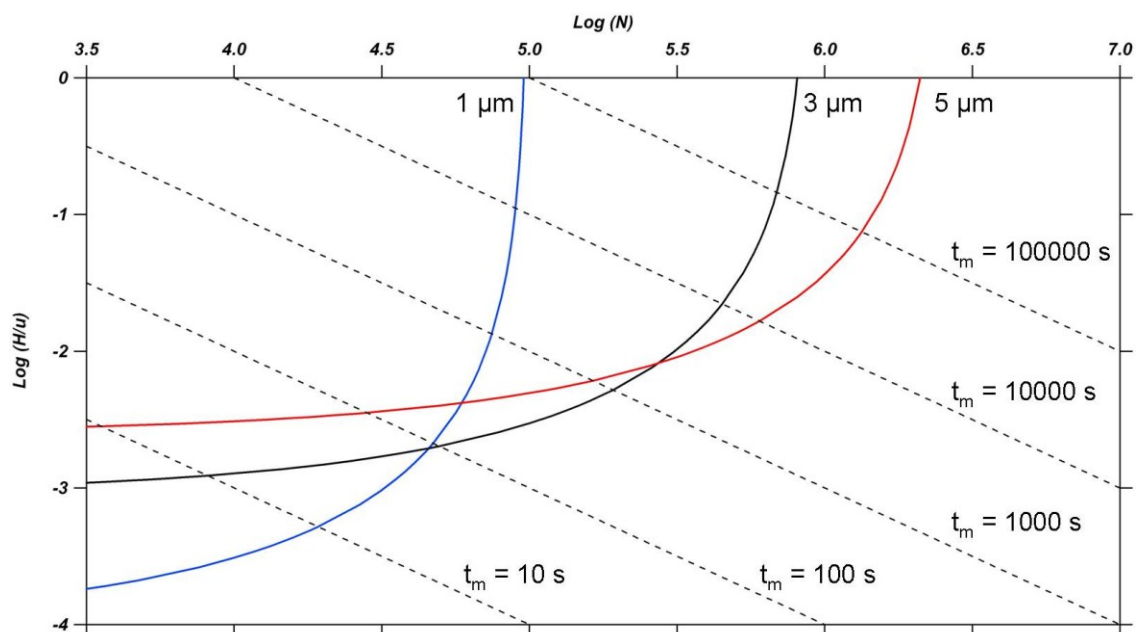


Figure 1-7: Kinetic plots for 1, 3, and 5 μm particles. $\Delta P = 400$ bar (~ 5800 psi); viscosity, $\eta = 1$ cP; interparticle porosity, $\varepsilon_i = 0.4$; diffusion coefficient, $D_m = 1 \times 10^{-5}$ cm/s; reduced van Deemter coefficients $A = 1.0$, $B = 1.0$, and $C = 0.1$.

CHAPTER 2: INVESTIGATIONS AND IMPROVEMENTS OF MICROCAPILLARY COLUMN PACKING AND PERFORMANCE

2.1 Introduction

The importance of packing procedures in producing stable, reproducible, highly efficient HPLC and UHPLC columns can not be underestimated. Historically, column packing has been regarded as an art form, but strides have been made in understanding the individual and synergistic effects that changing particular packing parameters may have upon a column's ultimate performance.

2.1.1 Slurry Packing

Early columns used for HPLC were packed with large ($\sim 25\text{-}50\text{ }\mu\text{m}$), irregularly shaped particles using vibration procedures or dry-pack methods that could reliably produce stable and efficient columns. As sub- $10\text{ }\mu\text{m}$ particles came into use, however, dry-pack methods were found insufficient and slurry packing procedures became routine. With this technique, a column blank is filled under pressure with a slurry of particles using one of a variety of approaches in effort to achieve stable, efficient packings. A balanced-density approach employs a slurry solvent with a density similar to that of the particles being packed, while a high-viscosity approach uses a solvent such as glycerin to slurry the particles. Both of these methods represent efforts to prevent particles from settling and size-segregating during the packing process. A low-viscosity unbalanced slurry approach became the norm with the introduction of sub- $5\text{ }\mu\text{m}$ particles with relatively narrow size distributions¹.

From a certain perspective, column slurry packing is relatively straight-forward. The particles of interest are suspended in an appropriate solvent and placed in a reservoir which is attached to a high-pressure pump. Pressure is applied to force the slurry through a column blank and, as the particles accumulate at the outlet frit at the end of the column, the packed bed is formed. Once the blank is packed, pressure is released, the column is removed, and a frit is placed at the inlet. A closer inspection reveals the slurry packing process to be quite complex, involving several interrelated parameters. Three major components of the slurry packing process involve colloid chemistry, slurry rheology, and particle filtration². Particle physiochemical properties such as surface modification, mechanical strength, and size-distribution along with interparticle forces, slurry solvent properties, slurry preparation, and post-packing column conditioning are just some of the considerations that must be taken into account. Survey of the scientific literature reveals that much of the column packing process and its desirable characteristics remain enigmatic, and contradictory opinions abound.

2.1.2 Bed Morphology and Its Influence on Chromatographic Performance

Column packing, as it relates to the structure of the packed bed and as it ultimately translates to chromatographic performance, is thought to affect the A-term most significantly. Heterogeneities in the packed bed result in a greater variety of available flow paths, thereby increasing eddy dispersion contributions to band broadening. Confined packings of spherical particles tend toward more ordered arrangements at the wall regions and more random, densely packed arrangements in the core region. These effects were investigated by Hsieh and Jorgenson by packing 5 μm particles into capillaries with inner diameters between 12 and 33 μm ³. A linear decrease in A-terms with decreasing inner diameter resulted in lower reduced plate heights for the narrower-bore columns. As the column-to-particle diameter

ratio becomes smaller, the denser core region of the packed bed effectively disappears, and the packing structure becomes more homogeneous over the column cross-section.

A second origin of radial heterogeneity is due to the high radial stress that is applied by the bed to the wall as a consequence of the friction between particles during the packing process⁴. This effect is thought to be highly dependent upon the experimental parameters. As a result of this phenomenon, packing density near the wall is higher than at the core region, and bed permeability is higher at the center of the column. Both of these wall effects, the previously described geometrical effect along with the more extended frictional effect, have been observed in computational bed reconstruction experiments performed by the Tallarek group⁵. Porosity profiles of a narrow-bore column approximately 40 particle diameters wide reveal a region of $\sim 2 d_p$ along the wall where mobile phase velocity is higher than average in the whole packing due to the geometrical effect. The adjacent region, consisting of approximately seven particle diameters, exhibits lower-than-average mobile phase velocities, most likely due to frictional effects during packing. The center region of the column, roughly $19 d_p$ across, exhibits homogenous flow profiles.

Giddings postulated that these contributors to eddy-dispersion were responsible for approximately one-half of the contribution to theoretically achievable minimum plate heights⁶. In fact, CEC studies, which are much less sensitive to heterogeneities in the packed bed, frequently result in reduced minimum plates heights near 1.0 ⁷. Likewise, pressure-driven LC experiments involving very large (~ 0.5 mm), monodisperse particles have resulted in equally low values for h_{min} ⁸. Computational fluid dynamics studies reveal that unconfined bulk packing exhibit significantly lower reduced longitudinal plate heights than confined packings which show a great deal of heterogeneity across the column diameter⁹.

Maintaining a constant rate of bed formation during the packing process represents one attempt to preserve packed bed homogeneity, both radially and longitudinally¹⁰. It is common that, when pressure is first applied and flow resistance is low, the initial portion of the packed bed forms quickly. This rapidly formed region typically exhibits a packing structure which is less dense than the subsequently formed segments of the bed. On the length scales common to commercially available columns (5 – 25 cm), longitudinal heterogeneities are of only minor concern¹¹. As longer columns are packed, however, changes in axial packing density may have greater affect on column efficiency.

Other experimental parameters found to affect bed density and A-term broadening include particle dispersity, with narrower size distributions tending to form less densely packed beds, and the speed with which particles are packed. Particles with high kinetic energies, typical in experiments utilizing low viscosity unbalanced slurries, will strike and displace particles already situated within the packed bed, thus leading to denser packing¹².

Packing density also affects B-term broadening inasmuch as variations in interstitial spaces affect longitudinal analyte diffusion. Lower packing densities imply larger interparticle mobile phase volumes and larger B-terms than would be expected in densely packed columns. C-terms are also somewhat affected by changes in density, although the correlation is a bit weaker as they depend primarily upon the analyte's diffusion coefficient and size of the packing material. An increase in packing density, however, reduces the distance between particles, thereby leading to faster mass transfer in the mobile phase and lower resistance to mass transfer³. Another study found that an increased packing density leads to a sharp increase in the C_M -term due to increased retention¹³.

2.1.3 Experimental Packing Conditions for Producing Desired Bed Morphologies

Even while considering the theoretical advantages and disadvantages of particular packed bed morphologies, it is still difficult to extrapolate back to a set of experimental conditions that will produce the desired characteristics. For example, how can radial homogeneity be maintained while addressing the realities of particle polydispersity and the wall effects described above, and what conditions will result in appropriate packed bed densities? Experimental conditions will be highly dependent upon the physiochemical properties of the particles, including surface chemistries and particle size. It is generally accepted that satisfactory packing results with particles $\geq 3 \mu\text{m}$ are relatively easy to achieve, but as smaller particles are used, surface chemistries presumably become increasingly important due to the surface area to volume relationship². Slurry solvent selection may, in turn, be largely affected based solely on particle size independent of functionality. From a commercial standpoint, the problem is compounded as seemingly slight variations on a particle batch-to-batch level may result in the need to tune packing conditions in effort to maintain reliable and stable packings.

Slurry solvent selection is generally made based on two criteria: (1) low viscosity in order to achieve high kinetic-energy packing and (2) that it “energy-matches” with the particles so that aggregation does not occur. For example, highly polar unmodified silica or particles functionalized with polar ligands should be slurried in some high surface energy, polar solvent, such as methanol. Modified particles, such as octadecylsilane-functionalized silica, should be slurried in lower surface energy, less polar solvents, such as tetrahydrofuran, methyl-tert-butyl ether, or mixtures of acetonitrile-chloroform, chloroform-methanol, or chloroform-acetone. The choice of slurry solvent to minimize particle-particle aggregation is thought to be especially important in packing standard-bore columns with inner diameters of

1 mm or greater¹. Ideal solvent choice when packing in capillaries is less understood with several contradictions cited in the available literature¹⁴.

The simplest method for determining the suitability of a solvent for packing a particular batch of particles consists of observing the slurry under an optical microscope. If the particles tend to aggregate, the solvent is considered an unlikely candidate for successful packing. However, even if particles are well dispersed, this is not conclusive evidence that the resultant column will be satisfactorily efficient and/or stable¹⁵.

The most common method for determining the extent of particle aggregation in a given solvent is measuring particle sedimentation rate¹⁶. The measured rate is compared to the theoretical rate (v_s) of single, well-dispersed particles of a given d_p .

$$v_s = \frac{(1 - \phi_p)^{-K_2} d_p^2 [\rho_{skel}(1 - \varepsilon_p) + \rho_l(\varepsilon_p - 1)]g}{18\eta} \quad (2-1)$$

where ϕ_p is the volume fraction of the particles, K_2 is a particle-solvent dependent constant, ε_p is the particle porosity, ε_f is the amount of pores filled with solvent, ρ_{skel} is the density of the particle skeleton, ρ_l is the solvent density, and g is the gravitational constant. Equation 2-1 can also be used to determine the effective particle diameter from a measured sedimentation rate. The effective diameter can then be used to assess the degree to which the particles tend to aggregate. The biggest drawback of the two methods for determining particle aggregation described here is that neither predict particle-solvent behavior under the high-pressure conditions used during packing experiments.

Another slurry parameter, particle concentration, may play an important role in the ability to pack reproducible, efficient, and stable columns. Literature suggests particle concentrations ranging between 7 and 40% (w/w%), but the best experimental conditions

will be heavily dependent upon particle functionality and size¹⁵. It is suggested that the best columns are produced when packing is fastest¹⁰. Any role that slurry concentration plays beyond facilitating fast packing is largely unexplored.

Relative particle size distribution (PSD) has also been identified as a potential determinant of successful column packing. Numerous studies, both experimental and theoretical, have been carried out in effort to determine the effects of large versus small PSDs. In a study involving 5 and 3 μm particles, Gritti et. al. concluded that the width of the PSD of a packing material has no significant effect on column efficiency in an RSD range between 15% and 40%¹⁷. The absolute particle size, however, has great effect on the quality of the packing. Smaller particles tend to pack less homogeneously than large particles, thereby increasing the contribution of eddy diffusion to chromatographic band broadening. Similar conclusion were reached in a study involving deliberately broadened PSDs where 3 or 5 μm particles were added in various wt/wt% to 1.9 μm particles. The mixed particle batches showed evidence of increased flow resistance due to the tendency for small particles to settle in the flow-through pores of larger particles, resulting in external porosities as low as 32%¹⁸. Intuitively, it might be expected that tighter PSDs would result in lower A- terms, a rationale often invoked when explaining the improved performance of sub-3 μm core-shell particles with RSDs \sim 5% over fully porous particles with much larger RSDs. An alternative explanation for the lower reduced plate heights of these particles involves the roughness of the external surface of these particles. This roughness locks particles into place during the packing process, thus keeping local external porosities across the column diameter essentially uniform¹⁹. Certain approaches have been taken to mitigate the reduced efficiencies which result from flow heterogeneities that are present within chromatographic packed beds without

attempting to eliminate these heterogeneities during the bed consolidation process. This was done by fitting the column outlet with ports designed to effectively segment the parallel flow profiles eluting from the column, and to sample only the center port²⁰.

In a 2006 review, Kirkland and Destefano compiled a list of experimental guidelines for successful column packing¹⁵. For achieving high efficiency and stable packing, it is suggested that during the packing process, (1) the particles should have a sufficiently narrow size distribution, (2) the column tubing should have a mirror-finish to minimize wall effects and fine formation, (3) packing pressure should be as high as possible, and (4) the slurry solvent should disperse the particle well. With respect to maintaining column stability after packing, it is suggested that it is important to close the packed bed quickly (i.e. set the inlet frit) to prevent the column from relieving bed compression. A number of these suggestions have become the subject of experimental and theoretical studies, and many are explored in the course of the present work with sub-2 μm particles.

2.2 Experimental

2.2.1 Chemicals

For the purposes of slurry packing and isocratic characterization of columns, HPLC grade acetone and HPLC grade acetonitrile were used as received from Fisher Scientific (Waltham, MA). Deionized water was obtained from a Nanopure ultrapure water system (Barnstead International, Dubuque, IA). Trifluoroacetic acid and formamide were used as received from Sigma Aldrich Chemical Company (Milwaukee, WI), and potassium silicate (Kasil) was obtained from PQ Corporation (Valley Forge, IA). The isocratic test mixture used to evaluate column performance contained L-ascorbic acid (Fisher Scientific), 1,4-dihydroxybenzene (hydroquinone), 1,3-dihydroxybenzene (resorcinol), 1,2-

dihydroxybenzene (catechol), and 4-methylcatechol from Sigma Chemical Company (St. Louis, MO).

2.2.2 General Capillary Column Packing Procedure

The general procedure for packing microcapillary columns has been expounded previously and will be outlined here in brief²¹. Any departures from this procedure and more specific experimental conditions will be noted in the appropriate sections. All columns were fused silica capillary tubes (Polymicro Technologies, Inc., Phoenix, AZ) with 360 μm outer diameters. Outlet frits were prepared by tapping 1 -2 mm of 2.56 μm nonporous silica particles (Bangs Laboratories, Fishers, IN) into the end of the capillary. The plug of particles was then sintered into place using an electric arc device to create a frit against which the packing material would accumulate.

The particles to be packed were suspended in a specified solvent and sonicated for approximately 10 minutes using a Cole Parmer Ultrasonic Cleaner 8891 (Vernon Hill, IL). Approximately 1 mL of slurry was transferred to the reservoir within a stainless steel packing bomb placed atop a stir plate. A stir bar at the bottom of the slurry reservoir acted to prevent particles from settling during the packing process. The fritted capillary, held by a UHPLC compression fitting, was inserted into the reservoir and secured. A 300:1 pneumatic amplifier pump, with a pressure maximum 50,000 psi (Haskel International Inc., Burbank, CA) was used to pump HPLC grade solvent (typically acetone) into the bomb and force the slurry through the capillary. Packing was initiated at approximately 100 psi and gradually increased to 30,000 psi at a rate of 6000 psi/cm of packed bed. Bed formation was monitored under an oil immersion microscope at 1000x until maximum pressure was reached. Once the desired column length had packed, gas pressure to the pneumatic pump was released. An

ultra-high pressure valve situated between the pump outlet and the packing bomb was slowly opened to release liquid pressure while care was taken not to disturb the packed bed, which was being monitored under magnification.

The capillary was removed from the packing bomb and transferred to a UHPLC injector to be flushed with 50/50 acetonitrile/water and 0.1% trifluoroacetic acid (TFA) at 50,000 psi. The pump pressure was bled off and the re-pressurized to 10,000 psi. A temporary inlet frit was set by heating the column a few centimeters from the end of the bed with a heated wire stripper (Teledyne Interconnect Devices, San Diego, CA). The liquid pressure was slowly released by opening the injector valve without disturbing the packed bed. The column was subsequently clipped to the final desired length and a permanent inlet frit set by pressing the exposed inlet end of the column onto a glass microfiber filter (Reeve Angel, Clifton, NJ) wetted with 1/1 vol/vol of Kasil and formamide. The frit was dried by placing the inlet end of the column several millimeters from the electrodes in the electrical arcing device, and gently arcing until a 0.5 mm portion of the polyimide coating was removed. This last step was taken to ensure that the polyimide would not swell over the capillary inlet and cause broadening effects when injections were made during isocratic performance characterization.

2.2.3 Column Evaluation

The experimental details of performing isocratic evaluation at UHPLC pressures have been described previously²¹. A single-stage pneumatic amplifier is used to pressurize the inlet of a triple-stage pump capable of generating pressures up to 75,000 psi. A UHPLC injector with the capillary column housed in a compression fitting attached is connected to the outlet of the triple-stage pump. Sample injections are performed by filling the central

port of the injector with the five-component isocratic test mixture ($\sim 200 \mu\text{M}$) and applying approximately 1,500 psi with the single-stage pump for ~ 1 s. The excess sample is flushed to waste before applying the column operating pressure with the triple-stage pump.

For amperometric detection, a $\sim 300 \mu\text{m}$ long carbon fiber microelectrode is inserted into the end of the packed capillary and held at +1.1 V vs. an Ag/AgCl reference electrode. The oxidation current of the eluting analytes is amplified and converted to a voltage with a SR750 current amplifier (Stanford Research Systems, Sunnyvale, CA) with a 3 dB low pass bandwidth filter at 15 Hz. The signal is digitized and data is acquired at 21 Hz using a LabView 6.0 program (National Instruments, Austin, TX). The chromatograms are digitally filtered to remove high-frequency noise and background subtracted to account for baseline drift. Theoretical plates (Equation 1-10) and retention times are determined for each peak using an iterative statistical moments algorithm in Igor Pro (Wavemetrics, Inc., Lake Oswego, OR). The second central moment (σ^2) is determined from data ± 3 standard deviations from the first moment (t_R). The average capacity factors, k' , a function of the differential pressure as analytes migrate the length of the column, are determined from the chromatograms using the following equation

$$k' = \frac{t_R - t_m}{t_m} \quad (2-2)$$

2.2.4 Segmented Column Performance

Inconsistent performance from columns packed in excess of 100 cm (to be discussed in Chapter 4) prompted investigations into the reasons for the diminished efficiencies of long columns. Axial heterogeneity was the suspected cause, and the degree of variation throughout the length of the column was assessed. 100 cm x 50 μm ID columns were packed with 1.9 μm C18 BEH particles slurried in acetone at a concentration of approximately 10

mg/mL. Columns were characterized under isocratic elution conditions in 50/50 acetonitrile/water and 0.1% TFA. The 100 cm columns were then bisected and refritted at the appropriate ends using the Kasil fritting technique described in the previous section. Each segment was characterized before subsequently bisecting each half again. In total, two 100 cm columns were packed, and four consecutive ~ 25 cm segments from each column were assessed. Column segments are labeled as '1', '2', '3', and '4' according to the direction of flow during packing. Segment '1' is the inlet end of the original 100 cm column and the last packed portion. Segment '4' is the outlet end of the original column; it packed first and most quickly.

Figure 2-1 shows the overlaid van Deemter curves for the inlet and outlet halves along with the h vs. v data points of the intact 100 cm column for each test analyte considered in isolation. As shown, the outlet half of the column outperformed the inlet half, and the intact 100 cm column data lies between the two extremes in the C-term region. The inlet was bisected into segments '1' and '2'; the outlet was bisected into segments '3' and '4'. The overlaid performance curves of these four segments are shown in Figure 2-2. A very clear trend is observed for segments '1', '2', and '3', with both h_{\min} and C-terms steadily decreasing. Segment '4', however, while having the lowest h_{\min} , exhibits a moderately higher C-term, and the van Deemter curve crosses over segment '3' in the high velocity region.

Packing density of each segment was assessed via two criteria: (1) the resistance to flow of each segment, which relates the operating pressure normalized to column length to the mobile phase velocity as determined by the elution time of L-ascorbic acid and (2) the relative retention factors of the test analytes. Figure 2-3 shows that resistance to flow is

higher in the latter packed regions of the column. Figure 2-4 shows the pressure-dependent retention data for each of the test analytes in isolation for all four segments. Once again, a clear trend is followed by segments '1', '2', and '3', with each of the curves running in parallel along the entire length of the utilized operating pressures. Segment '1' exhibits the highest retention, suggesting it to be the most densely packed of all four segments, and segment '3' is the least retentive and least densely packed. Again, segment '4' deviates from the well-behaved trend established by the latter packed segments, and the pressure dependent retentions associated with this first and most quickly packed portion of the column traverse the region between segments '2' and '3'.

The results from this experiment were corroborated. A second 100 cm column was characterized and segmented in the same manner described above. Figures 2-5, 2-6, and 2-7 show the overlaid performance curves, resistance to flow data, and retention data, respectively for the four segments. All trends are similar with the noted exception that column '4' is distinctly poorer performing than column '3'.

A previous study by Wong et. al. looking at the axial heterogeneity of downward slurry-packed columns reported on both performance and density trends¹¹. In that study, 5 cm x 4.6 mm columns were packed with 10 μ m silica particles in series to total lengths ranging between 5 and 30 cm. Column segments were assessed individually to obtain performance data, and the mass of packing material contained in each column was reported as a descriptor of bed density. For total column lengths greater than 20 cm, the 5 cm inlet (last packed) and outlet (first packed) columns were consistently the worst performing. The best performing column was typically the second column in the series followed in turn by each subsequently packed section. In determining the relative densities of the packed beds

for the series-connected columns, it was found that the outlet column (first packed) contained the most packing material by mass. Each subsequently packed column contained less material than the previous.

In explaining the results with regard to the outlet column, it was concluded that its relatively high density made perfectly intuitive sense. When packing is initiated, the velocity and momentum of the particles striking the outlet frit is the greatest of any particles impinging on the bed, thereby leading to this section having the highest packing density. It would be expected that this section would also perform the best given that a higher packing density implies less void volume between the particles and more uniform flow profiles. The authors explain the poor performance as an effect of the first few pumping strokes during the packing process which result in 135 – 200 bar pressure changes in the packed bed with each stroke. While the packed bed is still relatively short and unconsolidated, each stroke results in a series of expansions and compressions which act to create voids at the outlet as the particles cannot sufficiently reorganize with the bed building rapidly from behind. The relatively low momentum of the particles striking the packed bed at the inlet end as the length increases explains the low density. The poor performance of the last packed column is explained as a channeling effect which occurs as solvent impinges on the head of the column without the presence of a flow distributor.

The results of our segmented column study are similar to those reported by Wong et. al. inasmuch as column performance deteriorated in subsequently packed sections. Our findings also indicate that the outlet portion of the column did not follow the trend established by subsequent sections of the column, but performance was relatively good, especially with respect to segments '1' and '2'. The most probable explicator of this

deviation from the previously reported results is that the segments in our study were ~ 25 cm rather than 5 cm, suggesting that the indictable contributor to poorer-than-expected performance exists within a fairly short stretch at the immediate outlet of the column. In our procedure, packing was initiated at ~ 100 psi and gradually increased to 30,000 psi within 10 cm of packing. Attempts to determine the performance effects of this portion of packing at the outlet end will be discussed in section 3.2.4.

The most notable distinction between our results and those from the previous study is the inversion of the determined axial bed density. Our findings indicate that the latter, more slowly packed stretches of column are denser than even the first segment. This was somewhat counterintuitive, as it was expected that the first packed region, which is brought to the maximum packing pressure of 30,000 psi after just 10 cm of packing, would be the most compressed portion of the packed bed. In explaining this phenomenon, it is thought that the speed of packing at a given axial position plays a significant role. When packing is initiated, particles accelerate quickly toward the outlet frit and the bed builds at a rapid rate. At relatively fast rates of bed formation, individual particles impinging on the head of the column do not have sufficient time to reorganize themselves before being impinged upon by subsequent particles. This effect locks particles into place by not allowing them to resituate into larger void regions, thus creating a bed which is compressed by the relatively large pressure drop, but less resistive to flow due to interparticle voids left during rapid bed formation. As hydraulic resistance increases with the length of the packed bed, the slurry solvent flow rate slows dramatically, and individual particles impinging upon the head of the column have sufficient time to resituate into void regions before subsequent particles strike

and lock it into place. It is this effect which is believed responsible for the higher resistance to flow in latter packed segments of long columns.

2.2.5 Column Outlet Effect

The outlet segment in the experiment described in Section 2.2.4 did not follow the well established trends for performance or retentivity established by the subsequently packed three segments. Likewise, the Wong et. al. study noted poor performance from the first 5 cm segment in a series of columns packed to various total lengths. They attributed this phenomenon to pressure fluctuations during cycling of the pump which led to a series expansions and compressions of the packing before adequate bed consolidation could occur. In our case, working with microcapillary columns with inherently low flow rates and pneumatic pumps with relatively large volumes, no such pump cycling occurred. We therefore endeavored to track the root of the poor-than-anticipated performance of the outlet portion of the column.

In the typical procedure, packing pressure is increased at an approximate rate of 3000 psi/cm until the maximum 30,000 psi is reached when the packed bed is 10 cm long. Monitoring the process under 1000x magnification, it was observed that increasing the pressure resulted in several hundred micron compressions of the bed. To assess whether these discreet, successive compressions were in some way responsible for the performance deviations, a 50 cm x 50 μ m ID column was packed with 1.9 μ m BEH. Particles were slurried in acetone at \sim 3 mg/mL. Packing was initiated at \sim 100 psi and quickly brought to 30,000 psi after the bed had packed 1 cm. The column was isocratically characterized. Subsequently, 3 cm of column length was clipped from the outlet end, the column was

refritted using the Kasil technique, and again characterized. This procedure was repeated five times. In sum, column lengths of 50, 47, 44, 41, 37, and 33 cm were considered.

Figure 2-8 shows the reduced van Deemter curves of all six column lengths for each of the four retained test analytes considered in isolation. A subtle, yet interesting, trend can be noted with regard to this data. Clipping the initial 3 cm of column at the outlet end resulted in markedly improved performance. The most significant differences are in the C-terms, with nearly 10% improvements for the majority of analytes. The differences in A-terms are not as easily interpreted, as greater error exists in their determined values. As additional segments are clipped from the outlet, the performance steadily deteriorates. Resistance to flow changes for the different column lengths were not significant and did not allow for interpretation to be made.

The experiment was repeated, keeping all experimental conditions the same except for slurry concentration, which was raised to ~ 50 mg/mL. The reason for this change will be discussed at length in Section 2.2.6, but it suffices for now to say that better column performance has been consistently observed using higher slurry concentrations. A 49 cm x 50 μ m column was packed and subsequently clipped to lengths of 45, 41, 37, 33, and 28 cm.

Figure 2-9 shows the overlaid van Deemter curves. The performance of these columns was superior to those packed with the lower slurry concentration, and the column-to-column variation in the van Deemter coefficients is subtle. It is therefore difficult to trace the origin of performance deviations to any particular band broadening term. Considering column performance in general, however, the same trend is observed. Clipping the initial outlet segment improved performance relative to the original column. Subsequent clippings

resulted in consistent deterioration of performance. Once again, changes in resistance to flow from column-to-column are insignificant and not interpretable.

The findings of this experiment are in logical agreement with both the previously reported study by Wong et. al. and our results from the segmented column study described in Section 2.2.4. A very short segment at the column outlet, formed rapidly during initial bed consolidation seems to have slight deleterious effects on overall column performance. The inductible length appears to be < 5 cm. The effect also appears to be unrelated to differential compression of the bed as pumping pressure is increased in discrete intervals since maximum packing pressure was reached after just 1 cm of packing in the current experiment. A definitive conclusion remains elusive, however, as we are unable to probe the subtle interplay of eddy dispersion and resistance to mass transfer. It is possible that this early-formed portion of the bed experiences such a degree of axial and/or radial compression so as to affect performance until a cross-over point is reached where the effects of packing speed compensate those of density.

2.2.6 Slurry Concentration Effects

In noting the better performances and low flow resistances of the earliest packed portions of the segmented 100 cm columns (described in Section 2.2.4) and attributing these effects to the relatively fast packing rates of these segments, we sought a means of maintaining packing speed throughout the entire course of packing, with the ultimate aim of producing high-efficiency long columns in excess of 100 cm. One possible means to achieve this would be to maintain a high flow velocity by using low viscosity slurry solvents. In already using acetone as a slurry solvent ($\eta = 0.32$ cP at 20°C), few common solvents present themselves as viable alternatives. Another option would be to pack at elevated temperatures,

keeping the packed bed in a column heater to reduce solvent viscosity and flow resistance. Attempts at utilizing this last approach were made, but no notable improvements in column performance were observed.

The effect of increasing the concentration of the particle slurry used to pack microcapillary columns was investigated. In the past, this concentration was kept relatively low (≤ 5 mg/mL) in order to achieve slurries in which the particles were well dispersed. It had been intuited that large particle aggregates would lead to balky packing, which would ultimately result in void regions within the packed bed and deteriorated chromatographic performance. To determine the validity of this assumption, columns were packed with 5, 10, and 20 mg/mL slurries of 1.9 μm BEH particles in acetone. 50 μm ID capillaries were packed to approximately 55 cm, and prepared according to the procedure already noted. Figure 2-10 shows how bed length increased with respect to time throughout the packing process. Observing the process under magnification, packing was continuous in all instances, and it was noted that the beds were built up in the characteristic parabolic profiles as individual particles impinged upon the column head. The columns were characterized under isocratic conditions in 50/50 acetonitrile/water and 0.1% TFA. Figure 2-11 presents the overlaid van Deemter plots for each test analyte. The columns packed with the 5 and 10 mg/mL slurries performed almost identically in terms of respective h_{min} s and slopes in the C-term dominated region. The column packed with the 20 mg/mL slurry, however, outperformed them both according to these same criteria.

Even more concentrated slurries, 100 mg/mL of 1.9 μm BEH particles in acetone, were used to pack a pair of 50 μm ID columns. It was evident that particle-particle interactions were promoted, and large aggregates could be seen falling to the bottom of the

slurry vial only moments after removing it from the sonication bath. It was assumed that stirring of the slurry in the packing reservoir would negate this tendency, and nominal slurry concentration would be effectively preserved. Figure 2-12 illustrates the rapidity of packing with this concentration. Packing was far less smooth, although still continuous, when observed under magnification. Large aggregates could be seen entering the column blank at the inlet end of the capillary, and the packed bed was extended as these aggregates compressed onto the head of the forming column. As such, the typical parabolic profile of the packing was not observed. Figure 2-13 shows the overlaid van Deemter curves for these consecutively packed columns. Interestingly, the columns packed with these dense slurries performed very well and with excellent reproducibility; h_{\min} s were approximately 1.5 and uncorrected c-terms under 0.2. The performance results were somewhat counterintuitive, as it was apparent that particle aggregation was being promoted in the more concentrated slurries. This type of aggregation is traditionally advised against and avoided in column packing, especially for standard-bore analytical columns.

A collaborative study by the Jorgenson and Tallarek groups may provide a degree of insight into these results²². A series of columns with inner diameters ranging between 10 and 75 μm were packed with ~ 3 mg/mL slurries of 2.0 μm BEH particles in acetone and characterized. The chromatographic performances of these columns were then correlated to the morphological properties of the bed microstructures. Confocal laser scanning microscopy (CLSM) was used to visualize the packed beds, and computational reconstruction allowed for detailed analysis. Within the column set, two groups of packings were identified based upon the transcolumn porosity profiles. In general, poorer performing columns were noted to have looser packing along the wall regions and also exhibited a

greater extent of particle size segregation along the column radius. In this last instance, larger particles tended to occupy the central regions of the packed bed, and smaller particles tended toward the wall regions. The insights provided by this study may aid in explaining why slurry concentration affects ultimate chromatographic performance. Owing to the nature of the parabolic flow profile of the solvent in the capillary, the packed bed also forms at a faster rate in the center than at the walls. With lower slurry concentrations, particles are well dispersed and navigate the length of the column blank individually. We hypothesize that smaller particles can sample the slower flow profiles along the walls more effectively than can larger particles, thus leading to the size segregation of particles observed in the study described above. By using higher slurry concentrations, aggregation is promoted and particles are randomly associated in loose networks as they exit the packing reservoir and navigate the length of the capillary. As these aggregates impinge upon the head of the column, voids within the networks are compressed out, but radial homogeneity is preserved. In this way, wall effects in the bed microstructure are reduced and performance is improved.

For the sake of comparison, two ~ 25 cm columns were packed with high (100 mg/mL) and low (3 mg/mL) slurry concentrations. 75 μm ID capillaries were used so as to accentuate the potential extent of particle size segregation across the column diameter. Figure 2-14 shows the overlaid van Deemter curves of these two columns. The column packed with the 100 mg/mL slurry offers much better chromatographic performance, and the calculated van Deemter coefficients reveal significant differences in both the A- and C-terms. The improved A- term may reflect improved radial homogeneity for the reasons described above. The relative densities of the packed beds were assessed by both analyte retention (Figure 2-15) and resistance to flow (Figure 2-16). As was the case in the

segmented column experiment described in Section 2.2.4, the less densely packed column performs better. The reason for this difference in packing density may again relate to the speed of packing, where the denser slurry offers less time for particles to resituate into void regions at the head of the column before being impinged upon and locked into place. While a coherent picture of the effect of slurry concentration on chromatographic performance is emerging, the actual microstructure of the bed can only be elucidated microscopically.

CLSM data with respect to the observed trends will provide additional insight.

In addition to the potentially improved radial homogeneity of columns packed with concentrated slurries, the axial heterogeneity was also investigated. Once again, given the nature of the packing procedure, such longitudinal heterogeneity is inevitable because maximum packing pressure is reached quickly. Using the same technique described in Section 2.2.4, a 100 cm x 50 μ m ID column packed with a 100 mg/mL slurry of 1.9 μ m BEH particles in acetone was segmented into four \sim 25 cm segments. Once again, segments were designated '1', '2', '3', and '4', where '4' refers to the outlet portion which packed first, and '1' designates the inlet portion.

Figure 2-17 shows the van Deemter plots for each test analyte considered in isolation. The variation between column segments for this set is much narrower than for those derived from the 10 mg/mL slurries, shown in Figures 2-2 and 2-5. Reduced minimum plate heights range between 1.5 and 1.6 for all four segments, and c-terms for each analyte are generally within 10%. This testifies to a vast improvement in axial homogeneity. Figures 2-18 and 2-19 show the retentions of each column segment and their resistances to flow, respectively. While both assessments of column density are in agreement with each other, the associated trend is not as clear as in the case with the lower concentration slurry. The inlet segment '1',

the last and most slowly packed, was once again the most retentive and resistive to flow. Segments '2' and '3' packed faster and are less dense, which is consistent with the interpretations given on this point thus far. The outlet, segment '4', is once again anomalous amidst the established trend, and is the second densest of the segments. This fact is not easily explained, and it may again suggest a crossover point between the interplay of packing speed and the differential pressure drop across a given length of bed during the packing process. Stated another way, the outlet portion of the bed packs most quickly, making particle resituation and bed reorganization more unlikely. In itself, this should lead to a less dense bed. However, the maximum pressure of 30,000 psi is reached within the first 10 cm, thus axial compression is most extensive in this earliest portion of the packed bed. The resultant stresses of this large pressure drop may cause and accentuate the radial compression referred to in Section 2.1.2. This would in turn explain the consistently anomalous behavior of the column outlet performance and relative density.

2.2.7 The Effect of Packing and Flushing Pressure

As outlined in the general procedure in Section 2.2.2, maximum packing pressure is typically 30,000 psi. The bed is further consolidated by flushing in mobile phase at 50,000 psi before the inlet frit is placed. In general, it is recommended that columns should be packed at pressures 40% in excess of their routine operating pressures¹. After noting the trends in the data from Sections 2.2.4 and 2.2.6 with regard to packing density and chromatographic performance, we investigated the relative influences of these two high pressure steps on column performance.

In order to assess the effects of column packing pressure and post-packing flushing pressure, four 75 μ m ID columns were packed to approximately 30 cm each with 100 mg/mL

slurries of 1.9 μm BEH particles in acetone. One column was packed at a maximum pressure of 30,000 psi and subsequently flushed with mobile phase at 46,000 psi prior to setting the temporary inlet frit (30/46); a second column was packed at 30,000 psi and flushed at 23,000 psi (30/23); a third was packed at a maximum pressure of 10,000 psi and flushed at 46,000 psi (10/46); the final column of the series was packed at 10,000 psi and flushed at 23,000 psi (10/23). Efforts were made to avoid bed expansion during depressurization after the packing step by slowly releasing the pressure and monitoring the bed under magnification. In this way, it was hoped that bed morphology resulting from packing at 30,000 psi would be preserved even when flushing later at a lower maximum pressure of only 23,000 psi. All columns were characterized under isocratic elution conditions in 50/50 acetonitrile/water and 0.1% TFA. Maximum operating pressure did not exceed 25,000 psi during characterization. Column performance was assessed by the calculated van Deemter coefficients, and column permeability was compared by analyte retention and resistance to flow. Columns 10/23 and 10/46 were characterized again in 20/80 acetonitrile/water and 0.1% TFA to assess the effect of k' on the C-term. Trends were observed, and the experiment was repeated with a lower slurry concentration (~ 10 mg/mL). Only two columns were assessed: one packed at 30,000 psi and flushed at 46,000 psi (30/46[2]), and a second packed at 10,000 psi and flushed at 23,000 psi (10/23[2]). Again, maximum operating pressure did not exceed 25,000 psi during column characterization.

The van Deemter curves for all four columns packed with the 100 mg/mL slurry are overlaid for each analyte in Figure 2-20. The 10/23 performed best for all analytes with the most significant improvement being observed in the C- term region. The plot of retention factors versus operating pressures (Figure 2-21) and the resistance to flow plot (Figure 2-22)

reveal the same trend: the 10/23 column is the least densely packed, and the 30/46 column exhibits the highest packing density.

The trends carry over to the two columns packed at lower slurry concentration (~10 mg/mL). The 10/23[2] column outperforms the 30/46[2] column, as shown in Figure 2-23. Again, the most significant improvement is observed in the C-term region of the curves as the h_{\min} s are virtually identical. 10/23[2] is also less densely packed as attested by both the retention data (Figure 2-24) and resistance to flow data (Figure 2-25).

It is somewhat difficult to deconvolute the effects due to packing pressure from those due to flushing pressure, but an attempt can be made by simply noting the maximum pressures experienced by the columns in either step. The relative efficiencies of the two columns packed at 10,000 psi are sufficiently different to attribute the observed performance variation to the bed compression which occurs during the mobile phase flush. Visual observation revealed that the aforementioned bed compression was much greater in the 46,000 psi flush compared to the 23,000 psi flush, resulting in what might presumably be a slight decrease in interparticle porosity and a corresponding increase in k' due to increased bed density. Such a change could result in larger H_{CM} and H_{CS} contributions to chromatographic band broadening¹³. This is consistent with the observed data, as pronounced increases in these terms are expected with even small changes in k' values for low retention factors (< 0.5), where a sharp increase in C-term contributions at low retentions is followed by a leveling off at higher values of k' . By re-characterizing columns 10/23 and 10/46 in 20/80 acetonitrile/water it would be possible to probe the C- term dependence on k' . Additionally, at higher retentions slight changes in k' (< 0.05 units) between columns in this set would be unlikely to cause significant differences in the C-term. Unfortunately, after

switching to more a more aqueous mobile phase composition, early eluting peaks on column 10/23 exhibited a large degree of tailing, and subsequent examination of the packed bed revealed that gaps had formed, even as both the inlet and outlet frits remained intact. Column 10/46 exhibited no such bed collapse upon switching mobile phase compositions. This increased bed stability is likely attributable to the degree of bed compression afforded by flushing at higher pressure.

The performances of columns 30/23 and 30/46 are not sufficiently different to merit meaningful comparison to each other. If, however, they are considered together to reveal a third, moderately performing set lying between the extremes of the 10/23 and 10/46 columns, it may be possible to speculate the reason. Because both 30/23 and 30/46 experienced pressures in excess of anything experienced by 10/23, their deteriorated performances may be explained by the same reason invoked above. That is, the slightly higher packing densities of these columns resulted in higher H_{CM} and H_{CS} contributions. It still remains, though, to explain why these two columns performed better than 10/46, which experienced pressures as high or higher over the course of column preparation. In this instance, it may possibly be explained by pressure-dependent aggregation effects of the slurried particles during packing.

As will be discussed more extensively in Chapter 3, a certain degree of pressure-dependent aggregation is hypothesized based on observations of balky packing when using higher slurry concentrations and capillaries with very small IDs ($< 20 \mu\text{m}$). In the present case utilizing relatively large $75 \mu\text{m}$ ID capillaries, packing was continuous with either 10,000 psi or 30,000 psi packing pressures, but the size of particle aggregates is still assumed to be larger under higher pressures. For this reason, columns 30/23 and 30/46 may have had

better radial homogeneity than columns packed at 10 kpsi, thus leading to their improved performance with respect to 10/46.

2.2.8 Effect of Slurry Solvent

The observations discussed in Section 2.2.6 led us to speculate that improved radial homogeneity was one of the contributing factors to the improved chromatographic performance of columns packed with higher slurry concentrations. It is hypothesized that aggregates prevent particle size segregation from occurring as the length of the column blank is navigated from the packing bomb to the head of the packed bed. From this perspective, slurry solvent effects were investigated with respect to the degree of particle aggregation promoted. Methanol was singled out as the primary alternative to acetone for these studies. Its viscosity is relatively low (0.59 cP at 20°C) which allows for adequate flow velocity to be maintained throughout the packing process, and, compared to acetone, it promotes aggregation of BEH C18-functionalized particles.

A set of ~ 30 cm x 50 μ m ID columns was packed with slurry concentrations of 3, 10, 50, and 100 mg/mL of 1.9 μ m BEH particles in methanol. Isocratic performance in 50/50 acetonitrile/water and 0.1% TFA was compared in terms of calculated van Deemter coefficients. Figure 2-26 shows the overlaid van Deemter curves for each retained test analytes considered in isolation. Comparing the columns prepared with low (3 and 10 mg/mL) slurry concentrations to those prepared with high (50 and 100 mg/mL) slurry concentrations, there is clear difference in the calculated A-terms. The lower eddy-dispersion terms with high concentration slurries are consistent with the proposed mechanism of preserved radial homogeneity with higher concentrations. Also, it is noteworthy that there is a definite increase in the B-term with increasing slurry concentration.

It was clear that none of the columns offered performance as good as typical columns prepared with acetone as a slurry solvent. Also, it was inconclusive as to whether chromatographic performance was actually improved in moving to higher slurry concentrations with methanol as the slurry solvent. It was also noted that packing became balkier at 100 mg/mL, necessitating pressure release and reapplication to reinitiate packing. Additionally, methanol's viscosity is roughly twice that of acetone, so it was expected to take approximately twice as long to pack a given length of column. However, it took nearly 10x as long. These observations suggest that aggregates were becoming large enough at this nominal concentration so as to preclude entrance into the column blank inside the packing bomb. The balance between column inner diameter and slurry concentration (with resultant aggregate size) was investigated by looking at 75 and 150 μm ID columns packed with slurry concentrations of 50 and 100 mg/mL in methanol.

Figures 2-27 and 2-28 show the performances of $\sim 30\text{ cm} \times 75\text{ }\mu\text{m}$ ID columns packed with slurry concentrations of 50 and 100 mg/mL in methanol, respectively. The column packed at 50 mg/mL has h_{min} s and C-terms on par with similarly dimensioned columns packed in acetone at 100 mg/mL (see Figure 2-13). Increasing the slurry concentration to 100 mg/mL, however, resulted in slightly deteriorated performance with trends similar to those discussed above for the 50 μm ID columns. Once again, this is suggestive of an aggregate size/column inner diameter relationship.

It has been observed in our lab that both A- and C- terms increase with column inner diameter, and chromatographic performance suffers. Figures 2-29 shows the performance of a 23 cm x 150 μm ID column packed with a 100 mg/mL slurry in methanol. Figure 2-30 shows the performance of a 28 cm x 150 μm ID column packed with a 100 mg/mL slurry in

acetone. The performances of these columns are exceptional in comparison to results of larger ID columns packed with low slurry concentrations in the past²³. The uncorrected C-terms of the column packed in methanol (< 0.20) are amongst the best observed for these particles regardless of inner diameter.

2.3 Conclusions

Efforts have been made to demystify the capillary column packing process by investigating the effects of pressure, slurry concentration, and slurry solvent both individually and in concert. The investigation was sparked by the aim to pack high efficiency long microcapillary columns in excess of 100 cm, and working with columns of these lengths helped to reveal some subtle details that might have gone unobserved on smaller scales.

Our findings suggest an interesting interplay between packing speed and packing pressure, especially in the earliest packed portions of the column, which result in a short stretch of packed bed at the outlet which causes anomalous behavior amidst established performance and density trends. The large pressure drop across this relatively short column length in this region causes bed compression and stresses which have negative effects on subsequent chromatography. These conclusions are consistent with data from segmented long columns and from a series of shorter columns packed and flushed at different pressures. It seems likely that the pressure ramping profile during the packing process can be changed to reduce such effects. While large pressure drops may deteriorate chromatographic performance to slight degree, there is also evidence that the additional bed consolidation that occurs with higher pressures can stabilize the bed and prevent the formation of gaps when switching mobile phases.

Our findings with respect to improved chromatographic performance when using high particle slurry concentrations during the packing process may be related to both the packing speed afforded by this approach as well as to the prevention of particle size segregation across the diameter of the column. Fast packing does not allow adequate time for the resituation of individual particles into larger void regions at the head of the column. This leads to columns which are less resistant to flow, which is consistent with the earliest packed segments of long columns and columns packed with more concentrated slurries. The preservation of radial homogeneity is hypothesized to result from the random aggregation of particles in the packing bomb and the axial navigation of those aggregates through the column blank. Once the head of the column is reached, very large voids in the loose particle networks are compressed away, but randomness is preserved. This effect works to reduce the eddy dispersion contribution to chromatographic band broadening and is consistent with the observed reductions in A-terms for columns packed with concentrated slurries. Finally, the effect of particle aggregation resulting from slurry solvent was investigated. It was found that a balance between the aggregate size and column inner diameter exists. Columns can now be packed with excellent reproducibility across a large range of inner diameters with calculated van Deemter coefficients which are consistent with well-packed columns. Correlating the experimental conditions discussed in this chapter with the resultant bed morphologies via microscopic techniques may pave the way for further improvements.

2.4 References

- ¹ Snyder, L.R.; Kirkland, J.J.; Dolan, J. *Introduction to Modern Liquid Chromatography*. 3rd Ed., Wiley: New York, 2010.
- ² Shelly, D.C.; Edkins, T.J. *Journal of Chromatography* **1987**, 411, 185.
- ³ Hsieh, S.; Jorgenson, J.W. *Analytical Chemistry* **1996**, 68, 1212-1217.
- ⁴ Guiochon, G.; Drumm, E.; Cherrak, D. *Journal of Chromatography A* **1999**, 835, 41
- ⁵ Bruns, S.; Tallarek, U. *Journal of Chromatography A* **2011**, 1218, 1849-1860.
- ⁶ Giddings, J.C. *Dynamics of Chromatography: Principles and Theory*, Marcel Dekker Inc., New York, 1965
- ⁷ Stol, R.; Poppe, H.; Kok, W.T. *Analytical Chemistry* **2001**, 73, 3332-3339.
- ⁸ Knox, J.H. *Journal of Chromatography A* **2002**, 960, 7-18.
- ⁹ Khirevich, S.; Höltzel, A.; Seidel-Morgenstern, A.; Tallarek, U. *Analytical Chemistry* **2009**, 81, 7057-7066
- ¹⁰ Shelly, D.C.; Antonucci, V.L.; Edkins, T.J.; Dalton, T.J. *Journal of Chromatography* **1989**, 458, 267-279.
- ¹¹ Wong, V.; Shalliker, A.; Guiochon, G. *Analytical Chemistry* **2004**, 76, 2601-2608.
- ¹² Angus, P.D.A.; Demarest, C.W.; Catalano, T.; Stobaugh, J.F. *Journal of Chromatography A* **2000**, 887, 347-365
- ¹³ Gluckman, J.C.; Hirose, A.; McGuffin, V.L.; Novotny, M. *Chromatographia* **1983**, 17, 303-309.
- ¹⁴ Vissers, J.P.C.; Hoeben, M.A.; Laven, J.; Claessens, H.A.; Cramers, C.A. *Journal of Chromatography A* **2000**, 883, 11-25
- ¹⁵ Kirkland, J.J.; DeStafano, J.J. *Journal of Chromatography A* **2006**, 1126, 50 – 57.
- ¹⁶ Vissers, J.P.C.; Claessens, H.A.; Laven, J.; Cramers, C.A. *Analytical Chemistry* **1995**, 67, 2103-2109
- ¹⁷ Gritti, F.; Farkas, T.; Heng, J.; Guiochon, G. *Journal of Chromatography A* **2011**, 1218, 8209-8221

- ¹⁸ Liekens, A.; Billen, J.; Sherant, R.; Ritchie, H.; Denayer, J.; Desmet, G. *Journal of Chromatography A* **2011**, 1218, 6654-6662.
- ¹⁹ Gritti, F.; Guiochon, G. *Chemical Engineering Science* **2011**, 66, 3773-3782.
- ²⁰ Camenzuli, M.; Ritchie, H.J.; Ladine, J.R. Shalliker, R.A. *Journal of Chromatography A* **2012**, 1232, 47-51
- ²¹ MacNair, J.E.; Patel, K.D.; Jorgenson, J.W. *Analytical Chemistry* **1999**, 700 – 708.
- ²² Bruns, S.; Grinias, J.P.; Blue, L.E.; Jorgenson, J.W.; Tallarek, U. *Analytical Chemistry* **2012**, 84, 4496-4503.
- ²³ Jerkovich, A.D. *UNC Doctoral Dissertation* **2003**.

2.5 Figures

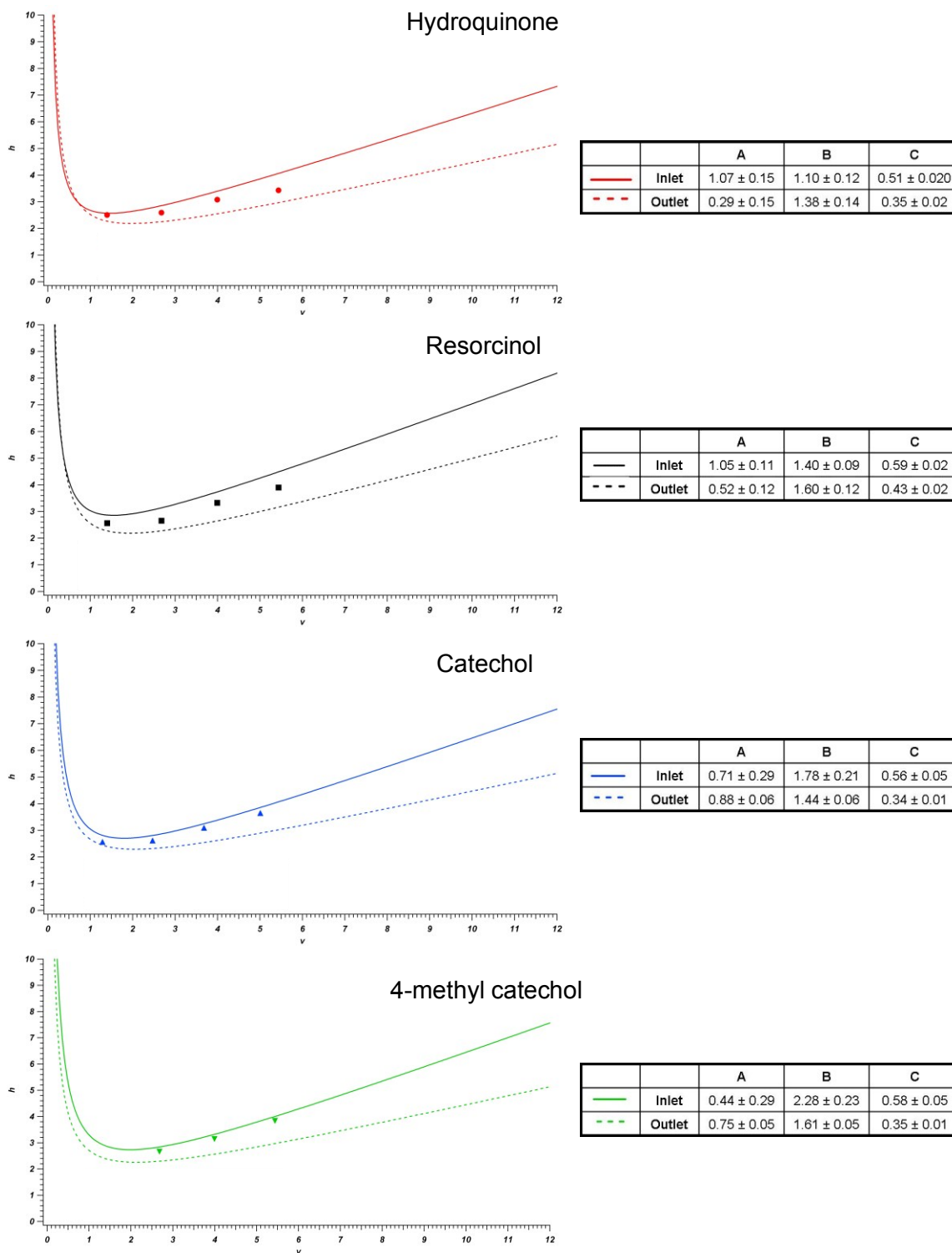


Figure 2-1: van Deemter curves of inlet and outlet halves of a bisected 100 cm x 50 μ m ID column packed with ~ 10 mg/mL slurry of 1.9 μ m BEH particles in acetone. Data points are for the intact 100 cm column.

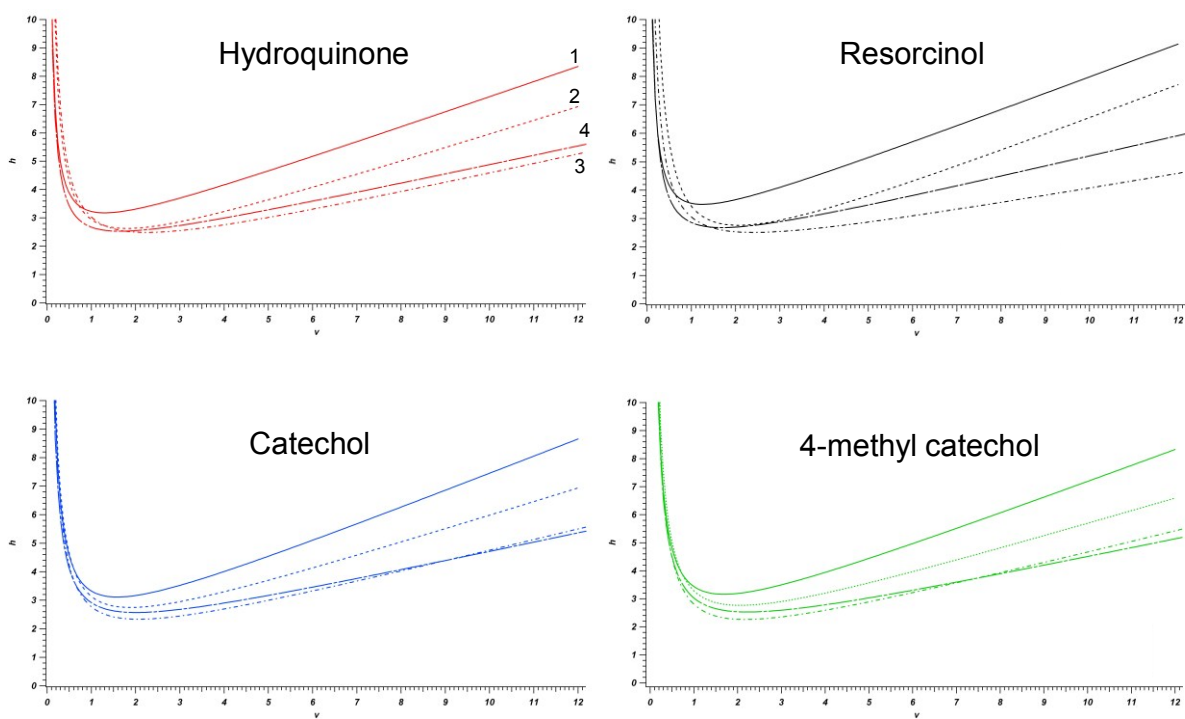


Figure 2-2: Overlaid van Deemter curves for all four ~ 25 cm segments of an originally 100 cm x 50 μm ID column packed with ~ 10 mg/mL slurry of 1.9 μm BEH particles in acetone.

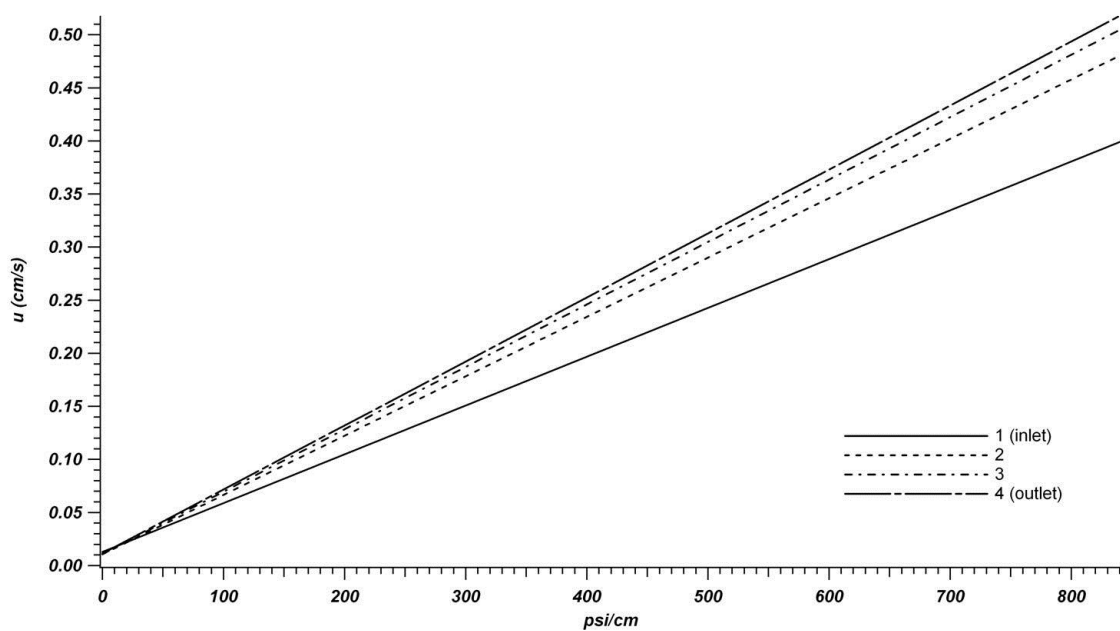


Figure 2-3: Resistance to flow data for all four ~ 25 cm segments of an originally 100 cm x 50 μm ID column packed with ~ 10 mg/mL slurry of 1.9 μm BEH particles in acetone.

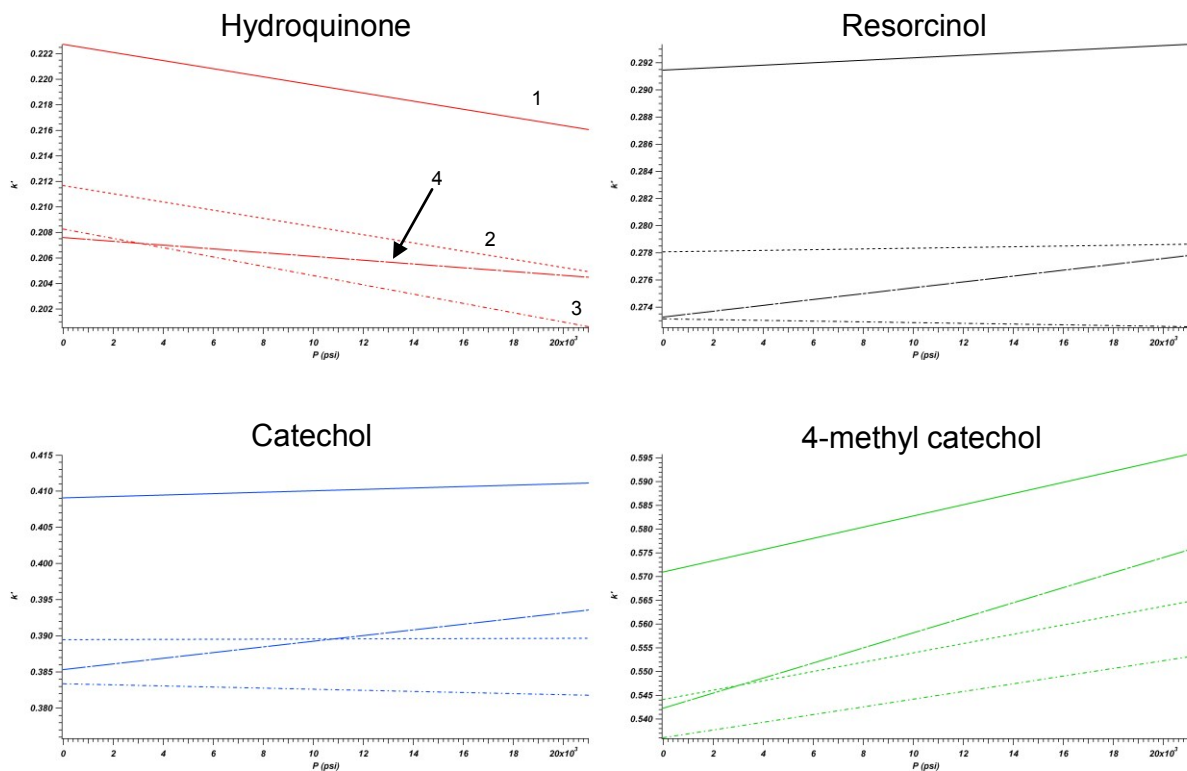


Figure 2-4: Retention data for all four ~ 25 cm segments of an originally 100 cm x 50 μ m ID column packed with ~ 10 mg/mL slurry of 1.9 μ m BEH particles in acetone.

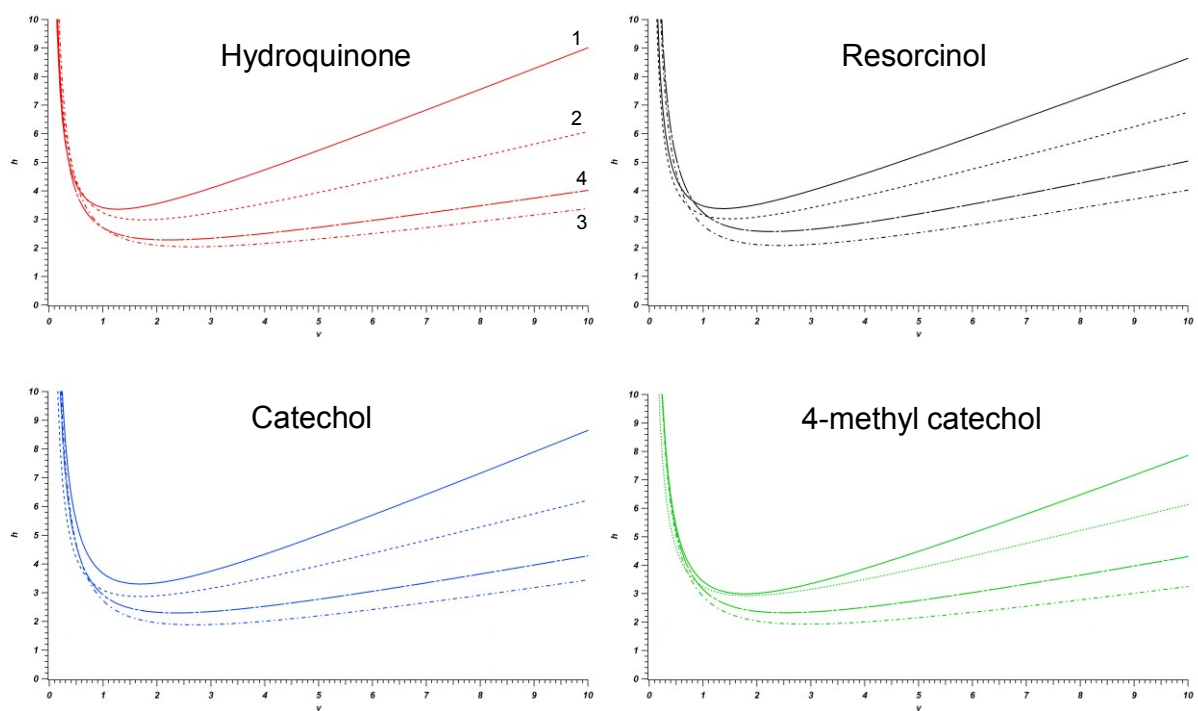


Figure 2-5: Replicate data of overlaid van Deemter curves for all four ~ 25 cm segments of an originally 100 cm x 50 μm ID column packed with ~ 10 mg/mL slurry of 1.9 μm BEH particles in acetone.

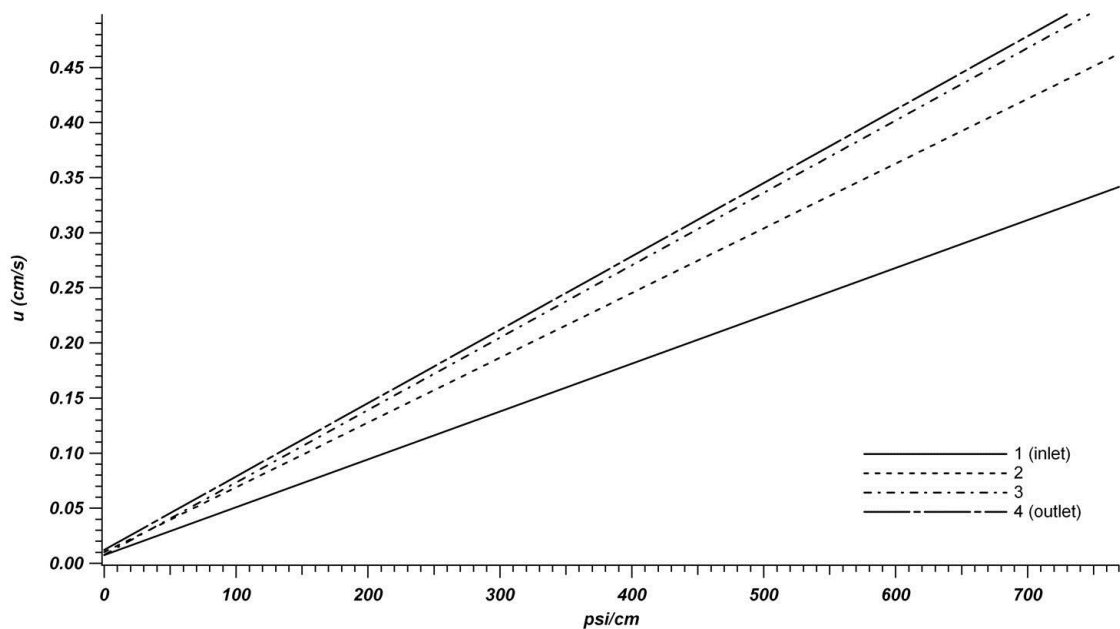


Figure 2-6: Replicate data of resistance to flow for all four ~ 25 cm segments of an originally 100 cm x 50 μm ID column packed with ~ 10 mg/mL slurry of 1.9 μm BEH particles in acetone.

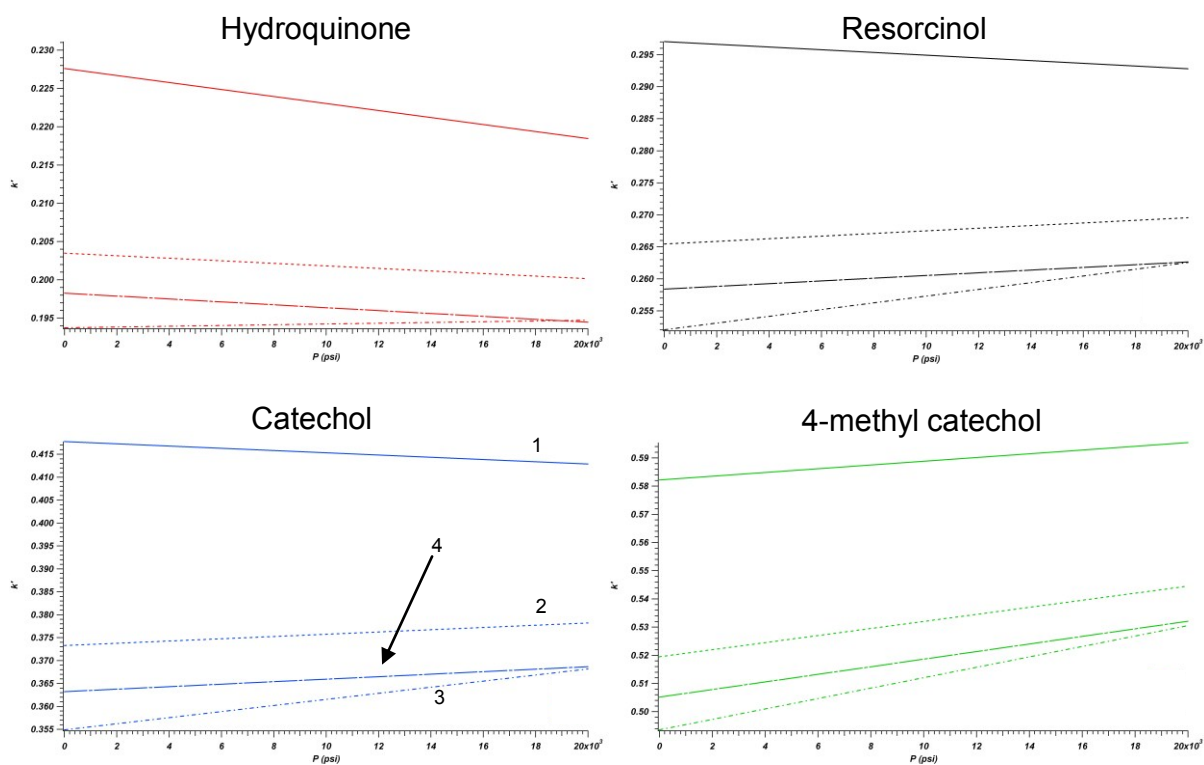


Figure 2-7: Replicate retention data for all four ~ 25 cm segments of an originally 100 cm x 50 μ m ID column packed with ~ 10 mg/mL slurry of 1.9 μ m BEH particles in acetone.

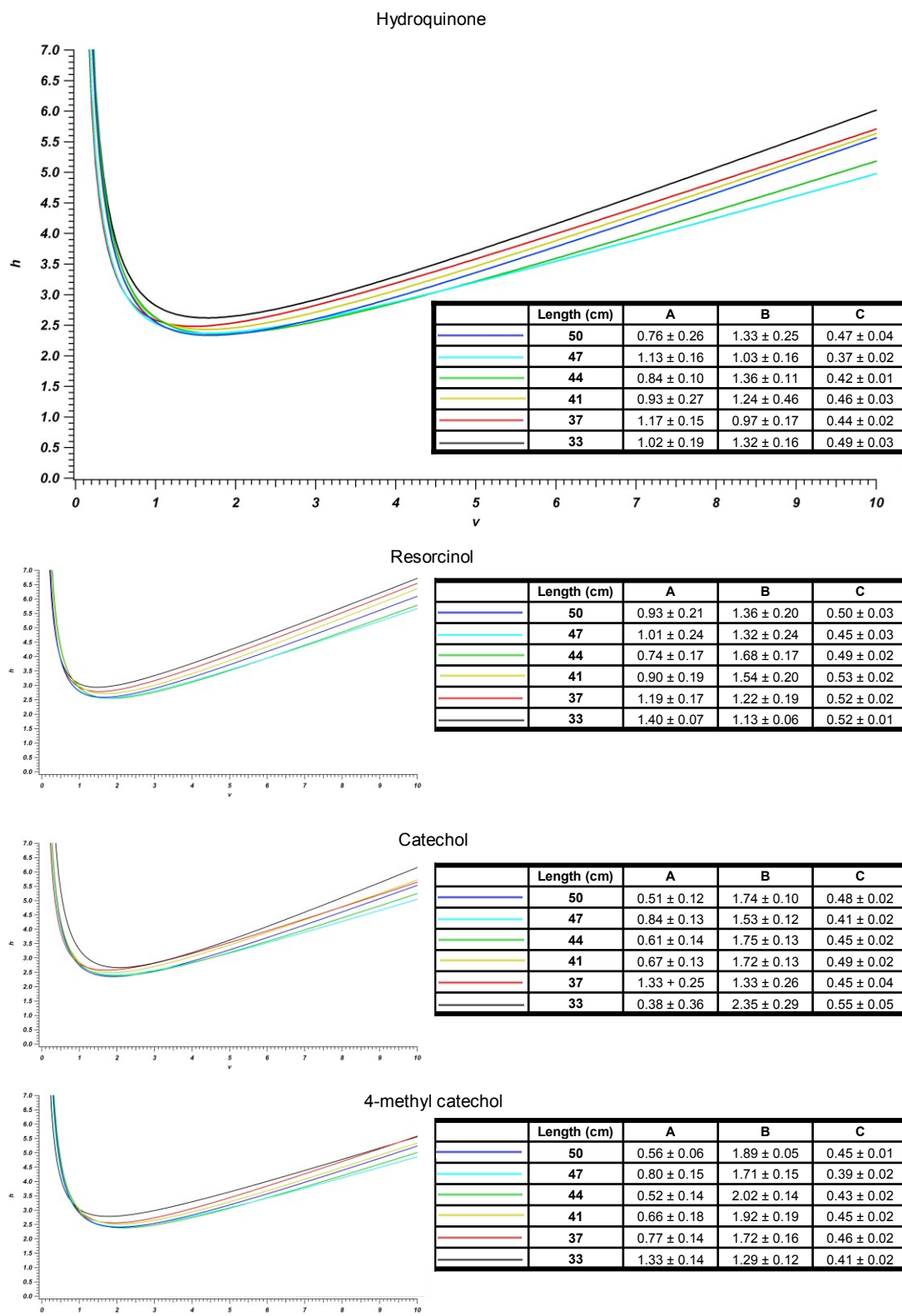


Figure 2-8: Overlaid van Deemter curves from column where increasing lengths of column were clipped from the outlet end. A ~ 3 mg/mL slurry of BEH particles in acetone was used to pack the original 50 cm x 50 µm ID column.

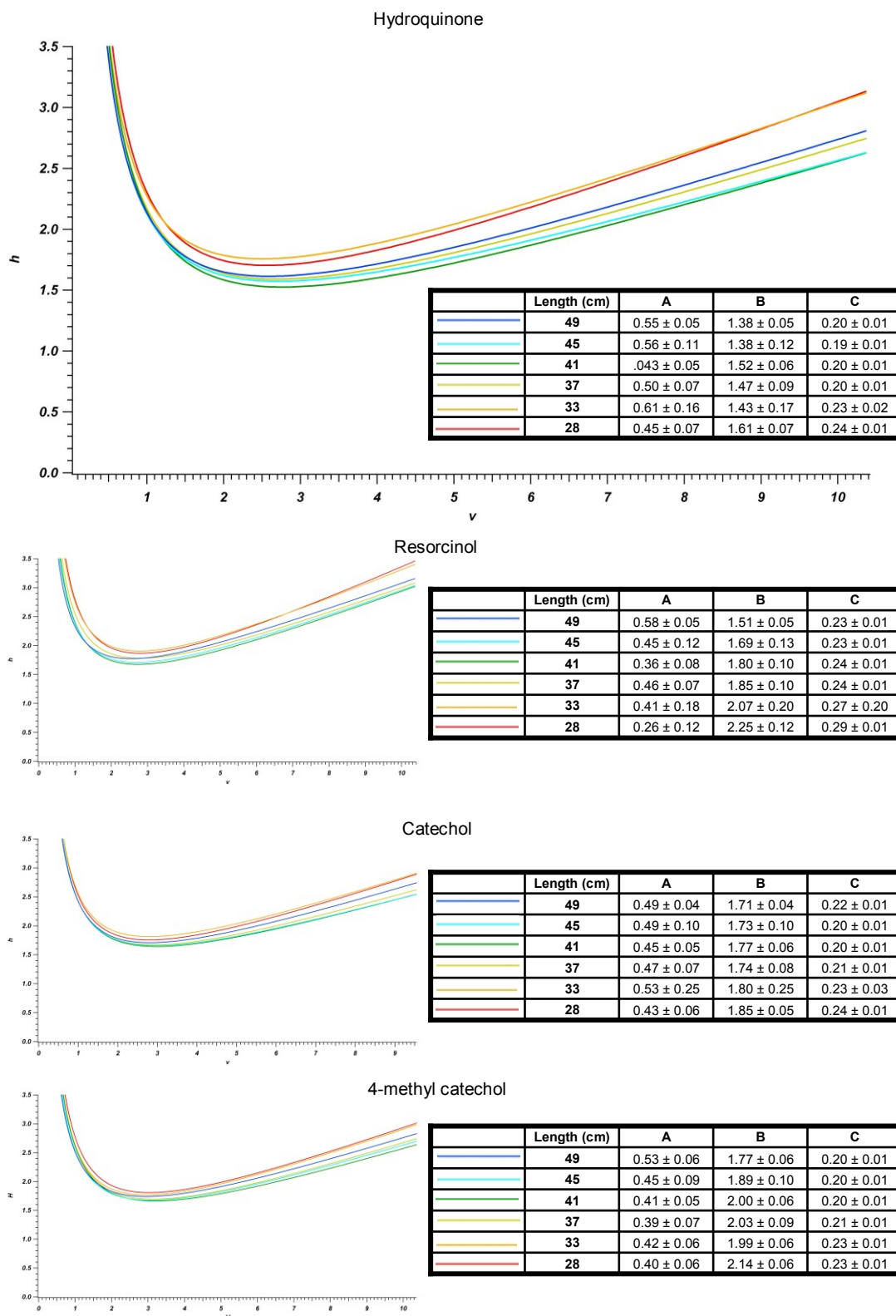


Figure 2-9: Overlaid van Deemter curves from column where increasing lengths of column were clipped from the outlet end. A ~ 100 mg/mL slurry of BEH particles in acetone was used to pack the original 49 cm x 50 μ m ID column.

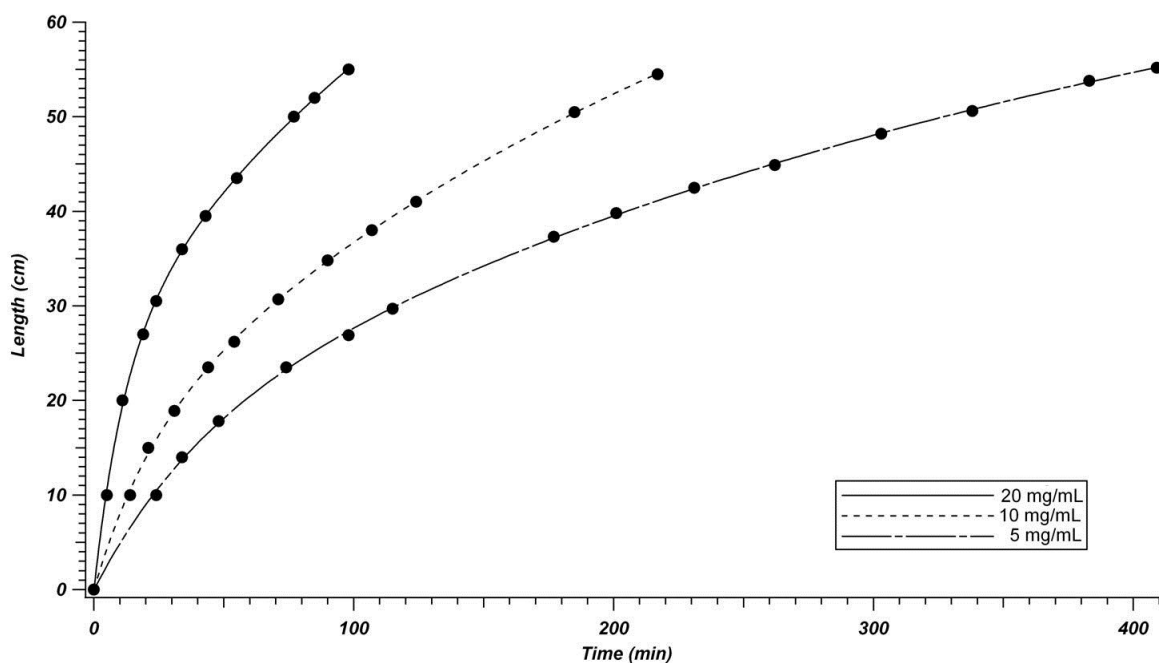


Figure 2-10: Rates of packing with 5, 10, and 20 mg/mL slurries of 1.9 μm BEH particles in acetone.

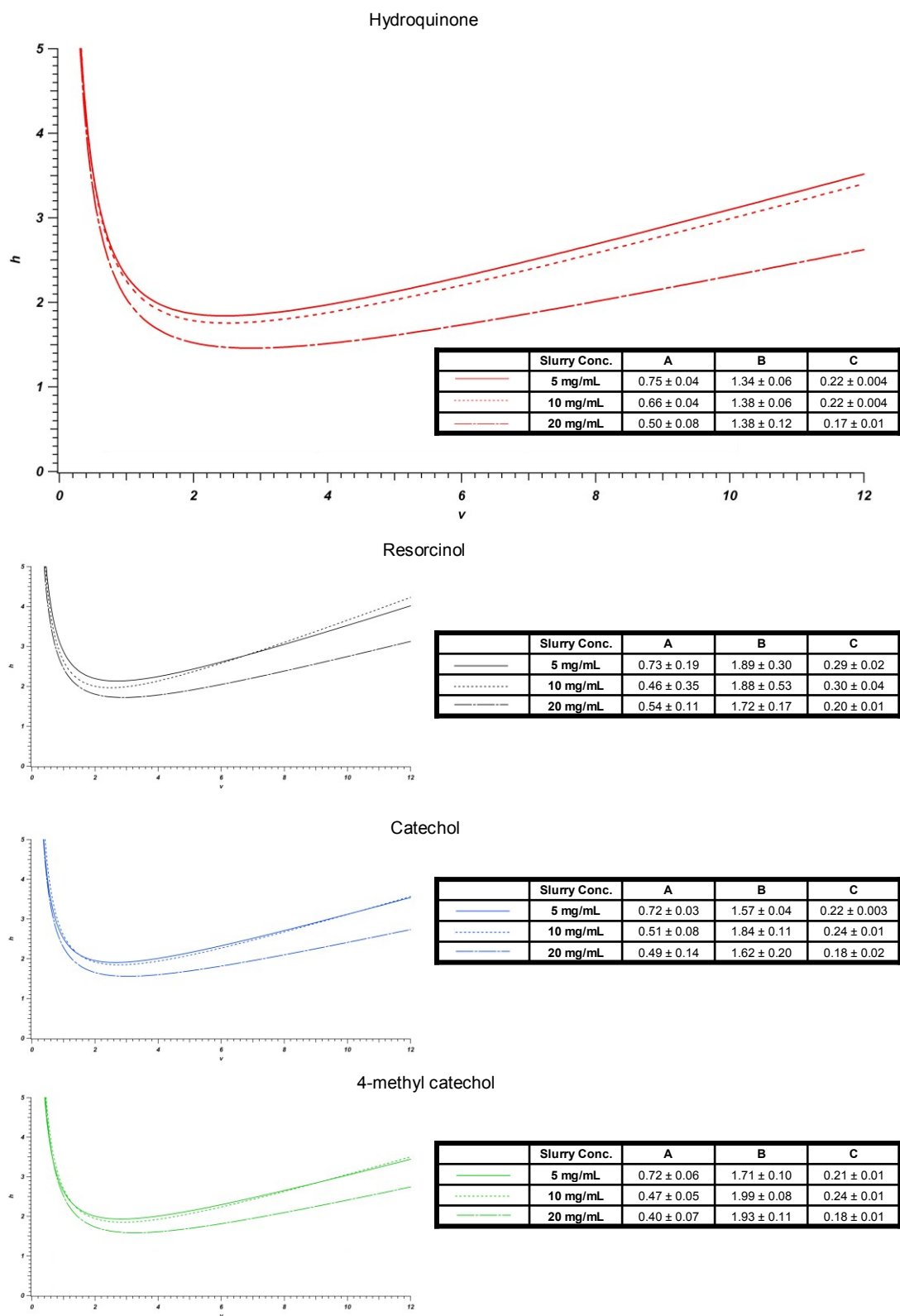


Figure 2-11: Performances of columns packed with 5, 10, and 20 mg/mL slurries of 1.9 μ m BEH particles slurried in acetone.

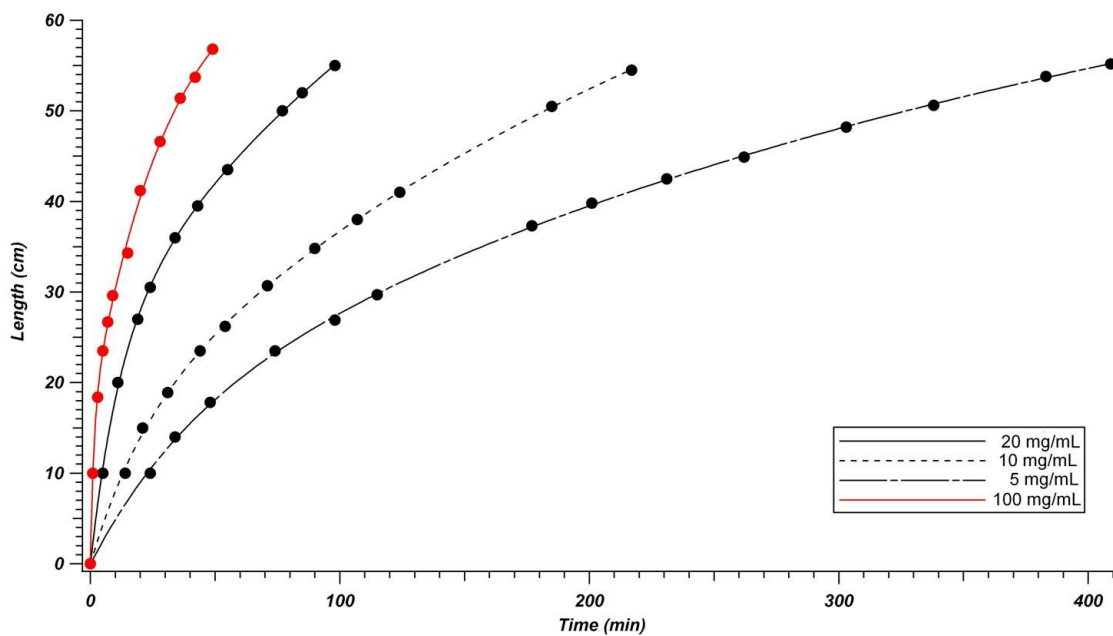


Figure 2-12: Rates of packing with 100, 20, 10, and 5 mg/mL slurries of 1.9 μm BEH particles in acetone. The 100 mg/mL slurry packing rate is highlighted in red.

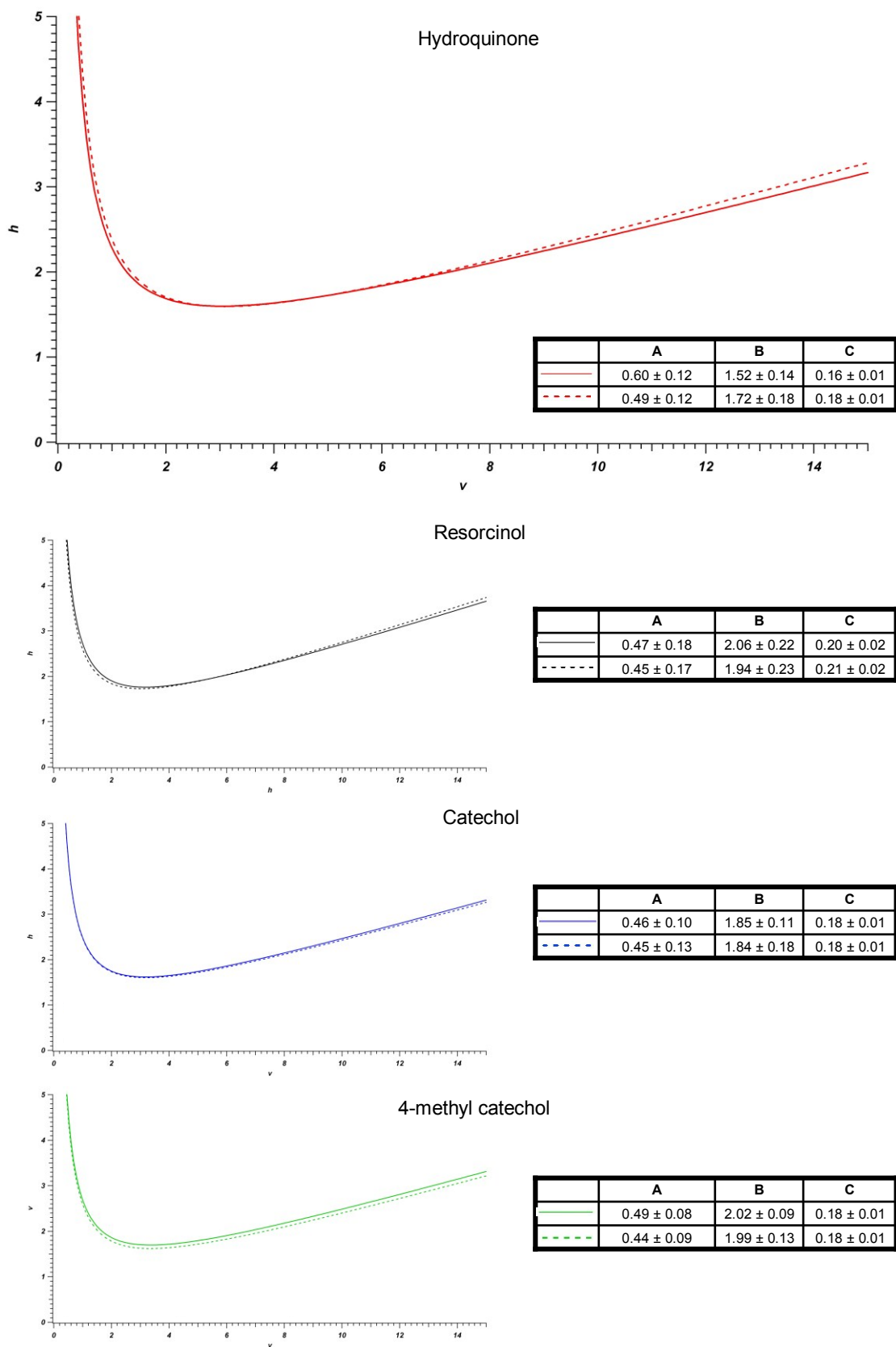


Figure 2-13: Overlaid van Deemter curves for consecutively packed 50 μ m ID columns

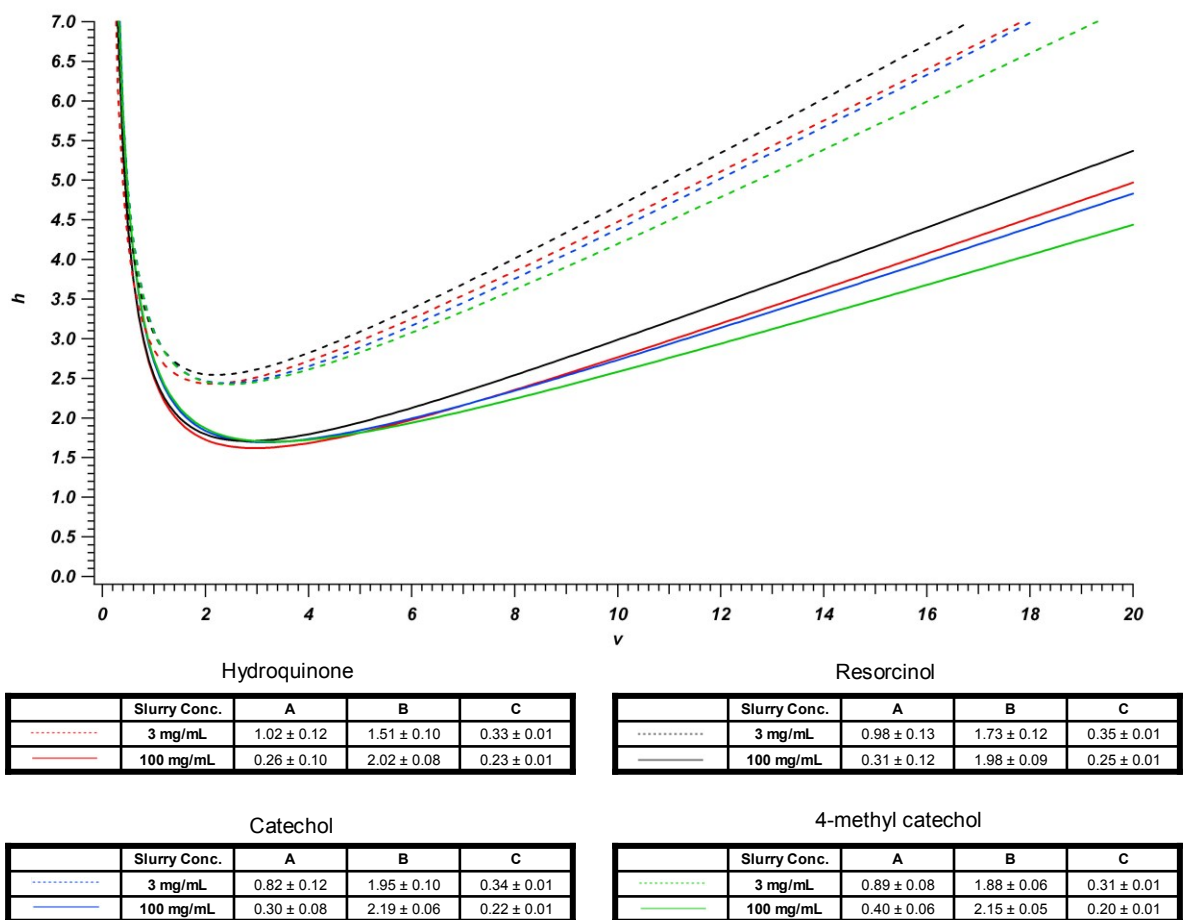


Figure 2-14: Comparison of performances for ~ 25 cm x $75 \mu\text{m}$ ID columns packed with 3 and 100 mg/mL slurries of $1.9 \mu\text{m}$ BEH particles.

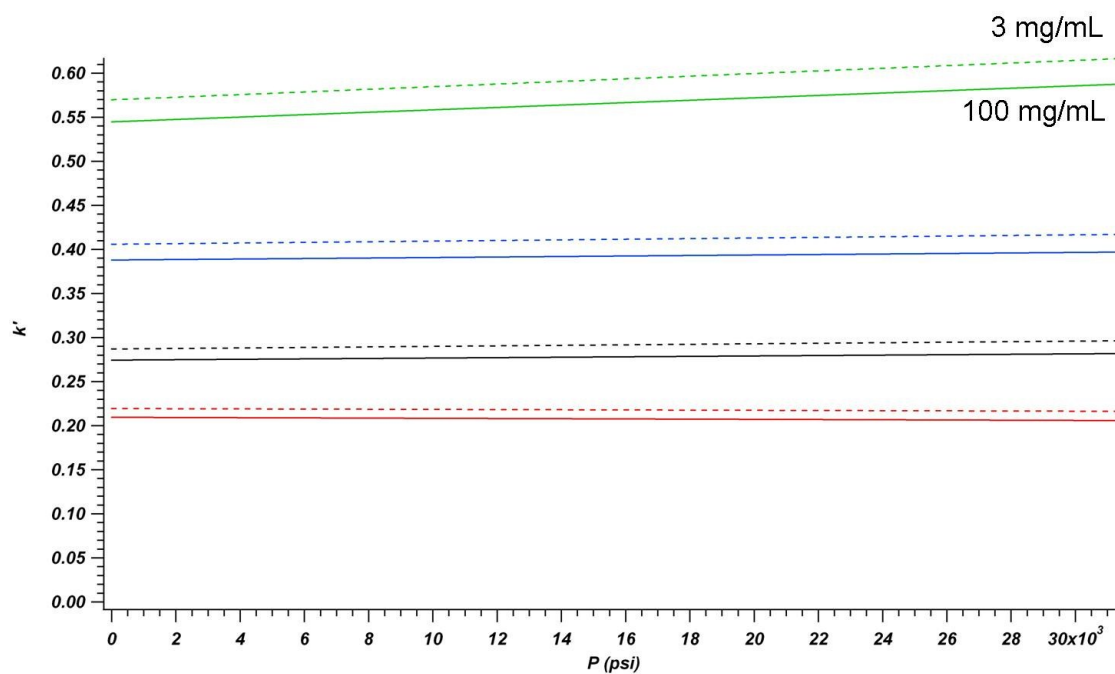


Figure 2-15: Comparison of column retention for ~ 25 cm x 75 μm ID columns packed with 3 and 100 mg/mL slurries of 1.9 μm BEH particles.

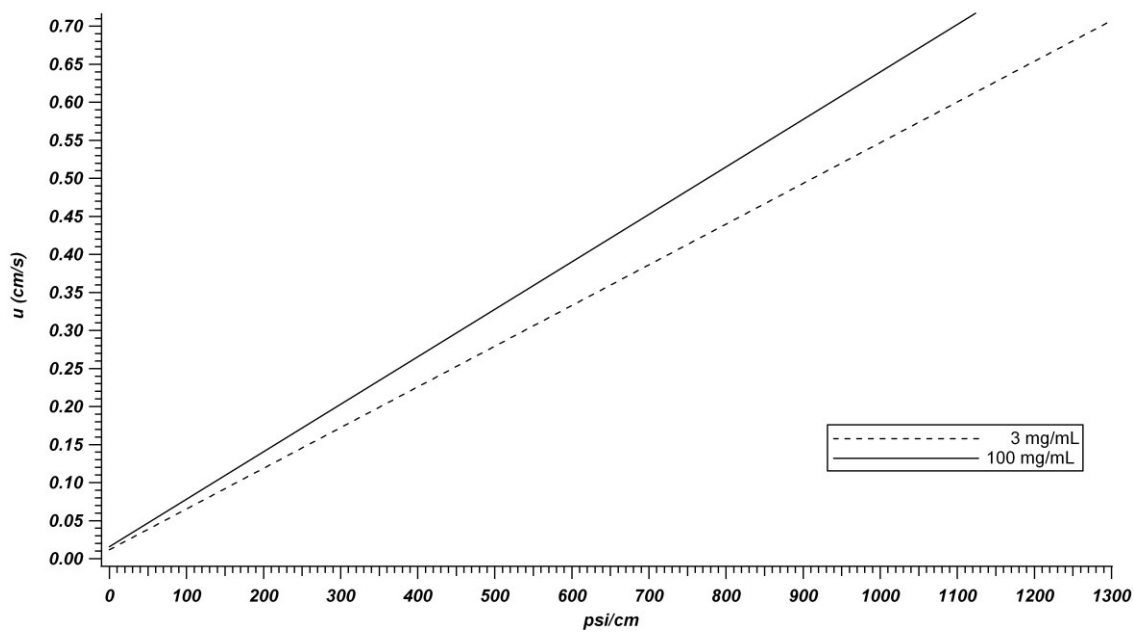


Figure 2-16: Comparison of column resistance to flow for ~ 25 cm x $75\ \mu\text{m}$ ID columns packed with 3 and 100 mg/mL slurries of $1.9\ \mu\text{m}$ BEH particles.

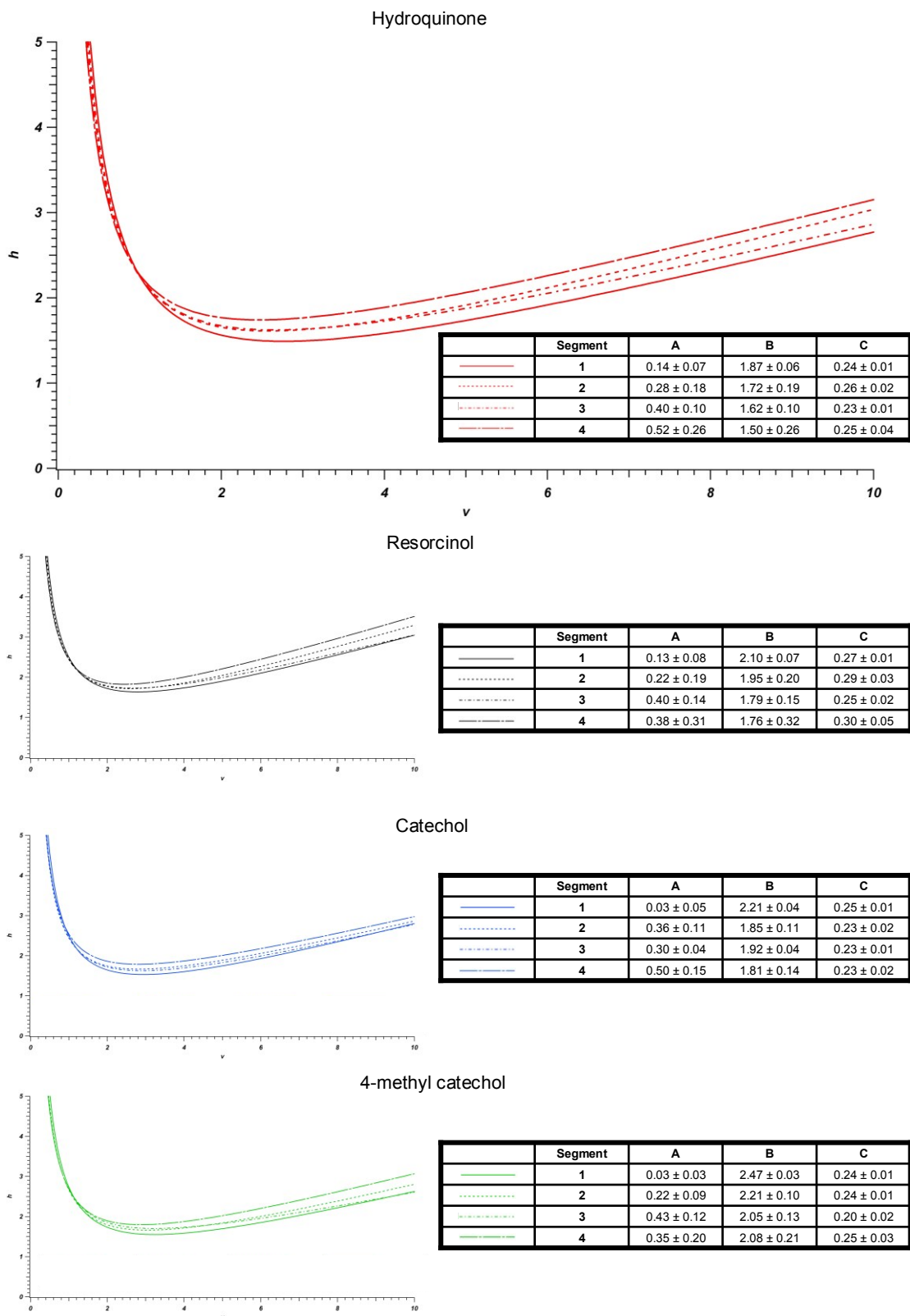


Figure 2-17: Overlaid van Deemter curves for all four ~ 25 cm segments of an originally 100 cm x 50 μ m ID column packed with ~ 100 mg/mL slurry of 1.9 μ m BEH particles in acetone.

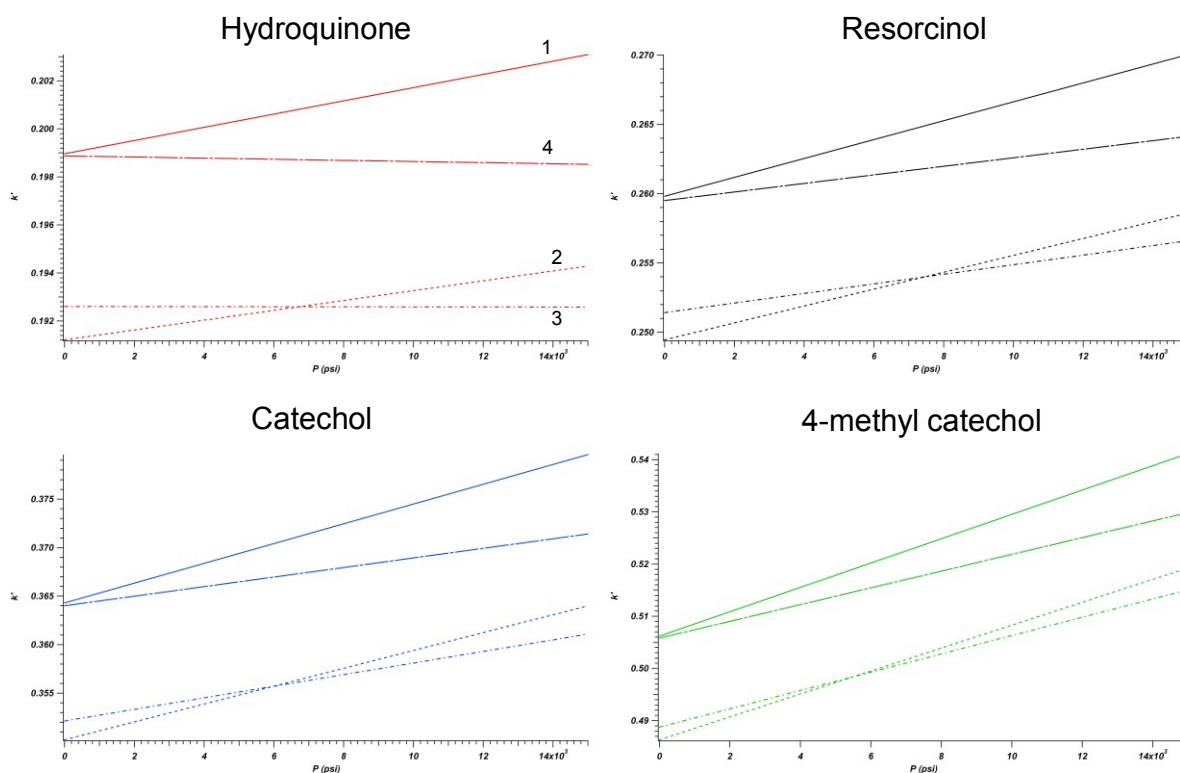


Figure 2-18: Retention data for all four ~ 25 cm segments of an originally 100 cm x 50 μm ID column packed with ~ 100 mg/mL slurry of 1.9 μm BEH particles in acetone.

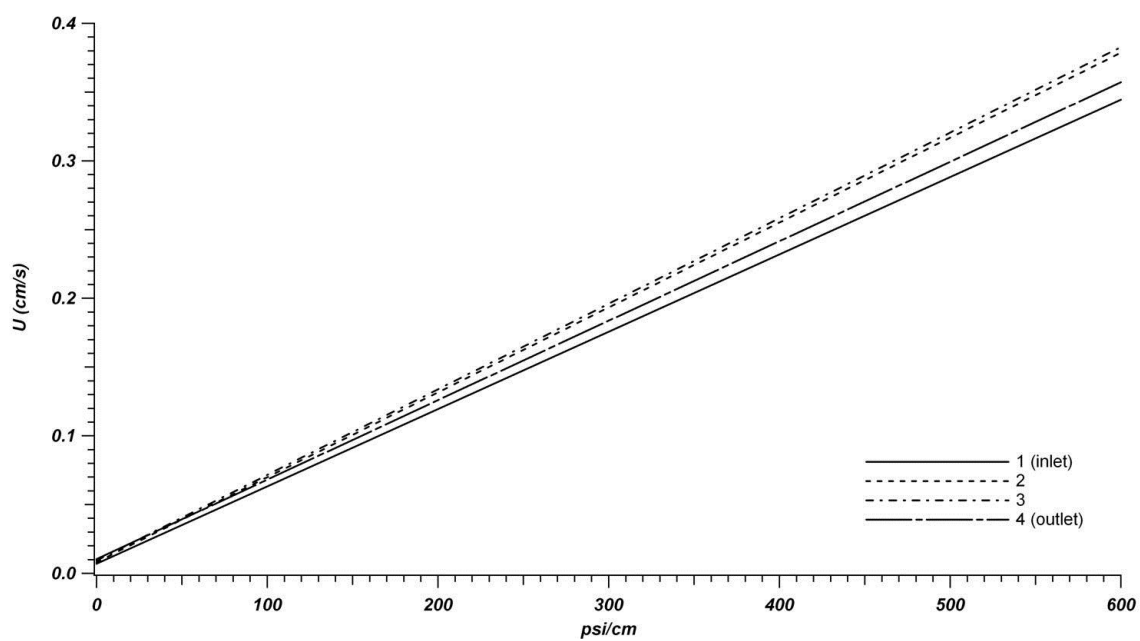


Figure 2-19: Resistance to flow data for all four ~ 25 cm segments of an originally 100 cm x 50 μm ID column packed with ~ 100 mg/mL slurry of 1.9 μm BEH particles in acetone.

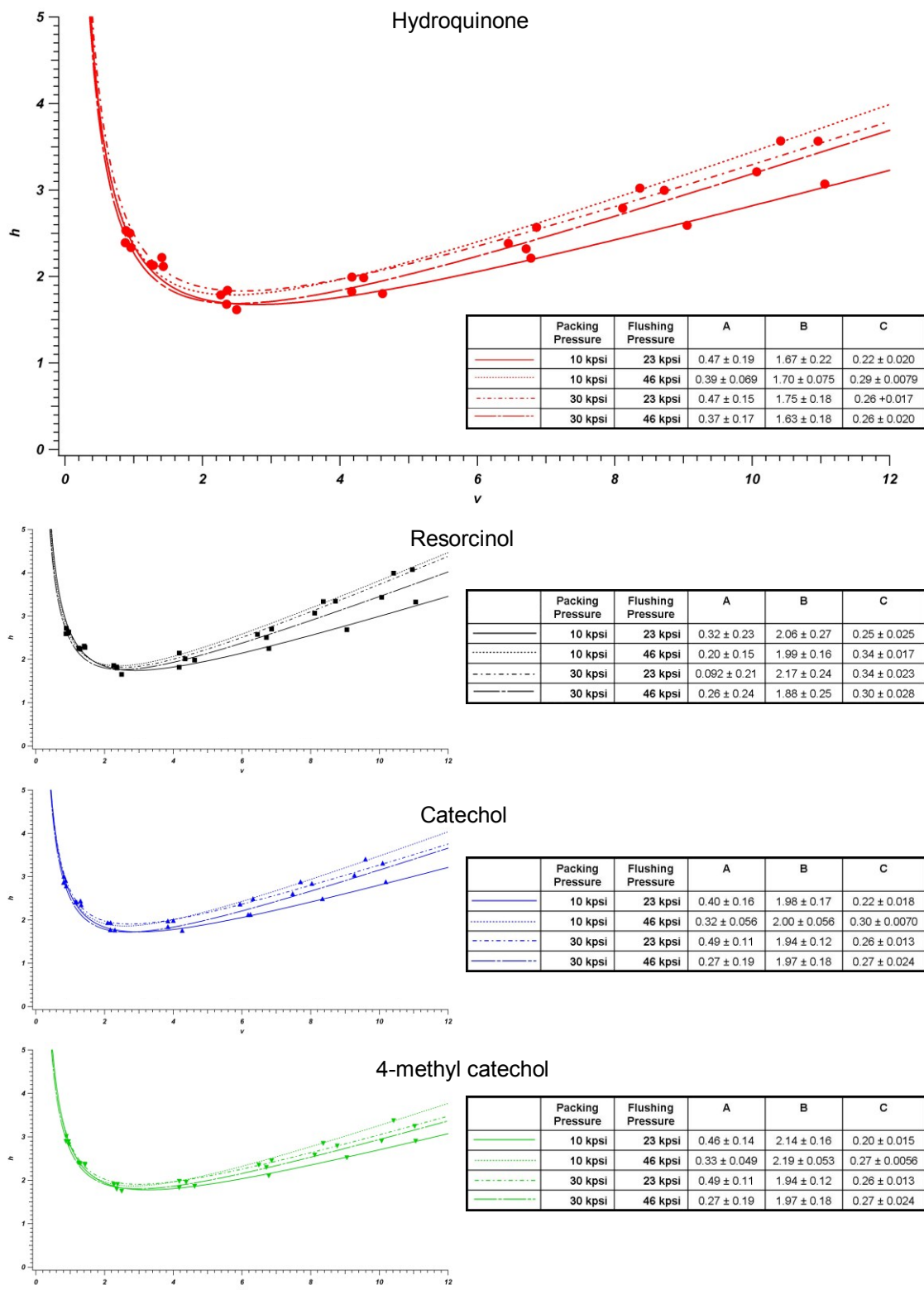


Figure 2-20: Overlaid van Deemter curves for permutations of ~ 25 cm columns packed at 10,000 or 30,000 psi and subsequently flushed at 23,000 or 46,000 psi. Columns were packed with ~ 100 mg/mL of 1.9 μ m BEH particles in acetone.

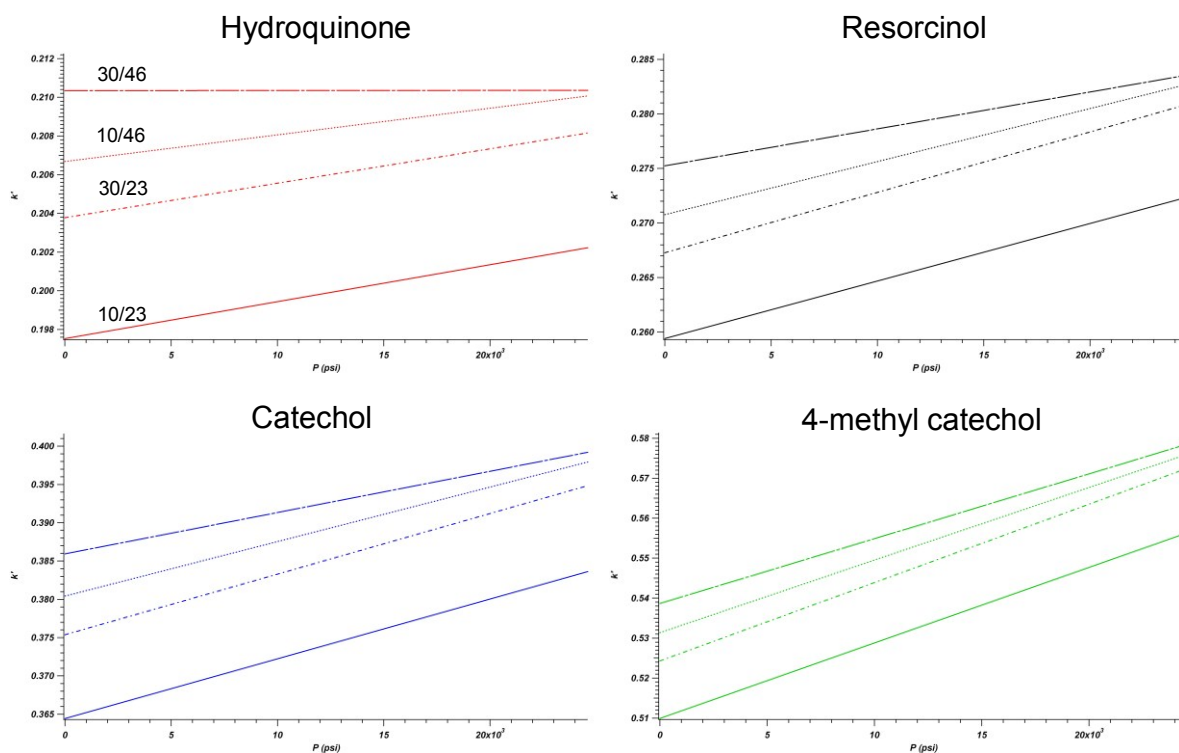


Figure 2-21: Retention data for permutations of ~ 25 cm columns packed at 10,000 or 30,000 psi and subsequently flushed at 23,000 or 46,000 psi. Columns were packed with ~ 100 mg/mL of 1.9 μ m BEH particles in acetone.

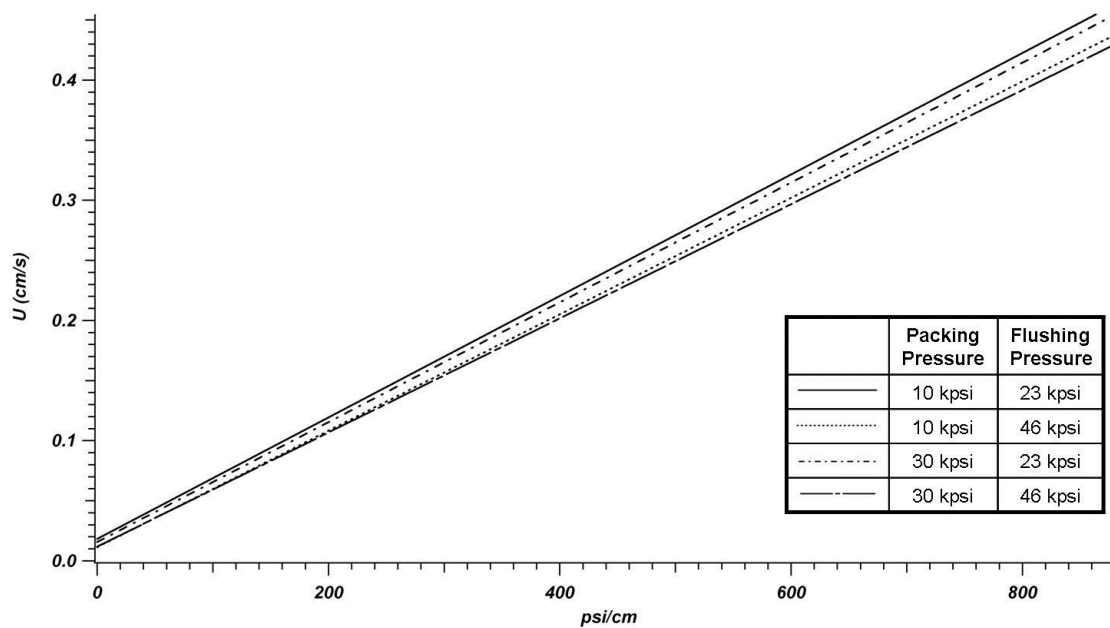
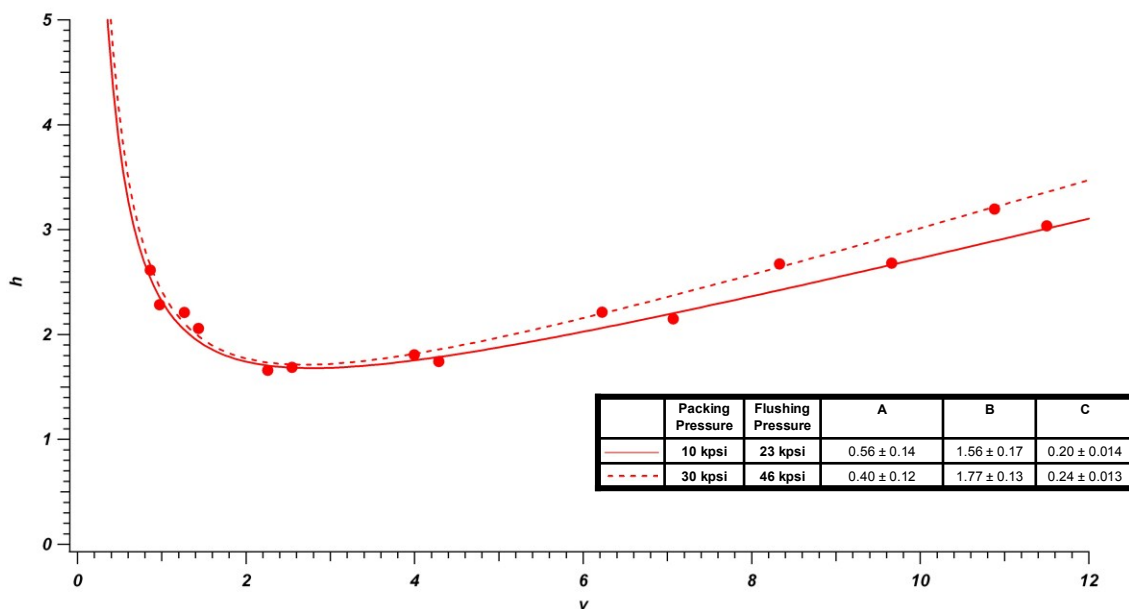
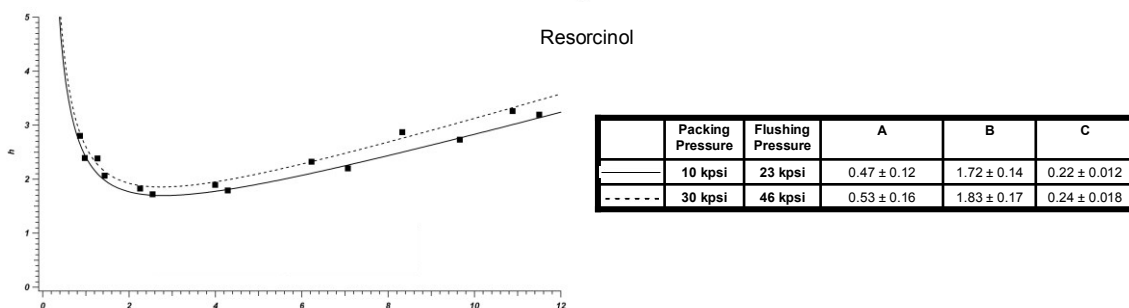


Figure 2-22: Resistance to flow data for permutations of ~ 25 cm columns packed at 10,000 or 30,000 psi and subsequently flushed at 23,000 or 46,000 psi. Columns were packed with ~ 100 mg/mL of 1.9 μm BEH particles in acetone.

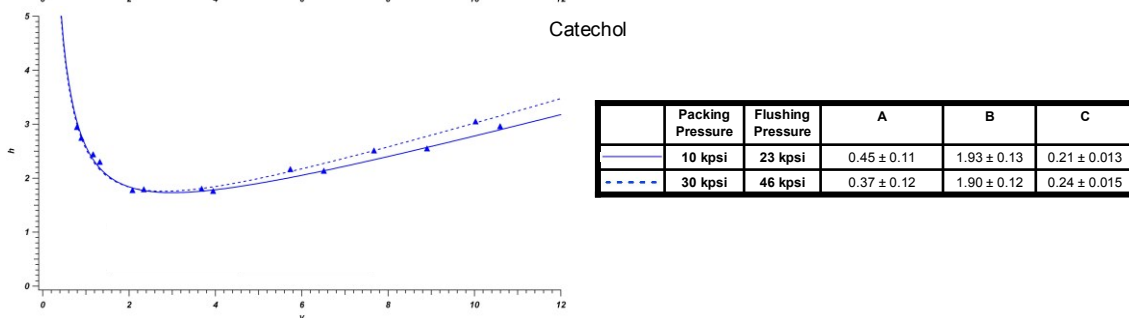
Hydroquinone



Resorcinol



Catechol



4-methyl catechol

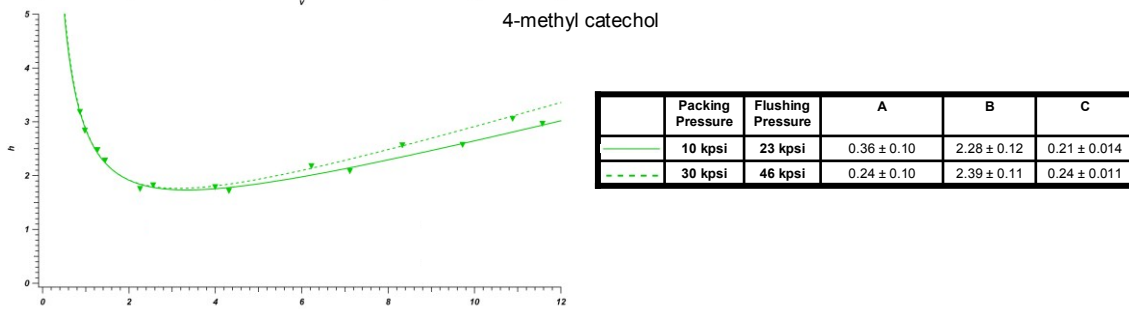


Figure 2-23: Overlaid van Deemter curves of ~25 cm column packed at 10,000 psi and flushed at 23,000 psi with a second column packed at 30,000 psi and flushed at 46,000 psi.

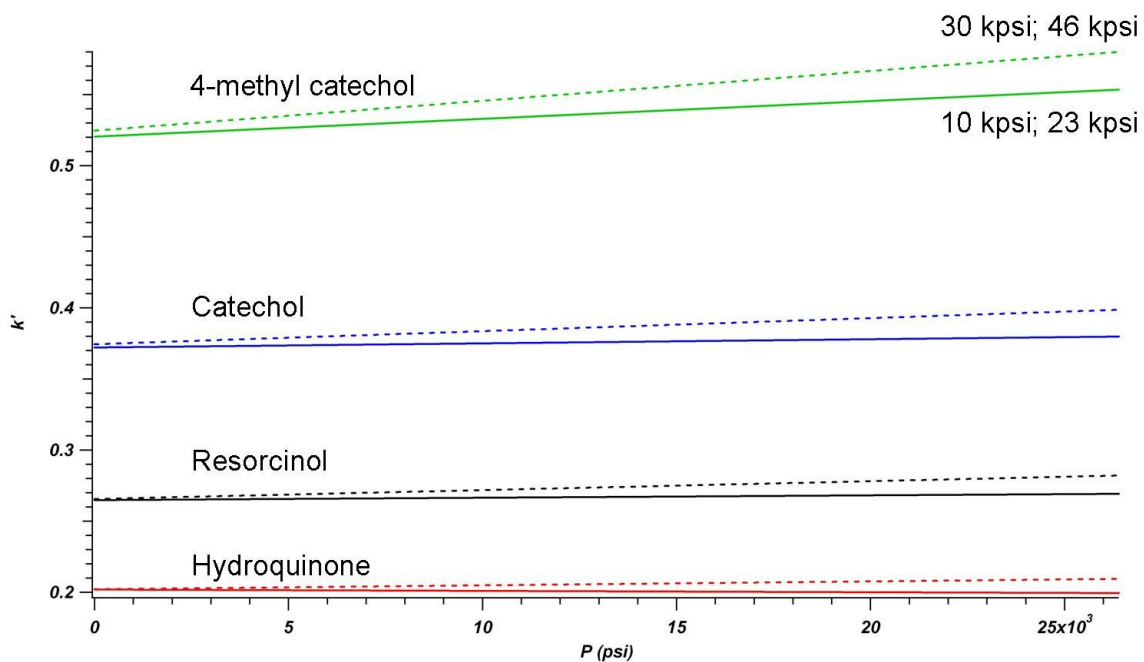


Figure 2-24: Retention data of ~ 25 cm column packed at 10,000 psi and flushed at 23,000 psi with a second ~ 25 cm column packed at 30,000 psi and flushed at 46,000 psi.

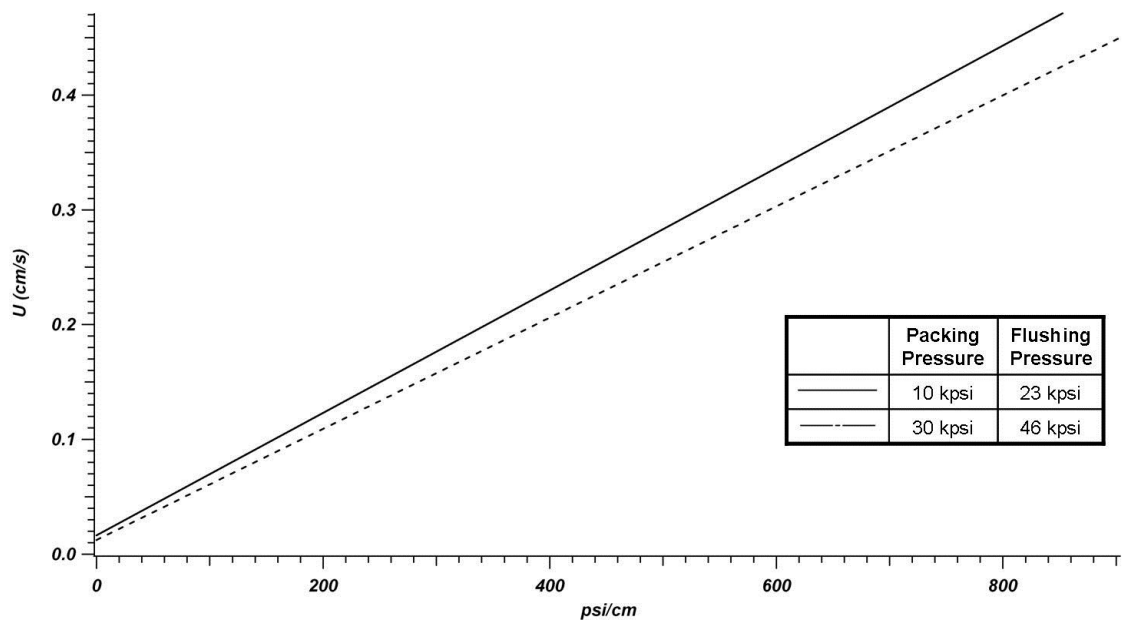


Figure 2-25: Resistance to flow data of ~ 25 cm column packed at 10,000 psi and flushed at 23,000 psi with a second column packed at 30,000 psi and flushed at 46,000 psi.

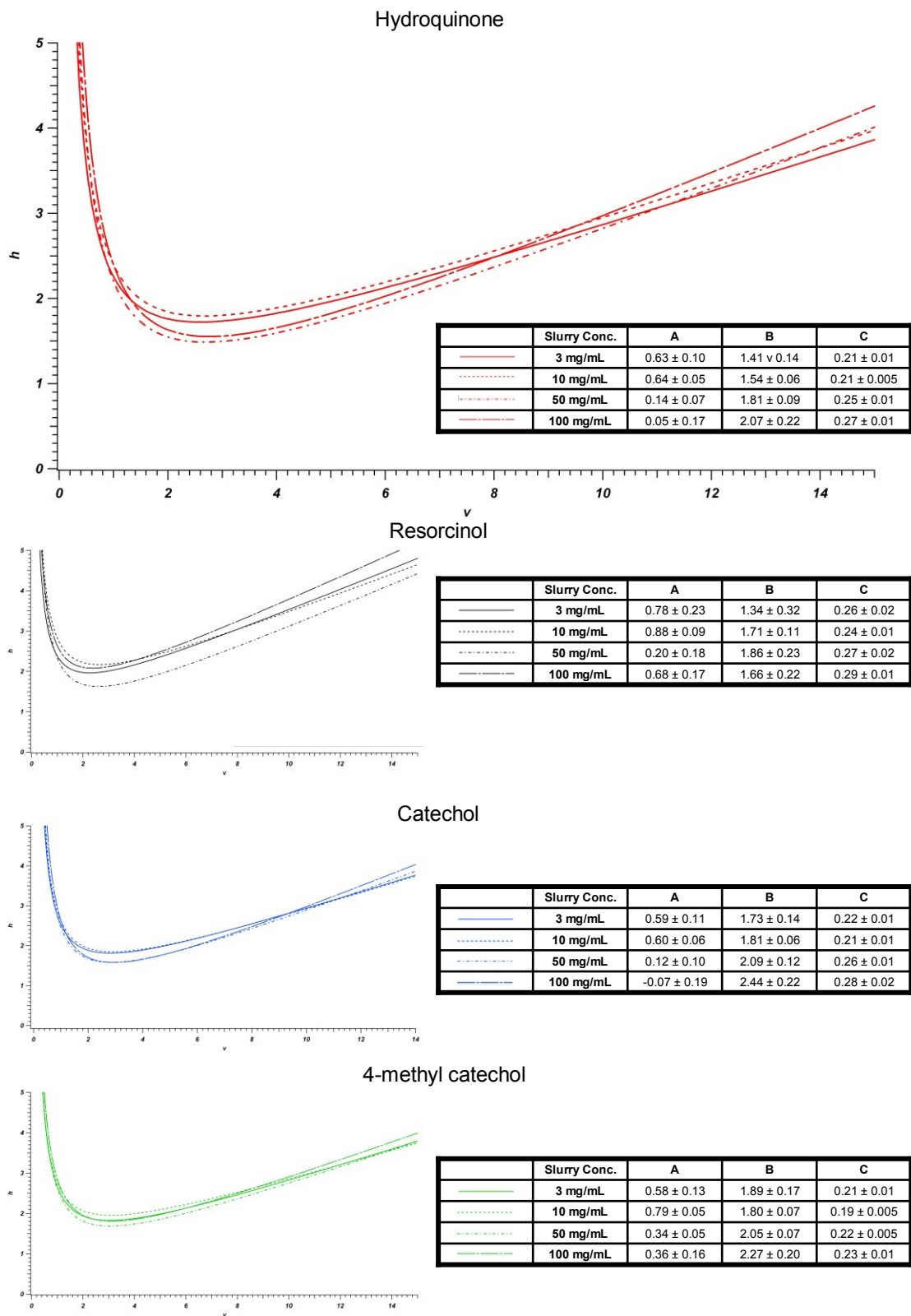


Figure 2-26: Performances of 50 μ m ID columns packed with 3, 10, and 50, and 100 mg/mL slurries of 1.9 μ m BEH particles in methanol.

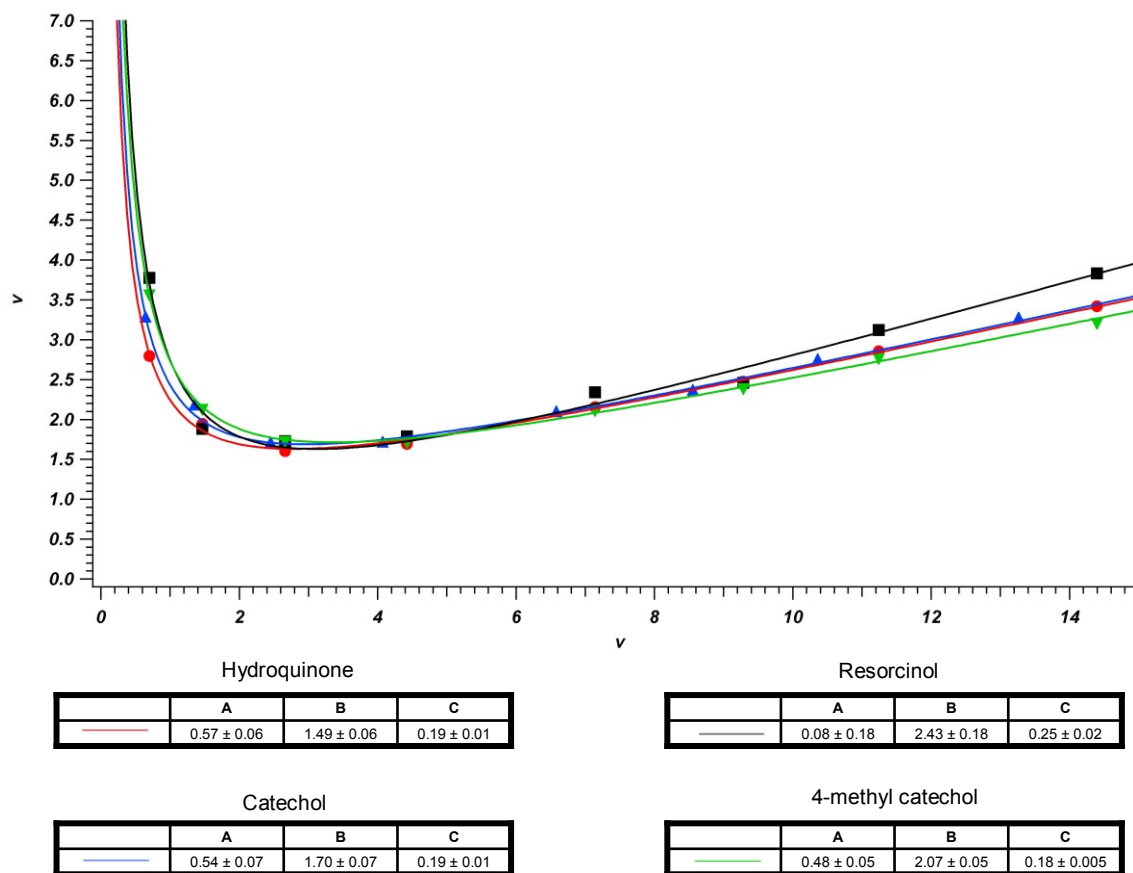


Figure 2-27: Performances of 75 µm ID column packed with 50 mg/mL slurry of 1.9 µm BEH particles in methanol.

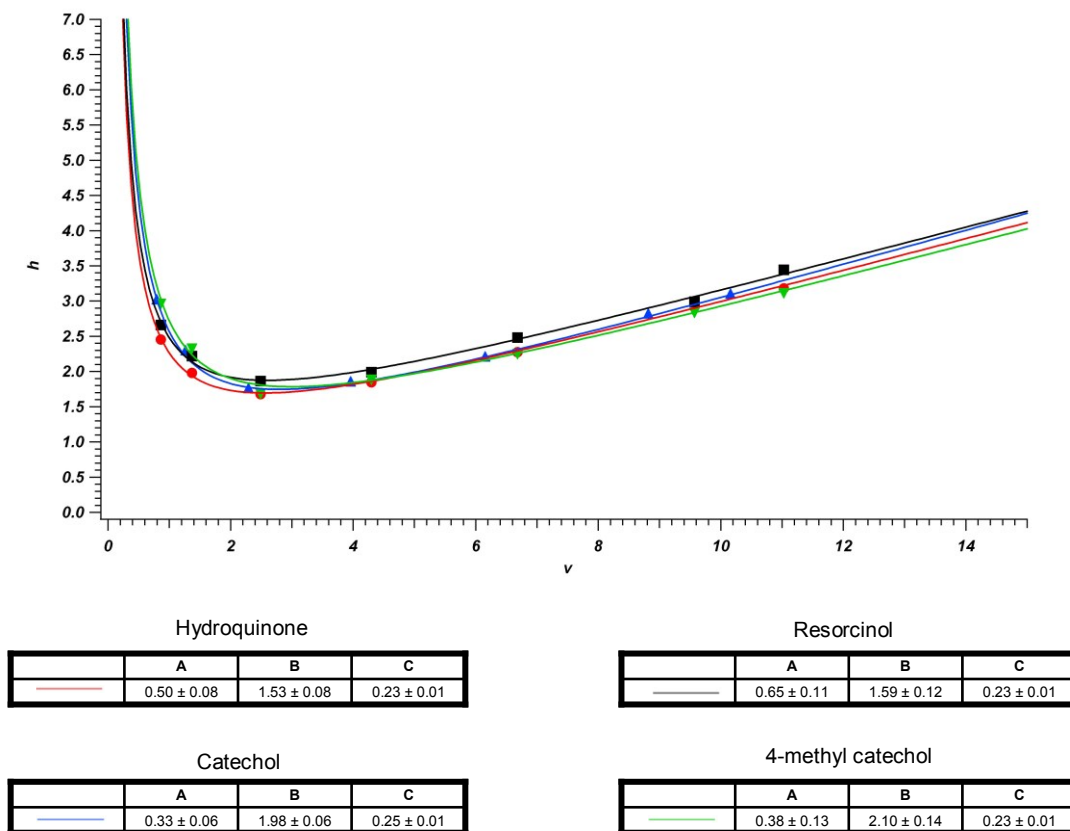


Figure 2-28: Performances of 75 µm ID column packed with 100 mg/mL slurry of 1.9 µm BEH particles in methanol.

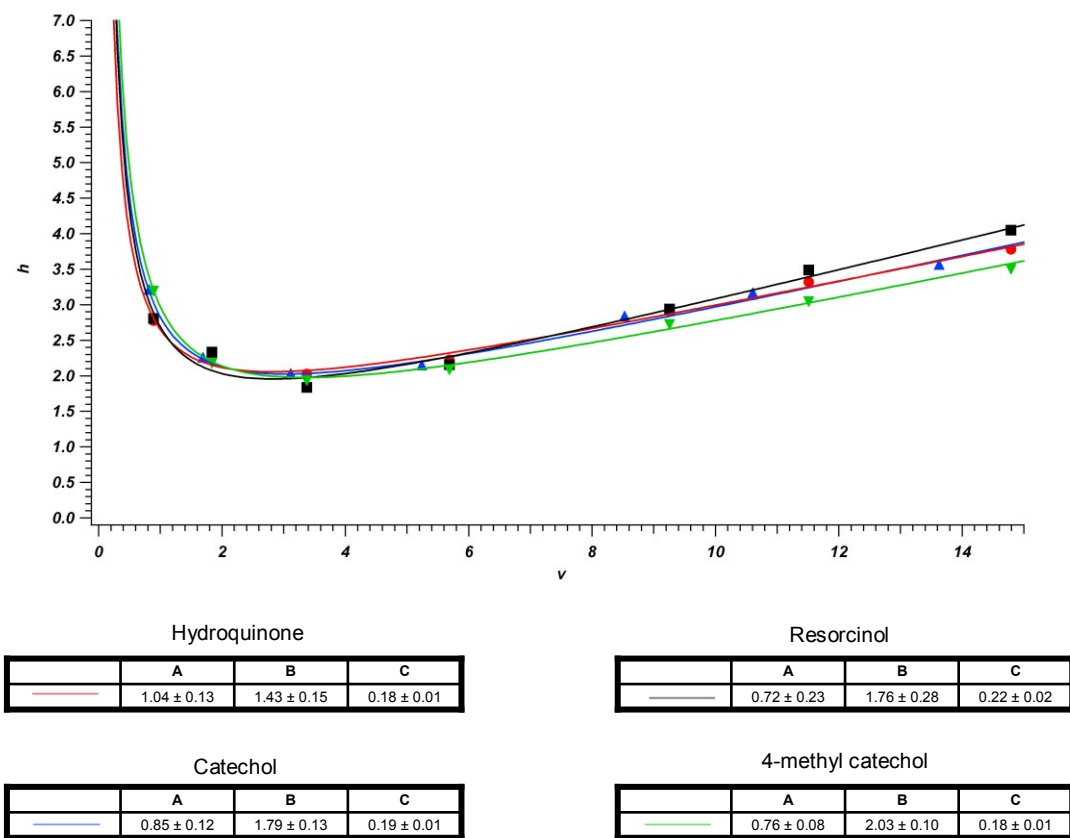


Figure 2-29: Performances of 150 μm ID column packed with 100 mg/mL slurry of 1.9 μm BEH particles in methanol.

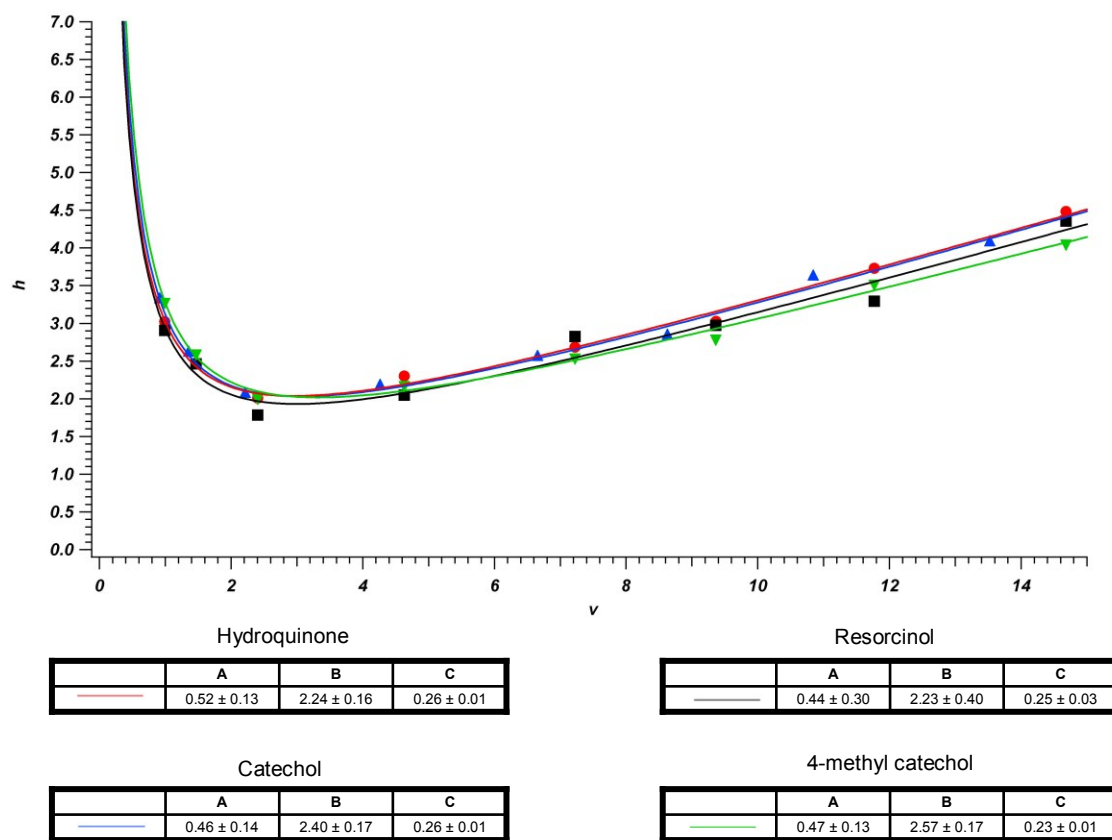


Figure 2-30: Performances of 150 μm ID column packed with 100 mg/mL slurry of 1.9 μm BEH particles in acetone.

CHAPTER 3: USE OF 1.0 MICRON-SIZED PACKING FOR FAST ANALYSES IN ULTRA HIGH PRESSURE CAPILLARY LIQUID CHROMATOGRAPHY

3.1 Introduction

To date, the vast majority of commercialized technologies borne of the chromatographic advancements ushered in by UHPLC have focused on generating moderately high pressures (up to 18,000 psi) for use with columns up to 25 cm long packed with 1.8 – 2.0 μm particles. While the separation speeds and efficiencies afforded by these approaches represent a major step forward when compared to typical HPLC performance, it is theoretically possible to achieve even faster and more efficient separations by moving to smaller particle diameters. This chapter explores the use of 1.0 μm porous particles as a stationary support for liquid chromatographic separations.

3.1.1 Alternative Approaches to Fast, Efficient Liquid Chromatographic Separations

Emphasis on increasing the speed of separations has led to advances in several areas in addition to sub-2 μm particle technologies. For example, monolithic columns are coherent rigid castings of silica or polymer made by in situ polymerization. The interstitial volumes of these columns are on the order of 80%, making their permeabilities much higher than those of packed bed columns. The lower flow resistance allows for either faster analyses or, alternatively, higher efficiencies in a given analysis times. Based upon column efficiency studies, some monolithic columns are estimated to have equivalent particle diameters of 4 – 5 μm . Theoretical investigations have sought to resolve whether higher pressure approaches

(UHPLC) or higher external porosity approaches (monoliths) are favorable. It is suggested that either approach has more or less the same effect on the kinetic performance of the chromatographic support, and that the favored approach comes down to mechanical and physiochemical considerations¹.

Superficially porous particles offer the promise of faster analysis times by using larger particles with performance characteristics that are competitive with smaller fully porous particles. By eliminating the porous core region of a particle, the stagnant mobile phase contribution to resistance to mass transfer broadening is significantly reduced. In this way, chromatographic performance is improved without the need for higher operating pressures².

Capillary electrochromatography (CEC) is another means to enhance transport inside of porous particles, thus increasing speed of analysis in certain applications. There is little evidence, however, for improved efficiency over entirely pressure driven flow techniques. In its simplest form, CEC employs fused silica capillaries packed with a stationary phase that has fixed charges at the surface. Application of a high electric field generates and maintains electrosmotic flow of eluent through the column. Analytes are separated due to partitioning between the stationary and mobile phases and, if they are charged, by differences in their electrophoretic mobilities³. Recently, the Wirth group has employed 330 nm non-porous silica spheres to form colloidal crystals inside of 75 μm ID fused silica capillaries. Isocratic electromigration across a 12 mm separation length is reported to generate plate counts in excess of 10^6 in 1.5 minutes for lysozyme⁴.

Similarly, non-porous 470 nm silica was used to form 21 mm colloidal crystals in 75 μm ID columns, and, using only pressure-driven flow, it is claimed that labeled bovine serum

albumin was separated to produce plate heights of ~ 15 nm in 40 seconds, corresponding to plate counts in excess of 10^6 and reduced plate heights of 0.032^5 . The authors attribute this remarkable performance to slip flow, which occurs in nanofluidics due to weak intermolecular interactions between the fluid and the walls (i.e. the hydrocarbon functionalized silica spheres, in this case). Compared to Hagen-Poiseuille flow, slip flow serves to narrow the velocity distribution across the flow channel, thus serving to decrease the distribution of analyte arrival times at the detection end of the column.

3.1.2 Theoretical Utility of 1.0 μm Porous Particle Supports

Recalling discussions from Chapter 1, it is generally regarded that “well-packed” chromatographic columns operated at optimum linear velocities have minimum plate heights on the order of two particle diameters:

$$H_{\min} \approx 2d_p \quad (3-1)$$

As such, smaller packing materials allow for lower minimum plate heights and greater column efficiencies. Moving to smaller particles diameters, however, necessitates much higher operating pressures to achieve a given mobile phase linear velocity, as shown in Equation 3-2 and discussed in Chapter 1.2.5.

$$\Delta P = \frac{\omega \eta L u}{d_p^2} \quad (3-2)$$

where ω is the flow resistance factor associated with the structure of the packed bed and η is the mobile phase viscosity. In addition, columns packed with smaller particles will also have faster optimum linear velocities, such that

$$\Delta P_{\text{opt}} \propto \frac{1}{d_p^3} \quad (3-3)$$

It can be seen, therefore, that moving from 2 μm particles (typical for commercial UHPLC applications) to 1 μm particles requires an 8-fold increase in pressure to operate a given column length at maximum efficiency. Given system operating pressure as a limiting factor, examination of the theoretical kinetic plots can provide insight into the most appropriate applications for a particular particle size. Figure 3-1 shows the performance of 1 μm versus 2 μm particles given pressure limitations of 15,000 and 40,000 psi. The following values were used in constructing the plots: viscosity, $\eta = 1$ cP; interparticle porosity, $\varepsilon_i = 0.4$; analyte diffusion coefficient, $D_m = 1 \times 10^{-5}$ cm^2/s ; reduced van Deemter coefficients $A = 1.5$, $B = 1.0$, and $C = 0.17$.

From Figure 3-1, the advantages of higher operating pressures can be assessed. For example, a separation performed with 2 μm particles and a column dead time of 100 s can be made significantly more efficient by using higher pressures. At 15,000 psi, the maximum achievable number of theoretical plates is approximately 58,000; at 40,000 psi, the maximum number of theoretical plates is nearly 80,000. Likewise, the advantages of using smaller particles can be assessed. Suppose a total analysis time need occur on a time scale commensurate with a 10 s column dead time. Using 2 μm particles and 15,000 psi operating pressures, approximately 10,000 plates can be generated. With 1 μm particles, 20,000 plates can be generated in the same time frame. At 40,000 psi, 2 μm particles can generate ~ 12,000 plates, while 1 μm particles provide ~ 28,000 plates.

The point of intersection for different particle diameters at a given operating pressure is a particularly interesting note of consideration for these plots. At 15,000 psi, this intersection occurs at $t_m \approx 170$ s, where ~ 85,000 plates can be generated for either 1 μm or 2 μm particles. If less than 85,000 plates are sufficient for a separation, 1 μm particles can

achieve a given efficiency in faster times. This is represented by moving vertically between the curves in Figure 3-1. Likewise, for a given dead time up to ~ 170 s, 1 μm particles can generate more plates than can columns packed with 2 μm particles. This is seen in moving along the isothermal lines. If more than 85,000 plates are required, however, using columns packed with 2 μm particles is the better option when limited to operating pressures of 15,000 psi. At 40,000 psi, this point of intersection occurs at ~ 460 s, where nearly 220,000 plates are generated. It is thus apparent that, 1 μm particles have their greatest utility for fast analyses.

While Figure 3-1 does not explicitly indicate the column lengths required to generate a given number of theoretical plates, the equations used in the construction of the plots reveal this information. Figure 3-2 more clearly illustrates the expected efficiencies of columns of various lengths packed with 1 μm particles given the same van Deemter coefficients used in constructing Figure 3-1. At 15,000 psi, it can be seen that a ~ 10 cm column is run most efficiently, producing over 40,000 plates with a t_m of just over 40 seconds. At 40,000 psi, a ~ 30 cm column produces over 100,000 with a t_m less than 2 minutes. Increasing the length over 3x to 100 cm will allow for $> 300,000$ plates, but t_m will exceed 20 minutes.

Previous work with 1.0 μm non-porous silica particles revealed relatively good performance with minimum plate heights ranging between 1.8 and 2.2 μm . C-terms, however, were larger than anticipated, and there was significant variability depending upon analyte retention⁶. One of the biggest drawbacks to working with non-porous materials is its low loading capacity, which can be expressed in terms of the phase ratio, β , the ratio between the surface area of the stationary phase and the mobile phase volume⁷:

$$\beta = (1 - \varepsilon_i) \frac{A_{SP}}{V_{SP} + \frac{\varepsilon_i}{\rho_{skel}}} \quad (3-4)$$

where ε_i is interparticle porosity, A_{SP} is the specific surface area of the packing material expressed in m^2/g , V_{SP} is the specific pore volume expressed in mL/g , and ρ_{skel} is the skeleton density of the packing material (2.2 g/mL for silica). For columns packed with $1.0 \text{ }\mu\text{m}$ non-porous particles and interstitial porosities of 40%, the phase ratio is approximately $9 \text{ m}^2/\text{mL}$. This relatively small value suggests low sample loadabilities, which results in greater peak broadening as the stationary phase is overwhelmed with even moderately sized injection volumes. By comparison, porous packing materials commonly have phase ratios on the order of $200 \text{ m}^2/\text{mL}$ or higher, allowing for sample loadabilities that are compatible with a wider array of detection schemes.

3.1.3 Previous Efforts with $1.0 \text{ }\mu\text{m}$ Porous Particles

In the preceding section, the theoretical considerations of $1 \text{ }\mu\text{m}$ particles and their situational preferentiality over larger particles make the important assumption that each particle size can be packed so as to produce equally efficient columns (i.e. columns having the same reduced van Deemter coefficients). This has not been realized, however, and previous efforts to pack efficient columns with $1 \text{ }\mu\text{m}$ porous particles within our lab have not proven entirely successful. Most notably, columns have exhibited greater than expected resistance to mass transfer contributions to analyte band broadening.

These previous efforts targeted methods to produce dense and stable packed beds, specifically focusing on slurry packing solvents and ultrasonic approaches to improve bed consolidation⁸. Column sonication studies were performed in effort to reorganize the packed bed, either during or after the packing process. It was thought that voids in the packing,

resulting from large particle aggregates, could be eliminated in this way, leading to better chromatographic performance. In most instances, there was evidence that sonication led to further bed compression, but these effects on ultimate column performance were somewhat varied. The slurry solvent studies were motivated by efforts to reduce particle-particle interactions so as to minimize aggregation during the packing process. For solvents that promote aggregation, it was thought that particle aggregates entering the column blank would tend to leave large void regions as the packed bed was formed, ultimately leading to poor chromatographic performance. Alternatively, the use of solvents which promote particle-solvent interactions would lead to individually solvated particles that packed uniformly and densely. Potential slurry solvents were screened by measuring the sedimentation rates of particles in various solvents. The measured rates were then compared to the theoretical settling rates of single, well-dispersed particles. This allowed for the determination of effective particle diameter and the degree of aggregation in a particular solvent. As explained in Chapter 2.1.3, the main drawback of this method is that the particle-solvent behavior under high-pressure conditions, such those used during packing experiments, is not effectively interrogated.

Acetone, THF, MEK, 50/50 (v/v) acetone/THF, 50/50 (v/v) acetone/MEK, and an aqueous solution of acid labile surfactant were used as slurry solvents to pack a series of 30 μm ID columns. Slurry concentration was approximately 2-3 mg/mL for each solvent. Each column was characterized isocratically across of range of operating pressures to determine the reduced van Deemter coefficients. The best overall performance was exhibited by the column packed in acetone, with h_{min} s ranging between 2 and 2.4 and uncorrected c-terms

ranging between 0.4 and 0.5. Packed bed densities, as assessed by analyte retention (k' vs. ΔP), consistently revealed that columns packed in acetone were the least densely packed⁸.

The slurry solvent investigation suggested no clearly superior alternatives to acetone for producing columns with performance characteristics approaching those theoretically predicted. Reduced minimum plate heights remained significantly higher than the best performing columns packed with larger particles, and reduced C-terms were also approximately 2x higher than anticipated. We endeavored, therefore, to employ the findings discussed in Chapter 2 in effort to improve the performance of microcapillary columns packed with 1.0 μm porous BEH particles.

3.2 Experimental

3.2.1 Chemicals

To slurry pack and isocratically characterize columns, HPLC grade acetone and HPLC grade acetonitrile were used as received from Fisher Scientific (Waltham, MA). Deionized water was obtained from a Nanopure ultrapure water system (Barnstead International, Dubuque, IA). Trifluoroacetic acid and formamide were used as received from Sigma Aldrich Chemical Company (Milwaukee, WI). Potassium silicate (Kasil) was used as obtained from PQ Corporation (Valley Forge, IA). The isocratic test mixture used to evaluate column performance contained L-ascorbic acid (Fisher Scientific), 1,4-dihydroxybenzene (hydroquinone), 1,3-dihydroxybenzene (resorcinol), 1,2-dihydroxybenzene (catechol), and 4-methylcatechol from Sigma Chemical Company (St. Louis, MO). All fused silica capillary was obtained from Polymicro Technologies, Inc. (Phoenix, AZ).

3.2.2 Initial Efforts to Pack Capillary Columns With 1.0 μm Porous Particles

In work with 1.0 μm porous BEH particles, the general column packing procedure as outlined in Chapter 2.2.3 was used with slight modifications. All columns discussed in this chapter packed with 1.0 μm particles featured outlet frits that allowed for the insertion of the carbon microfiber used in electrochemical detection. Frits were formed by tapping a $\sim 1\text{mm}$ plug of 1.5 μm nonporous silica particles (EiChrom, Dillon, IL) into the capillary. A tungsten wire was used to push the plug approximately 0.5 mm further into the capillary, and the particles were sintered in place using an electric arc device. During packing, the pressure was increased at a rate of approximately 6,000 psi/cm of packed bed to a maximum pressure of 30,000 psi unless otherwise noted.

Initial efforts to improve the performances of capillary columns packed with 1.0 μm porous BEH particles involved increasing the concentration of the particle slurry used in the packing process, in accordance with findings discussed in Chapter 2.2.6 with respect to 1.9 μm particles. It was suggested there that the improved chromatographic performance observed when using higher concentration slurries may be due to the promotion of aggregation, whereby particles over the entire range of the size distribution are randomly associated in relatively loose networks. As these aggregates of randomly associated particles navigate the column blank and impinge upon the head of the forming column, voids are compressed out and radial homogeneity is preserved. In work with 1.9 μm particles, slurry concentrations of $\sim 100\text{ mg/mL}$ were used, and with sonication, particles were visually well-dispersed. Aggregates tended to settle quickly upon removal from the sonication bath, but stirring within the packing reservoir kept particles suspended. With 1.0 μm particles, large aggregates were observed at much lower concentrations, and particles were not visually well-dispersed with concentrations in excess of 30 mg/mL, even upon sonication. Owing to this

fact and to the scarcity of available particles, ~ 20 mg/mL acetone slurries were used. This is 7–10x more concentrated than slurries used in previous work⁸.

30 μm ID columns were packed to 20-30 cm lengths, consistent with maximum achievable efficiency predictions at 40,000 psi as shown in Figure 3-2. After packing to length, columns were flushed in 50/50 acetonitrile/water and 0.1% TFA at 50,000 psi prior to setting Kasil inlet frits. Column performance was relatively poor in most instances, with peak tailing evident. In many instances, bed collapse was evident as there would be a sudden deterioration in performance when operating at higher pressures, exemplified in Figure 3-3. Examinations of the packed beds afterwards often revealed gaps at different axial positions of the columns while both inlet and outlet frits remained intact. Even under high pressures, these gaps remained fixed, and subsequent sonications of the columns were rarely successful in re-forming continuous packed beds. This suggested that particles were not being leached through the frits, but that the packed beds were inherently unstable in different solvent compositions.

Bed instability was also observed in columns packed with 1.9 μm particles, as described in Chapter 2.2.7. The column beds packed and flushed at lower pressures collapsed upon switching to more aqueous mobile phases. In the current work with 1.0 μm particles, the flushing procedure was modified in attempt to avoid dramatic solvent switching effects that could lead to gaps. Rather than the sudden application of 50,000 psi flushing pressures, several column volumes of mobile phase were pumped through the columns in 5,000 psi increments until the maximum flushing pressure of 50,000 psi was reached. In this way, it was hoped that the packed beds would compress so as to leave little possibility for later bed collapse. The strategy was successful, and Figure 3-4 shows the chromatographic

performance of a 20 cm x 30 μm ID column packed with 1.0 μm BEH particles, operated at 40,000 psi. The van Deemter performances of hydroquinone, catechol, and 4-methyl catechol are shown in Figure 3-5. Minimum reduced plate heights are under 2.0 and uncorrected C-terms are under 0.3 for all analytes.

3.2.3 Effect of Slurry Concentration in Packing 1.5 and 1.0 μm Porous Particles

To assess the improvement in chromatographic performance owed to packing with higher slurry concentrations, two ~ 15 cm x 30 μm ID columns were packed with 1.0 μm BEH particles, one at 20 mg/mL and one at 2 mg/mL in acetone. The shorter column lengths allowed for more characterization of the C-term dominated region at faster linear velocities. Figure 3-6 shows the overlaid van Deemter curves for the two columns. The column packed with the 20 mg/mL slurry performs superiorly with h_{min} s of approximately 1.75 for all four test analytes and uncorrected C-terms ranging between 0.30 and 0.34. In contrast, the column packed with the 2 mg/mL slurry achieves minimum plate heights of 2.2 and C-terms in excess of 0.43. Figures 3-7 and 3-8 show the overlaid retention and resistance to flow data for both columns. Consistent with the 1.9 μm particle data presented in Chapter 2.2.6, the column packed with the higher slurry concentration is less densely packed. Again, this is likely attributable to the relative packing rates of the two columns, which is nearly 10x faster with the 20 mg/mL slurry. With faster packing, there is less time for particles to resituate into larger void regions before being impinged upon and locked into place by subsequently packing particles, thus leading to less densely packed beds.

While performance is markedly improved in comparison to our previous efforts with 1.0 μm particles, the relative performance of larger, 1.9 μm particles is still significantly better, consistently achieving h_{min} s of ~ 1.5 and uncorrected C-terms < 0.20 . As an

intermediate between the 1.9 and 1.0 μm particles, the slurry concentration experiment was performed with 1.5 μm BEH particles⁹. Two $\sim 25\text{ cm} \times 50\text{ }\mu\text{m}$ ID columns were packed with slurry concentrations of 30 mg/mL and 3 mg/mL. Figure 3-9 shows the overlaid van Deemter curves for the two columns, and the column packed with the 30 mg/mL slurry significantly outperforms the column packed at the lower concentration. Reduced minimum plate heights ranged between 1.7 and 1.75, and C-terms between 0.27 and 0.30. Resorcinol, characteristically the poorest performing of the test analytes, had a h_{min} and C-term of 1.8 and 0.35, respectively. In general, these two assessors correspond to improved relative performance when moving from columns packed with smaller to larger particle diameters. Again, retention data (Figure 3-10) and resistance to flow data (Figure 3-11) show that the column packed with the 30 mg/mL slurry was less densely packed than the column packed with 3 mg/mL.

3.2.4 Effect of Column ID on Performance of Columns Packed with 1.5 and 1.0 μm Particles

In the experiments involving the assessment of column performance with respect to slurry concentration for all three particle diameters (1.9, 1.5, and 1.0 μm), column inner diameters were selected from availability such that d_c/d_p would be similar in each case. Performance with respect to column ID was also assessed for both 1.5 and 1.0 μm particles. 30 mg/mL slurries of 1.5 μm particles in acetone were used to pack 30, 50, and 75 μm ID columns, and performance was assessed. Figure 3-12 shows the overlaid performance curves for each of the four retained test analytes. There is a clear trend toward better performance with smaller column diameters, although the calculated van Deemter coefficients are not especially revealing as to where this improvement originates. It seems clear that the C-terms

of the 30 μm ID column are lower than those of the two larger ID columns, but there is too much error in the A-terms to draw significant conclusions about relative axial homogeneities.

20 mg/mL slurries of 1.0 μm particles in acetone were used to pack 15, 30, and 50 μm ID columns. Notably, for the 15 μm ID column at 30,000 psi, packing was balky and prone to frequent stops. At 24,000 psi, however, packing was continuous. Figure 3-13 shows the overlaid van Deemter curves and calculated coefficients for hydroquinone, catechol, and 4-methyl catechol considered in isolation. Once again, narrower ID columns outperform larger ID columns. There is a clear trend toward increasing C-terms with larger IDs, but A-terms actually decrease. Because these columns were relatively long at ~ 30 cm and run with maximum operating pressures of 40,000 psi, there is insufficient characterization of the C-term region. Characterization at faster linear velocities would likely have served to give more accurate calculations of the A- and C-terms.

3.2.5 Effect of Packing Pressure on Performance of Columns Packed with 1.0 μm Particles

It was consistently observed that columns with narrower inner diameters (≤ 20 μm) could not be packed with high-concentration slurries at 30,000 psi without stopping frequently, thus requiring depressurization and rapid re-pressurization to initiate packing again. With each stoppage there exist a period of time where the head of the column is impinged upon only by solvent. This allows sufficient time for the reorganization of particles into void regions, leading to denser packings which we have observed to perform poorly. Rapid depressurization would certainly negate this effect, but at the cost of greater disturbance to the already packed bed. The problem could be remedied by either decreasing the maximum packing pressure or by decreasing the slurry concentration to achieve continuous packing. These observations suggest a relationship between slurry concentration,

packing pressure, and effective aggregate size. As the size of the aggregates approach the diameter of the column, packing becomes balky. Aggregate size appears to increase with both packing pressure and slurry concentration.

The effect of packing pressure on performance of columns packed with 1.0 μm particles was assessed by packing three $\sim 20\text{ cm} \times 30\text{ }\mu\text{m}$ columns at maximum pressures of 10,000 psi, 20,000 or 30,000 psi with a 20 mg/mL acetone slurry. All three columns packed continuously, regardless of maximum packing pressure, and the rates of packing accorded with packing pressure. Columns were subsequently flushed at 50,000 psi in 50/50 acetonitrile/water and 0.1% TFA prior to setting the inlet frits. Columns were isocratically characterized with electrochemical detection of a test mixture containing ascorbic acid, hydroquinone, catechol, and 4-methyl catechol. Figure 3-14 shows the overlaid van Deemter curves for each of the retained analytes considered in isolation. Examination of the calculated van Deemter coefficients reveals that all three columns perform very similarly, with reduced minimum plate heights ≤ 2.0 and C-terms ranging between 0.30 and 0.36. It therefore appears that - at these column lengths, particle diameters, and operating pressures - so long as continuous packing can be maintained, ultimate chromatographic performance is relatively unaffected by packing pressure.

3.2.5 Evaluation of 10 μm ID Columns Packed with 1.9, 1.5, and 1.0 μm Porous Particles

Although reduced minimum plate heights under 2.0 have been achieved with great reproducibility, the uncorrected C-terms of columns packed with 1.0 μm particles are consistently higher than theoretically predicted values (~ 0.30 vs. 0.20). One means to assess the performance of a packing material somewhat independently of packed bed structure is to pack columns of sufficiently narrow inner diameter. As described in Chapter 2.1.2,

cylindrically confined packings of spherical particles tend to exhibit three distinctive regions of interstitial porosity profiles. This leads to radial heterogeneities and additional eddy-dispersion contributions which are responsible for approximately one-half of theoretically achievable minimum plate heights. Firstly, a geometrical effect is induced by the walls of the column, along which flow tends to be fastest. A second region originates from the frictional effects of packing, causing packing density in the regions near the walls to be higher than the third distinctive region – the bulk core of the column. As column diameter becomes smaller, the core region of the packed bed effectively disappears. The packing structure becomes more homogeneous and there is very rapid diffusional averaging over the cross-section of the column.

In order to better assess the performance potentials of 1.9, 1.5, and 1.0 μm particles, and to compare them independently of packing structures, each particle type was packed in 10 μm ID capillaries. Although d_c/d_p was not the same for all three particle sizes, this was the smallest available inner diameter that could accommodate the insertion of the $\sim 8 \mu\text{m}$ carbon microfiber used in electrochemical detection. As mentioned in the previous section, as column ID becomes smaller, the packing pressure and/or the particle slurry concentration must be reduced to facilitate continuous packing. As such, a 25.8 cm column was packed with a 5 mg/mL slurry of 1.9 μm BEH particles at 18,000 psi; a 26.3 cm column was packed with a 30 mg/mL slurry of 1.5 μm BEH particles at 15,000 psi; and a 14.3 cm column was packed with a 20 mg/mL slurry of 1.0 μm BEH particles at 15,000 psi. All three columns were subsequently flushed at 50,000 psi and isocratically characterized in 50/50 acetonitrile/water and 0.1% TFA. Figure 3-15 shows the overlaid van Deemter curves for hydroquinone, catechol, and 4-methyl catechol considered in isolation. Each of the reduced

minimum plate heights and C-terms are the best observed in this dissertation work with respect to each particle diameter. It is still the case, however, that there is a clear trend toward better relative performance when moving from smaller to larger particle diameters. h_{\min} s and C-terms for the 1.9 μm particles range between 1.2 – 1.3 and 0.14 – 0.15, respectively. For 1.5 μm particles, h_{\min} s and C-terms range between 1.5 – 1.6 and 0.20 – 0.22. Finally, for 1.0 μm particles, h_{\min} s and C-terms range between 1.6 – 1.7 and 0.27 – 0.28. Investigators have reported that H_{\min} becomes smaller for smaller particle diameters, but that h_{\min} is higher than expected for sub-2 μm particles^{10,11}. This suggests that the advantage of using smaller particle diameters is not as large as expected. One study has also suggested that the contribution of desorption of the analyte from the stationary phase, C_s , becomes a significant contributor to C_{total} as particle diameter becomes smaller. In other words, desorption time becomes significant compared to the time it takes to diffuse in and out of a particle. As such, a theoretical limit of the C-term is approached¹².

Considering the van Deemter coefficients shown in Figure 3-15 to be the best achievable for each particle diameter (to date), the utility of 1.0 μm particles in preference to larger 1.9 μm particles can be assessed using kinetic plots in the same way described in Section 3.1.2. Figure 3-16 shows these plots for an operating pressure of 40,000 psi. The solid traces represent the performances of 1.9 and 1.0 μm particles using the actual van Deemter coefficients calculated from the 10 μm ID columns. The dashed red trace represents the theoretical performance of 1.0 μm particles if they performed as well as the 1.9 μm particles (i.e. the reduced van Deemter coefficients calculated from the 1.9 μm particles are applied to the 1.0 μm particles).

In comparing the actual performances of the 1.0 and 1.9 μm particles, it can be seen from the point of intersection that the preferential use of the smaller particles occurs with column dead times faster than ~ 140 s. In this time, it is estimated that both particle sizes can generate approximately 170,000 plates. If greater efficiencies are required, the 1.9 μm particles should be used; if fewer plates are required, the smaller particles can generate more plates in a given time or a given number of plates in less time.

Comparison of the actual performance of the 1.0 μm particles to the theoretically achievable performance can be done in a number of informative ways. The greatest differences are observed in very fast analyses which generate less than 100,000 plates. For example, with a 10 s column dead time, $\sim 31,000$ plates are estimated using the real van Deemter coefficients. Theoretically, $> 45,000$ plates can be generated if the 1.0 μm particles performed as well as the larger particles – a 50% increase. Likewise, if 100,000 plates are needed for a particular separation, actual performance predicts a required column dead time of ~ 44 s. Theoretically, this separation could be performed nearly 50% faster, with a column dead time of ~ 30 seconds. Considering the intersection point of the theoretical performance of 1.0 μm particles and actual performance of 1.9 μm particles, preferred use of the smaller particles would be extended to column dead times of approximately 180 s, in which $\sim 210,000$ plates could be generated.

3.3 Conclusions

Slightly modified column packing procedures for fully porous 1.0 μm BEH particles have been used to greatly improve the performance of microcapillary columns packed with these particles. Previous work in our lab focused primarily on achieving stable, densely packed beds by the use of various slurry solvents to effectively disperse individual particles

during the packing process. In this way it was hoped that large void regions would be eliminated and chromatographic performance would be improved. Investigation of several solvents and binary solvent mixtures, however, revealed acetone slurries to produce the most efficient columns, although reduced minimum plate heights and C-terms were still relatively high. Findings presented in Chapter 2 of this work reiterated the importance of speed during the column packing process and also the benefits of packing with higher concentration slurries. By promoting particle aggregation, concentrated slurries not only increase packing rates, but it is hypothesized that they also preserve homogeneity of the polydisperse packing material across the column diameter.

Concentrated slurries and efforts to prevent the formation of gaps arising from mobile phase composition changes have produced the best columns to date for 1.0 μm particles, with minimum plate heights of approximately 1.8 μm and uncorrected C-terms of ~ 0.30 . Interestingly, there is a clear trend toward better relative performance when moving from smaller to larger particle diameters, as reflected in many of the experiments described in this chapter. This is shown most clearly in Figure 3-16, and in the calculated C-terms for the 10 μm ID columns. Also somewhat surprisingly, there is little difference in performance between 30 and 10 μm ID columns packed with 1.0 μm particles. Figure 3-17 shows the kinetic performances of the 30 μm ID column packed with a 20 mg/mL slurry from Section 3.2.3 and the 10 μm ID column from Section 3.2.5. Significant differences are not manifest until the B-term dominated portions of the curves, which correspond to column dead times where the use of columns packed with 1.9 μm particles is preferred. Overall, further improvements in the relative performance of 1.0 μm particles (i.e. reductions of the uncorrected C-terms to ≤ 0.20) accomplishes little in extending the utility of these particles

over 1.9 μm particles unless much higher operating pressures become routine. On the other hand, further improvements would permit for very fast analyses which do not require a large number of theoretical plates to be performed approximately 50% faster.

3.4 References

- ¹ Desmet, G.; Cabooter, D.; Gzil, P.; Verelst, H.; Mangelings, D.; Heyden, Y.V.; Clicq, D. *Journal of Chromatography A* **2006**, 1130, 158-166.
- ² Guiochon, G.; Gritti, F. *Journal of Chromatography A* **2012**, 1218, 1915-1938.
- ³ Unger, K.K.; Huber, M.; Hennessey, T.P.; Hearn, M.T.W.; Walhagen, K. *Analytical Chemistry* **2002**, 74, 200A-207A.
- ⁴ Wei, B.; Malkin, D.S.; Wirth, M.J. *Analytical Chemistry* **2010**, 82, 10216-10221.
- ⁵ Wei, B.; Rogers, B.J.; Wirth, M.J. *Journal of the American Chemical Society* **2012**, 134, 10780-10782.
- ⁶ MacNair, J.E.; Patel, K.D.; Jorgenson, J.W. *Analytical Chemistry* **1999**, 71, 700-708.
- ⁷ Neue, U.D. *HPLC Columns: Theory, Technology, and Practice*; Wiley-VCH, Inc.: New York, NY, **1997**.
- ⁸ Lieberman, R.A. *UNC Doctoral Dissertation* **2009**.
- ⁹ Mellors, J.S.; Jorgenson, J.W. *Analytical Chemistry* **2004**, 76, 5441-5450.
- ¹⁰ De Villiers, A.; Lestremau, F.; Szucs, R.; Gelebart, S. David, F.; Sandra, P. *Journal of Chromatography A* **2006**, 1127, 60.
- ¹¹ Nguyen, D.T.T.; Duillarme, D.; Rudaz, S.; Veuthey, J.L. *Journal of Chromatography A* **2006**, 1128, 105.
- ¹² Wirth, M.J. *Journal of Chromatography A* **2006**, 1148, 128-130.

3.5 Figures

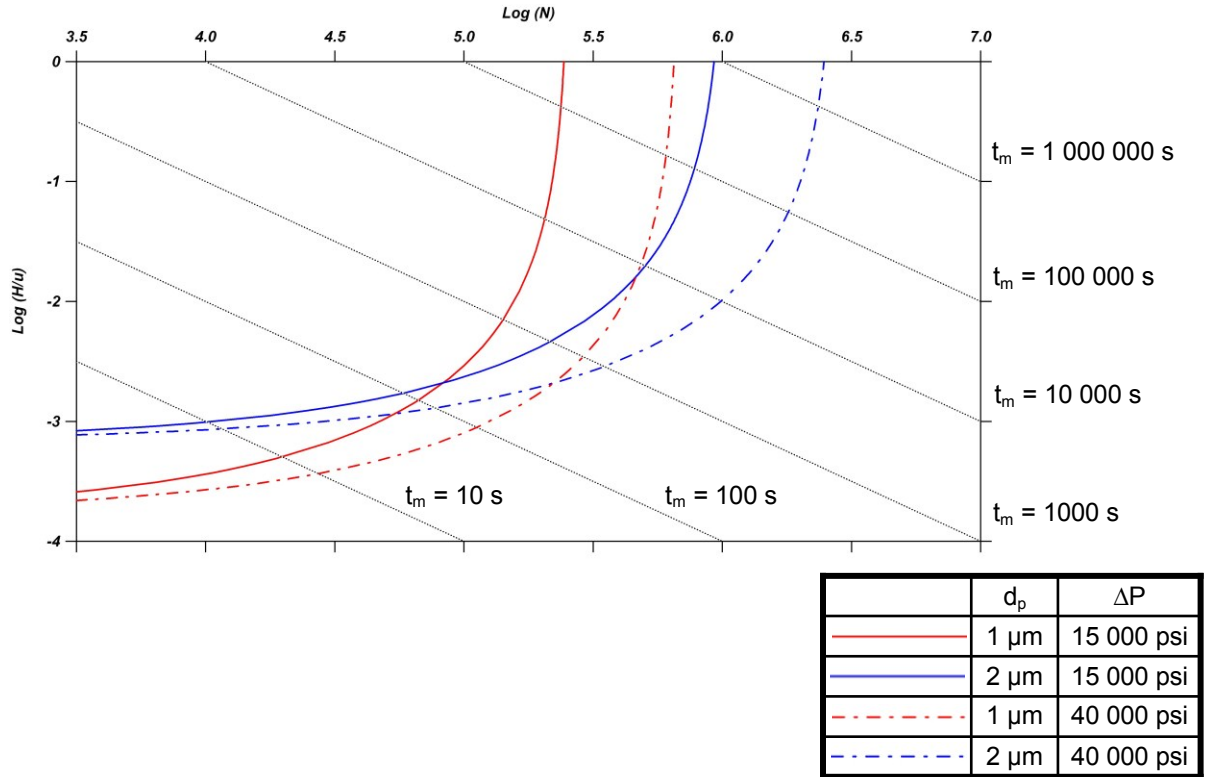


Figure 3-1: Kinetic plots showing the performance of 1 vs. 2 μm particles with pressure limitations of 15,000 psi (solid lines) and 40,000 psi (dashed lines). Plots are constructed assuming viscosity, $\eta = 1$ cP; interparticle porosity, $\varepsilon_i = 0.4$; analyte diffusion coefficient, $D_m = 1 \times 10^{-5} \text{ cm}^2/\text{s}$; reduced van Deemter coefficients $A = 1.5$, $B = 1.0$, and $C = 0.17$.

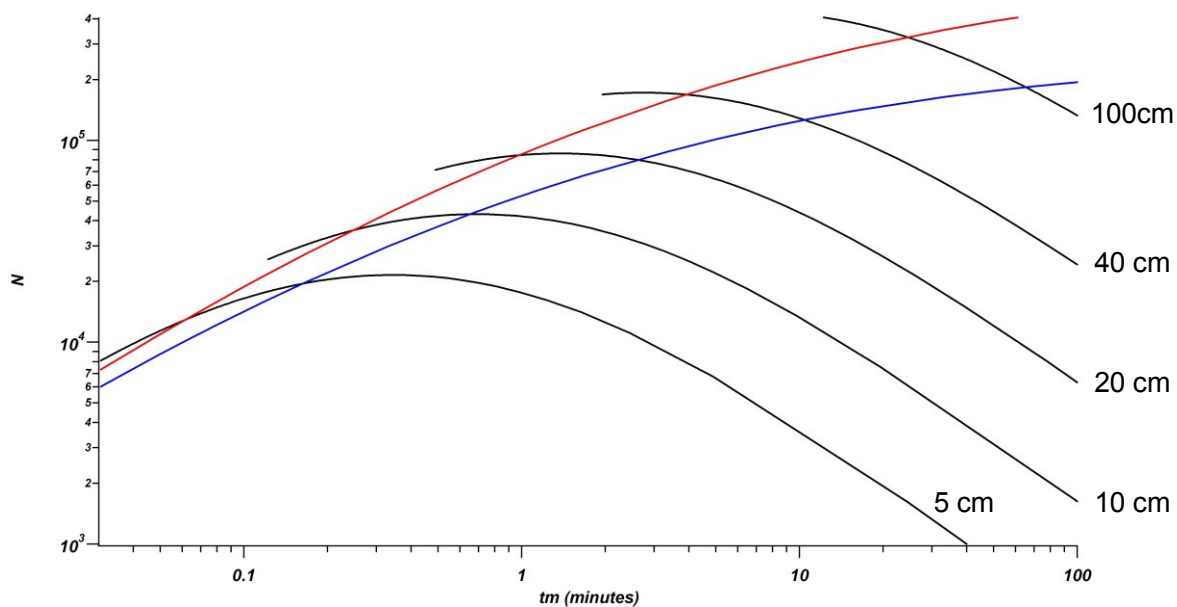


Figure 3-2: Expected performance of columns of various lengths packed with 1 μm particles operated at 15,000 psi (blue trace) and 40,000 psi (red trace). Plots are constructed assuming viscosity, $\eta = 1$ cP; interparticle porosity, $\varepsilon_i = 0.4$; analyte diffusion coefficient, $D_m = 1 \times 10^{-5}$ cm^2/s ; reduced van Deemter coefficients $A = 1.5$, $B = 1.0$, and $C = 0.17$.

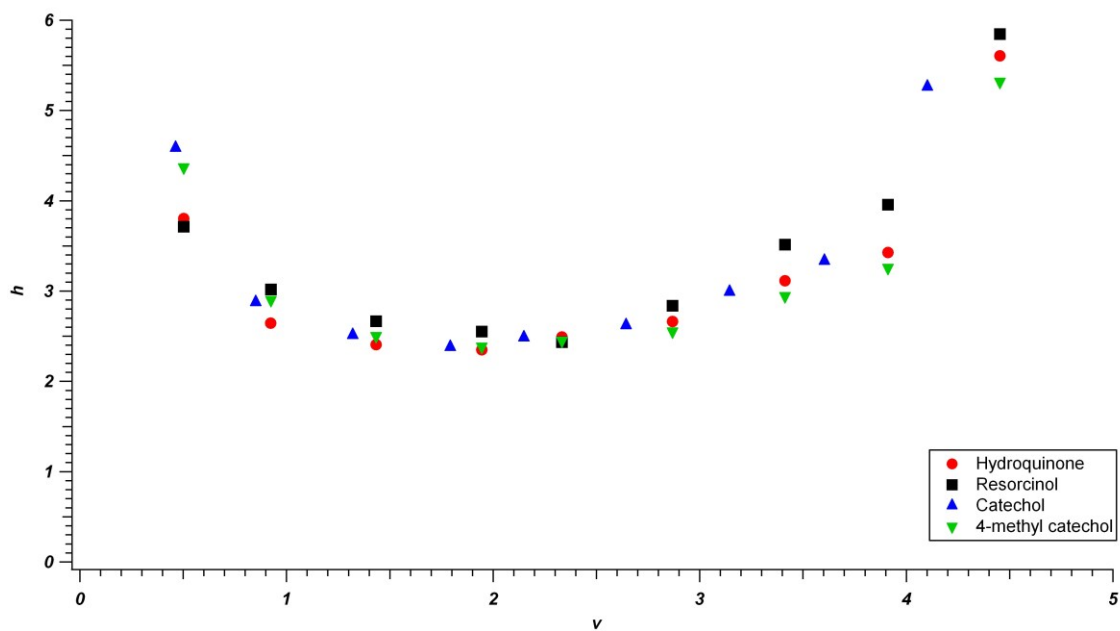


Figure 3-3: h vs. v plots for 19 cm x 30 μ m ID column packed with 1.0 μ m BEH particles run in 50/50 acetonitrile/water and 0.5% TFA. The sudden deterioration in performance at higher linear velocities was caused by bed collapse.

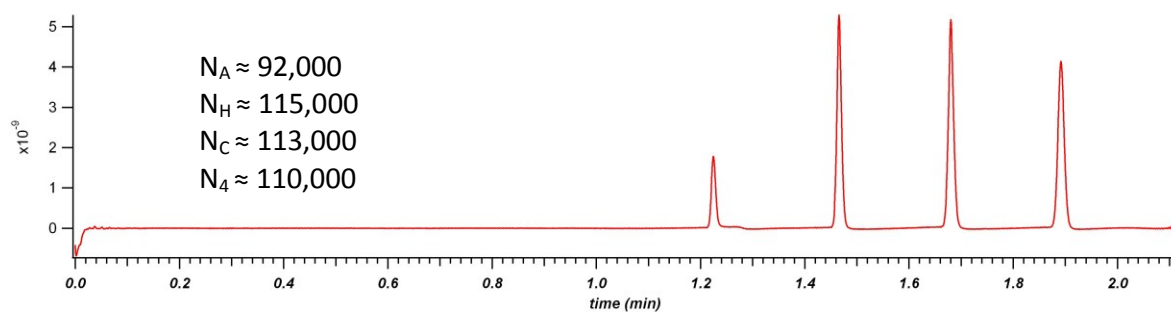


Figure 3-4: Chromatogram of 20 cm x 30 μm ID column packed with 1.0 μm BEH operated at 40,000 psi in 50/50 acetonitrile/water and 0.1% TFA.

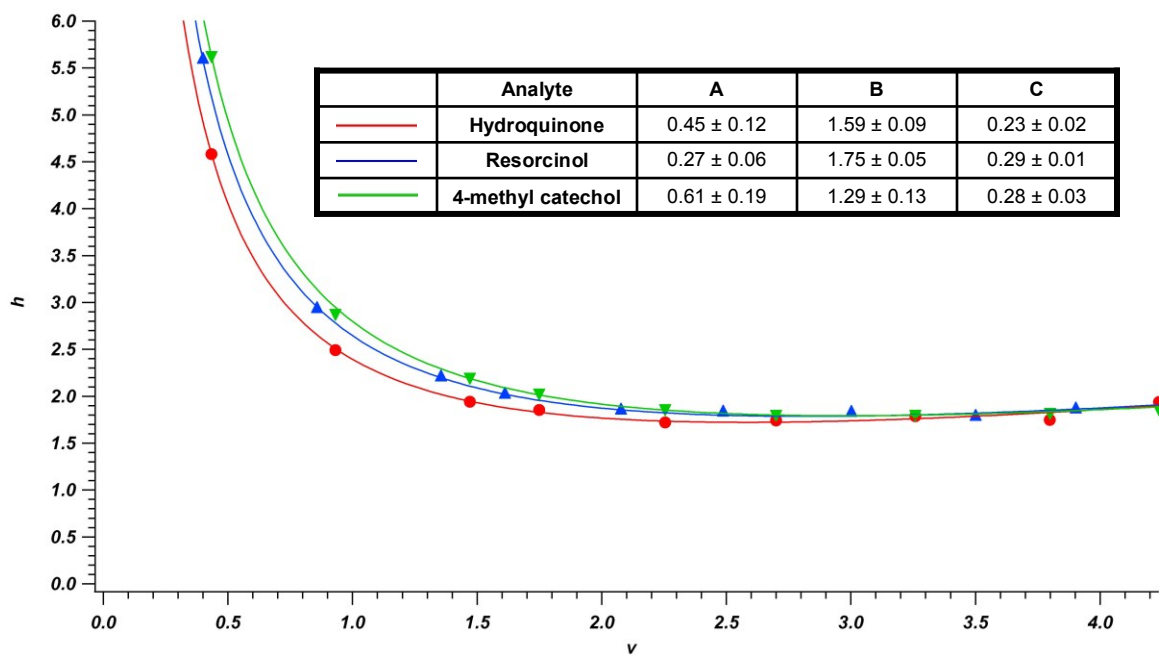


Figure 3-5: van Deemter performance of a 20 cm x 30 μm ID column packed with 1.0 μm BEH particles run in 50/50 acetonitrile/water and 0.5% TFA.

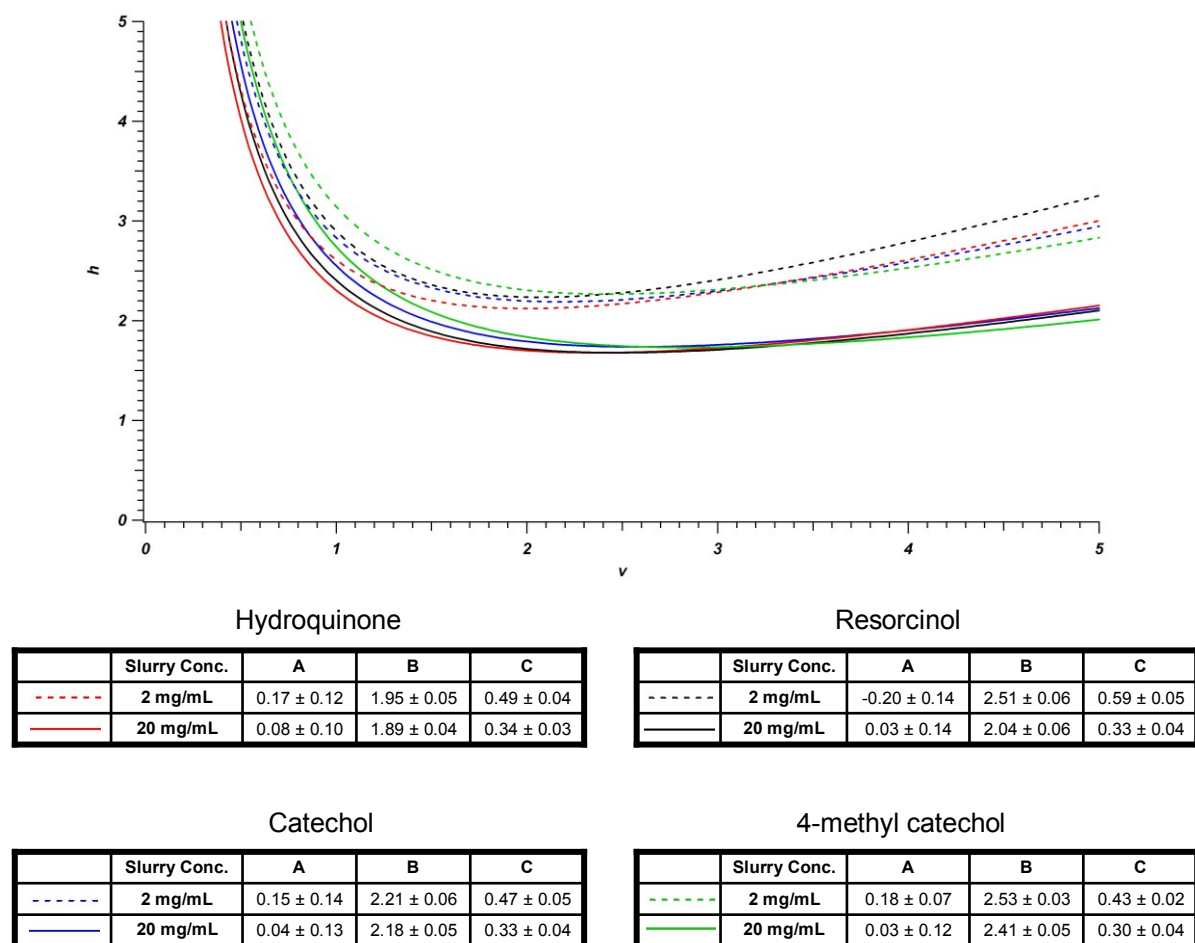


Figure 3-6: Comparison of performances of 30 μm ID columns packed with 2 mg/mL (14.6 cm) and 20 mg/mL (15.1 cm) slurries of 1.0 μm BEH particles.

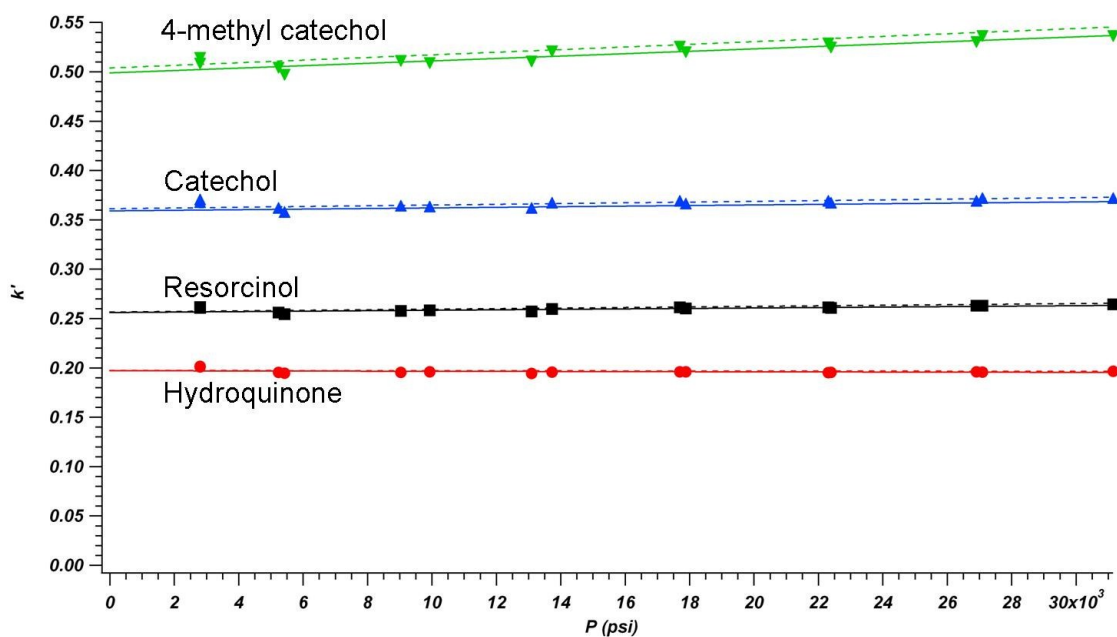


Figure 3-7: Comparison of column retention for ~ 15 cm x 30 μ m ID columns packed with 2 (dashed lines) and 20 mg/mL (solid lines) slurries of 1.0 μ m BEH particles.

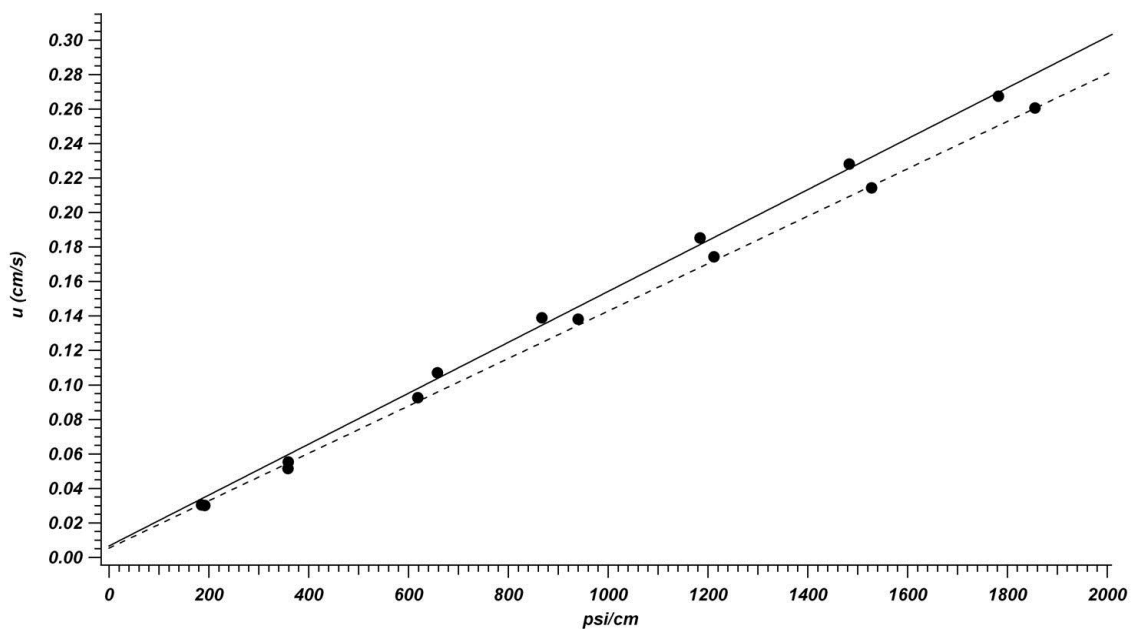
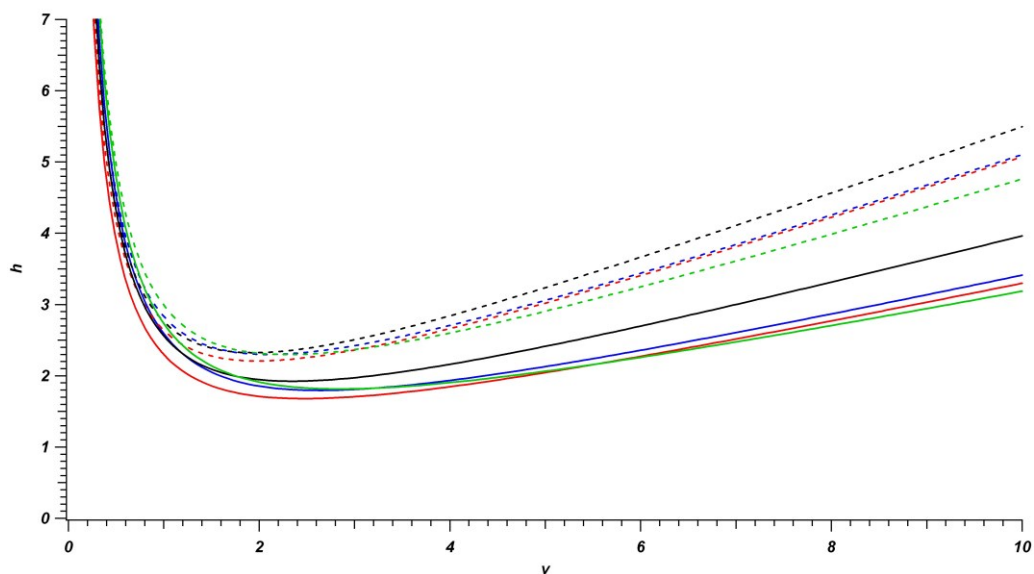


Figure 3-8: Comparison of column resistance to flow for ~ 15 cm x $30\ \mu\text{m}$ ID columns packed with 2 (dashed line) and 20 (solid line) mg/mL slurries of $1.0\ \mu\text{m}$ BEH particles.



Hydroquinone

	Slurry Conc.	A	B	C
---	3 mg/mL	0.44 ± 0.11	1.75 ± 0.07	0.45 ± 0.02
—	30 mg/mL	0.27 ± 0.06	1.75 ± 0.05	0.29 ± 0.01

Resorcinol

	Slurry Conc.	A	B	C
---	3 mg/mL	0.42 ± 0.16	1.85 ± 0.11	0.49 ± 0.03
—	30 mg/mL	0.29 ± 0.12	2.18 ± 0.08	0.35 ± 0.02

Catechol

	Slurry Conc.	A	B	C
---	3 mg/mL	0.43 ± 0.11	1.96 ± 0.07	0.45 ± 0.02
—	30 mg/mL	0.23 ± 0.09	2.07 ± 0.07	0.30 ± 0.01

4-methyl catechol

	Slurry Conc.	A	B	C
---	3 mg/mL	0.40 ± 0.12	2.18 ± 0.08	0.41 ± 0.02
—	30 mg/mL	0.29 ± 0.10	2.18 ± 0.08	0.27 ± 0.01

Figure 3-9: Comparison of performances of 25.4 cm x 50 μ m ID columns packed with 3 mg/mL and 30 mg/mL slurries of 1.5 μ m BEH particles.

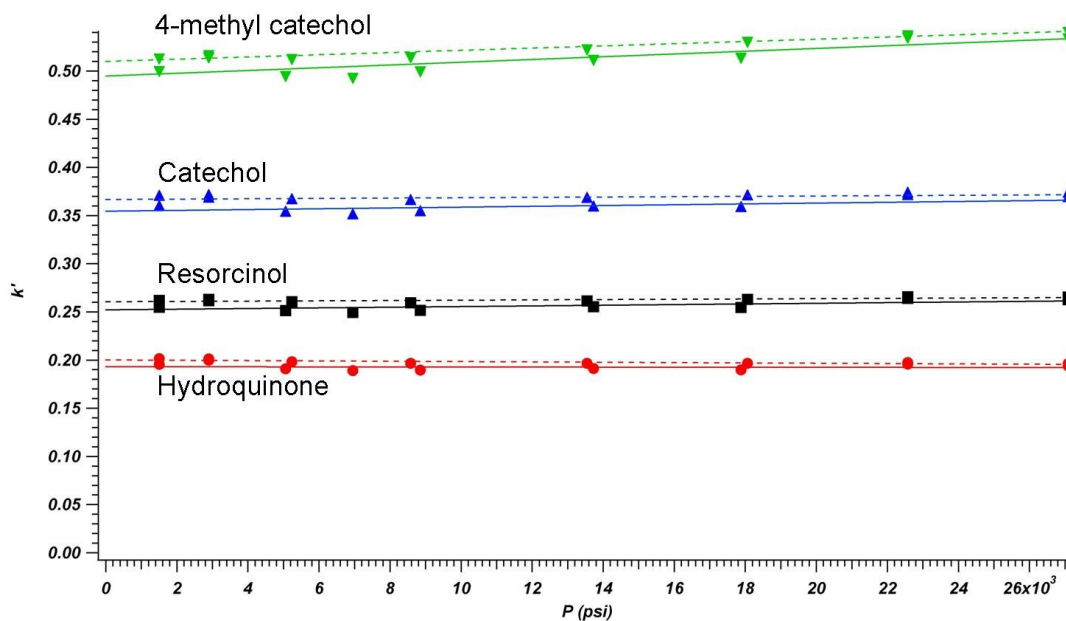


Figure 3-10: Comparison of column retention for 25.4 cm x 50 μm ID columns packed with 3 (dashed lines) and 30 mg/mL (solid lines) slurries of 1.5 μm BEH particles.

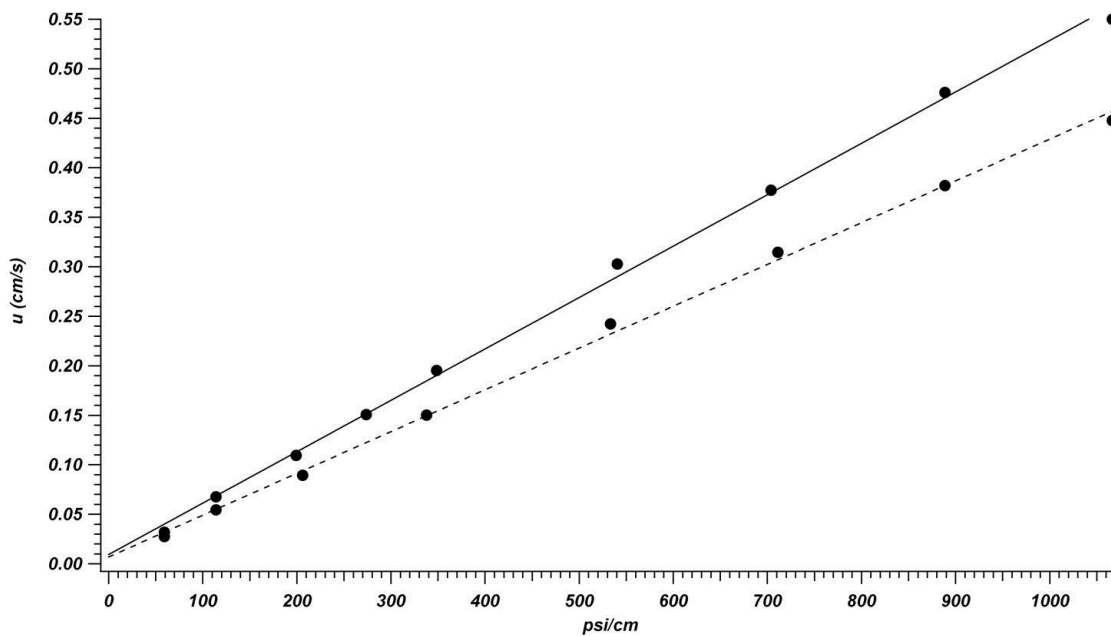


Figure 3-11: Comparison of column resistance to flow for 25.4 cm x 30 μm ID columns packed with 3 (dashed line) and 30 (solid line) mg/mL slurries of 1.5 μm BEH particles.

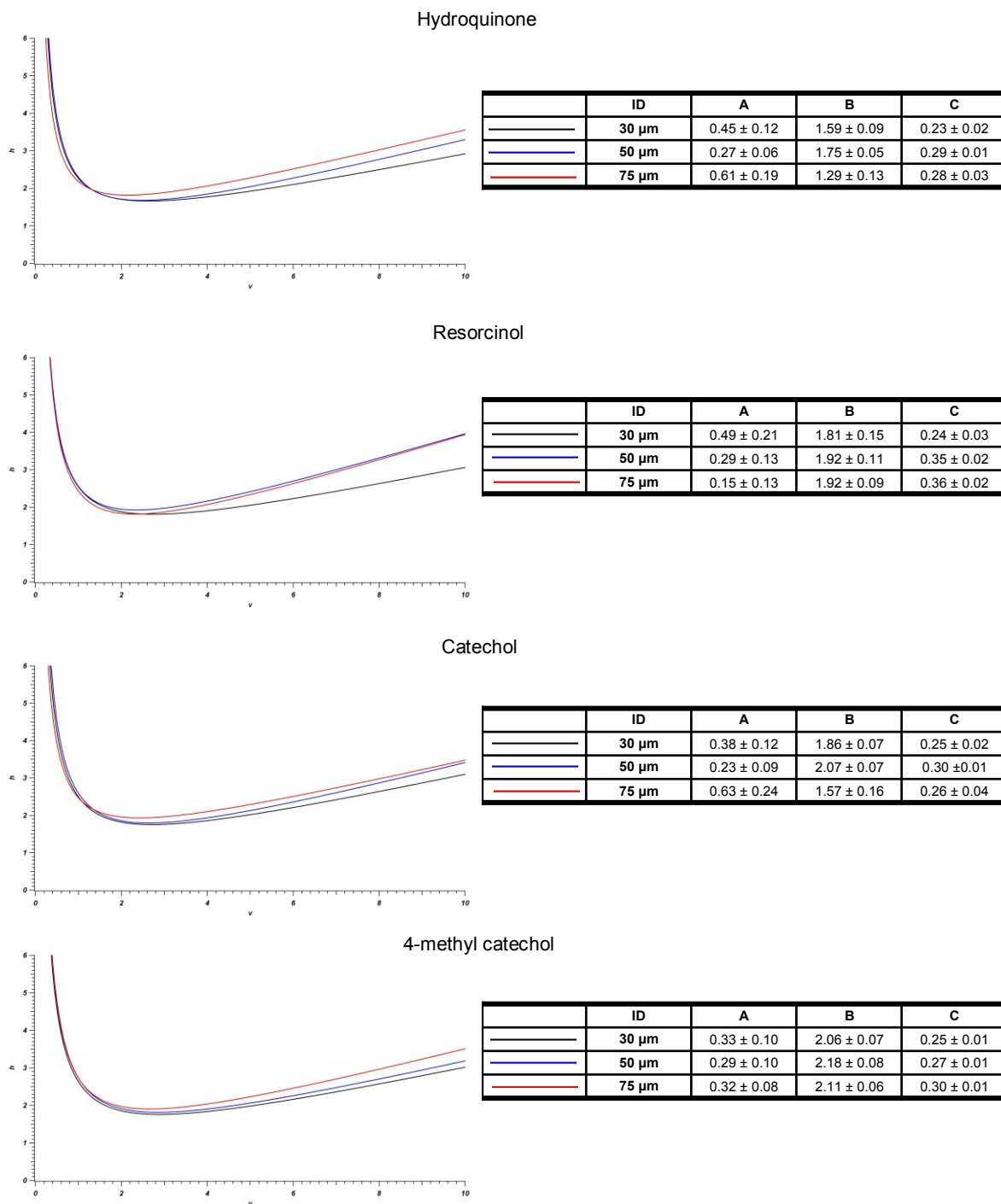


Figure 3-12: Effect of column inner diameter on chromatographic performance for columns packed with 1.5 μm BEH particles. Columns dimensions were 25.7 cm x 30 μm ID, 25.4 x 50 μm ID; 25.8 x 75 μm .

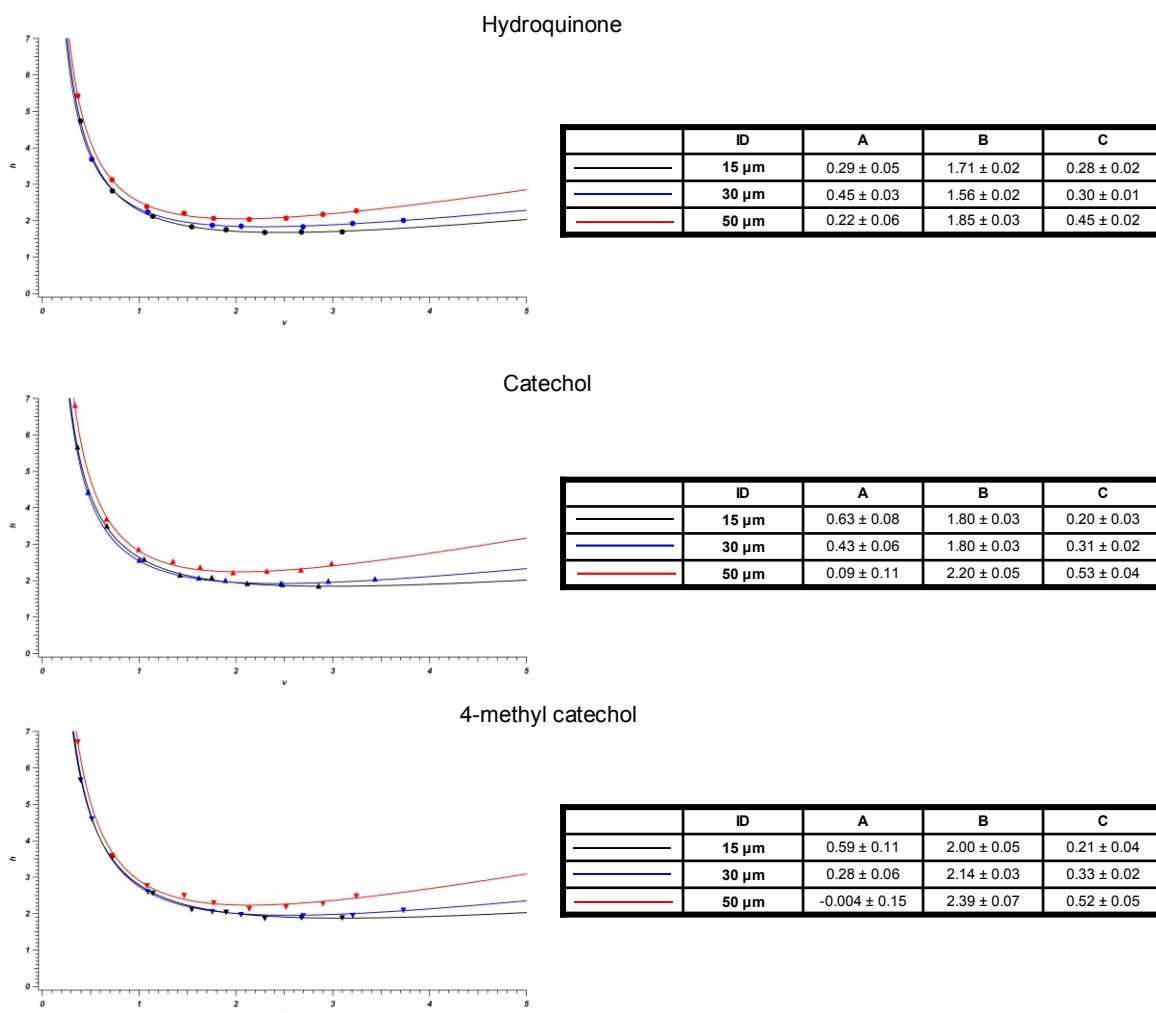
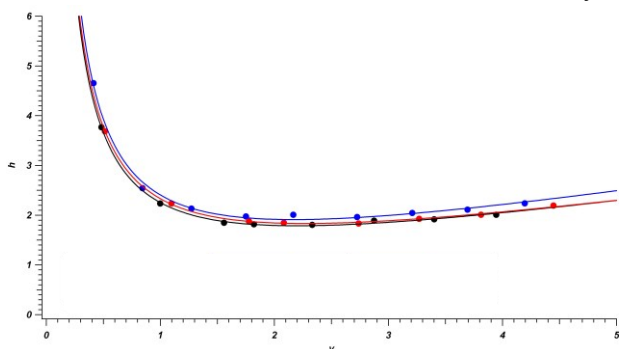


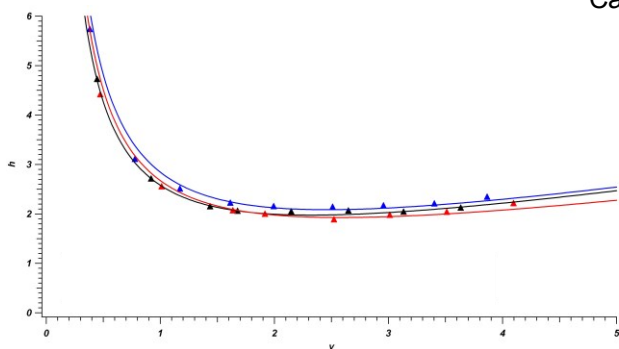
Figure 3-13: Effect of column inner diameter on chromatographic performance for columns packed with 1.0 μm BEH particles. Columns dimensions were 28 cm x 15 μm ID; 20 cm x 30 μm ID; 30.2 x 50 μm .

Hydroquinone



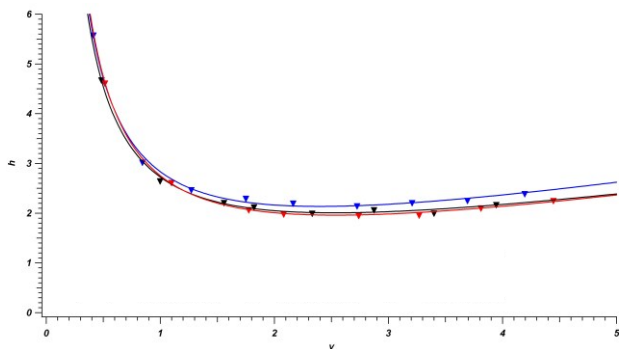
	Packing Pressure	A	B	C
—	10 kpsi	0.36 ± 0.06	1.57 ± 0.03	0.32 ± 0.02
—	20 kpsi	0.34 ± 0.11	1.70 ± 0.06	0.36 ± 0.03
—	30 kpsi	0.42 ± 0.04	1.60 ± 0.02	0.31 ± 0.01

Catechol



	Packing Pressure	A	B	C
—	10 kpsi	0.38 ± 0.08	1.86 ± 0.04	0.34 ± 0.03
—	20 kpsi	0.34 ± 0.08	2.15 ± 0.04	0.36 ± 0.02
—	30 kpsi	0.38 ± 0.07	1.99 ± 0.05	0.30 ± 0.02

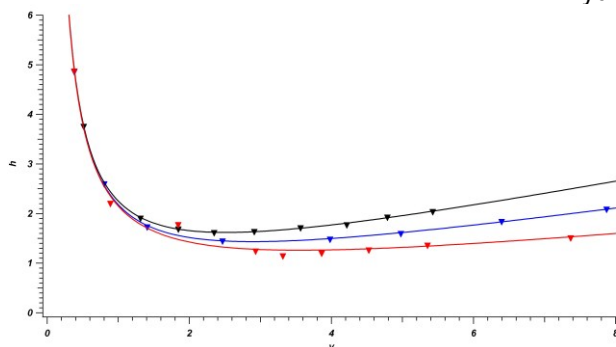
4-methyl catechol



	Packing Pressure	A	B	C
—	10 kpsi	0.45 ± 0.11	1.97 ± 0.06	0.31 ± 0.03
—	20 kpsi	0.42 ± 0.11	2.06 ± 0.06	0.36 ± 0.03
—	30 kpsi	0.26 ± 0.05	2.16 ± 0.03	0.33 ± 0.01

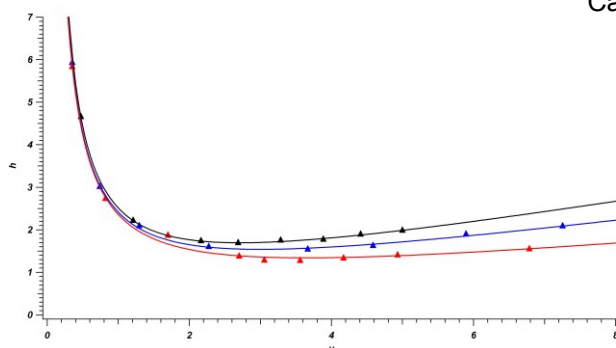
Figure 3-14: Effect of maximum packing pressure on chromatographic performance for columns packed with 1.0 μm BEH particles. Columns dimensions were 19.8 cm x 30 μm ID (10,000 psi); 20 cm x 30 μm ID (20,000 psi); and 20 x 30 μm (30,000 psi).

Hydroquinone



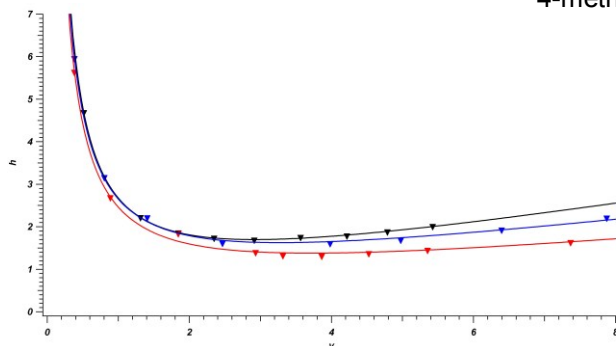
	d_p	A	B	C
—	1.0 μm	0.24 ± 0.03	1.74 ± 0.02	0.27 ± 0.01
—	1.5 μm	0.23 ± 0.03	1.74 ± 0.02	0.21 ± 0.005
—	1.9 μm	0.29 ± 0.07	1.72 ± 0.06	0.14 ± 0.01

Catechol



	d_p	A	B	C
—	1.0 μm	0.18 ± 0.03	2.06 ± 0.02	0.28 ± 0.01
—	1.5 μm	0.23 ± 0.05	1.97 ± 0.03	0.22 ± 0.01
—	1.9 μm	0.27 ± 0.05	1.94 ± 0.03	0.15 ± 0.01

4-methyl catechol



	d_p	A	B	C
—	1.0 μm	0.15 ± 0.02	2.26 ± 0.01	0.27 ± 0.005
—	1.5 μm	0.33 ± 0.08	2.13 ± 0.04	0.20 ± 0.01
—	1.9 μm	0.30 ± 0.06	2.06 ± 0.05	0.15 ± 0.01

Figure 3-15: Performance of 10 μm ID columns packed with 1.0 μm BEH (14.3 cm), 1.5 μm BEH (26.3 cm), and 1.9 μm BEH (25.8 cm).

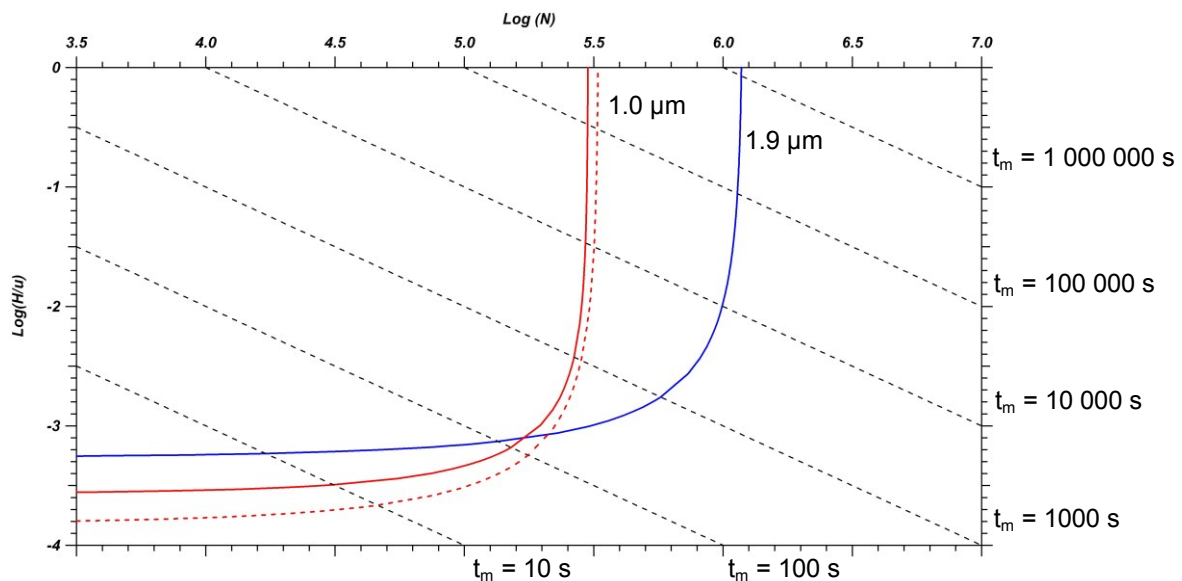


Figure 3-16: Kinetic plots showing the performance of 1.0 vs. 1.9 μm particles with pressure limitations of 40,000 psi. Reduced van Deemter coefficients of $A=0.30$, $B=2.06$, and $C=0.15$ are used in the construction of the 1.9 μm curve (blue trace) and the theoretical 1.0 μm curve (dashed red trace). Reduced van Deemter coefficients of $A=0.15$, $B=2.26$, and $C=0.27$ are used in the construction of the 1.0 μm curve (red trace). Plots are constructed assuming viscosity, $\eta = 1 \text{ cP}$; interparticle porosity, $\varepsilon_i = 0.4$; analyte diffusion coefficient, $D_m = 1 \times 10^{-5} \text{ cm}^2/\text{s}$.

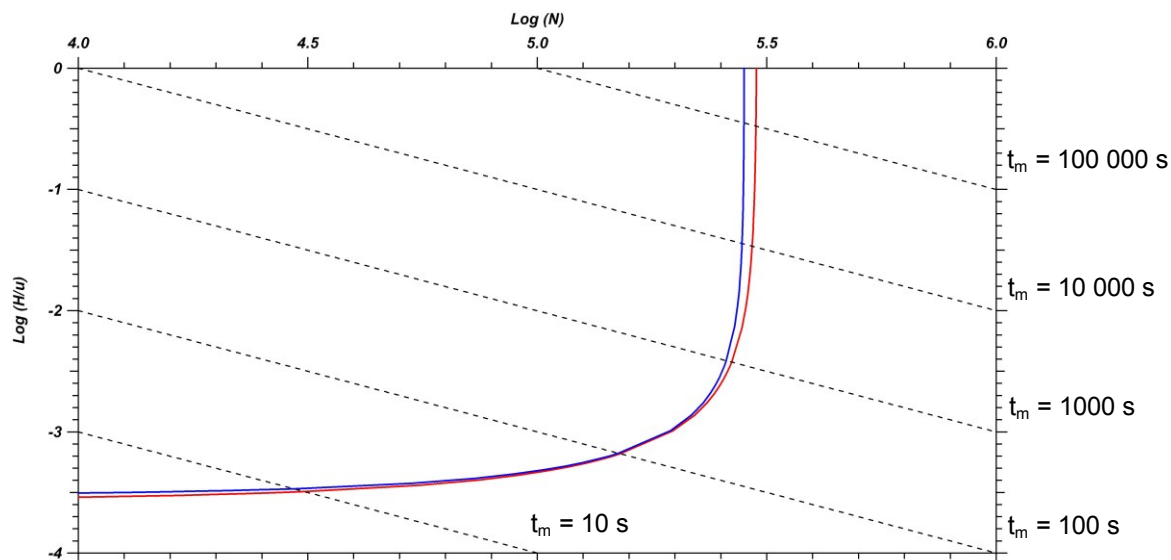


Figure 3-17: Kinetic plots showing the performance of 1.0 μm particles with pressure limitations of 40,000 psi packed in 10 μm and 30 μm ID capillary. Reduced van Deemter coefficients of $A=0.15$, $B=2.26$, and $C=0.27$ are used in the construction of the 10 μm ID curve (red trace). Reduced van Deemter coefficients of $A=0.03$, $B=2.41$, and $C=0.30$ are used in the construction of the 30 μm ID curve (blue trace). Plots are constructed assuming viscosity, $\eta = 1 \text{ cP}$; interparticle porosity, $\varepsilon_i = 0.4$; analyte diffusion coefficient, $D_m = 1 \times 10^{-5} \text{ cm}^2/\text{s}$.

CHAPTER 4: LONG MICROCAPILLARY COLUMNS AT ELEVATED TEMPERATURE AND PRESSURE FOR HIGH-EFFICIENCY ONE-DIMENSIONAL SEPARATIONS

4.1 Introduction

High separation efficiency in liquid chromatography is a persistent ambition. The advent of ultrahigh pressure liquid chromatography (UHPLC) ushered in a new era of separations where speed and efficiency were effectively combined. Commercialization of the technology has emphasized a reduction in analysis time congruent with the use of moderate-length (10-25 cm) columns packed with $\sim 2\ \mu\text{m}$ particles and operated at 1000 bar ($\sim 15,000\ \text{psi}$) to provide up to 60,000 theoretical plates. Highly complex samples, however, such as those encountered in “-omics” fields, call for even greater efficiencies, comparable to those available with capillary electrophoresis and gas chromatography. This chapter explores the efficiency gains possible in combining ultrahigh pressure (up to 50,000 psi), small particles (sub- $2\ \mu\text{m}$), and elevated temperatures (up to 85°C) in pursuit of that goal.

4.1.1 Survey of High-Efficiency Packed-Column Liquid Chromatography Separations

The most straight-forward way to generate higher efficiencies in one-dimensional liquid chromatography is to pack longer separation paths. An early attempt at this approach is represented by Scott and Kucera, who constructed a 14 m long column by coupling 1 m x 1 mm columns packed with $5\ \mu\text{m}$ particles in series. The column was used to separate C2 to C8 alkylbenzenes on the basis of exclusion and produced 650,000 plates in 9 hours. Under retention conditions, approximately 510,000 plates were achieved¹. Menet et al. attempted to

achieve the one-million plate mark, also by coupling 1 m x 1 mm columns in series, but packed with 7-8 μm particles, to a total length of 22 m. Operated at 600 atm (8,800 psi), 920,000 plates were generated for a dead-time marker in approximately 19 hours. Decreased efficiencies were observed for more retained species², and approximately 600,000 plates were observed at $k' \approx 3$. Their efficiency data showed that the 22 m column was operated well below its optimum velocity due to limitations in the pumping hardware being utilized³.

Recognizing that the number of achievable plates is restricted by the pumping capabilities, attempts at high efficiency separations using columns with high permeabilities have been explored. In a particular interesting approach, Tanaka et. al. packed a 1 mm ID glass column with 10 μm silica particles and subsequently pulled it to produce a 16.2 m x 44 μm ID column with octadecylsilylation carried out in situ. Operating at approximately 1500 psi, 500,000 theoretical plates were achieved with a dead time of 27 minutes⁴. In breaking the previous barriers imposed by pumping capabilities, MacNair and coworkers achieved > 300,000 plates in under 6 minutes by packing relatively long microcapillary columns with sub-2 μm particles^{5,6}.

In 2005, capitalizing on advances brought on by UHPLC technologies, Smith's group performed proteomics experiments which utilized 40 – 200 cm 50 μm ID columns packed with 1.4 – 3 μm particles at pressures up to 20,000 psi to obtain peak capacities of 1000 – 1500. More than 2000 proteins were identified and over 5000 metabolites in separate 12 hour ion trap MS/MS analyses⁷. Recently, 100 cm x 25 μm columns packed with 5 μm particles were operated ~1500 psi and flow rates ≤ 10 nL/min to achieve high peak capacities (~750) with a 10 hour gradient. Over 4000 proteins were identified across duplicate runs⁸. In this last example, peak capacities are notably lower than those achieved by Smith, but the

authors propose that a favorable convergence of figures of merit (low flow rate, high ionization efficiency, and state-of-the-art mass spectrometry) lead to the increased number of identifications.

4.1.2 Alternative Means of Achieving High Separation Efficiency in Liquid Chromatography

4.1.2.1 Multidimensional Separations

Multidimensional separations are one way to approach the problem of insufficient separation efficiency, especially in cases of complex samples containing dozens to hundreds or even thousands of components, such as in “-omics” applications. In such instances, peak capacity is the major concern, and utilization of the entire separation space becomes priority. Two-dimensional separations will result in the multiplication of the peak capacities from both single dimensions provided that two criteria are met. First, the separation modes must be orthogonal, and second, the resolution from the first dimension cannot be lost in the transfer to the second dimension. For example, a 2D separation with a peak capacity of 200 in the first dimension (typical of standard HPLC column performance) and a more modest capacity of 10 in the second dimension would result in an overall peak capacity of 2000. Efficient use of this entire space becomes difficult, however, and the theoretically achievable multiplicative peak capacity is never realized⁹. In the cases of proteomics and metabolomics, samples can be so complex that increasing the efficiency of one or both dimensions could be extremely helpful.

4.1.2.2 Superficially Porous Particles

Core-shell, or superficially porous, particles are an attempt to modify particle architecture in effort to improve column performance. A solid core particle is surrounded by a porous shell which effectively limits the diffusion of analytes to only a fraction of the total

particle diameter. The largest improvements in performance of superficially porous over fully porous particles are therefore due to the reduced volume of stagnant mobile phase contained within the pores, H_{CSM} , but improvements in the A- and B- terms have also been observed. Thus, larger superficially porous particles can be used to achieve column efficiencies that are obtained with smaller fully porous particles at lower operating pressures¹⁰. Long columns efficiently packed with particles that have structural parameters tuned for particular applications may prove useful.

4.1.2.3 Porous Layer Open Tubular (PLOT) Columns

Porous layer open tubular (PLOT) columns are an alternative route in the pursuit of high-efficiency one-dimensional separations. This type of column uses an open tube with adsorbent-coated inner walls. PLOT columns were initially developed for use in GC due to high permeability and low reduced plate heights. In liquid chromatography applications, however, the stability of the sorbent layer is problematic, and the practical constraints of extra-column volumes arise. In order to achieve efficiencies on par with those of packed particle columns, PLOTs must have inner diameters of 10 μm or narrower for large analytes with small diffusion coefficients, such as proteins.

Attempts at very high efficiencies using these columns include Tijssen's work with a 275 cm x 32 μm ID column. Alkaline etching was used to produce a highly adsorptive siliceous layer on the inner wall, which served as the stationary phase. Operated at optimum velocity, 2.8×10^6 plates were generated ($H = 9.8 \mu\text{m}$) in 6.5 hours¹¹. Other work has shown similar results with greater than 10^6 plates achieved for unretained species in long analysis times with low operating pressures (< 400 bar), but drastic decreases in efficiencies for even moderately retained species ($k \sim 0.1$)^{12,13,14}.

4.1.2.4 Monolithic Columns

Monolithic columns, coherent rigid castings of silica or polymer made by in situ polymerization of the material, have gained a great amount of attention since the mid-1990s. Monolithic beds contain both large macropores with diameters $\sim 2\ \mu\text{m}$ and small mesopores $\sim 10\ \text{nm}$. The interstitial volumes of these columns is typically around 80%, causing their permeabilities to be much higher than those of packed bed columns and reducing the operating pressures needed to run them at a particular flow rate. Some studies estimate monolithic columns to have equivalent particle diameters of 4 -5 μm based upon column efficiencies. Theoretical studies taking a kinetic plot approach to compare the performances of monoliths and packed bed columns with respect to analysis times for both very fast, low efficiency ($N < 50,000$) and slower, high efficiency ($N > 100,000$) runs have been performed. For analyses with lower required efficiencies, sub-3 μm packed bed columns were vastly superior; for runs with higher required efficiencies, monolithic approaches were shown to be potentially better¹⁵.

Tanaka et. al. prepared long monolithic silica-C18 capillary columns (100 μm ID) with lengths ranging between 90 and 440 cm and operated at pressures up to 6800 psi to achieve 100,000 – 500,000 theoretical plates with dead times between 5 and 40 minutes. When three columns with high permeabilities were connected in series to give a 1250 cm separation path length, $\sim 10^6$ plates were achieved at $k' = 2.4$ and a column dead time of 150 minutes¹⁶.

4.1.2.5 Micropillar Array Columns (PACs)

High-precision etching was proposed by Regnier as a solution to particle slurry-packed column-to-column reproducibility¹⁷. The technique offers the ability to control the

position of each individual particle-equivalent, or pillar, and also the possibility of eliminating all possible sources of eddy-diffusion by decreasing the heterogeneity of the flow paths in the microstructured channels. Using a deep reactive ion etching process, 10 μm diameter pillar arrays were created in channels of various widths to determine the dispersion profile of an unretained fluorescent marker. As long as the sidewall regions of the channels were appropriately designed, very high efficiencies were achieved, with reduced plate heights as small as $h = 0.2$ ¹⁸. Reversed-phase pressure-driven separations were later performed with pillar diameters of 4.4 μm and an external porosity of 55% to achieve 4000 – 5000 plates in a 1 cm channel¹⁹.

Desmet et. al. recently used the same approach in an attempt to achieve 10^6 plates using theoretically optimized parameters²⁰. A 310 cm long separation channel was arranged on a 4 inch silicon wafer with 10 μm wide asymmetric turns connecting 5 cm 150 μm wide PAC channels. Pillar diameter and interpillar distance were 5.2 μm and 2.3 μm , respectively, to yield an interpillar porosity of approximately 54%. Operating at 350 bar (~ 5000 psi), a dead time marker eluted in 18.4 minutes to yield 1.07×10^6 plates. For even moderately retained species, however, minimum plate heights were over 3 times higher. The authors speculate that this diminished performance is due to the loadability of the PACs and suggest that porous pillars or superficially porous pillars are needed to address this issue. These approaches, however, would likely introduce additional heterogeneities into the microstructure, thereby abating some of the advantages afforded by the highly ordered arrays.

4.1.3 Temperature as a Parameter in Liquid Chromatography

The influence of temperature in liquid chromatography, specifically its effects on column efficiency and the behavior of solutes, has been widely studied and yielded conflicting results. Nonetheless, the use of higher temperatures remains an attractive option because it represents a simple means of controlling some of the important physical parameters in LC such as viscosity, mobile phase polarity, and solute diffusivity. Some of the improvements in performance that have been observed when operating at elevated temperatures include the ability to perform faster analyses without loss of efficiency and the reduction of organic content in the mobile phase. Temperature has also been used to improve selectivity in certain cases.

4.1.3.1 The Effect of Elevated Temperature on Column Efficiency

In as far as elevated temperatures affect chromatographic performance, Chen and Horvath concluded that the van Deemter coefficients remain constant and that only mobile phase viscosity and solute diffusivity vary with temperature²¹. Experimental viscosity and diffusivity measurements are thus needed to assess and meaningfully compare performances across a range of temperatures, but obtaining this data can be somewhat arduous. The Wilke-Chang equation, an empirical expression based on extensive experimental investigations, can be used to estimate diffusivity with a fair degree of accuracy²².

$$D_{A,B} = 7.4 \times 10^{-8} \frac{(\Phi_B M_B)^{1/2} T}{\eta_B V_A^{0.6}} \quad (4-1)$$

where $D_{A,B}$ is the diffusion coefficient of an infinitely dilute solute A in solvent B, M_B is the molecular weight of solvent B, T is the absolute temperature, η_B is viscosity of B at T , V_A is the molar volume of solute A at its normal boiling temperature, and Φ_B is the association factor of solvent B. Recommended values for Φ are 2.26 for organic solutes diffusing into

water, 1.9 for methanol, and 1.0 for unassociated solvents such as acetonitrile²³. For mixed solvents, the association factor can assigned as:

$$\Phi M = \sum_{j=1}^n x_j \Phi_j M_j \quad (4-2)$$

where x_j is the mole fraction of solvent j . Viscosity estimates for water-acetonitrile mixtures as a function of temperature (up to 120°C) and composition can be found from the following empirical equation, developed by Chen and Horvath²¹:

$$\eta(\alpha, T) = \exp \left[\begin{aligned} &\alpha \left(-3.476 + \frac{726}{T} \right) \\ &+ (1-\alpha) \left(-5.414 + \frac{1566}{T} \right) \\ &+ \alpha(1-\alpha) \left(-1.762 + \frac{929}{T} \right) \end{aligned} \right] \quad (4-3)$$

where α is the volume fraction of acetonitrile.

Using the unreduced form of the van Deemter equation with A-, B-, and C-coefficients of 1.5, 1.0, and 0.17, respectively, the effect of temperature on the theoretical H versus U curves for 1.9 μm particles is shown in Figure 4-1. Higher temperatures generate higher optimal linear velocities and the slope becomes flatter in the resistance to mass transfer-dominated region of the curve. If reduced parameters were utilized, the plots at different temperatures would be perfectly superimposable.

4.1.3.2 The Effect of Elevated Temperature on Retention

The retention time of an analyte on a particular column can be greatly reduced with increasing temperature. On one hand, the ability to flow at higher linear velocities at a given operating pressure due to decreased solvent viscosity at higher temperatures can be used to reduce analysis times. On the other hand, increasing temperature also tends to reduce solute

retention factors, k' . The Van't Hoff equation shows how k' is a function of the free energy changes involved in a solute's interaction with both the mobile and the stationary phases.

$$\log k' = -\frac{\Delta H_0}{2.3RT} + \frac{\Delta S_0}{2.3R} + \log \phi \quad (4-4)$$

where ΔH_0 and ΔS_0 are the system enthalpy and entropy, R is the universal gas constant, and ϕ is the phase ratio. For neutral solutes, the plot of $\log k'$ versus $1/T$ is usually linear. Even while temperature can be used to affect solute retention, solvent strength typically plays a larger role. In general, a 1% (v/v) increase in organic modifier has roughly the same effect as a 5°C increase in temperature on elution times and retention factors on an C18 column²⁴.

4.1.4 Kinetic Plots: The Combined Effects of Small Particles, High Pressures, and Elevated Temperatures

In considering the theoretical separation efficiencies afforded by packing long microcapillary columns with sub-2 μm particles and using operating pressures in excess of 40,000 psi, it is helpful to examine kinetic plots. In this way, pressure limitations can be considered in conjunction with analysis time in order to assess the feasibility of a particular approach. Figure 4-2 presents a series of curves representing columns of various lengths packed with 1.9 μm particles. Each point on the curves refers to a column dead time (along with a corresponding operating pressure) and the theoretically achievable number of plates. The plots are constructed using reduced van Deemter coefficients of 1.0, 1.0, and 0.1 for A-, B-, and C-, respectively. The red line indicating a 40,000 psi operating pressure demarcates the accessible separation parameters, which lie below the line, from those which are inaccessible, which lie above. For example, 250,000 plates can be generated in just over 10 minutes with a 100 cm column and less than 40,000 psi; but 10^6 plates cannot be generated in under 40 minutes with even a 400 cm column unless more than 40,000 psi operating

pressures are available. Figure 4-3 shows the newly accessible separation speeds and efficiencies which become available upon moving from commercially available UHPLC equipment (15,000 psi) to higher pressures (40,000 psi). Moving horizontally across this region shows the increase in speed which can be accomplished while maintaining a given plate count; moving vertically highlights the increased efficiencies which become possible while maintaining a given analysis time. Figure 4-4 shows the combined effect of introducing elevated temperatures (85°C vs. 25°C) and higher pressures (40,000 psi vs 15,000 psi) on achievable speeds and efficiencies with 1.9 μm particles. The curves represent the maximum achievable plate count for a given dead time.

4.1.5 Peak Capacity in Gradient Elution of Peptides

While plate count is the most common means of measuring column efficiency, it cannot easily be used to assess gradient separations. Plate count, in fact, can be determined in gradient chromatography if the instantaneous retention factor at the point of elution is known, but this knowledge often requires a series of tedious experiments. Peak capacity is a much more common assessor of gradient performance and can be defined as the number of peaks that can fit into an elution time window t_1 to t_2 with a fixed resolution, typically $R_s = 1$ (4 σ). As mentioned in Chapter 1, peak capacity as a descriptor of separation efficiency under isocratic elution conditions is of limited value because the upper end of the retention window is essentially unbounded. Under gradient elution conditions, however, the upper bound is defined by the length of the gradient. Peak capacity can thus be written as

$$n_C = 1 + \int_{t_1}^{t_2} \frac{1}{4\sigma} dt \quad (4-5)$$

Using a fixed resolution of 1, peak capacity can also be defined as

$$n_C = 1 + \sum_n R_s \quad (4-6)$$

If the peak width over the entire chromatogram is very similar, as is often the case in gradient elution schemes, the simplest practical measurement of peak capacity is

$$n_C = 1 + \frac{t_g}{\bar{w}} \quad (4-7)$$

where t_g is the gradient run time and \bar{w} is the average peak width²⁵.

For a generic reversed-phase gradient carried out under linear solvent-strength conditions and without sample-imposed limitations, the maximum peak capacity that can be obtained has been derived as

$$n_C = 1 + \frac{\sqrt{N}}{4} \times \frac{1}{G+1} \ln \left(\frac{G+1}{G} e^{S \times \Delta c} - \frac{1}{G} \right) \quad (4-8)$$

where G , the gradient steepness factor, is defined as

$$G = S_{k'} \times \Delta c \times \frac{t_0}{t_g} \quad (4-9)$$

and typically ranges between 0.05 and 1.0, where very flat gradients take on lower values.

$S_{k'}$ is the slope of the plot of the natural logarithm of the retention factor versus solvent composition, and Δc is the change in solvent composition over the course of the entire gradient²⁶.

For the gradient separation of peptides, which will be of primary concern in this present chapter, Δc is usually around 0.5 and the value of S is typically high. In other words, the solvent composition at elution of a given analyte hardly differs with different gradients, and Equation 4-8 simplifies to

$$n_C = 1 + \frac{\sqrt{N}}{4} \times \frac{S_{k'} \times \Delta c}{G+1} \quad (4-10)$$

From Equation 4-10, it can be seen that three operational parameters can be varied to achieve the desired peak capacity. The first is the number of theoretical plates, which depends upon the column length, particle size, and flow rate, as has been discussed previously. The second is the gradient span, which is typically 50% for peptide separations. The final parameter is the gradient run time, the effect of which is more clearly illustrated in Equation 4-9. Higher peak capacities can be obtained by increasing the ratio of gradient run time to column dead time. Using Equation 4-10, peak capacity is plotted in Figure 4-5 as a function of gradient time for a 15 cm x 4.6 mm column packed with 5 μm particles. A value of 40 is assigned to S , typical for peptides of molecular weight around 1800; and the gradient span is 0.5. A fixed flow rate of 1 mL/min is assumed, with a maximum pressure not exceeding 6000 psi. N is calculated using estimated van Deemter coefficients: A is $1.5d_p$, B is $1D_m$, and C is $d_p^2/(6D_m)$. The diffusion coefficient is estimated as $8.0 \times 10^{-6} \text{ cm}^2/\text{s}$. As can be seen, the peak capacity continues to increase with longer analyses, but at a much slower rate. A peak capacity of 250 is achieved in 1 hour, but only ~ 40 peak capacity units are gained by extending the analysis to 3 hours.

Figure 4-6 shows the effect of flow rate on the resultant peak capacity. Interestingly, while the minimum plate height on the van Deemter curve occurs around 0.08 mL/min for peptides on this column, the maximum peak capacity for a 1 hour gradient is at a flow rate over 8x faster, at 0.66 mL/min. It is evident that using a flow rate which minimizes the isocratic HETP will not necessarily result in the highest peak capacity under gradient elution conditions. This conclusion is in good agreement with experimental findings^{27,28}. On the other hand, while using lower flow rates may not result in maximal peak capacities, the sensitivity of the assay may be greatly improved²⁵.

The effect of using smaller particles is illustrated in Figure 4-7, comparing theoretical peak capacities from 15 cm columns packed with 5 and 1.9 μm particles over a fixed gradient time. The flow rate providing the optimal peak capacity in the column packed with smaller particles is higher than that for the column packed with larger particles, which is consistent with isocratic performance characteristics. The pressure needed to reach the optimal flow rate is significantly higher when using smaller particles.

The use of elevated temperatures in gradient elution has also been used to reduce run times without drastic losses in efficiency. Because retention factors tend to decrease with increasing temperature, approaches have been taken to preserve the retention factor by reducing the amount of organic modifier in the mobile phase. In this way, total peak capacity should remain relatively unaffected. Using temperature as a variable parameter in gradient elution liquid chromatography has also been used to increase efficiencies when operating far from predicted optimal flow rates, whether for reasons of pressure limitations or concerns over sensitivity. It has also been used to provide alternate selectivities.

4.2 Experimental

4.2.1 Chemicals

For the purposes of slurry packing and isocratic characterization of columns, HPLC grade acetone and HPLC grade acetonitrile were used as received from Fisher Scientific (Waltham, MA). Deionized water from a Nanopure ultrapure water system (Barnstead International, Dubuque, IA) was used. Trifluoroacetic acid and formamide were used as received from Sigma Aldrich Chemical Company (Milwaukee, WI), and potassium silicate (Kasil) was obtained from PQ Corporation (Valley Forge, IA). The isocratic test mixture used to evaluate column performance contained L-ascorbic acid (Fisher Scientific), 1,4-

dihydroxybenzene (hydroquinone), 1,3-dihydroxybenzene (resorcinol), 1,2-dihydroxybenzene (catechol), and 4-methylcatechol from Sigma Chemical Company (St. Louis, MO). When using mass spectrometric detection, Optima grade water and acetonitrile with 0.1% formic acid were used (Fisher Scientific).

4.2.2 Isocratic Characterization at Elevated Temperatures

All columns for this series of experiments were fused silica capillary tubes (Polymicro Technologies, Inc., Phoenix, AZ) with 50 μm inner diameters and 360 μm outer diameters. A 66 cm x 50 μm ID column was packed with a ~ 3 mg/mL slurry of 1.9 μm BEH particles in acetone and characterized according to the procedures described in Sections 2.2.2 and 2.2.3.

The column was characterized at room temperature (23°C), 45°C, 65°C, and 85°C with 50/50 acetonitrile/water and 0.1% TFA. Columns were heated in an aluminum heating block, as shown in Figure 4-8. Temperature was maintained through feedback control of cartridge heaters within the block using a CN9600 Series temperature controller (Omega, Stamford, CT). With this configuration, approximately 6 cm of column at the inlet end remained unthermostatted, as it was contained within the UHPLC injector. The outlet end of the column protruded from the heating block ~ 0.5 cm and was butt-connected to 8.5 cm of 15 μm ID open capillary. The carbon microfiber was inserted into the end of this open capillary for detection of the eluting electroactive test compounds. Figure 4-9 shows chromatograms collected at each temperature near optimum operating pressure. Tailing becomes increasingly prevalent with increasing temperature. Figure 4-10 shows the overlaid reduced van Deemter curves for hydroquinone at each temperature, exemplifying the deteriorating performance.

Because the heat transfer through microcapillary columns is fast enough to rule out the effects of insufficiently heated mobile phase, the unthermostated portion of the column within the injector was identified as the probable cause for the poor efficiencies at elevated temperatures. The UHPLC injector was modified to allow for the insertion of four cartridge heaters and a thermocouple to maintain a matched temperature with the aluminum heating block through a second temperature controller as shown in Figure 4-11. The experiment described above was repeated with a 60 cm x 50 μ m ID column packed with 1.9 μ m BEH particles. Again, approximately 0.5 cm of column outlet protruded from the heating block to allow for butt-connection to \sim 8.5 cm of 15 μ m ID open capillary. A weaker mobile phase, 70/30 acetonitrile/water and 0.1% TFA, was used to characterize the columns at 23, 45, 65, and 85°C. Even with this improved configuration, however, a short segment of column (\sim 1.5 - 2 cm) between the injector and the aluminum heater is not in direct contact with either metal block. The segment runs the length of the hollow bolt which attaches the UHPLC compression fitting to the injector. Polystyrene foam was used to insulate this region of the experimental setup in attempt to reduce the temperature differentials as the column exits the injector and enter the heater.

Figure 4-12 shows the chromatograms collected at each temperature near optimum operating pressure. Far less tailing is evident when compared to the chromatograms in Figure 4-9, but the later eluting peaks begin to show some fronting/tailing, especially at 85°C. This may be due to differential temperature effects between the injector and heater. The pressure dependent retention data for each temperature is shown in Figure 4-13. Extrapolating to atmospheric pressure in each instance allows for the construction of Figure 4-14, which shows how the predicted reductions in retention factors are observed according

to the van't Hoff equation discussed in Section 4.1.3.2. Unreduced van Deemter plots for hydroquinone at each temperature, presented in Figure 4-15, show that the predicted behavior, as modeled in Figure 4-1 and discussed in Section 4.1.3.1, is achieved. Running at elevated temperatures moves the minimum plate heights to faster linear velocities, and the slopes of the curves in the C-term region are effectively reduced. h vs. v plots for each of the four retained test analytes considered in isolation are shown in Figure 4-16. Reduced parameters were calculated from estimated pressure-dependent mobile phase viscosities and scaled diffusion coefficients. The overlay of the data across the entire temperature range is a good indicator that temperature is an effective means to reduce analysis time while maintaining the efficiency of the separation.

It should be noted that elevated temperatures can lead to and accelerate the degradation of sample on the column. In the present case, this is most apparent for 4-methyl catechol. The lack of 85°C data in Figure 4-16 is due to 4-methyl catechol being entirely oxidized on the column and undetected electrochemically. Figure 4-17 shows the degradation of this peak at 65°C with elution time of the peak corresponding to operating pressure. On a related note, extended periods of column operation at 85°C were not observed to significantly affect sample retention, and the packing material was deemed stable for use at high temperature.

4.2.3 100 cm Microcapillary Columns

Early attempts to pack long microcapillary columns to lengths of approximately 100 cm met with various degrees of success. 50 μ m ID capillary tubes were packed with 1.9 μ m BEH particles slurried in acetone with concentrations ranging between 5 and 10 mg/mL. Columns were subsequently flushed in 50/50 acetonitrile/water and 0.1% TFA at 50,000 psi

before fritting. Figure 4-18 shows the overlaid van Deemter curves of catechol for five columns packed over a period of approximately three months. Performance is highly variable, even as experimental packing conditions are kept virtually the same. Minimum reduced plate heights for the five columns ranged between 1.60 and 3.25; average maximum theoretical plate counts ranged between 350,000 and 160,000.

4.2.3.1 Column ID Effects

It has been consistently observed that the inner diameter of packed microcapillary columns can greatly influence chromatographic performance. Hsieh and Jorgenson investigated this effect by packing 5 μm particles into capillaries with inner diameters ranging between 12 and 33 μm . As column diameter decreased, the geometrical wall effect became the dominant influence on the structure of the packed bed, and the denser core region of the packing effectively disappeared. Both the A- and C- terms were observed to decrease with column diameter, and column permeability increased²⁹. Similarly, the Tallarek group has correlated the morphologies of the bed microstructures for columns of increasing inner diameters to chromatographic performance using confocal laser scanning microscopy (CLSM). Larger ID columns with poorer performance tended to exhibit a greater degree of particle size segregation along the column diameter. Wider-bore columns also showed a greater difference in transcolumn porosity profiles than did narrower, better performing columns³⁰. With these observations in mind, we packed a series of 100 cm columns with inner diameters of 30, 50, and 75 μm and compared their performances.

Columns were packed and evaluated according to the general procedures described in Section 2.2.2 and 2.2.3. ~ 5 mg/mL of 1.9 μm BEH particles were slurried in acetone and columns were packed at maximum pressures of 30,000 psi. Columns were subsequently

flushed at maximum pressures of 50,000 psi in 50/50 acetonitrile/water and 0.1% TFA.

Figure 4-19 shows the overlaid van Deemter curves of the three columns for each retained test analyte considered in isolation. As anticipated, column efficiency deteriorates when moving to larger inner diameters. Average maximum theoretical plate counts were 340,000 for the 30 μm ID column; 240,000 for the 50 μm ID column; and 215,000 for the 75 μm ID column.

4.2.3.2 Gradient Elution Characterization of 100 cm Microcapillary Columns

The isocratic performances of the 30, 50, and 75 μm ID columns were correlated to their performances under gradient elution conditions. As described in Section 3.1.5, the resultant peak capacities of gradient elution separations are a complex function of column efficiency, gradient composition, gradient steepness, flow rate, as well as analyte properties. Peak capacities under a given set of system operating parameters were determined for a tryptic digestion of bovine serum albumin, a relatively simple model that allowed for tracking particular peaks throughout the runs.

The UHPLC gradient system has been described and characterized previously and is schematized in Figure 4-20³¹. A Waters 1525 binary gradient pump (Waters Corp., Milford, MA), modified to pump brake fluid, is connected to a custom hydraulic amplifier (Waters Corp.) with 30:1 amplification to generate ultrahigh pressures up to 40,000 psi. The outlet of the amplifier is connected to a low-volume four-port cross (Valco Instrument Co., Houston TX). The analytical microcapillary column, an open tubular flow splitter, and gradient inlet tubing comprise the remaining three port connections.

The binary gradient is generated using a Waters CapLC system and is loaded in reverse onto a 0.020 in. ID stainless steel gradient storage loop situated between the low-

volume cross and the hydraulic amplifier. The flow resistance of the long analytical column and small inner diameter flow splitter serve to effectively load the entire gradient onto the storage loop. After the gradient is loaded, an integrated autosampler is used to make the sample injection and to load it onto the loop. Two high-pressure pin valves (Valco) serve to isolate the low-pressure CapLC instrumentation from the ultrahigh pressures supplied by the amplifier. Once gradient and sample loading is complete, these valves are closed and the hydraulic amplifier is engaged to push the sample and gradient from the loop into the low-volume cross and onto the analytical column.

System pressure is determined by the specified volumetric flow rate of the hydraulic amplifier and the length and diameter of the open-tubular capillary flow splitter. The flow through long microcapillary columns is low, on the order of a few hundred nL/min, and accurate flow control of the custom amplifier requires flows above $\sim 1 \mu\text{L}/\text{min}$. The configuration of the port connections in the low-volume cross dictates a split ratio whereby much of the preloaded sample and gradient volume is diverted through the splitter to waste, and only a small fraction is directed onto the analytical column. Thus, the dimensions of the capillary splitter and the specified volumetric flow rate determine the playback time of a particular preloaded gradient volume.

The first set of gradient elution experiments compared the peak capacities of the 30, 50, and 75 μm ID columns from Section 4.2.3.1 over a range of 1-50% acetonitrile gradient times. Gradients were loaded and played back at $4 \mu\text{L}/\text{min}$ at $\sim 24,000$ psi for total gradient times of approximately 60, 120, 180, and 240 minutes. Peak capacities were calculated by selecting 12 – 15 characteristic peaks over the entire elution window, measuring peak widths at half-height, and determining the 4σ peak base widths. The total gradient time was then

divided by the average peak base width. Detection was accomplished with electrospray time-of-flight mass spectrometry (ESI-TOF-MS). The analytical column was butt-connected via a Teflon sleeve to a ~ 20 cm x $10\ \mu\text{m}$ ID segment of open tubular fused silica tubing. This capillary was interfaced to a $20\ \mu\text{m}$ pulled to $10\ \mu\text{m}$ ID fused silica PicoTip (New Objective, Woburn, MA) within the nanospray source at 90° to the inlet cone of the LCT-TOF mass spectrometer (Micromass, Ltd.). A spray voltage of 2 kV was used, with subtle adjustments made as ESI spray became unstable over time. Sample and extraction cone voltages were set to 35 and 10 V respectively. Figure 4-21 shows the chromatograms from the $50\ \mu\text{m}$ ID column and Figure 4-22 shows the resultant peak capacities as a function of gradient length for all three columns. Superior isocratic performance translates to gradient elution performance, exemplified in $\sim 30\%$ improvement in peak capacity when comparing the 75 to the $30\ \mu\text{m}$ ID column. This is in relatively good agreement for the square-root relationship of N to peak capacity shown in Equations 4-8 and 4-10. The roll-off in efficiency, characterized in Figure 4-5, is also apparent.

As concluded in Section 4.2.2, running the column at elevated temperatures allows column efficiency to be maintained while reducing analysis time. Under gradient elution conditions, viscosity changes throughout the course of the run as mobile phase composition changes. At elevated temperatures, the reduction in mobile phase viscosity is not proportional across all compositions. For example, at 25°C , 20/80 acetonitrile/water has a viscosity of approximately 0.87 cP, while 40/60 acetonitrile/water has a viscosity of 0.83 cP - a 7% difference. At 65°C , the viscosities of 20/80 and 40/60 acetonitrile/water are 0.48 and 0.47, respectively - a 3% difference. As discussed in Section 4.1.3.2, analyte retention also decreases with temperature, and a weaker mobile phase is required in order to maintain a

given retention factor, k' . For these reasons, a strict multiplier cannot easily be applied to predict how much faster a given efficiency can be accomplished as a function of temperature, but a general trend is still observed. The 100 cm x 30 μ m ID column was characterized under gradient elution conditions with 1–50% acetonitrile at temperatures of 25, 35, 45, and 65°C. The low volume four-port cross was placed in a column heater provided by Waters Corp. to temperature control the analytical column in conjunction with the flow splitter. Figure 4-23 shows peak capacity versus the retention window for all four temperature sets. The retention window corresponds to the time between an early eluting and a late eluting characteristic peaks. Column efficiency is maintained while analysis time is reduced in proportion to the reduction in mobile phase viscosity at elevated temperatures.

The final parameter of investigation for this set of gradient elution experiments was the effect of volumetric flow rate on resultant peak capacity. As discussed in Section 4.1.5, experimental investigations with peptides have shown that flow rates significantly higher than those consistent with maximum van Deemter efficiencies should be used to achieve maximum peak capacities, although explanations for this phenomenon are scarce³². Using the 100 cm x 30 μ m ID column, several series of gradient volumes were played back at different flow rates. In this way, the percentage change of mobile phase composition per column volume (i.e. gradient slope) was maintained while flow rate, and thus total analysis time, was varied. Four different gradient slopes (12.5%, 4.1%, 3.1%, and 1.5% change per column) were characterized over a range of mobile phase linear velocities from 0.03 cm/s to 0.14 cm/s (as determined from column dead times), corresponding to operating pressures ranging from ~ 6,000 psi to ~26,000 psi at 25°C. Peptide separations are generally carried out with gradient slopes < 2% change/column volume to achieve maximum resolution.

The results of this investigation are summarized in Figure 4-24, which plots peak capacity versus linear velocity. Regardless of the gradient slope, a general trend holds whereby decreasing the flow rate serves to increase the resultant peak capacity. In the present case, peak capacities for a 3% change per column volume can be increased ~ 30% by cutting the flow rate in half until a peak capacity of ~ 600 is reached in a 16 hour total run time. Assuming a diffusion coefficient for peptides of $5 \times 10^{-6} \text{ cm}^2/\text{s}$, the optimum interstitial velocity according to van Deemter theory for 1.9 μm particles is approximately 0.079 cm/s. As discussed in Section 1.2.4, this corresponds to a linear velocity of ~ 0.04 cm/s as determined by the elution of a dead time marker in a column packed with fully porous particles. Surprisingly the peak capacities achieved on this 100 cm column are highest at these low linear velocities and markedly lower at faster flow rates. This is at odds with both previously reported experimental data and the predictions discussed in Section 4.1.5.

4.2.3.3 Slurry Concentration Effects

The employment of high concentration slurries, originally discussed in Section 2.2.6, has also proven beneficial in packing columns in excess of 100 cm. A 105 cm x 50 μm ID and 103 cm 50 μm ID column were packed with a 100 mg/mL slurry of 1.9 μm BEH particles. The columns were isocratically characterized in 50/50 acetonitrile/water and 0.1% TFA. Performances were excellent with theoretical plate counts in excess of 350,000, minimum reduced plate heights of ~ 1.5, and uncorrected C-terms of ~ 0.2 for both columns. These results are commensurate with some of the best performance characteristics seen for much shorter columns, such as those shown in Chapter 2, Figure 2-13. Chromatograms of each column operated near optimum linear velocity are shown in Figure 4-25. Figure 4-26 shows the overlaid van Deemter performances for each retained test analyte considered in

isolation. In addition to performance, column permeability is also similar. Figure 4-27 shows the pressure dependent retention data, and Figure 4-28 shows the resistance to flow as determined by the elution time of ascorbic acid.

As already discussed in Section 2.2.6 and shown in Figure 2-17, axial homogeneity is also well preserved when packing long columns with highly concentrated slurries. We attribute this to the relative speed of packing, as packing with slurry concentrations between 3 and 10 mg/mL consistently yielded deteriorated performance and more densely packed beds. Packing times of 100 cm columns typically ranged between 100 and 120 minutes with 100 mg/mL slurries, so long as the nominal concentration in the slurry packing reservoir was maintained through adequate stirring.

4.2.4 200 cm Microcapillary Columns

Again, moving to higher particle slurry concentrations was a key component in the ability to pack highly efficient 200 cm columns reproducibly. In early efforts with 5 – 10 mg/mL slurries, packing was slow, and total packing time ranged 48 – 72 hours. Chromatographic performance was also highly variable, and the best columns resulted in maximum theoretical plate counts in the range of 450,000 to 500,000 plates, corresponding to minimum reduced plate heights higher than 2.0. Often times, however, plate counts barely attained to maximum values of 400,000.

Figure 4-29 shows chromatograms collected at 23°C and 65°C for a well-performing 180 cm x 50 µm ID column operated at 45,000 psi. The elevated temperature runs were performed using the set-up described earlier with the injector and column heater held at matching temperatures. Theoretical plate counts for ascorbic acid at room temperature are in excess of 2×10^6 plates due to its extremely low retentivity. At 65°C, retention is presumably

even lower, and plate counts exceed 3×10^6 . For retained analytes, plate counts range between 470,000 and 510,000. Figure 4-30 shows the h versus v data collected at both 23°C and 65°C. Van Deemter coefficients are not calculated due to the lack of adequate sampling in the C-term dominated regions. It will also be noted that, at 65°C, hydroquinone has very low reduced minimum plate heights ranging between $\sim 0.9 - 1.3$. Fronting/tailing at the baseline region of more retained peaks, such as catechol, may be due to the differential heating of the short ~ 1.5 -2.0 cm segment of column between the injector and heater, as described in Section 4.2.2. Once again, the lack of 4-methyl catechol data in the elevated temperature runs is indicative of its oxidation on the column, which renders it electrochemically undetectable.

Using 100 mg/mL slurries, 200 cm columns typically packed in approximately 8 hours and consistently displayed excellent chromatographic performance. Figure 4-31 shows a chromatogram of a 214 cm x 50 μ m ID column packed with a 100 mg/mL slurry of 1.9 μ m BEH particles, operated at 38,500 psi. Theoretical plate counts range between 560,000 and 650,000, with h_{\min} s between 1.6 and 2.0. In our work, these values are the best obtained amongst columns packed to this length, but fall somewhat short of the performance characteristics of 100 cm columns packed under similar experimental conditions. We again attribute this decline in relative efficiency to axial heterogeneity, as discussed in Section 2.2.4. The speed of packing which results from the use of concentrated packing slurries delays the qualitative onset of diminished efficiency and increased resistance to flow, as described in Section 2.2.6 with respect to 100 cm columns. As even longer columns are packed, however, such as in the present case, the effects of significantly slowed packing are again manifested.

A 216 cm x 50 μ m ID column packed with a 100 mg/mL slurry of 1.9 μ m BEH particles was characterized under gradient elution conditions with the same approach described in Section 3.2.3.2. Runs were performed at room temperature with 1-50% acetonitrile gradients and 0.1% formic acid for a tryptic digest of BSA. Operating pressures were \sim 30,000 psi. Mass spectrometric data was collected with a Waters QTOF Premier with a spray voltage of \sim 2 kV, adjusted as necessary to maintain stable spray. 12 – 15 characteristic peaks were selected from the retention windows of each run and 4σ peak base widths were calculated from the measured widths at half height. Figure 4-32 shows representative chromatograms of each run, corresponding to 120, 240, and 360 minute gradients. Peak capacities for the 360 minute gradient exceeded 900. Figure 4-33 shows the peak capacity vs. retention window data for the column run at 25 and 65°C. Once again, peak capacity is effectively preserved while significantly cutting the analysis time by running at elevated temperatures. Although the analyses were not performed, further slowing the flow rates and lengthening the analysis times may have allowed for even higher peak capacities to be attained, as was observed with the 100 cm column characterizations.

4.2.5 > 200 cm Microcapillary Columns

With \sim 200 cm columns capable of generating > 600,000 plates in reasonable analysis times ($t_m \approx$ 25 minutes at 45,000 psi), efforts were made at packing still longer columns which would approach the 10^6 plate benchmark. Using 100 mg/mL particle slurries, attempts to pack efficient microcapillary columns in excess of 300 cm were made. Packing was relatively fast, and columns packed in \sim 24 hours. Maximum packing pressures of 30,000 psi and mobile phase flushing pressures of 50,000 psi were used prior to setting the permanent inlet frits. Performances of such columns, however, were extremely poor, resulting in

theoretical plate counts of 400,000 to 600,000 at 40,000 psi operating pressures. These results were difficult to explain, even when considering the expected effects of axial heterogeneity. To trace the origin of the poor performance, a 330 cm column was segmented into thirds. The first packed segment, '1', was isocratically characterized and compared to the last, slowest packed segment, '3'. Figure 4-34 shows the overlaid h vs. v data for both segments. Although there was no clear drop-off in performance for the latter packed segment, both were equally poor with h_{\min} s around 3.0. Additionally, the experiment was performed such that the data corresponding to the highest operating pressures (38,200 psi) was collected later. Subsequently collected replicate data showed a marked decrease in efficiency, as represented by the data points at $v \approx 3.5$. This behavior indicated that the packed bed had collapsed in the previous high-pressure run.

The influence of the post-packing mobile phase flush at high pressure with respect to relatively short 30 cm columns was discussed in Chapter 2. It was concluded that while the additional bed compression resulting from a 46,000 psi flush in comparison to a 23,000 psi flush had a slightly negative influence on column performance, the improved bed stability was an overriding benefit. In the present case, the differential pressure drop across a given length of column is considerably lower than in the previously discussed series of experiments. For a 300 cm column flushed at 50,000 psi, each 100 cm segment is compressed in accordance with a $\sim 17,000$ pressure drop. Flushing at higher pressures, however, was viewed as impractical as the UHPLC fittings were prone to failure above 60,000 psi. In attempt to assess the influence of the high-pressure flush as a limiting factor in preparing efficient long columns, two ~ 100 cm x 50 μm ID columns were packed with a 100 mg/mL slurry of 1.9 μm BEH particles at 30,000 psi and subsequently flushed at either

50,000 psi or 23,000 psi. Figure 4-35 shows the overlaid van Deemter curves for both columns. Superior performance resulted from the column flushed at higher pressure, with h_{\min} s of approximately 1.5 and uncorrected C-terms under 0.2. Both quantifiers were significantly higher with the column flushed at 23,000 psi, with h_{\min} s of 2.0 and C-terms approaching 0.3.

The apparent importance of a sufficient degree of post-packing bed compression suggested that packing columns in excess of 200 cm was an impractical means of attaining the goal of 10^6 theoretical plates. A modular approach revealed itself as a promising alternative. By packing shorter columns, on the order of 100 – 200 cm, and connecting them in series, efficiencies consistent with columns of those lengths could be maintained over longer separation paths. It was of vital importance, though, that the series connections be made with absolutely zero dead-volume.

To demonstrate the necessity of eliminating all connecting volume, consider a theoretical 100 cm x 50 μ m ID column packed with 1.9 μ m particles capable of generating 360,000 plates ($h = 1.46$) at $v_{\text{opt}} = 3.0$. An analyte with $k' = 0.5$ elutes after 15.9 minutes with a base peak width (4σ) of 6.36 seconds. With a volumetric flow rate of 74.4 nL/min, this corresponds to a peak volume of only 7.9 nL. If a 7.9 nL dead volume region is subsequently considered as the injection volume onto a matching 100 cm column in series, a resulting peak volume upon elution from the second column can be estimated according to the following equation³³:

$$V_p = \left(\left[\frac{4}{3} \right] V_s^2 + V_{p,0}^2 \right)^{0.5} \quad (4-11)$$

where V_p is the peak volume upon elution, V_s is the sample volume, and $V_{p,0}$ is the baseline peak volume for a very small sample. In other words, a dead volume gap at the outlet of the

first column serves to re-equilibrate the eluting Gaussian peak, and a new sample plug of uniform concentration is introduced onto the second column. The re-equilibrated sample plug will then broaden as it migrates the length of the second 100 cm column (also capable of generating 360,000 plates for a sufficiently small sample injection). Assuming a gap volume equivalent to the peak volume, 7.9 nL, and efficient evacuation of the dead-volume region, the 4σ width of the peak eluting from the second 100 cm x 50 μm column in series would be 9.7 seconds with a retention time of 31.8 minutes. This corresponds to a total plate count of 618,000 for the 200 cm separation path, significantly less than the expected 720,000 plates ($4\sigma = 8.99$ seconds). In reality, however, convection and diffusion phenomena would not permit the efficient evacuation of the entire sample from the dead volume region and the sample volume injected onto the second column would be significantly larger than that estimated here and would also result in notable peak tailing.

To design a suitable zero dead-volume connector that could hold at operating pressures in excess of 40,000 psi, the UHPLC compression fitting was modified to accommodate a longer PEEK ferrule (~ 0.6 inches). Capillary columns were abutted in the center of the ferrule, and compression of the PEEK served to squeeze each capillary along this length. Figure 4-36 illustrates the design and mechanism of the connection. Capillary faces were polished using a Model 395 Dremel tool (Dremel, Racine, WI) outfitted with a diamond polishing wheel prior to making the connection in effort to eliminate void regions where eluent could enter.

It was decided that, rather than several 100 cm columns in series, a single connection consisting of two high efficiency ~ 170 cm columns was the most practical approach to achieve 10^6 theoretical plates. While elution volumes and variances are additive, plate

counts are not. The total plate count for a series of coupled columns is therefore calculated as³⁴:

$$N_T = \frac{(\sum V_R)^2}{\sum \sigma^2} \quad (4-12)$$

where N_T is the total plate count for the series of columns and V_R is the retention volume. If columns are of the same type (i.e. elution volume), but different performance, the total plate count is greatly influenced by the poorest performing column in the series as illustrated by the following equation³⁴.

$$N_T = \frac{n_c^2}{\sum \frac{1}{N}} \quad (4-13)$$

where n_c is the number of columns in series. For this reason, only similarly performing columns were connected.

A series connection between two ~ 165 cm columns was made, each capable of generating over 550,000 plates ($h_{min} \sim 1.5$). Columns were packed to length in the previously described manner using a 100 mg/mL slurry of 1.9 μ m BEH particles, and flushed at 50,000 psi prior to setting inlet frits. The connection was made such that the outlet (i.e. the first pack portion) of the first column was abutted to the inlet of the second column in the modified UHPLC fitting. Performance of the ~330 cm column could not be assessed, however, as eluting peaks had very low intensities and poor peak profiles. Increasing sample concentration did little to aid in the assessment. Failure to load adequate amounts of sample has frequently been observed as the result of gap formation due to broken inlet frits, but visual examination of the packed bed under magnification revealed that the column was intact. Upon reapplication of 40,000 psi running pressure, an array of gaps at the outlet of

the first column in the series was noted while monitoring the packed bed under magnification. The gaps were relatively evenly spaced over a ~ 15 cm length and estimated to range between 5 and 20 microns in length. Continuing to view the bed under magnification, it was noted that releasing the pressure at the head of the column resulted in the gradual disappearance of the gaps. Pressure reapplication resulted in gap reformation.

These observations led us to speculate that the elastic expansion of the silica microcapillary and the concurrent compression of the BEH particles under high pressure were responsible for the appearance and disappearance of the microgaps at the outlet of the first column in the bank. In the packing and high-pressure flushing steps of column preparation, the outlet region remains at atmospheric pressure. When this region is subsequently connected in series with another column of similar length, it is effectively floated at > 20,000 psi causing small expansion of the column inner diameter and sufficient space for reorganization of the packed bed. With depressurization, the expanded capillary returns to its original dimensions, and the packed bed seemingly mends.

To address this phenomenon, the first column to be connected in the series was packed to length, flushed at 50,000 psi, and the inlet frit was set. The column was then flushed at 50,000 psi in the opposite flow direction, and a new frit was set at the original outlet end of the column. In this way, it was hoped that each end of the column, having experienced 50,000 psi, would be adequately compressed and stable to remain intact while floated at pressure in the series connected chain. Figure 4-37 shows two chromatograms, collected at 40,000 and 45,000 psi operating pressures, for a 170 cm x 50 μ m ID column (flushed at 50,000 psi in both directions) and a 190 cm x 50 μ m ID column packed with 1.9 μ m BEH particles connected in series. The test mixture contained ascorbic acid,

hydroquinone, catechol, and 4-methyl catechol. With a dead time of 105 minutes ($v = 1.6$), more than 10^6 theoretical plates were achieved, even for retained analytes.

4.3 Conclusions

We have explored the use of long microcapillary columns packed with sub-2 μm particles and operated at UHPLC pressures in effort to achieve very high efficiencies. Improved knowledge of the capillary column packing process has allowed for columns on the order of 100 – 200 cm to be packed which can generate 360,000 – 650,000 plates in reasonable analysis times. We have also shown that column efficiency can be preserved under both isocratic and gradient elution conditions while working at elevated temperatures to speed the time of analysis. This work suggests that peak capacities approaching 1000 can be attained for peptide samples in approximately 3 hours by employing elevated temperatures, provided that samples are not thermally unstable. In weighing the cost of analysis time against the value of information gained, even higher peak capacities can presumably be obtained by operating a slower flow rates than those discussed with regard to the gradient characterization of the 216 cm column in Section 4.2.4. Settings in which a long column, high resolution approach may prove especially beneficial are in the analysis of extremely complex samples, such as those encountered in “-omics” fields, where hundreds or thousands of components can complicate the interpretation of data. This type of approach should also be considered compatible with multi-dimensional separations, which can serve to further increase resolving power.

4.4 References

- ¹ Scott, R.P.W.; Kucera, P. *Journal of Chromatography* **1979**, 169, 51-72.
- ² Menet, H.G.; Careil, P.C.; Rosset, R.H. *Analytical Chemistry* **1984**, 56, 1770
- ³ Menet, H.; Gareil, P.; Caude, M.; Rosset, R. *Chromatographia* **1984**, 18, 73
- ⁴ Tanaka, N.; Kinoshita, H.; Araki, M.; Tsuda, T. *Journal of Chromatography* **1985**, 332, 57 – 69.
- ⁵ MacNair, J.E.; Lewis, K.C.; Jorgenson, J.W. *Analytical Chemistry* **1997**, 69, 983-989.
- ⁶ MacNair, J.E.; Patel, K.D.; Jorgenson, J.W. *Analytical Chemistry* **1999**, 71, 700-708.
- ⁷ Shen, Y.; Zhang, R.; Moore, R.J.; Kim, J.; Metz, T.O.; Hixson, K.M.; Zhao, R.; Livesay, E.A.; Udseth, E.A.; Smith, R.D. *Analytical Chemistry* **2005**, 77, 3090-3100.
- ⁸ Zhou, F.; Lu, Y.; Ficarro, S.B.; Webber, J.T.; Marto, J.A. *Analytical Chemistry* **2012**, ASAP
- ⁹ Stoll, D.R.; Li, X.; Wang, X.; Carr, P.W. *Journal Chromatography A* **2007**, 1168, 3-43.
- ¹⁰ Guiochon, G.; Gritti, F. *Journal of Chromatography A* **2012**, 1218, 1915-1938.
- ¹¹ Tijssen, R.; Bleumer, J.P.A.; Smith, A.L.C.; Van Kreveld, M.E. *Journal of Chromatography* **1981**, 218, 137 – 165.
- ¹² Kucera, P.; Guiochon, G. *Journal of Chromatography* **1984**, 283, 1-20.
- ¹³ Liu, G.; Djordjevic, N.M.; Erni, F. *Journal of Chromatography* **1992**, 592, 239-247.
- ¹⁴ Swart, R.; Kraak, J.C.; Poppe, H. *Journal of Chromatography A* **1995**, 689, 177-187.
- ¹⁵ Desmet, G.; Clicq, D.; Gzil, P. *Analytical Chemistry* **2005**, 77, 4058 – 4070.
- ¹⁶ Miyamoto, K.; Hara, T.; Kobayashi, H.; Morisaka, H.; Tokuda, D.; Horie, K.; Koduki, K.; Makino, S.; Núñez, O.; Yang, C.; Kawabe, T.; Ikegami, T.; Takubo, H.; Ishihama, Y.; Tanaka, N. *Analytical Chemistry* **2008**, 80, 8741 – 8750.
- ¹⁷ Slentz, B.E.; Penner, N.A.; Regnier, F. *Journal of Separation Science* **2002**, 25, 11011-1018.
- ¹⁸ De Pra, M.; Kok, W.T.; Gardeniers, J.G.E.; Desmet, G.; Eeltink, S.; van Nieuwesteele, J.W.; Schoenmakers, P.J. *Analytical Chemistry* **2006**, 78, 6519 – 6525.

- ¹⁹ De Malsche, W.; Eghbali, H.; Clicq, D.; Vangeloooven, J.; Gardeniers, H.; Desmet, G. *Analytical Chemistry* **2007**, 79, 5915 – 5926.
- ²⁰ De Malsche, W.; Op De Beeck, J.; De Bruyne, S.; Gardeniers, H.; Desmet, G. *Analytical Chemistry* **2012**, 84, 1214 – 1219.
- ²¹ Wilke, C.R.; Chang, P. *American Institute of Chemical Engineers Journal* **1955**, 1, 265.
- ²² Guillarme, D.; Heinisch, S.; Rocca, J.L. *Journal of Chromatography A* **2004**, 1052, 39-51.
- ²³ Chen, H.; Horvath, C. *Analytical Methods and Instrumentation* **1993**, 1, 213-222.
- ²⁴ Zhu, C.; Goodall, D.M.; Wren, S.A.C.; *LCGC Asia Pacific* **2005**, 8, 48-59.
- ²⁵ Neue, U.D. *Journal of Chromatography A* **2005**, 1079, 153.
- ²⁶ Wang, X.; Stoll, D.R.; Schellinger, A.P.; Carr, P.W. *Analytical Chemistry* **2006**, 78, 3406
- ²⁷ Liu, H.; Finch, J.W.; Lavalley, M.J.; Collamati, R.A.; Benevides, C.C.; Gebler, J.C. *Journal of Chromatography A* **2007**, 1147, 30
- ²⁸ Neue, U.D. *Journal of Chromatography A* **2008**, 1184, 107-130.
- ²⁹ Hsieh, S.; Jorgenson, J.W. *Analytical Chemistry* **1996**, 68, 1212-1217.
- ³⁰ Bruns, S.; Grinias, J.P.; Blue, L.E.; Jorgenson, J.W.; Tallarek, U. *Analytical Chemistry* **2012**, 84, 4496-4503.
- ³¹ Eschelbach, J.W.; Jorgenson, J.W. *Analytical Chemistry* **2006**, 78, 1697-1706.
- ³² Liu, H.; Finch, J.W.; Lavalley, M.J.; Collamati, R.A.; Benevides, C.C.; Gebler, J.C. *Journal of Chromatography A* **2007**, 30-36.
- ³³ Snyder, L.R.; Kirkland, J.J.; Dolan, J. *Introduction to Modern Liquid Chromatography*. 3rd Ed., Wiley: New York, 2010.
- ³⁴ Neue, U.D. *HPLC Columns: Theory, Technology, and Practice*; Wiley-VCH, Inc.: New York, NY, **1997**.

4.5 Figures

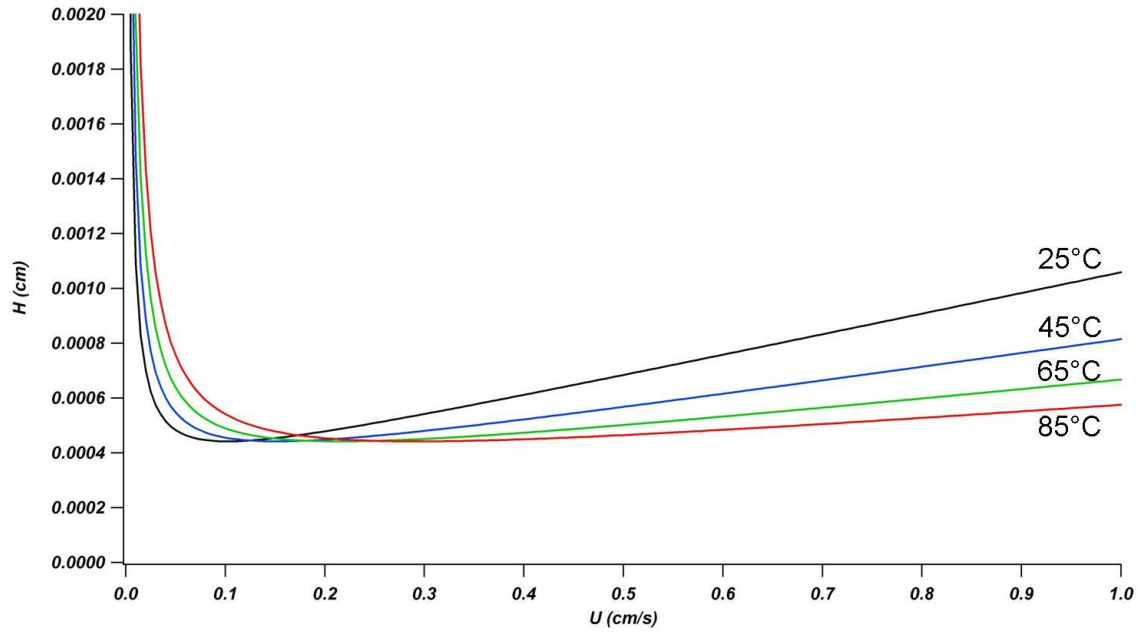


Figure 4-1: Theoretical H vs. U curves for 1.9 μm particles at 25, 45, 65, and 85°C, using reduced A-, B-, and C- terms of 1.5, 1.0, and 0.1, respectively. Mobile phase viscosities are calculated according to the Chen-Horvath equation, and diffusion coefficients are scaled accordingly.

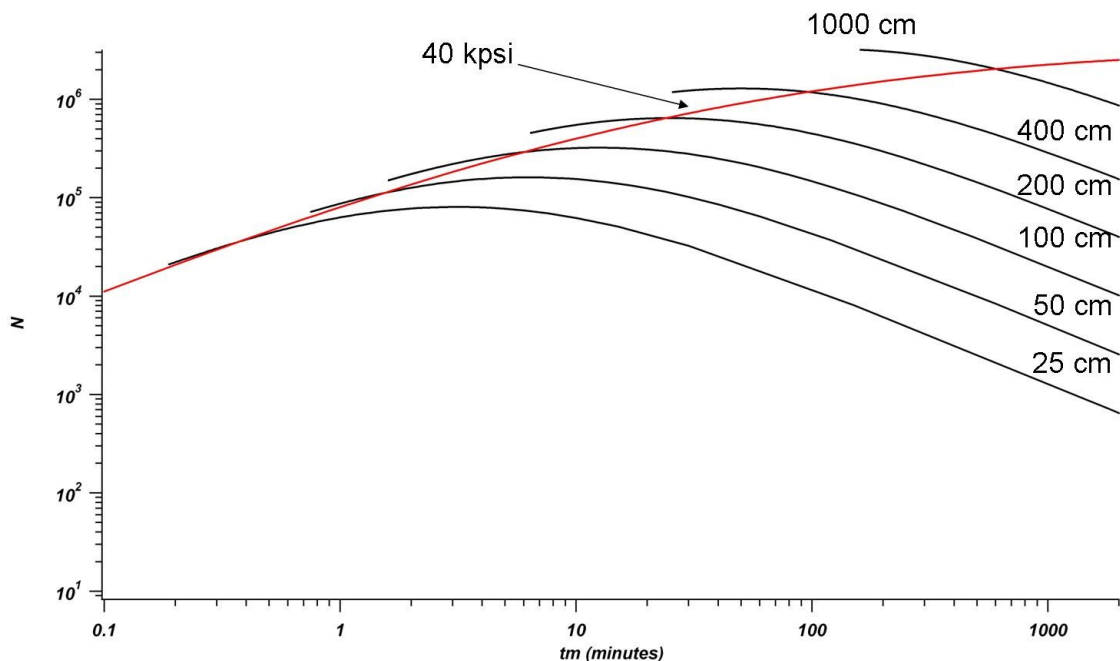


Figure 4-2: Series of theoretical curves representing the performance of 25 cm – 1000 cm columns. Curves are constructed using reduced van Deemter coefficients of 1.0, 1.0, and 0.1 for A-, B-, and C-, respectively. Mobile phase viscosities of 0.89 cP and diffusion coefficients of $8.0 \times 10^{-6} \text{ cm}^2/\text{s}$ are assumed. Each dead-time corresponds to an operating pressure. The intersection of the red trace with the curves shows expected performance when operating at 40,000 psi.

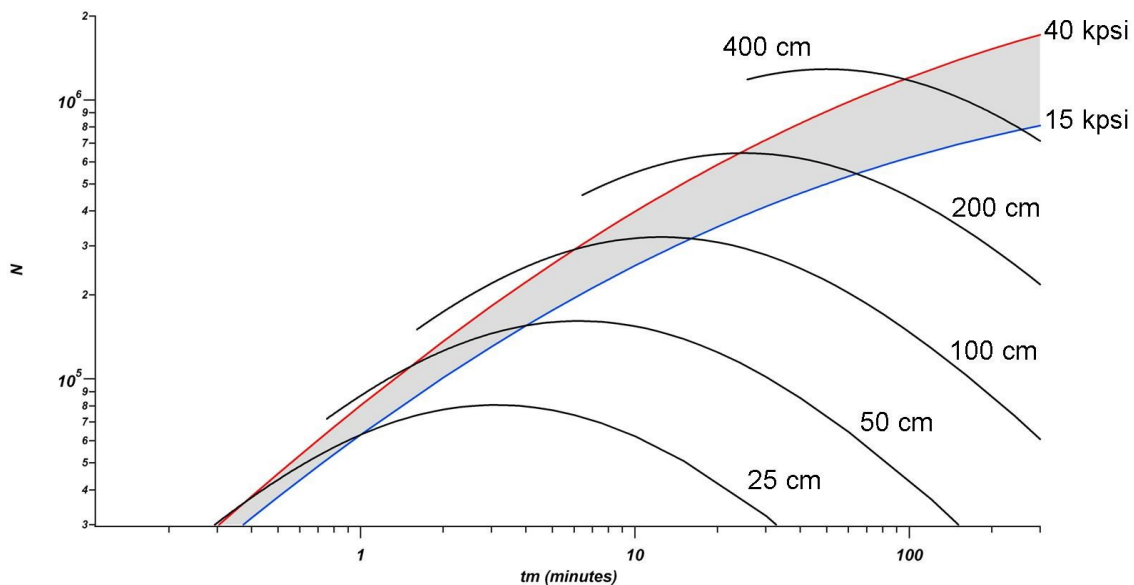


Figure 4-3: Theoretical plates vs. column dead times for 25 cm – 400 cm columns. The separation speeds and efficiencies that become newly accessible upon increasing maximum operating pressure from 15,000 psi to 40,000 psi are represented in the shaded region.

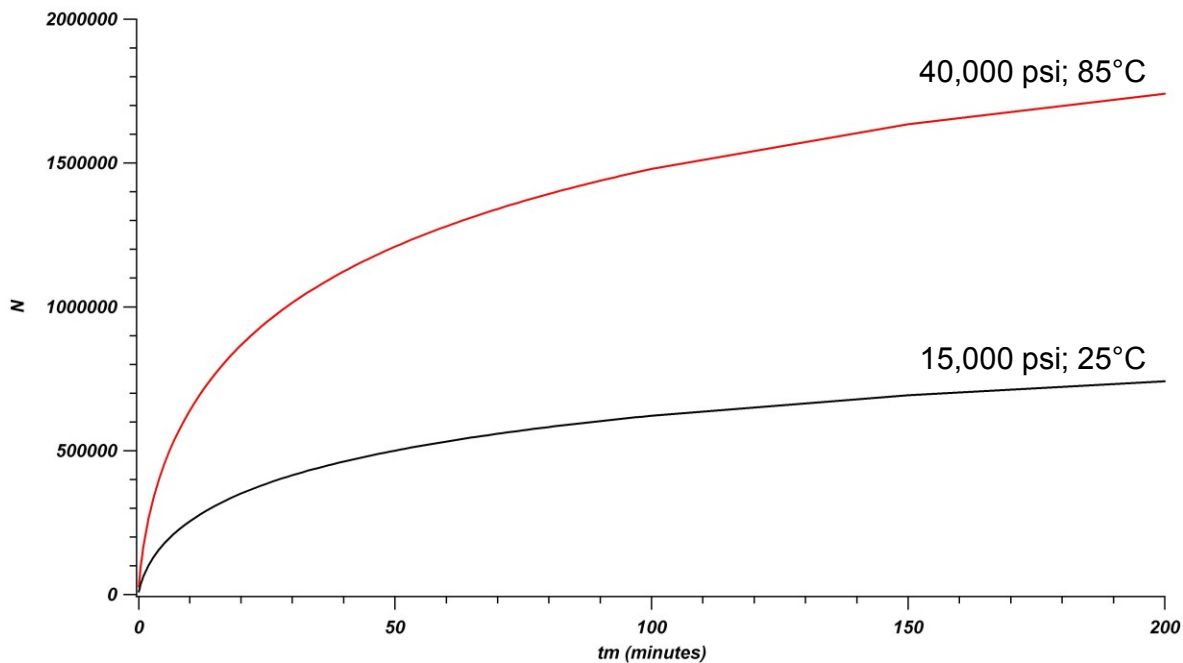


Figure 4-4: Maximum number of theoretical plates vs. column dead times for columns packed with 1.9 μm particles given a limiting operating pressure. The black curve represents columns run at 25°C and 15,000 psi. The red trace highlights the increase in accessible efficiencies that become available when operating at 85°C and 40,000 psi. Each dead-time corresponds to a column length.

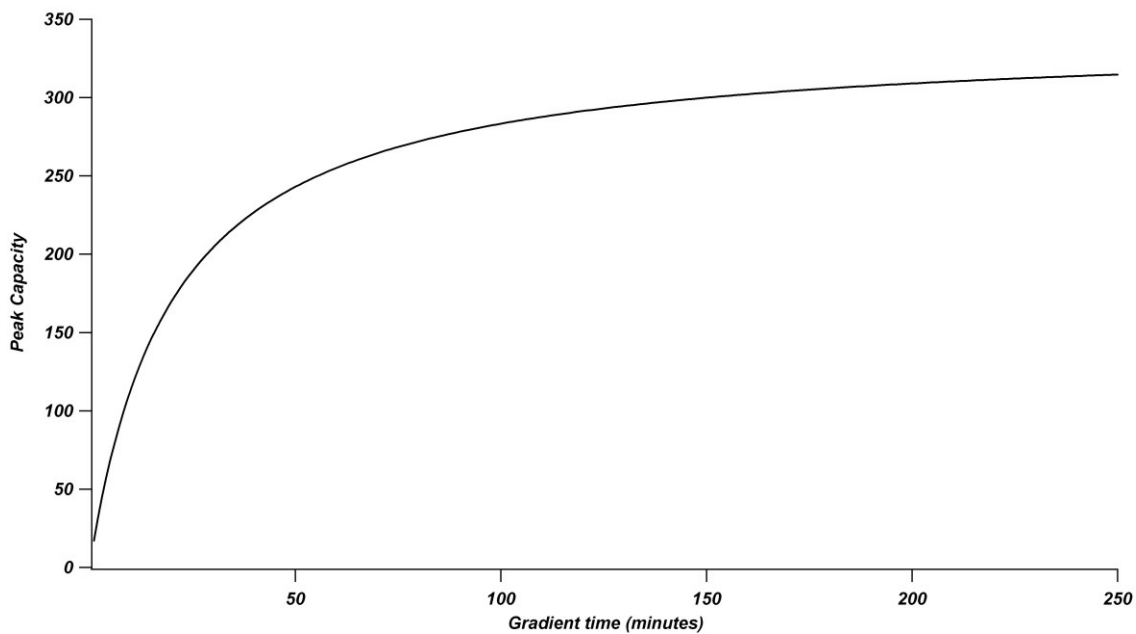


Figure 4-5: Peak capacity as a function of gradient time using Equation 4-10 for a 15 cm x 4.6 mm column with 5 μm particles and a fixed flow rate of 1.0 mL/min. Theoretical plates are estimated using $A=5d_p$, $B=1D_m$, and $C=d_p^2/(6D_m)$. A diffusion coefficient of $8.0 \times 10^{-6} \text{ cm}^2/\text{s}$ is assumed.

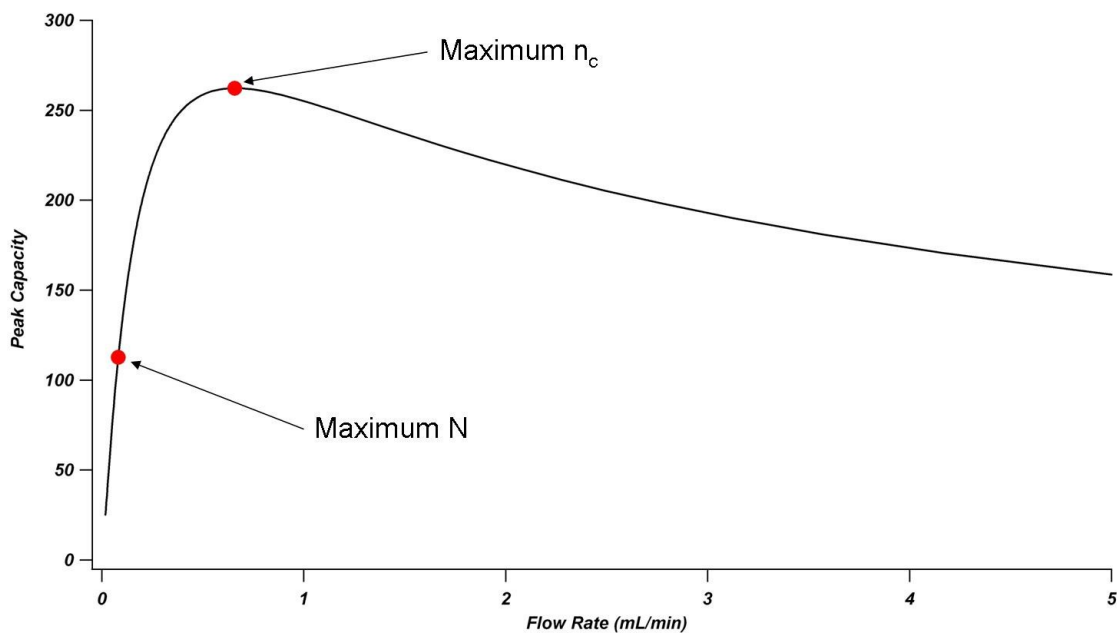


Figure 4-6: Peak capacity as a function of flow rate for a 15 cm x 4.6 mm column packed with 5 μ m particles. Gradient time is fixed at 1 hour. Maximum N as determined by the van Deemter coefficients $A=5d_p$, $B=1D_m$, and $C=d_p^2/(6D_m)$ occurs at a flow rate 8x slower than that which yields the highest peak capacity.

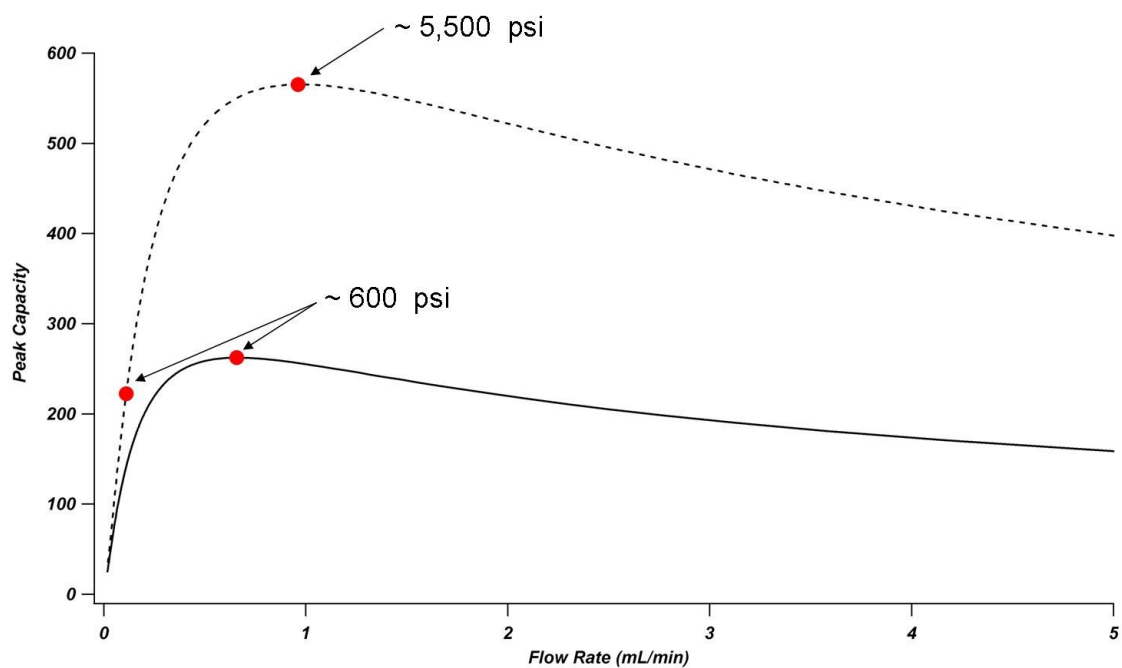


Figure 4-7: Peak capacity as a function of column flow rate for 15 cm x 4.6 mm columns. The solid trace is for 5 μm particles; the dashed trace is for 1.9 μm particles. Gradient time is fixed at 1 hour.

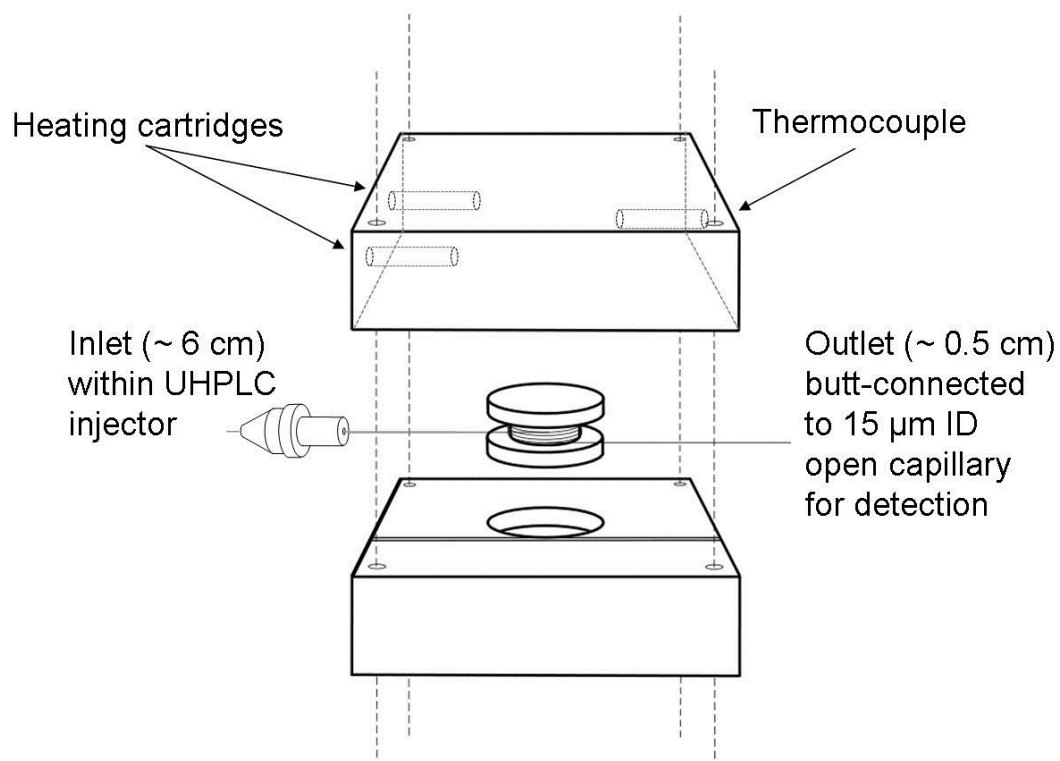


Figure 4-8: Experimental set-up for performing isocratic characterization at elevated temperatures. The majority of the column is housed within an aluminum heating block, held at temperature through feedback control of two heating cartridges. The first ~6 cm of column is unthermostatted within the column injector. 0.5 cm of column outlet protrudes from the heating block and is butt-connected to an open capillary for electrochemical detection.

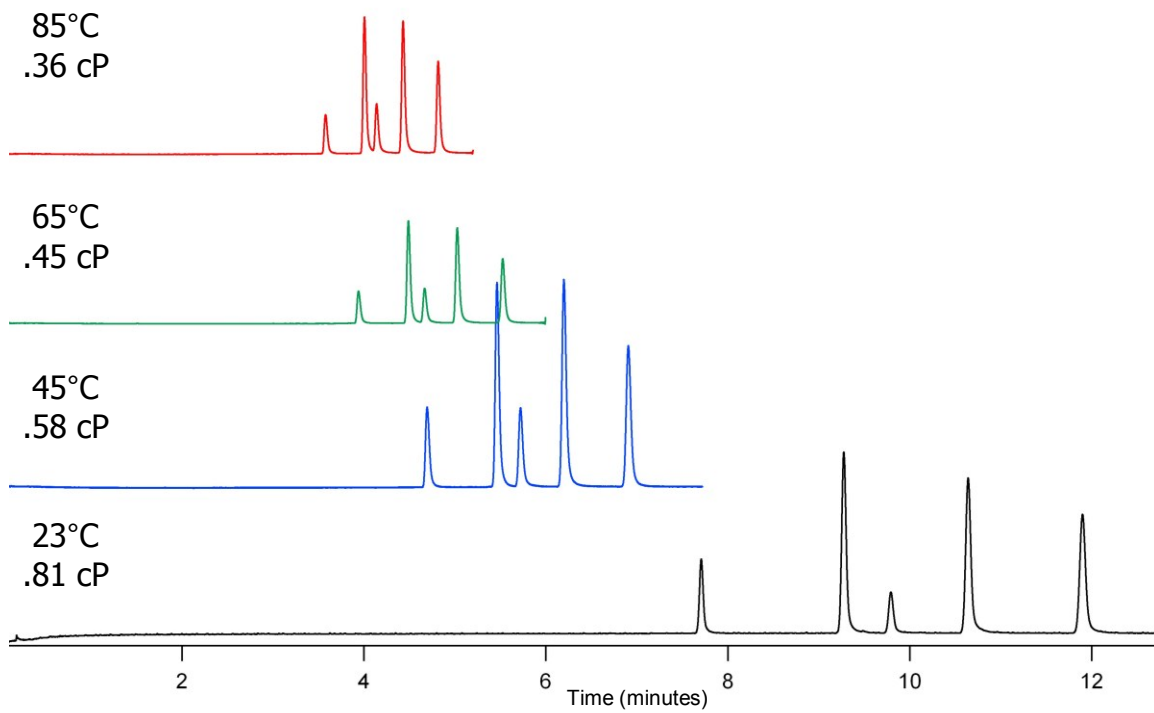
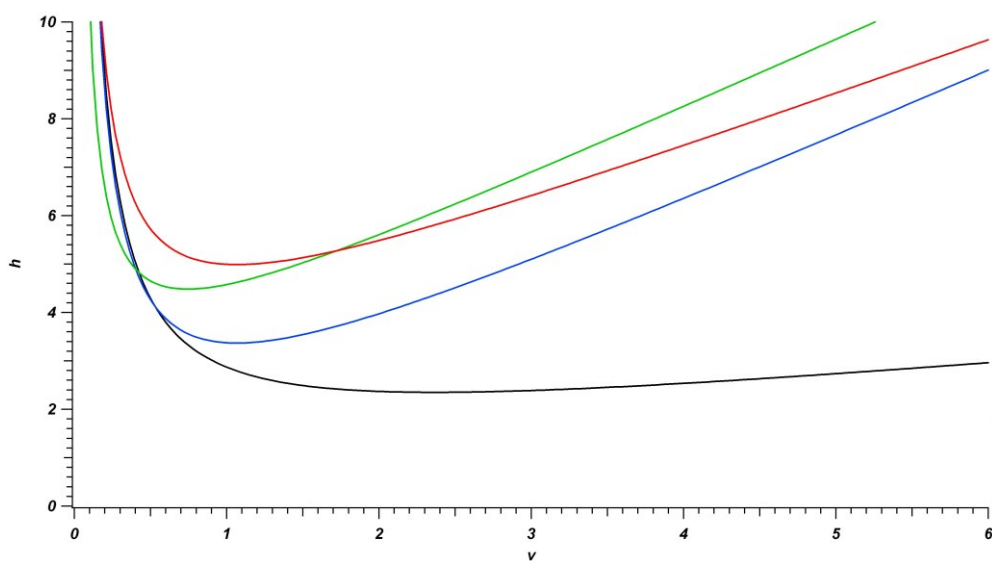


Figure 4-9: Chromatograms collected near optimum linear velocity for a 66 cm x 50 μm ID column packed with 1.9 μm BEH particles at 23, 45, 65, and 85°C in 50/50 acetonitrile/water and 0.1% TFA.







	Temp.	A	B	C
	23°C	1.03 ± 0.09	1.56 ± 0.04	0.28 ± 0.02
	45°C	0.40 ± 0.86	1.58 ± 0.31	1.39 ± 0.30
	65°C	2.37 ± 0.36	0.79 ± 0.09	1.42 ± 0.18
	85°C	2.54 ± 0.23	1.30 ± 0.09	1.15 ± 0.07

Figure 4-10: Overlaid reduced van Deemter curves for hydroquinone collected at 23, 45, 65, and 85°C for a 66 cm x 50 µm ID column packed with 1.9 µm BEH particles.

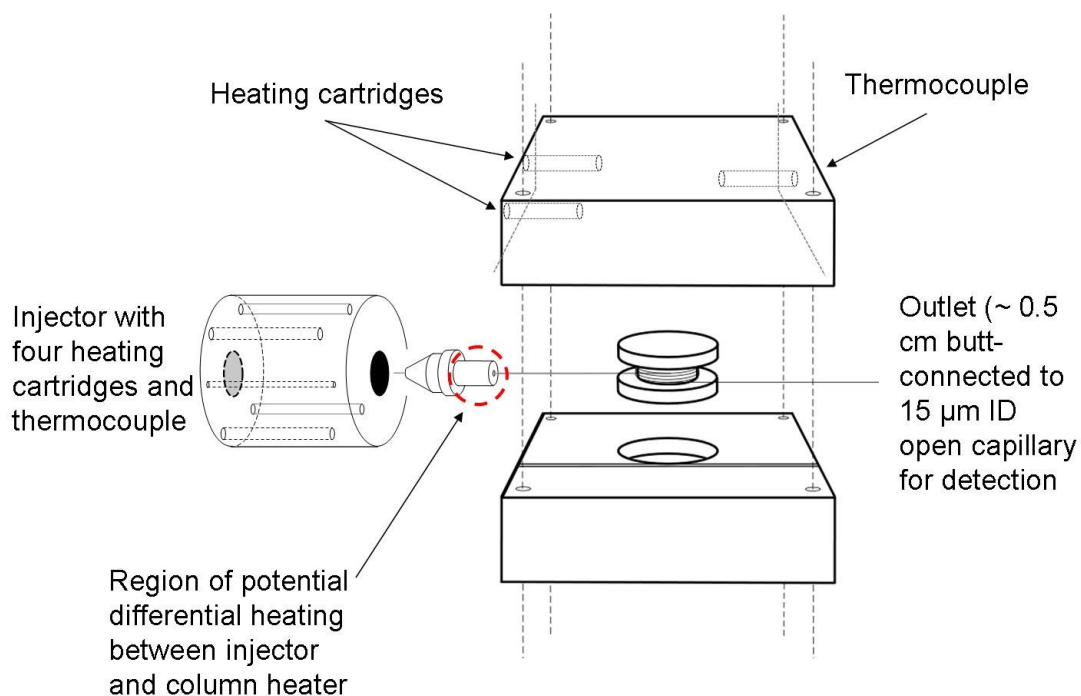


Figure 4-11: Modified experimental set-up for performing isocratic characterization at elevated temperatures. The majority of the column is housed within an aluminum heating block, held at temperature through feedback control of two heating cartridges. The injector is held at matching temperature using four heating cartridges. Approximately 2 cm of column resides between the injector and heating block. 0.5 cm of column outlet protrudes from the heating block and is butt-connected to an open capillary for electrochemical detection.

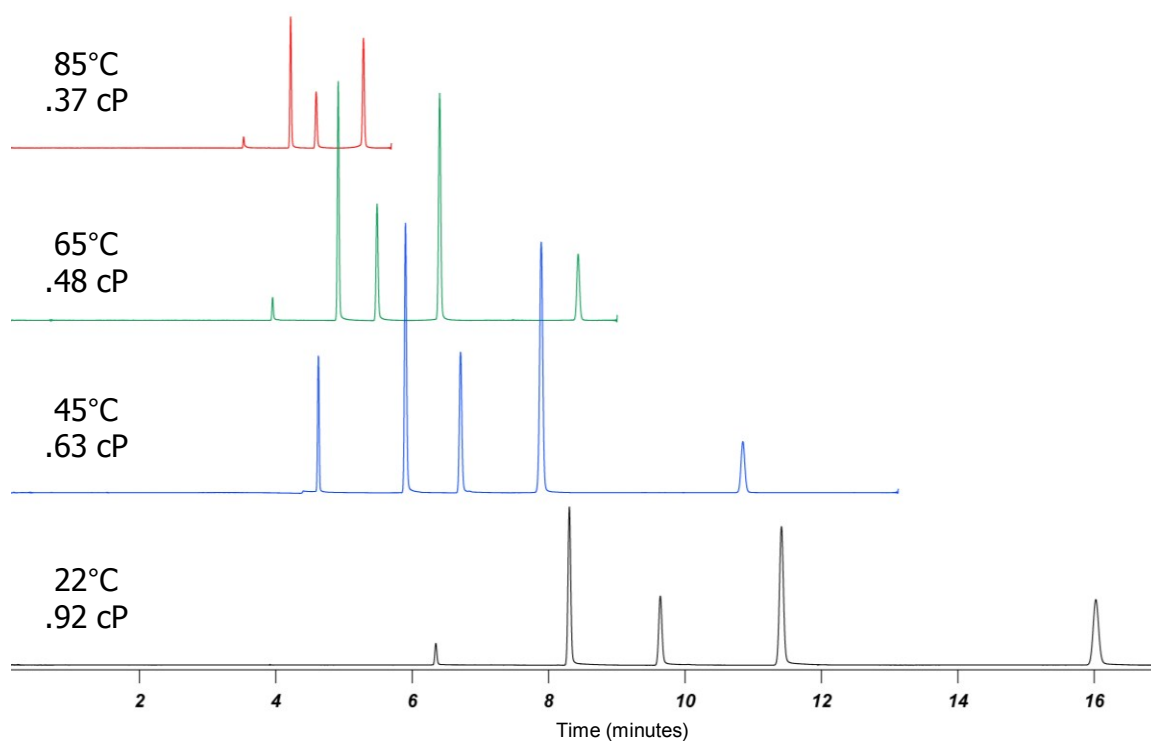


Figure 4-12: Chromatograms collected near optimum linear velocity for a 60 cm x 50 μ m ID column packed with 1.9 μ m BEH particles at 23, 45, 65, and 85°C using 30/70 acetonitrile/water and 0.1% TFA.

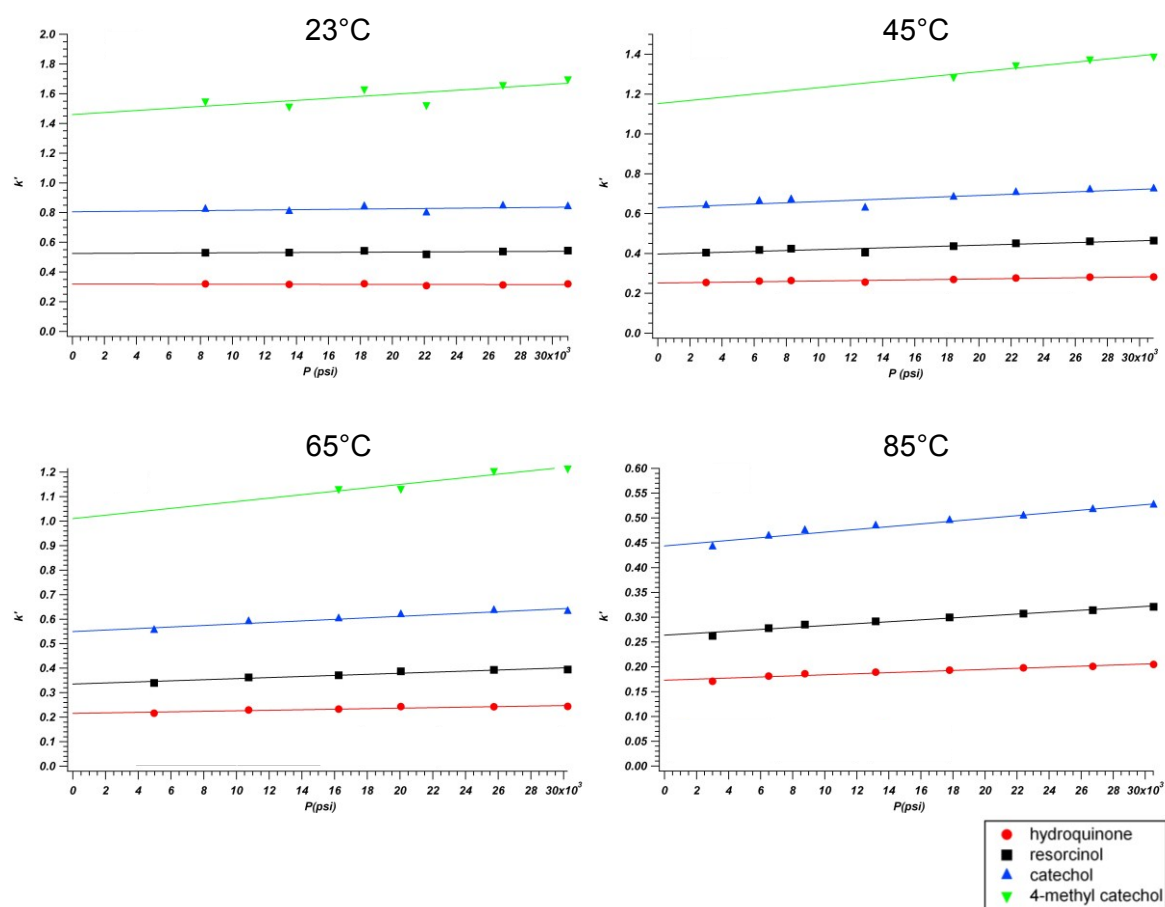


Figure 4-13: Retention as a function of operating pressure at 23, 45, 65, and 85°C for a 60 cm x 50 μ m ID column packed with 1.9 μ m BEH in 30/70 acetonitrile/water and 0.1% TFA.

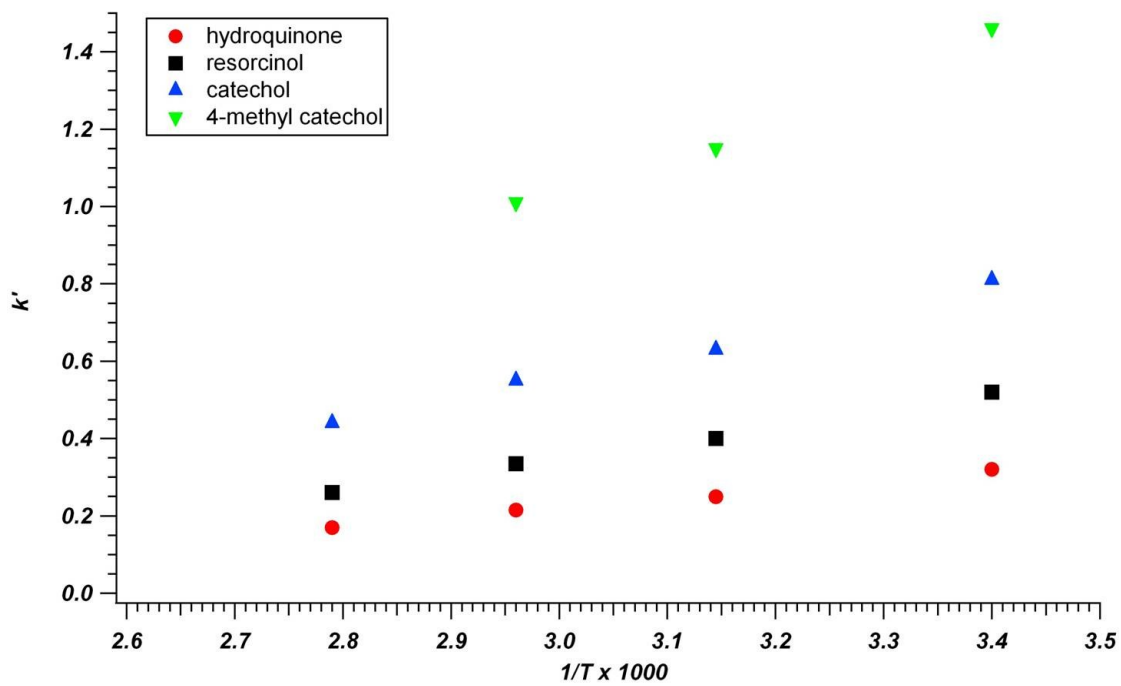


Figure 4-14: Van't Hoff plot of the retained test analytes at 23, 45, 65, and 85°C in 30/70 acetonitrile/water and 0.1% TFA.

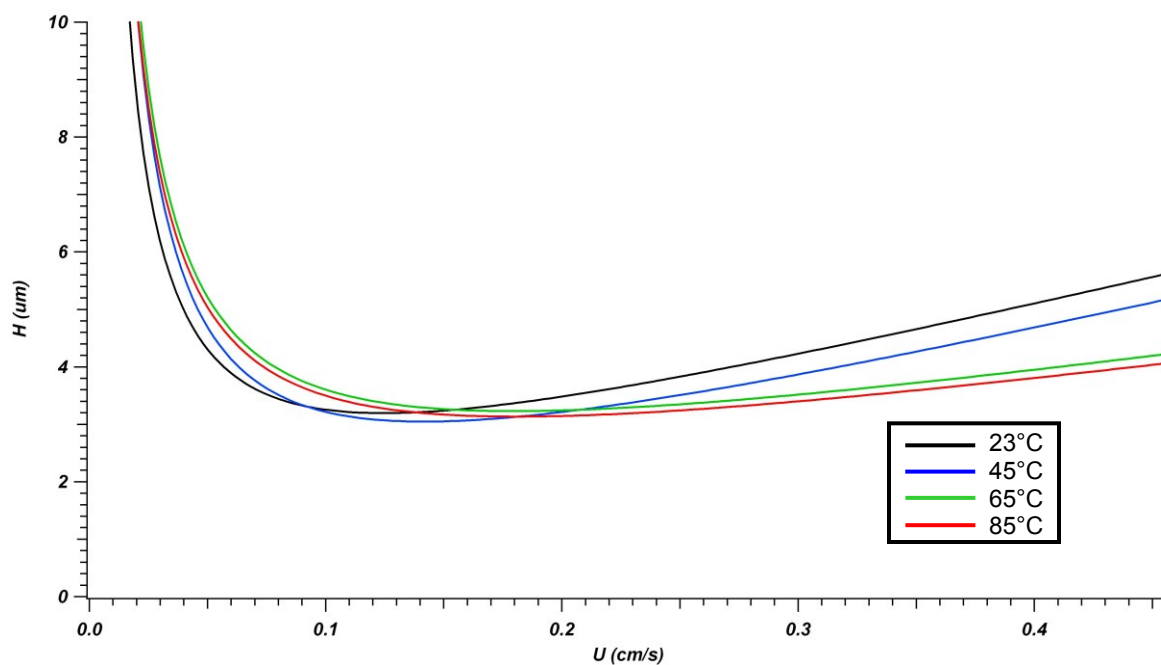


Figure 4-15: H vs. U plots for hydroquinone at 23, 45, 65, and 85°C. Comparison with theoretical predictions in Figure 4-1 reveals the expected increase in U_{opt} at elevated temperatures and preserved column efficiency.

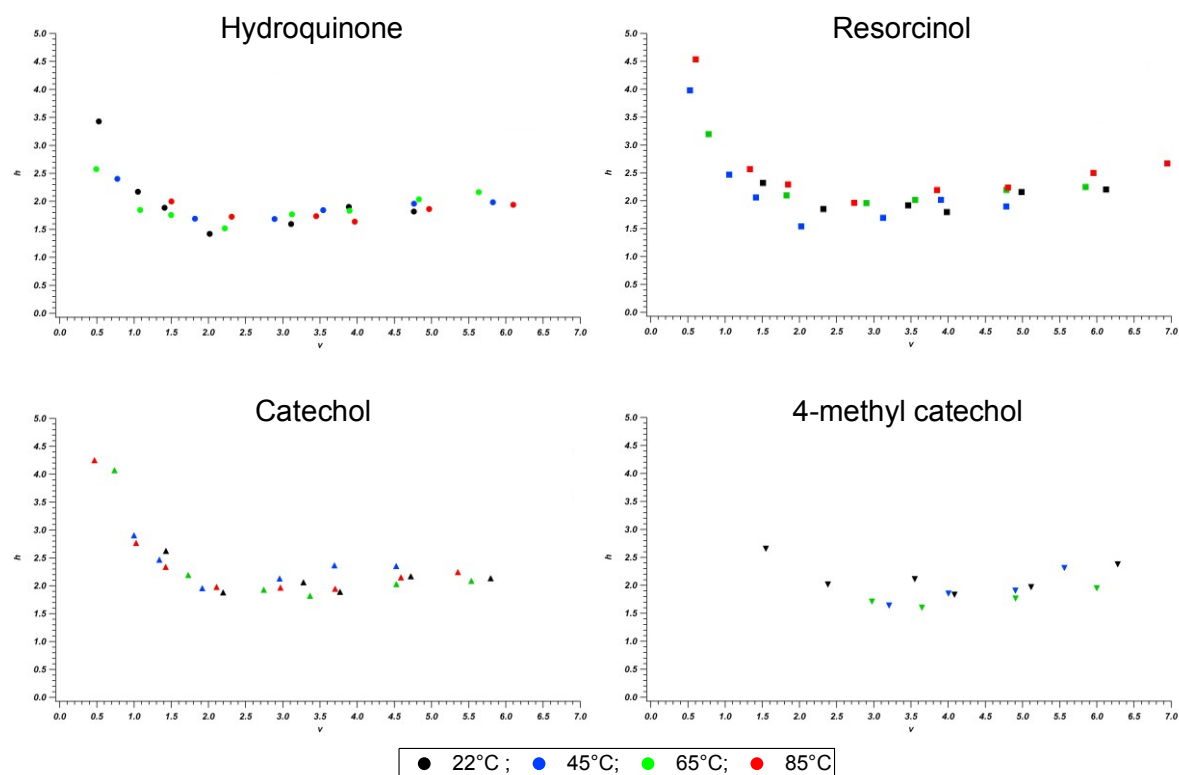


Figure 4-16: Overlay of reduced van Deemter plot for each analyte at 23, 45, 65, and 85°C. Reduced parameters at elevated temperatures are calculated from estimated pressure-dependent mobile phase viscosities and corresponding increases in analyte diffusion coefficients.

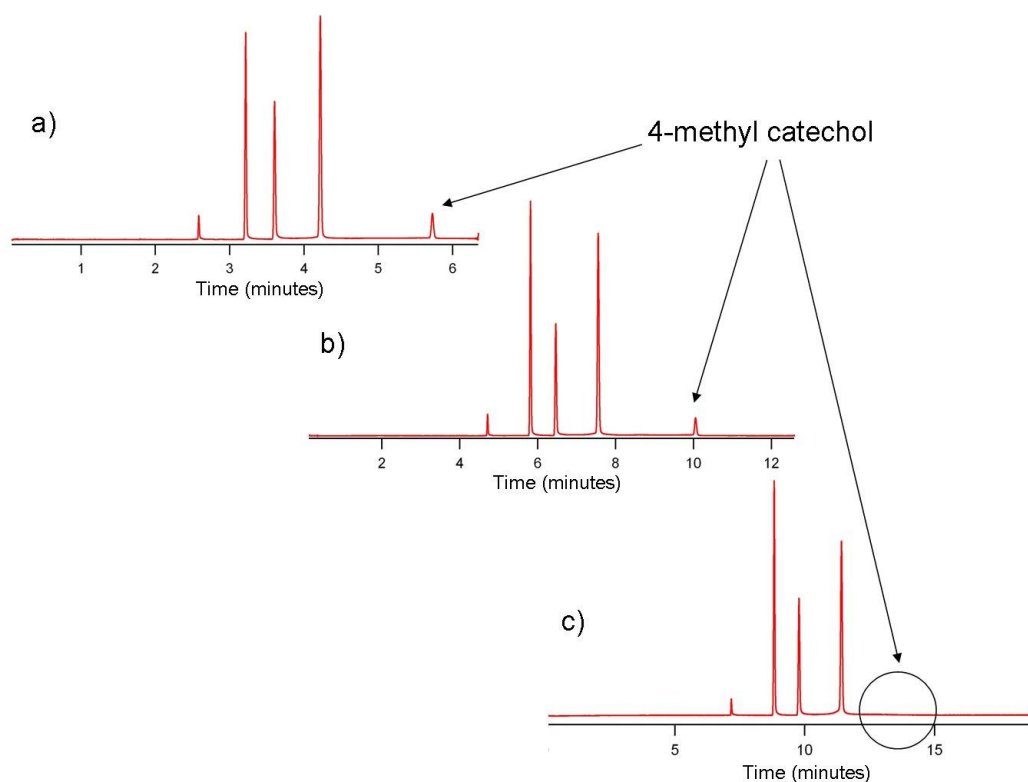


Figure 4-17: Chromatograms highlighting the on-column oxidation of 4-methyl catechol. With longer analysis times, the peak is rendered electrochemically undetectable. a) 33,000 psi; b) 18,000 psi; c) 12,000 psi.

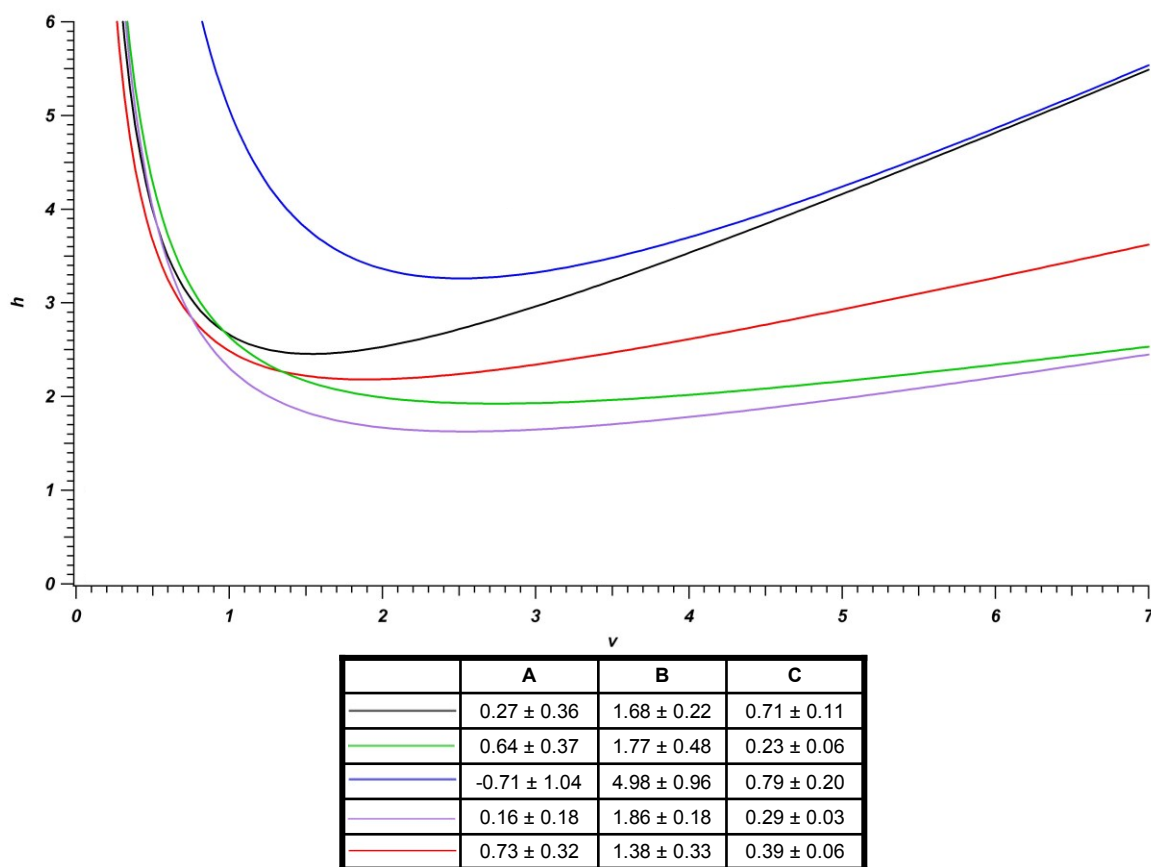


Figure 4-18: Overlay of van Deemter performances for five ~100 cm x 50 μ m ID columns packed over a three month period. Experimental packing conditions were virtually identical with particle slurry concentrations ranging between 5-10 mg/mL.

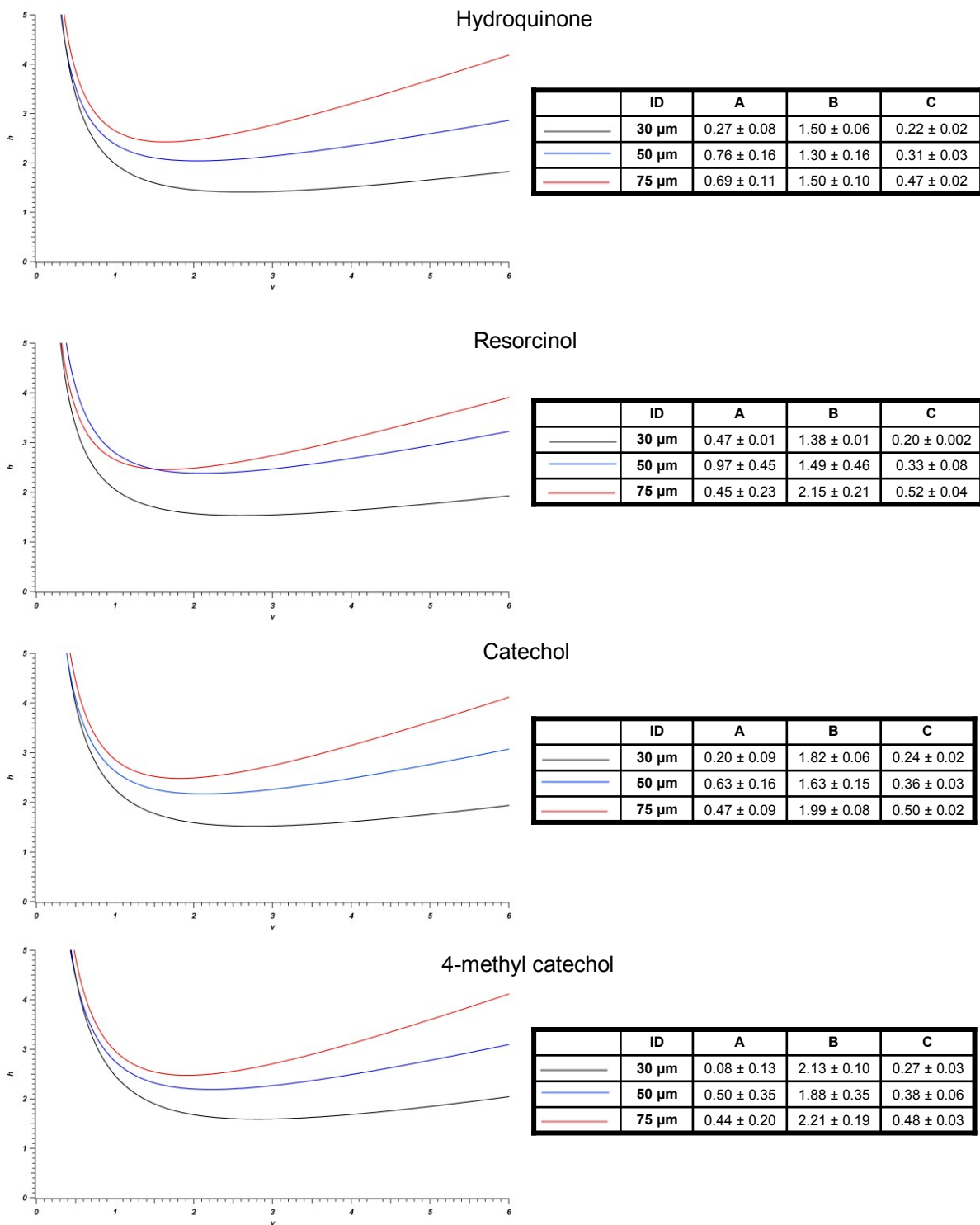


Figure 4-19: Effect of column inner diameter on performance of ~100 cm columns. As observed in the past, performance improves dramatically with decreasing ID.

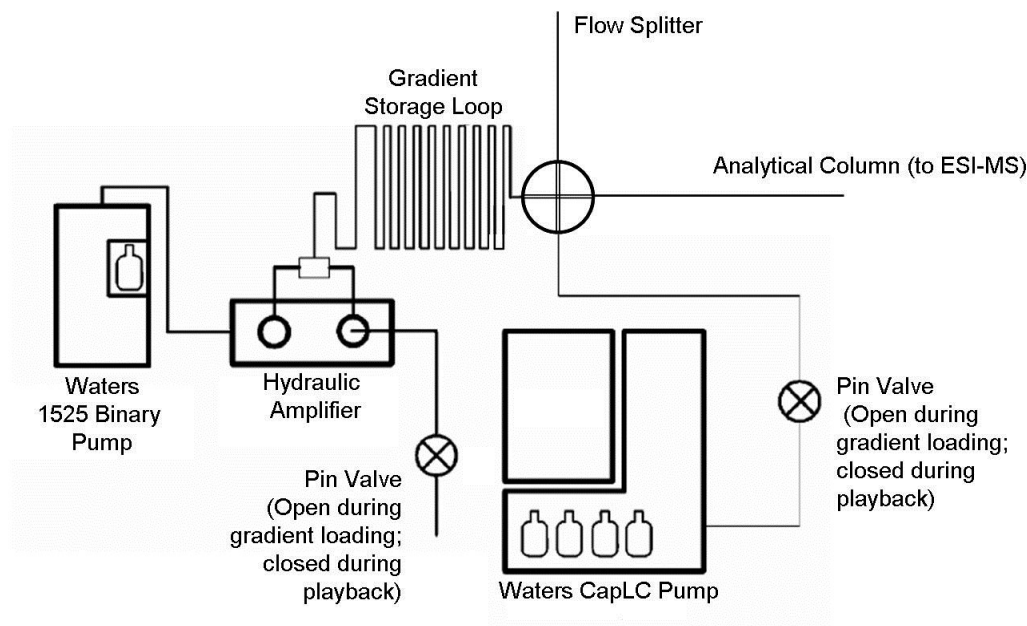


Figure 4-20: Schematic view of UHPLC gradient system. The gradient is generated by a Waters CapLC pump and loaded onto an external storage loop, followed by the sample. Flow resistances of the packed analytical column and small-ID flow splitter ensure that the vast majority of flow reaches the loop. Once the sample is loaded, both pin valves are closed, and the hydraulic amplifier is engaged to push the sample and gradient into the micro-volume cross. Much of the sample and gradient is diverted to waste through the flow splitter, while a small volume makes it onto the analytical column for analysis.

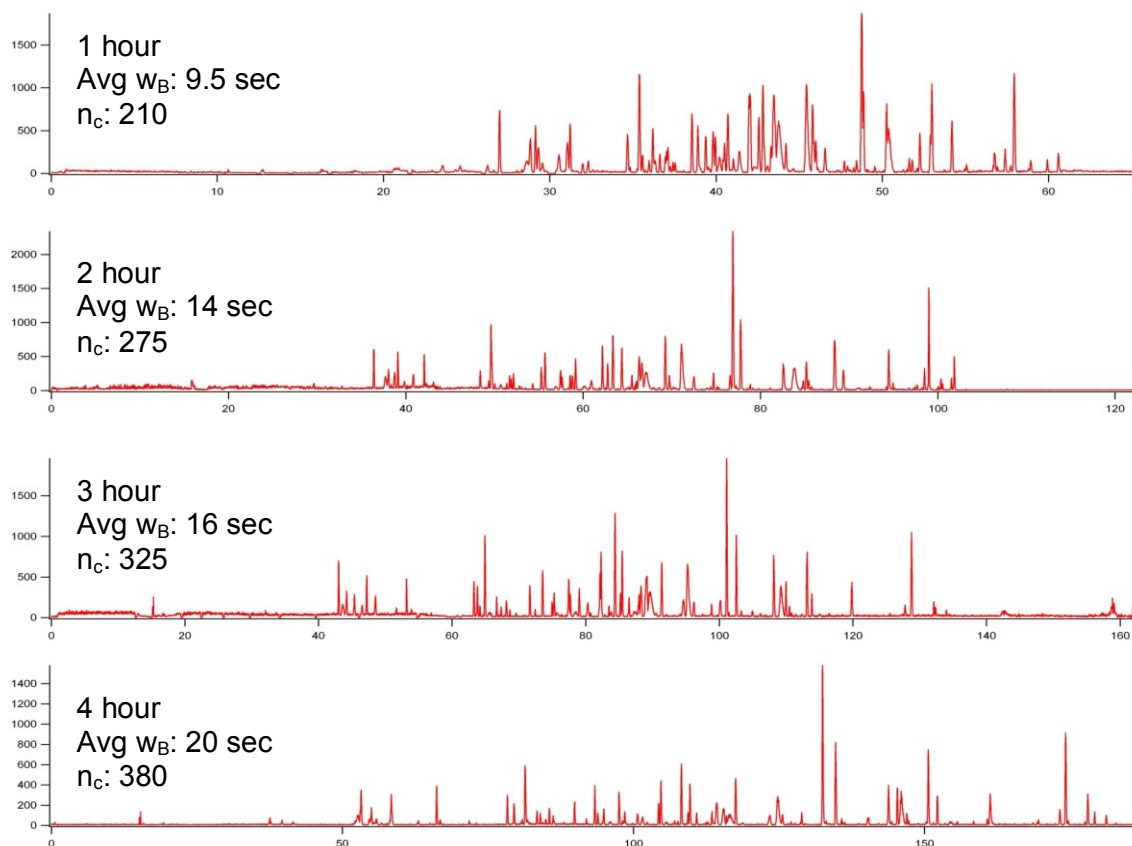


Figure 4-21: Representative chromatograms of a tryptic digest of bovine serum albumin run in 1-50% acetonitrile gradients corresponding to total run times of 60, 120, 180, and 240 minutes. Runs were performed on a 100 cm x 50 μ m ID column packed with 1.9 μ m BEH particles. Operating pressure was \sim 24,000 psi, but varied throughout the runs with changing mobile phase viscosities. Mass spectrometric detection was accomplished using a Waters LCT-TOF.

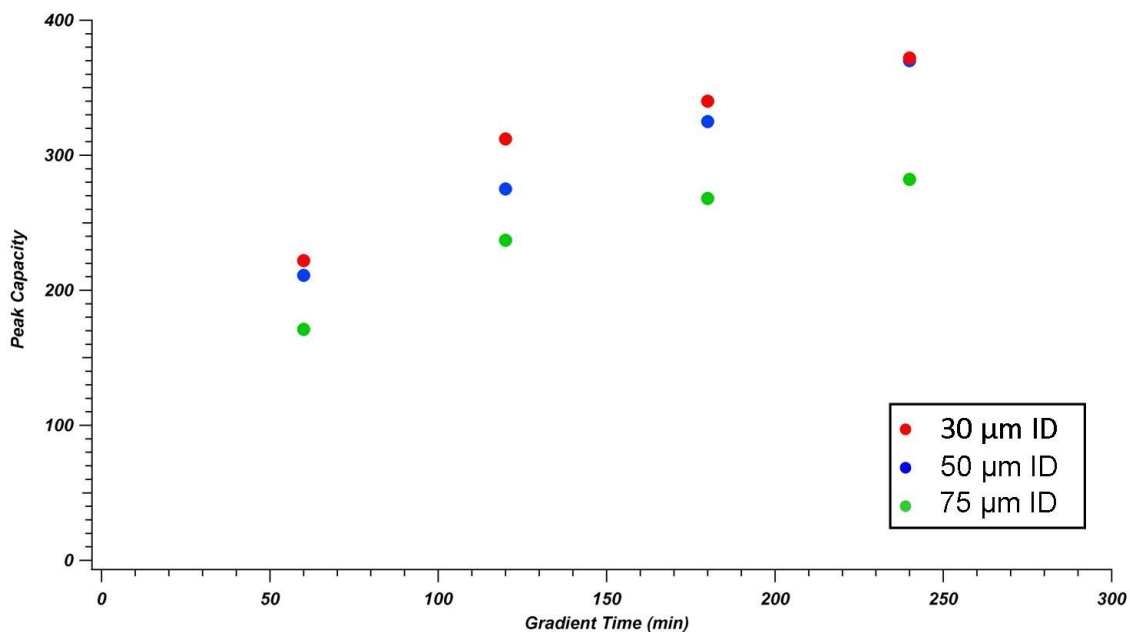


Figure 4-22: Peak capacities vs. gradient time for 100 cm columns with different inner diameters. Isocratic performance was best for the 30 μm ID column and worst for the 75 μm ID column. Peak capacities were calculated by determining 4σ base widths of representative peaks in 1-50% acetonitrile gradients for a BSA tryptic digest sample.

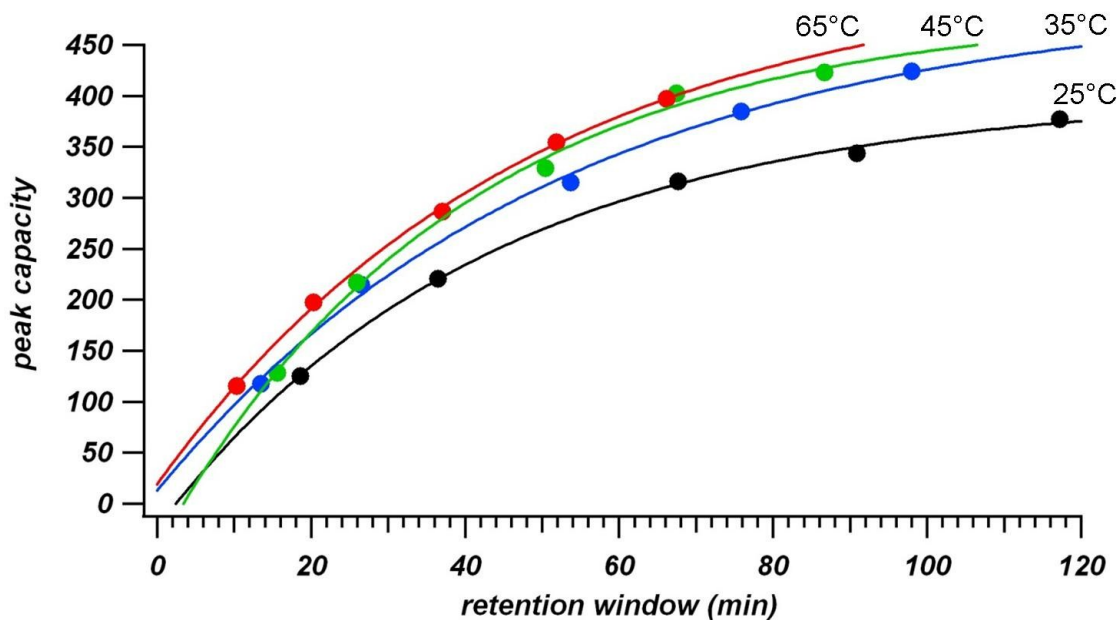


Figure 4-23: Peak capacity vs. retention window for a 100 cm x 30 µm ID column packed with 1.9 µm particles. 1-50% acetonitrile gradients for a BSA tryptic digest sample were run and peak capacities determined from 4σ base widths of representative peaks. Retention windows were determined from the elution times of two characteristic peaks, and peak capacities calculated by dividing the retention window by the average peak width.

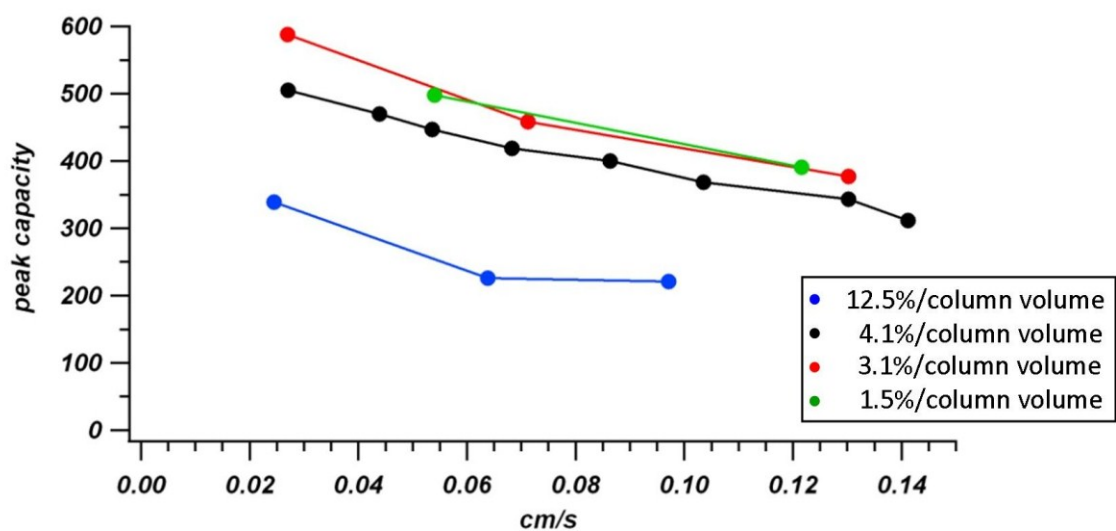


Figure 4-24: Peak capacity vs. mobile phase linear velocity as determined by the column dead time for four gradient steepnesses, represented by % change of mobile phase composition per column volume.

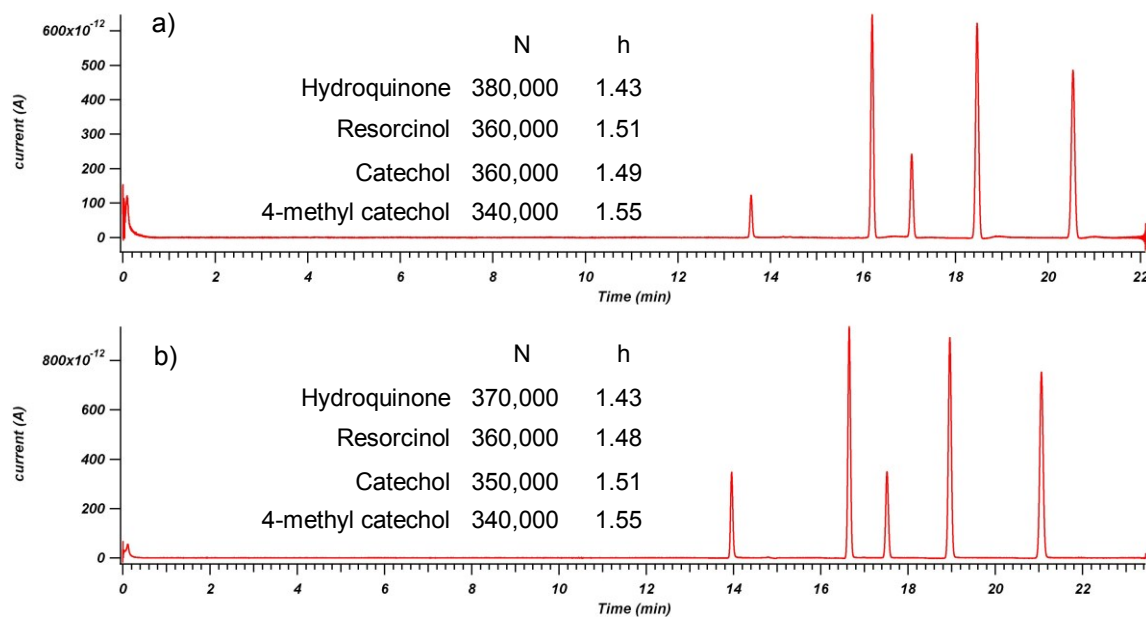


Figure 4-25: Representative chromatograms of a) 105 cm and b) 103 cm x 50 μm ID columns packed with a 100 mg/mL slurry of 1.9 μm BEH particles.

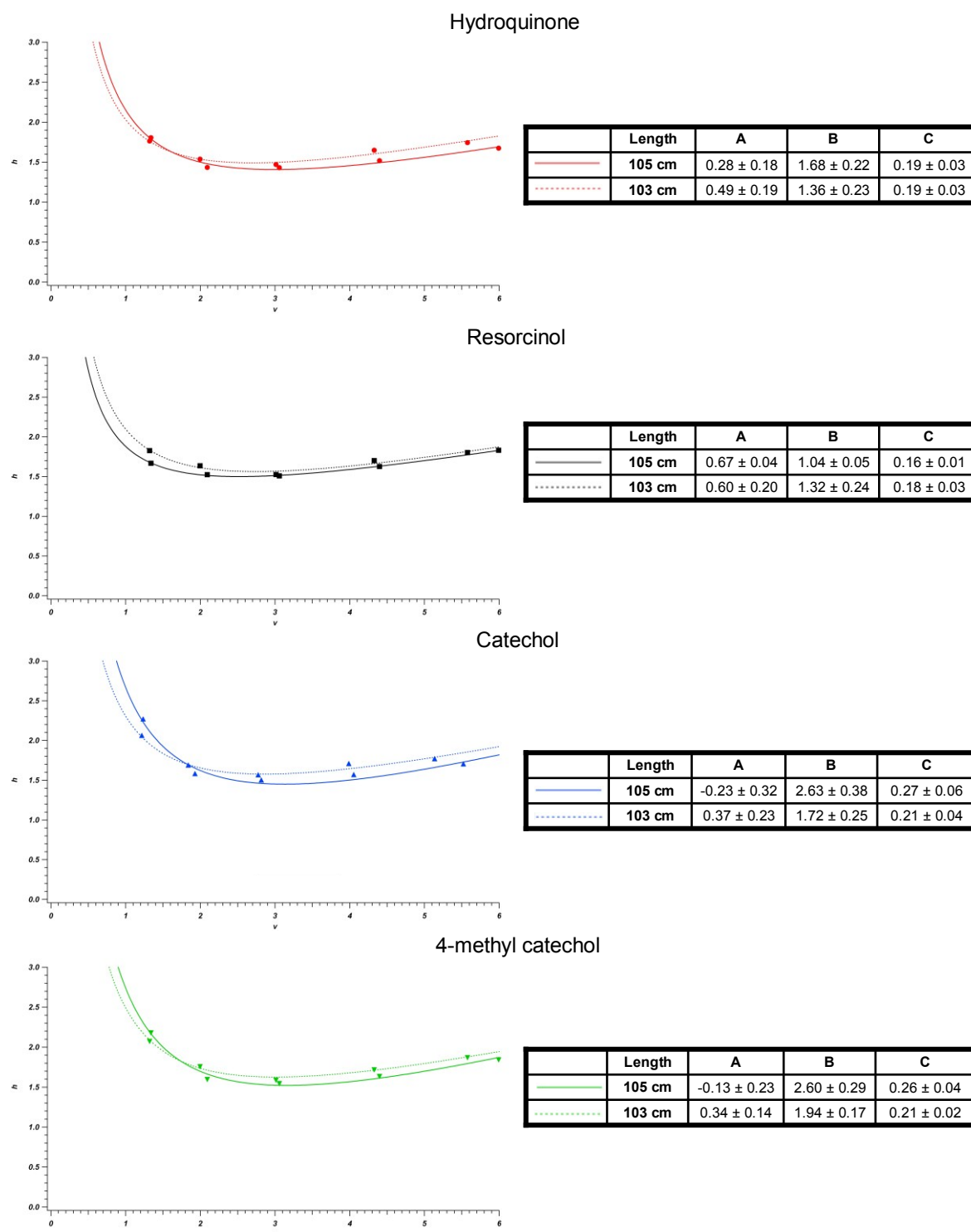


Figure 4-26: Reduced van Deemter curves of the consecutively packed 105 cm and 103 cm x 50 μ m ID columns packed with 100 mg/mL slurries of 1.9 μ m BEH.

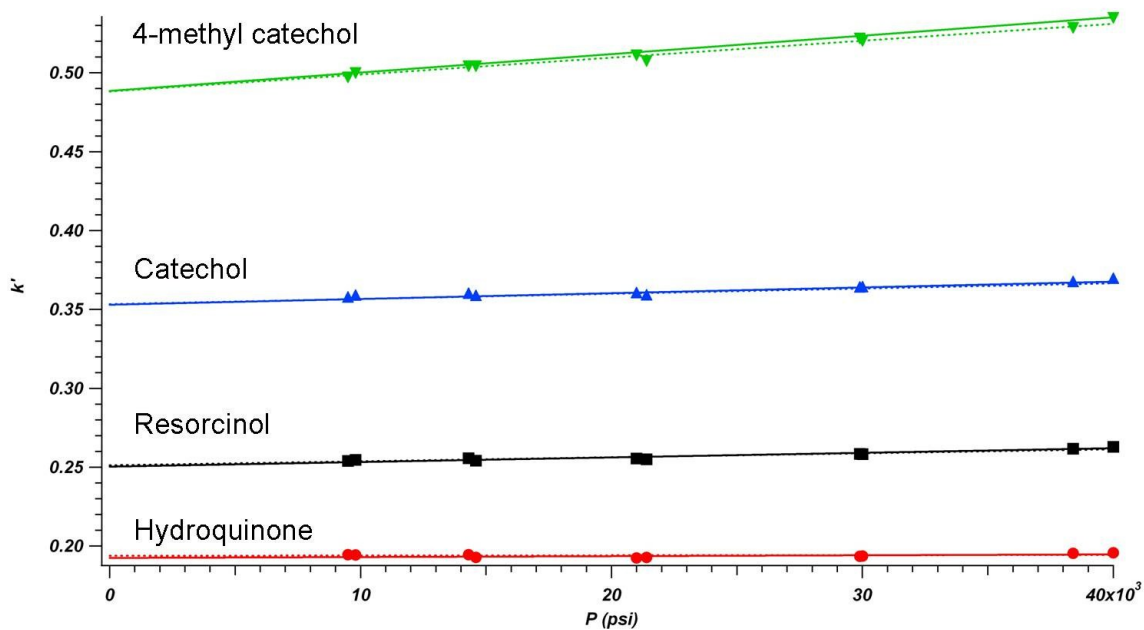


Figure 4-27: Retention data for the consecutively packed 105 (solid trace) cm and 103 cm (dashed trace) columns, highlighting the similarity of column permeability.

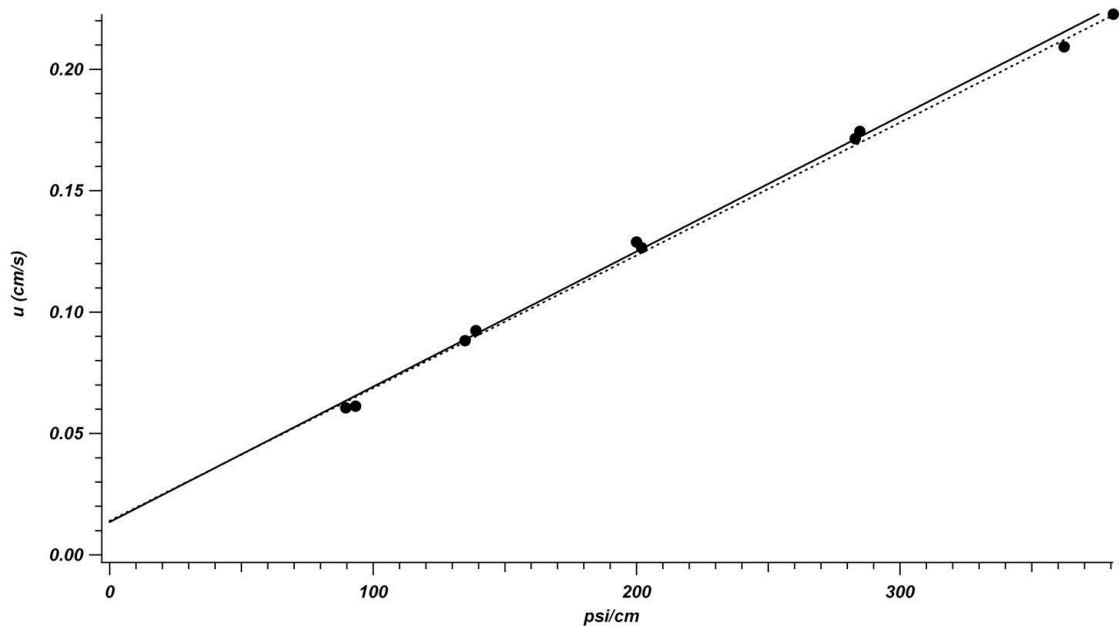


Figure 4-28: Flow resistances of the consecutively packed 105 cm (solid trace) and 103 cm (dashed trace) columns.

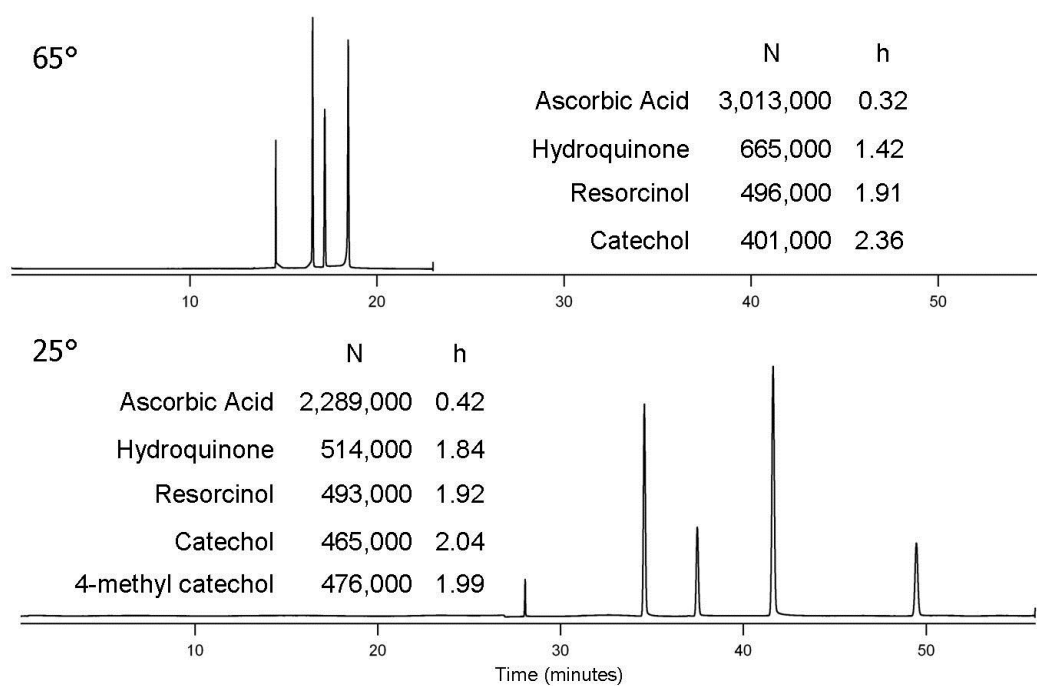


Figure 4-29: Chromatograms collected at 25°C and 65°C for a 180 cm x 50 µm ID column operated at 45,000 psi.

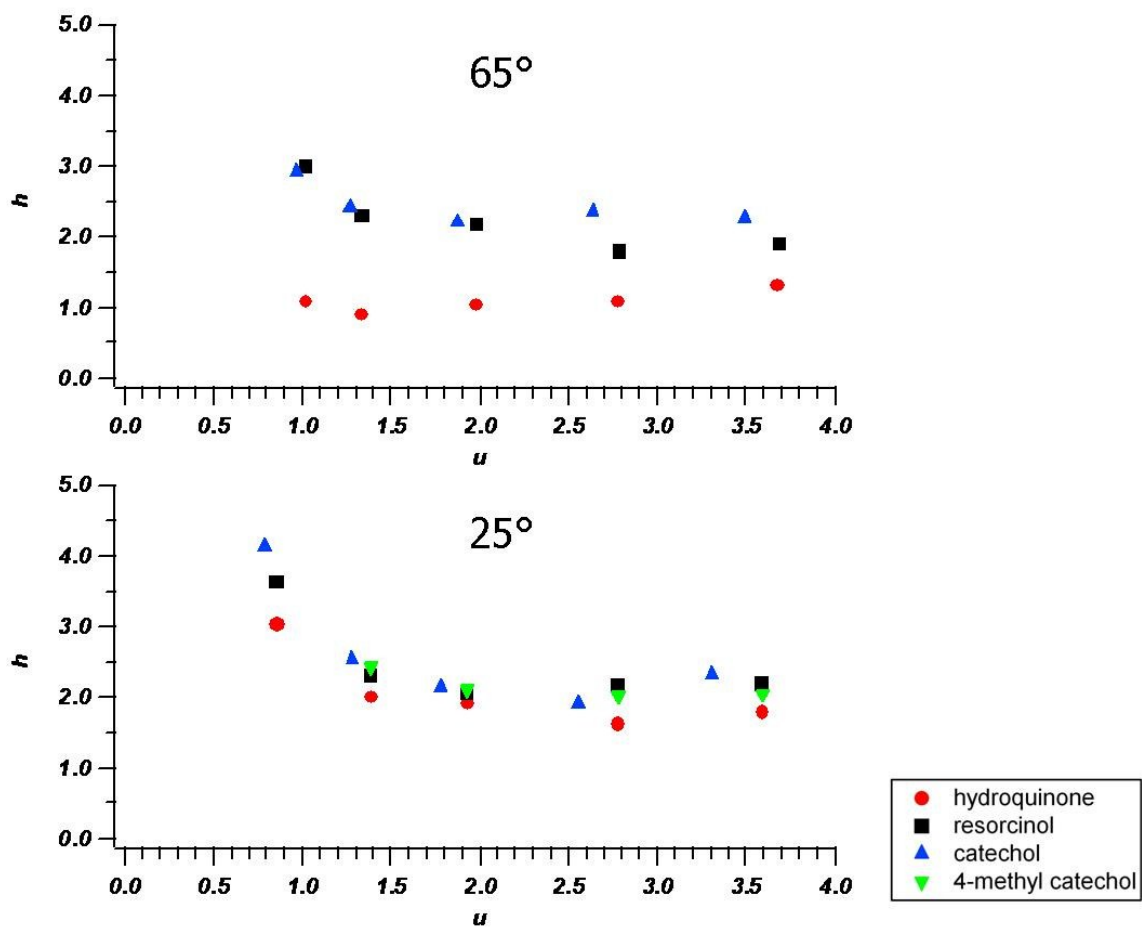


Figure 4-30: h vs. u plots of the 180 cm x 50 μ m ID column. 4-methyl catechol is oxidized on-column at 65 $^{\circ}$ C.

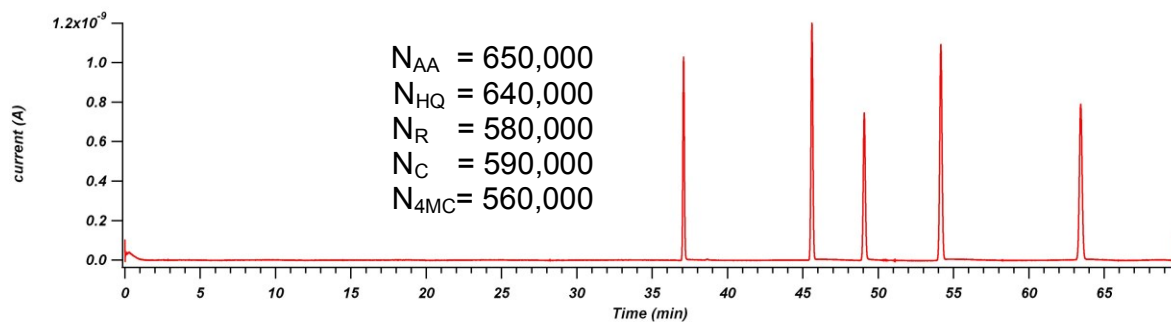


Figure 4-31: Representative chromatogram of a 214 cm x 50 μ m ID column packed with a 100 mg/mL slurry of 1.9 μ m BEH particles, operated at 38,500 psi. The improved performance when packing with concentrated slurries is reflected in the number of theoretical plates.

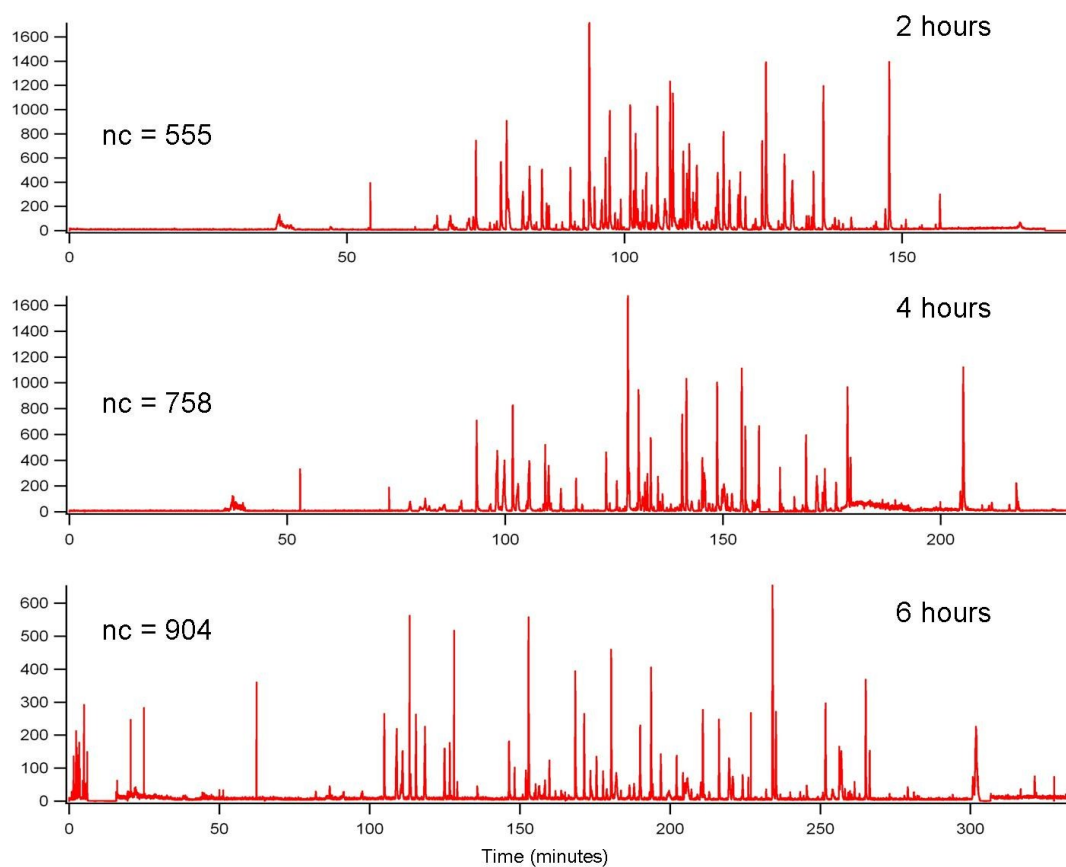


Figure 4-32: Chromatograms and determined peak capacities for a 216 cm x 50 μ m ID column packed with 1.9 μ m BEH. 1-50% acetonitrile gradients of 120, 240, and 360 minutes for a BSA tryptic digest sample were run and peak capacities determined from 4σ base widths of representative peaks.

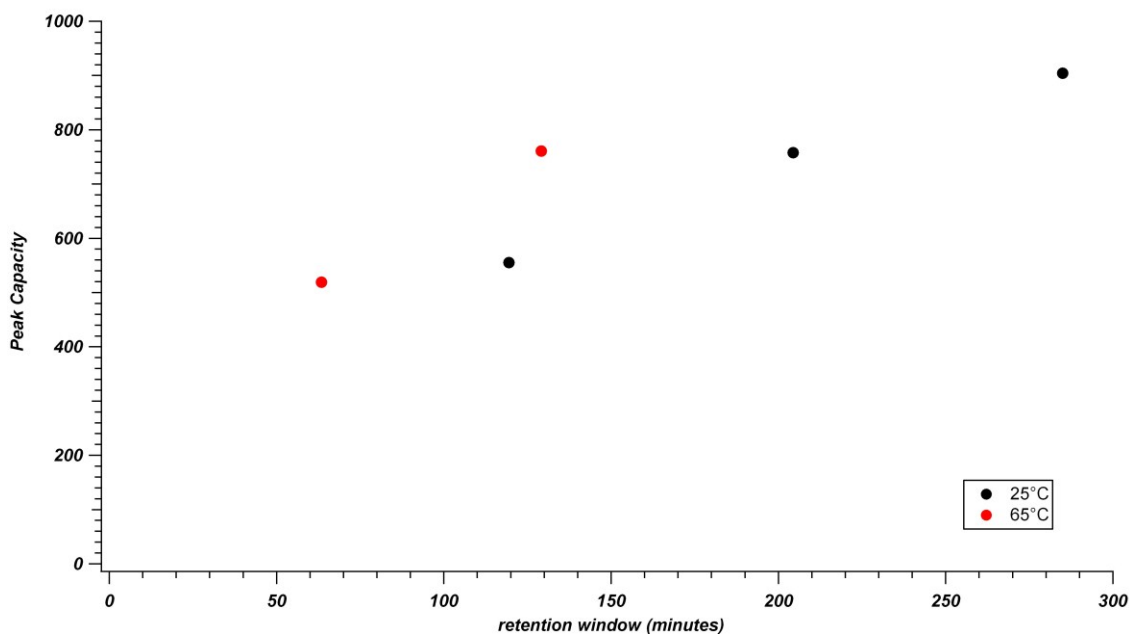


Figure 4-33: Peak capacity vs. retention window for a 216 cm x 50 μm ID column packed with 1.9 μm BEH particles. 1-50% acetonitrile gradients for a BSA tryptic digest sample were run and peak capacities determined from 4σ base widths of representative peaks. Retention windows were determined from the elution times of two characteristic peaks, and peak capacities calculated by dividing the retention window by the average peak width.

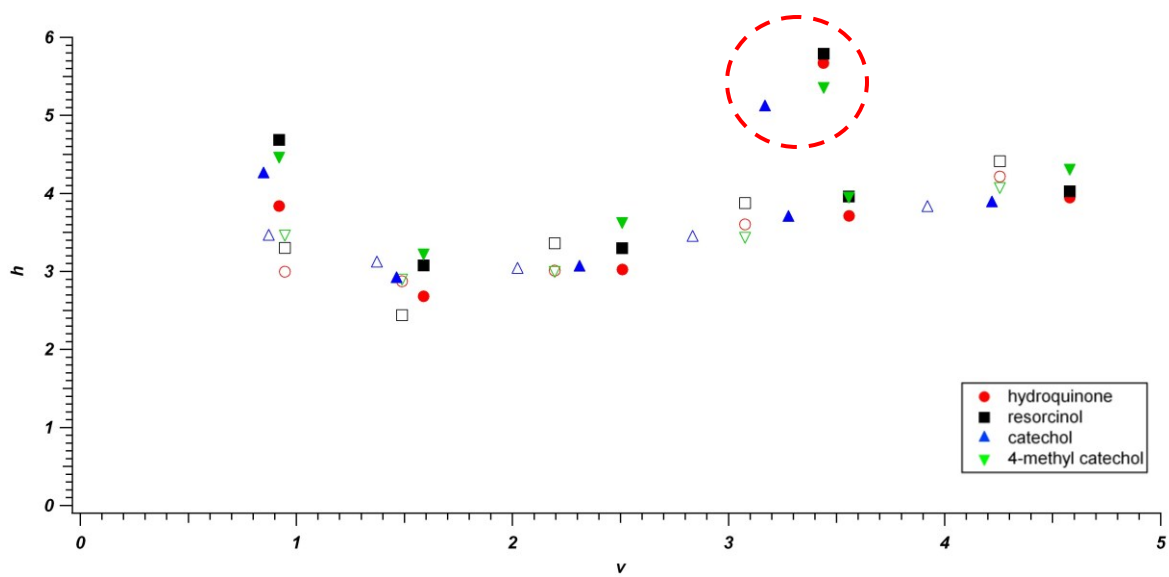
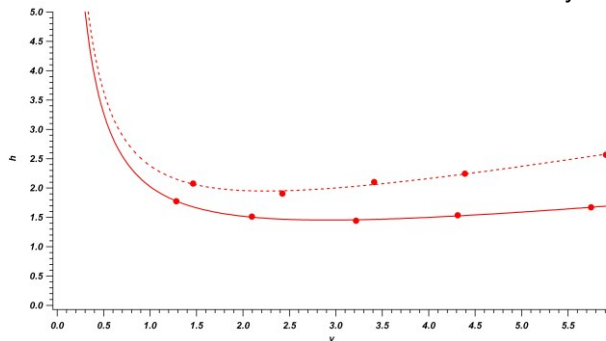


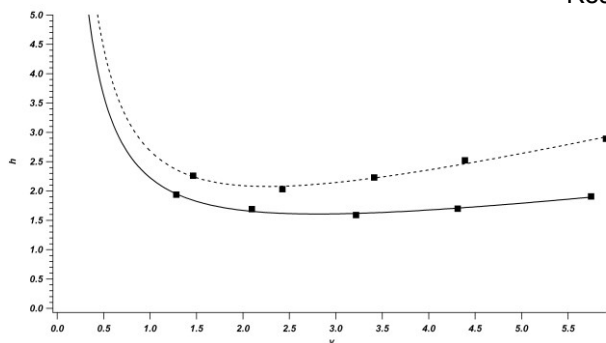
Figure 4-34: Overlaid h vs. ν data for the first (closed markers) and last packed (open markers) ~ 100 cm segments of a originally 330 cm x 50 μm ID column packed with 1.9 μm BEH particles. Data highlighted in the red circle shows deteriorated performance subsequent to collected data at the highest operating pressures, signaling packed bed instability.

Hydroquinone



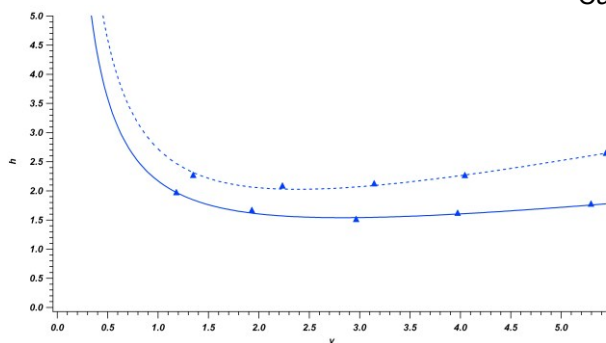
	Flushing	A	B	C
—	50 kpsi	0.55 ± 0.07	1.32 ± 0.08	0.16 ± 0.01
- - -	23 kpsi	0.70 ± 0.22	1.40 ± 0.28	0.28 ± 0.03

Resorcinol



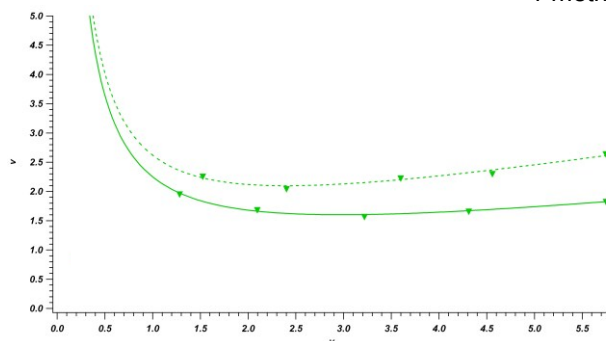
	Flushing	A	B	C
—	50 kpsi	0.54 ± 0.15	1.49 ± 0.18	0.19 ± 0.02
- - -	23 kpsi	0.37 ± 0.28	1.94 ± 0.37	0.38 ± 0.04

Catechol



	Flushing	A	B	C
—	50 kpsi	0.47 ± 0.17	1.51 ± 0.18	0.19 ± 0.03
- - -	23 kpsi	0.58 ± 0.14	1.70 ± 0.17	0.32 ± 0.02

4-methyl catechol



	Flushing	A	B	C
—	50 kpsi	0.61 ± 0.13	1.48 ± 0.15	0.17 ± 0.02
- - -	23 kpsi	0.82 ± 0.26	1.53 ± 0.34	0.27 ± 0.04

Figure 4-35: Overlaid reduced van Deemter plots of 100 cm x 50 μ m ID columns packed at 30,000 psi and subsequently flushed at either 23,000 psi or 50,000 psi. The column flushed at 50,000 psi performs superiorly.

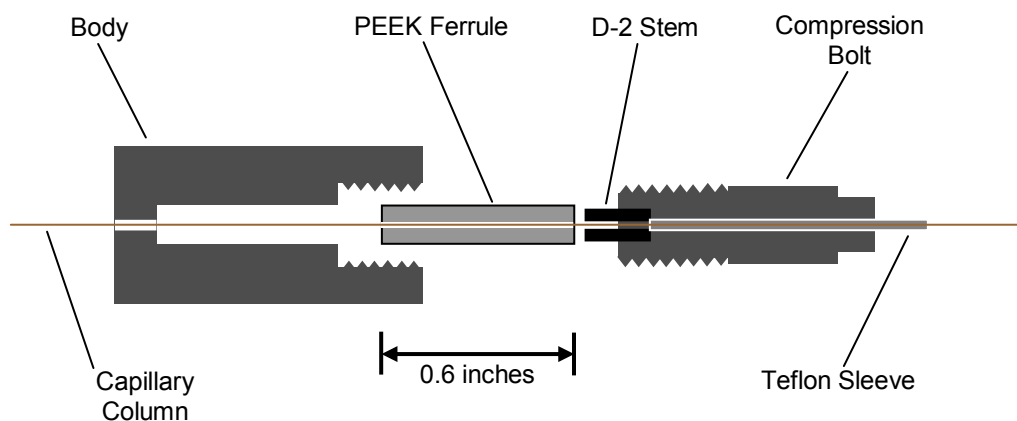


Figure 4-36: Modified UHPLC compression fitting to allow for the zero dead-volume connection of two microcapillary columns in series. The body is machined from 17-4 PH stainless steel, the compression bolt from 316 stainless steel, and the stem from D-2 air hardened tool steel. Capillary columns are abutted in the center of the PEEK ferrule and compression serves to grip the columns axially without twisting the silica faces over one another, thereby preventing breakage.

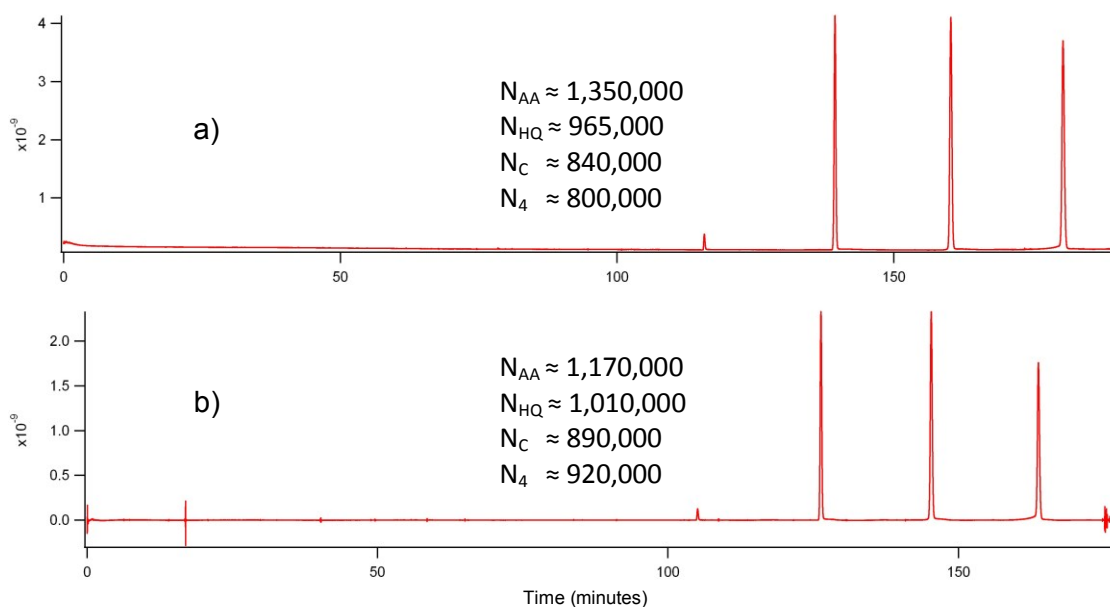


Figure 4-37: Chromatograms collected at a) 40,000 psi and b) 45,000 psi of a 360 cm x 50 μm ID column packed with 1.9 μm BEH particles. Total column length was achieved by the series connection of a 190 cm and 170 cm column in the compression fitting shown in Figure 4-36.

CHAPTER 5: CONSTANT PRESSURE GRADIENT-CAPABLE PLATFORM FOR HIGH-EFFICIENCY ONE-DIMENSIONAL UHPLC SEPARATIONS

5.1 Introduction

In Chapter 4 of this work, long microcapillary columns packed with sub-2 μm particles and operated at UHPLC pressures up to 40,000 psi were shown to be an effective means of achieving high theoretical plate counts and peak capacities. Columns packed with 1.9 μm BEH particles to lengths of ~ 200 cm were shown capable of generating $> 650,000$ plates and peak capacities approaching 1000 in under 6 hour analyses times. Additionally, elevated temperatures of 65°C were effectively employed to cut run times by approximately 50%. These results suggest a real applicability of high-efficiency one-dimensional liquid chromatographic approaches to “-omics” fields, such as proteomics, metabolomics, lipidomics, etc.^{1,2}. Such samples can be very complex and contain hundreds or thousands of components, the chromatographic resolution of which would be highly beneficial for data interpretation. This chapter describes the construction and characterization of a constant pressure gradient-capable platform for UHPLC proteomic applications.

5.1.1 Previous UHPLC Gradient System

The previous UHPLC gradient system³, described more thoroughly in Chapter 4.2.3.2 and schematized in Figure 4-20, utilized a Waters 1525 binary gradient pump (Waters Corp., Milford, MA), modified to pump incompressible brake fluid, connected to a custom-built hydraulic amplifier with 30:1 amplification to output pressures up to 40,000 psi.

Acetonitrile/water gradients were generated using a Waters CapLC and loaded in reverse

onto a stainless steel storage loop. Once the gradient was loaded, an integrated autosampler was used to make a sample injection and load it onto the loop in front of the gradient. After isolating the low-pressure CapLC instrumentation with two pin valves (Valco Instrument Co., Houston TX), engagement of the hydraulic amplifier pushed the sample and gradient from the loop into a low-volume four-port cross (Valco) and onto the head of the analytical column before mass spectrometric detection.

As shown in Chapter 4 of this work, long microcapillary columns are an effective means of producing high peak capacities in manageable analyses times when utilizing UHPLC pressures at elevated temperatures. To demonstrate the utility of this approach in a proteomics setting, the relative performances of a long microcapillary column and a commercially available column were compared in the separation of a yeast cell lysate tryptic digest. Figure 5-1a shows the separation performed on a Waters nanoAcquity with the commercial column (25 cm x 75 μm ID; 1.9 μm BEH) using a 90 minute gradient of 5 – 40 acetonitrile and 0.1% formic acid at 40°C. Figure 5-1b shows the same sample separated on a 200 x 50 μm column packed with the same particles using a 6 hour, 1-50% acetonitrile gradient at 25°C. Figure 5-1c shows an expanded view of a ~ 100 minute span of this separation, better highlighting the improved resolution. Finally, Figure 5-1d shows the same separation on the 200 cm column run at 65°C to cut the run time by approximately 50% while maintaining column performance.

As can be seen, this approach to UHPLC with gradient capability worked extremely well aside from a few notable constraints - the most significant of these being the requirement of split flow and the inherent pressure limitations of the hydraulic amplifier ($\leq 40,000$ psi). The need for split flow arose from the method of flow control, which, for the

sake of accuracy and reproducibility, required flow rates higher than 1.0 $\mu\text{L}/\text{min}$. Routine operation of the instrumentation utilized flow rates of 4.0 $\mu\text{L}/\text{min}$ at $< 30,000$ psi, which were much higher than the volumetric flow rates through the microbore analytical columns used with the system. In the case of 100 – 200 cm columns packed with 1.9 μm particles, typical flow rates at 30,000 psi ranged between 85 – 170 nL/min at 25°C. As such, only 2 – 4% of the sample and loaded gradient were directed onto the analytical column while the majority was split through a narrow-bore open capillary to waste. The biggest drawbacks, however, were the mechanical failures of several key components in the system. The hydraulic amplifier was an entirely custom design, and as the check valves, pump heads, and software became increasingly unreliable, a new approach was ultimately necessitated.

5.1.2 Conceptual Features of New Gradient UHPLC System

The unfortunate demise of the previous UHPLC gradient system nevertheless gave an opportunity to supplement many of its most attractive features (i.e. its automated operation) with the potential to run at even higher pressures. Operating pressures in excess of 50,000 psi could be readily achieved by using a pneumatically driven pump in place of the hydraulic amplifier. This would also allow for the achievement of flow rates dictated entirely by the characteristics of the analytical column. In the previous design, flow rate was dialed in, and a flow splitter was customized through its length and diameter to regulate system pressure – thereby indirectly specifying flow through the analytical column. Additionally, without flow splitting, the entire sample injection and gradient volumes could be directed onto the column, thus avoiding waste of potentially valuable sample.

Using a pneumatically driven Haskel pump to provide flow, however, demands that constant pressure operation of the gradient system be a reasonable alternative to constant

flow – the standard mode of operation for commercial UHPLC instrumentation. In a way, the viability of a constant pressure approach was already attested to with the previous UHPLC gradient system, which was somewhat inaccurately dubbed as constant flow. Firstly, constant flow was attempted through open-loop control on the low-pressure end of the hydraulic amplifier, and the lack of adequate feedback resulted in significant changes in flow throughout the courses of gradient runs. Secondly, with the use of gradients, mobile-phase viscosity varied over the course of runs. Ideally, the dead-times of the analytical column and the splitter capillary would be the same such that the mobile-phase compositions contained within both at any given time would be identical. The impracticality of using extremely long, large ID splitters to achieve this led to viscosity mismatches and flow rate variations throughout the courses of runs³.

The changes in flow rates that occur throughout the courses of gradient runs in constant pressure operation can be estimated by looking at the viscosities of acetonitrile/water mixtures at different temperatures, using the equation developed by Chen and Horvath⁴:

$$\eta(\alpha, T) = \exp \left[\begin{array}{l} \alpha \left(-3.476 + \frac{726}{T} \right) \\ + (1 - \alpha) \left(-5.414 + \frac{1566}{T} \right) \\ + \alpha(1 - \alpha) \left(-1.762 + \frac{929}{T} \right) \end{array} \right] \quad (5-1)$$

where α is the volume fraction of acetonitrile and T is the absolute temperature. Figure 5-2 shows the viscosities of 0/100 – 100/0 mixtures of acetonitrile/water at 25, 45, 65, and 85°C. At 25°C, there are significant changes in viscosity over the range of mobile phase compositions, progressing through a maximum of 0.89 cP at approximately 20% acetonitrile

to only 0.35 cP at 100% acetonitrile. For most gradient separation applications, however, the range of utilized mobile phase compositions is much narrower. Figure 5-3 shows the viscosities at each temperature normalized to the maximums in the range from 0-50% acetonitrile – a typical range for peptide separations. Examination of these plots reveals that as temperature increases, the relative differences in viscosities over the course of the gradient, and thus resulting flow rates, become smaller. For example, at 25°C, there is a ~ 13% difference between the highest and lowest mobile phase viscosities; at 65°C, there is only a ~ 5% difference. This suggests that, at elevated temperatures – which have proven beneficial for managing the analyses times⁵ required with long capillary column – operation at constant pressure tends toward greater resemblance to constant flow operation. It should be noted that these calculated viscosities do not account for behavior under UHPLC pressures⁶.

As a final note to the validity of a constant pressure approach, a recent theoretical comparison of the performance of gradient elution chromatography at constant pressure and constant flow rate was made by Gritti and Guiochon⁷. A number of important assumptions were made, including the negligibility of eluent compressibility and pressure effects on retention. While these assumptions may not hold at UHPLC pressures, their calculations indicated that for a given analysis time, the same volume gradient profiles resulted in the very same peak capacities for both modes of operation^{7,8}. Ultimately, however, so long as chromatographic performance could be deemed good and reproducibility was satisfactory, the constant pressure approach would prove to be a useful means of generating high efficiency separations.

5.2 System Design and General Operation

The general scheme of operation was carried over from the previous UHPLC system in the design of the constant pressure system which incorporated the pneumatic pump in place of the hydraulic amplifier to drive the high pressure separations. A Waters nanoAcquity was modified to serve in place of the CapLC module for gradient generation and sample handling. The most significant modifications were made with regard to the flow paths from the nanoAcquity to the external gradient storage loop and the effective isolation of the commercial instrument when operating at high pressure. A mechanism for sample trapping was also incorporated into the initial design.

A major benefit of incorporating the nanoAcquity into the system design is the ability to handle the entire UHPLC-MS operation through Masslynx, the system's associated software. From the nanoAcquity console, the inlet method editor can be used to set the on/off states for each of the solenoid-controlled valves to change appropriately throughout the courses of the methods specified in Masslynx. At least three methods are required to complete a chromatographic run using this system: a gradient loading method, a sample loading and trapping method, and a final method to allow for UHPLC operation and mass spectrometric data collection. As a practical consideration for the long chromatographic runs typical when using long columns, a fourth categorical method must be employed. "Linker" methods preserve the valve state configuration during UHPLC runs while enabling data to be collected under newly specified file names so that maximum file sizes are not exceeded. Unfortunately, as Masslynx proceeds sequentially through the list of specified methods, several seconds of data acquisition are lost in the switching times.

Figure 5-4 shows the general schematic of the modified instrumentation. For high pressure operation, a triple-stage Haskel pump (Burbank, CA) capable of generating 75,000

psi with 1000:1 amplification was used. Approximately 100 cm of 15 μ m ID open capillary held by a UHPLC compression fitting connected the flow from the outlet of the pump to the outlet of the gradient storage loop through a microvolume tee (Valco) . This narrow bore capillary was used to restrict the volumetric flow rate should a large leak occur downstream. Operation of the Haskel pump and manipulation of the on/off states of the pneumatically actuated pin valves was achieved through separate regulation of compressed gas pressure supplied and split from a single nitrogen tank. Pressure was regulated to \sim 40 psi for supply to a bank of 3-way/2-position solenoid valves to operate the five different 40,000 psi-rated pin valves located throughout the system. Pressure was also regulated before a 3-way/2-position solenoid valve for supply to the hydraulic amplifier.

As mentioned above, three distinct flow paths are utilized in the course of a chromatographic run by manipulating the on/off states of the five pin valves. Gradients are once again loaded in reverse onto a \sim 500 μ L external storage loop of 0.005 in ID, 1/32 in OD stainless steel tubing. Figure 5-5 shows the flow path used to perform gradient loading, with the on/off pin valve states highlighted. From the nanoAcquity inject valve, the trapping valve is bypassed to direct flow to a first microvolume tee. Additional connections to this tee direct flow either to waste when the nanoAcquity vent pin valve (labeled pin valve '1' in Figure 5-5) is open or further downstream when closed. With pin valve '1' closed and the nanoAcquity pin valve (pin valve '2') open, flow proceeds to a second microvolume tee, where flow is directed either onto the storage loop or through a \sim 6.5 cm trap column. With the gradient storage isolation pin valve (pin valve '3') and vent pin valve (pin valve '4') located at the outlet of the loop open, the trap pin valve (pin valve '5') is closed to load the gradient. Gradients were typically loaded at \sim 5 μ L/min to take advantage of the

nanoAcquity's closed-loop pump control for accurate and reproducible gradient generation. Owing to the extra volume introduced by the many fluidic connections leading from the nanoAcquity to the storage loop, additional gradient volume was flowed to ensure that initial playback conditions were fully loaded onto the loop. It should be mentioned at this point that, because no flow rate is specified in the constant pressure UHPLC playback of the pre-loaded gradients, gradient loading methods are specified by the total gradient volume. Average volumetric flow rate can be approximated over the course of a chromatographic run to estimate total analysis time

Once the gradient is loaded, and sample trapping is to be utilized, the states of the pin valves are changed to direct flow through the ~ 6.5 cm trap column, as shown in Figure 5-6. Both pin valves '3' and '4' are closed, and pin valve '5' is opened. The sample injection is made, and flow is directed through the trap column to a third microvolume tee. While the sample is trapped, the inherently high flow resistance of the long analytical column acts to direct the vast majority of flow through pin valve '5' to waste. Sample was typically trapped while flowing with several sample loop volumes of 0.5% acetonitrile.

For high pressure operation of the analytical separation, the valve states are manipulated a third time, as shown in Figure 5-7. Pin valves '2', '4', and '5' are closed, pin valve '3' is opened, and the Haskel pump is engaged. Flow is thus directed to push the gradient off of the storage loop, through the trap and analytical columns before mass spectrometric detection. Pin valve '1', connected at the first tee, is open to serve a dual purpose. Firstly, it allows flow from the nanoAcquity to gradually ramp down, as it was observed that the instantaneous mechanical obstruction of the flow path caused the back-pressure of the instrument to increase sharply, even with zero flow specified. Secondly, it

serves to divert flow and isolate the nanoAcquity from the UHPLC pressures should the nanoAcquity pin valve fail during operation.

5.3 Chromatographic Performance of Constant-Pressure UHPLC System

5.3.1 Utilized Microcapillary Columns

While capable of performing at higher operating pressures, initial characterizations of the constant-pressure system were done at 30,000 psi and 65°C. The trap and analytical columns were both maintained at temperature in a column heater provided by Waters. ~ 6.5 cm x 150 µm ID trap columns were packed with 5 µm Symmetry-C18 particles (Waters Corp.). Analytical columns were packed to optimal lengths according to the theoretically predicted performances of 1.9, 1.5, and 1.0 µm particles shown in Figures 5-8, 5-9, and 5-10, respectively. As such, ~ 200 cm columns were packed with 1.9 µm BEH particles; ~ 100 cm columns were packed with 1.5 µm particles; ~ 25 cm columns were packed with 1.0 µm particles. All columns had 75 µm IDs in order to allow for volumetric flow rates compatible with electrospray ionization. Larger IDs also allow for larger gradient volumes to be loaded. Because there are a number of fluidic connections and several regions of substantial volume (ex. the microvolume tees, internal chambers of the pin valves, the trap column), larger gradient volumes served to reduce the effects of gradient mixing in these regions.

5.3.2 Results with Sample Trapping

Early efforts with the UHPLC system were characterized by a number of complications, many of which were foreseen given the nature of constant pressure operation and the practicalities of making numerous fluidic connections operated at high pressures. In several instances, chromatograms revealed either no evidence of sample or peak elution profiles which corresponded to significantly smaller gradient volumes than those specified by

the methods (i.e. the elution windows were very short). Each of these observations was evidence of a leak at some fluidic connection in the system. Given that there is no pressure or flow rate readout when operating during high-pressure playback, the leaks could only be detected by visual observation. When no leaks could be seen and chromatographic elution windows roughly corresponded to those expected, the system was considered to be operating properly. These subjective criteria could be deceiving, however. With total gradient volumes of only a few tens of microliters, undetected nano-leaks at the fluidic connections or within the pin valves could impact the chromatographic reproducibility. The second problem consistently encountered in the operation of the system was the frequent clogging of capillary tubing comprising the various flow paths. This often resulted in the nanoAcquity exceeding its maximum pressure of 10,000 psi during gradient loading. It is suspected that chipping of the silica capillary when making the high-pressure connections is the primary reason for this problem.

Separation of a cell lysate digest of yeast grown on dextrose was performed with a 200 cm x 75 μ m ID column packed with 1.9 μ m BEH particles. Figure 5-11 shows the resultant chromatogram from a \sim 35 μ L gradient of 4 – 40% acetonitrile. With an estimated column volume of 6 μ L, this is a relatively steep gradient - 6.2% change per column volume. The widths at half height of 15 peaks across the separation window from \sim 55 to \sim 220 minutes were measured, and 4σ base widths were calculated assuming Gaussian peak shapes. Average base width was approximately 0.47 minutes, giving a peak capacity over the 165 minute separation window of \sim 350. By comparison, a separation performed on the previous UHPLC gradient system with a 216 cm column gave a peak capacity of approximately 760 in a nearly identical separation window, as shown in Figure 4-32. Closer inspection of the peak

profiles revealed tailing for almost every peak, as shown by the overlaid single ion chromatograms in Figure 5-12.

Similarly, yeast cell lysate separations were performed on ~ 100 cm x $75\ \mu\text{m}$ ID columns packed with $1.5\ \mu\text{m}$ BEH particles. Figure 5-13a shows the performance of a 117 cm column with a $25\ \mu\text{L}$ gradient of 3 – 40% acetonitrile, a $\sim 5.2\%$ change per column volume. Within the separation window from 18 – 100 minutes, a peak capacity of only ~ 200 is achieved. Increasing the gradient volume to $45\ \mu\text{L}$ (2.9% change per column volume), the peak capacity is increased to ~ 310 within a 140 minute separation window (Figure 5-13b). The separation was performed on a different 100 cm column with a $85\ \mu\text{L}$ gradient of 1 – 40% acetonitrile (1.3% change per column volume) to give a peak capacity of ~ 510 within a 280 minute separation window (Figure 5-13c). Each of these results is poorer than expected and, once again, peaks are notably tailing, as illustrated in Figure 5-14.

Finally, separations were performed on a 25 cm x $75\ \mu\text{m}$ ID column packed with $1.0\ \mu\text{m}$ BEH particles. Although peak capacities were not expected to be as high as with much longer columns, moderate peak capacities in very short analyses times are theoretically achievable. Resultant peak capacities were determined from separations of the yeast sample using 15, 25, and $35\ \mu\text{L}$ gradient volumes of 1 – 40% acetonitrile, corresponding to approximately 2.0, 1.2, and 0.8% mobile phase composition changes per column volume, respectively. Figure 5-15 shows representative chromatograms for each gradient.

Separations were only moderately improved by lengthening the gradient with peak capacities increasing from ~ 118 through ~ 126 , to ~ 134 in 37, 65, and 80 minute retention windows. These marginal improvements in peak capacities with shallow gradients are fairly consistent with both theoretical predictions, as shown in Figure 4-5, and the experimental data for 100

cm columns packed with 1.9 μm particles, shown in Figure 4-23. Unfortunately, these results represent neither an improvement in peak capacity nor speed when compared to the performance of a commercially available 25 cm x 75 μm ID column packed with 1.9 μm BEH particles operated on the Waters nanoAcquity. Characterizations of the nanoAcquity column were performed using a BSA tryptic digest and 15, 30, 60, 90, and 120 minute gradients of 5 – 40% acetonitrile at 35°C. Figure 5-16 plots peak capacity versus retention window for both 25 cm columns packed with either 1.0 or 1.9 μm particles.

5.3.3 Results with Direct Injection

The chromatographic results shown in the previous section were relatively underwhelming considering the performances of the long microcapillary columns discussed in Chapter 4. Smaller injection volumes did little to reduce the peak tailing characterized in Figures 5-12 and 5-14, and it seemed that some new feature of the constant pressure system was acting to broaden the peaks and reduce peak capacities to approximately 50% of expected values. Since the overall system design was very similar in principle to the previous UHPLC system, attention was turned to the newly implemented trapping mechanism as the potential source of diminished performance. The trap columns, packed with 5 μm C18 Symmetry particles, were relatively long in order to accommodate the fittings needed to make the high-pressure fluidic connections. 6.5 cm x 150 μm ID trap columns have an approximate column volume of 0.8 μL which is significant relative to the volumes of the utilized analytical columns. Commercial nanoAcquity columns are outfitted with trap columns packed with the same material, but are only 2 cm long. It is possible that sample is significantly broadened on the trap column before being released with the appropriate mobile phase composition to the analytical column. Additionally, Symmetry particles have greater

hydrophobic character than the BEH C18 particles used to pack the analytical columns. It is therefore likely that, upon being released from the more retentive trap column, the sample is not refocused at the head of the analytical column, leading to large volume sample injections which serve to broaden the peaks. In the direct inject operation of the previous UHPLC system, sample was concentrated at the head of the analytical column with sufficiently aqueous mobile phase. With the incorporation of the trap column into the new system design, it was hoped that larger total sample injections could be made without overloading the stationary phase, thus allowing for the analysis of low abundance species and/or low-concentration samples. The observed peak broadening, however, nullified the potential advantages of the trapping method and warranted returning to the direct injection approach.

As such, the fluidic connections were rerouted as shown in Figure 5-17. Pin valve '1' remains closed during the gradient and sample loading methods, while pin valves '2' and '4' remain open. The need for pin valves '3' and '5' are eliminated in this direct injection scheme. In this way, the sample is loaded onto the storage loop rather than a trap column, as shown in Figure 5-18. Sufficient volume of aqueous mobile phase is flowed through the sample loop to ensure sample is not prematurely clipped before it is loaded onto the storage loop. When running at UHPLC pressures, the pin valves '2' and '4' are closed, and the Haskel pump is engaged. Once again, pin valve '1' remains open to allow flow from the nanoAcquity to gradually ramp down and to provide a safety mechanism for the instrument should the nanoAcquity pin valve fail during high-pressure operation, as shown in Figure 5-19.

Using a 100 cm x 75 μm ID column packed with 1.5 μm BEH particles, separations of an E.coli digestion standard were performed with 1 – 40% acetonitrile gradients at 65°C.

25, 50, 100, 150, and 200 μL total gradient volumes were utilized, corresponding to percent acetonitrile changes per column volume of 4.7, 2.3, 1.2, 0.9, and 0.6%, respectively. Figure 5-20 shows the resultant chromatograms, and Figure 5-21 plots the peak capacity versus retention window data. With the 100 μL gradient, a peak capacity of ~ 670 is achieved in a total analysis time of ~ 220 minutes. Doubling the gradient length to 200 μL resulted in a peak capacity of ~ 771 in a total analysis time approaching 400 minutes. These results are vastly superior to those achieved in trapping mode. Comparatively, peak shape is also improved, with markedly less tailing, as exemplified by the single ion chromatograms in Figure 5-22.

The results are promising, even though the previous analyses of the 100 cm and 216 cm columns packed with 1.9 μm BEH particles make it difficult to specify the utility of the 100 cm column packed with 1.5 μm particles. Extrapolation of the plot in Figure 4-23 reveals that the 100 cm column packed with 1.9 μm particles should achieve peak capacities approaching 450 given a 120 minute retention window at 65°C. Likewise, the 216 cm column could be expected to achieve a peak capacity of ~ 700 in a similar retention window. In the present case, the 100 cm column packed with 1.5 μm particles achieves a peak capacity of ~ 500 within a similar time frame according to Figure 5-21. Figure 5-23 reveals the similarities in column efficiencies that can be expected for columns packed with either 1.9 or 1.5 μm particles operated at 30,000 psi and 65°C. The plots represent the maximum number of theoretical plates that can be achieved in a given dead time, for which there are corresponding column lengths for each particle size. The plots intersect such that a ~ 138 cm column packed with 1.9 μm particles produces as many plates in the same amount of time as a ~ 110 cm column packed with 1.5 μm particles. It appears, therefore, that until operating

pressures in excess of 30,000 psi become routine with the system, it is probably best to pack long columns with 1.9 rather than 1.5 μm particles. This is especially true given our current ability to pack the larger particles with better relative efficiencies, as discussed in Chapter 3.

5.4 Conclusions

The design and implementation of the constant pressure gradient-capable UHPLC system shows great promise, although to this point its full potential has yet to be realized. Its most attractive aspect over the previous system, the ability to operate at much higher pressures, has been under-explored due to the limitations of several key components. The high-pressure fittings used to make the fluidic connections and the maximum pressure ratings of the pin valves used to manipulate the flow paths are the greatest concerns. Although these components have been tested and are capable of operating at pressures in excess of 50,000 psi, their extended reliabilities are essential in providing reproducible chromatographic results. This is especially true given the nature of the pneumatically amplified gradient playback without flow readout or split-flow operation. Undetected nano-leaks at any of the numerous connections or within the pin valve housings can be detrimental when working with relatively small pre-loaded gradient volumes. With the previous system, very small leaks could be undetected, but given that the vast majority of gradient and sample volumes were split to waste, the effects were often negligible.

The direct injection mode of operation has proven to be a great improvement over the originally conceived trapping operation. It is likely that the length of the utilized trap columns and their large volumes relative to the total volumes of the analytical columns were responsible for deteriorated performances. Additionally, the high retentivity of the particles used in the trap columns relative to the C18 BEH particles did not allow for sample to

refocus at the head of the analytical column prior to the separation. The results achieved with the 100 cm column packed with 1.5 μm BEH particles in direct injection mode are very promising. Further characterizations of the system with longer columns packed with 1.9 μm particles are needed, and the ability to operate at higher pressures would help to establish a clear regime where 1.5 μm particles are preferred when only moderately high peak capacities are needed. Similarly, the ability to operate above 30,000 psi would allow shorter columns packed with 1.0 μm particles to achieve peak capacities comparable to commercially available columns, but in much faster analysis time.

5.5 Figures

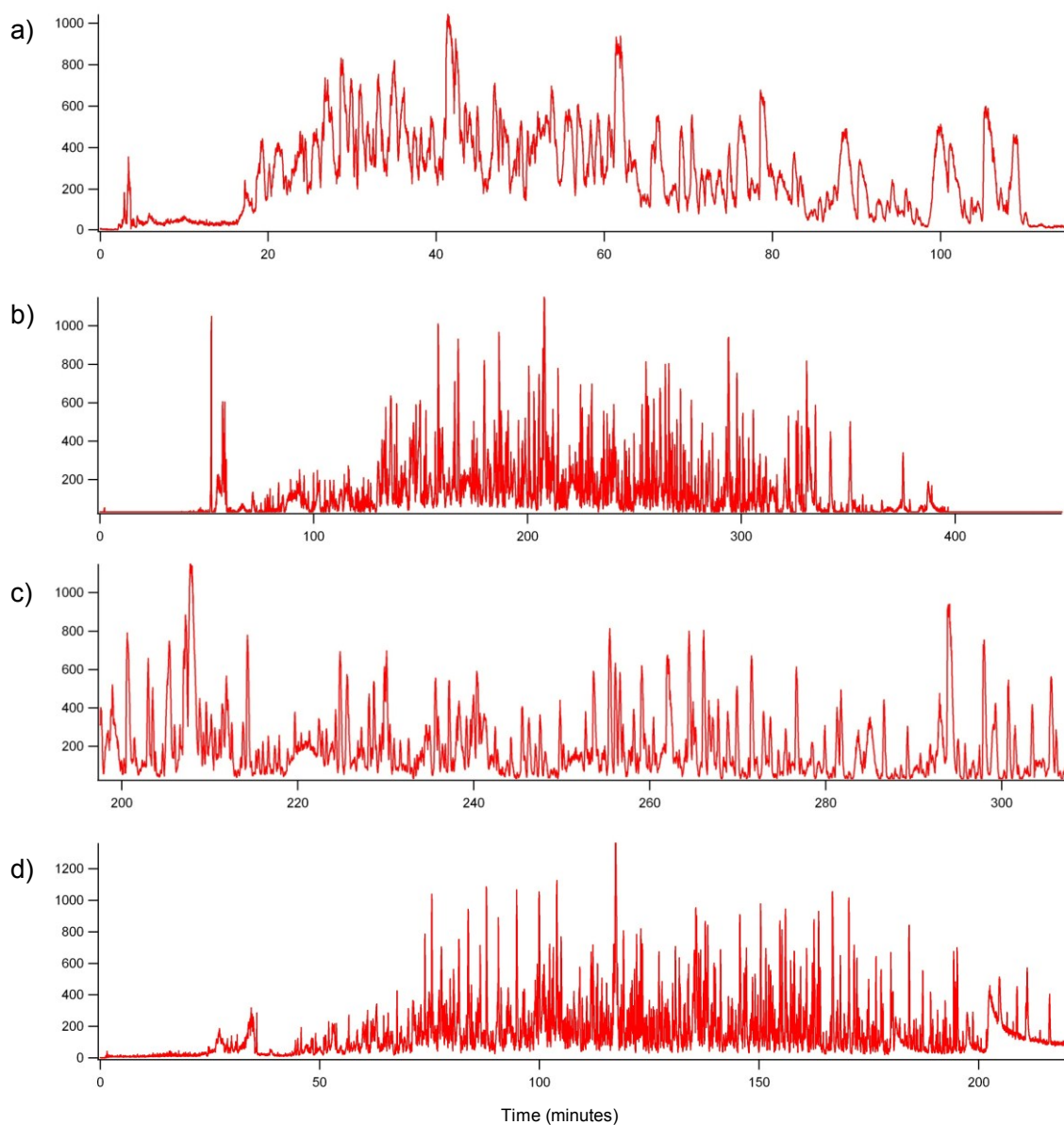


Figure 5-1: Chromatograms of a yeast cell lysate digest. a) A 90 minute 5-40% acetonitrile gradient performed on a commercial 25 cm x 75 μm ID packed with 1.9 μm BEH particles at 40°C; b) A 6 hour 1-50% acetonitrile gradient performed on a 200 cm x 50 μm ID column packed with 1.9 μm BEH at 25°C; c) An ~ 100 minute expanded view of the separation in (b); d) The same gradient utilized in (b) played back at 65°C

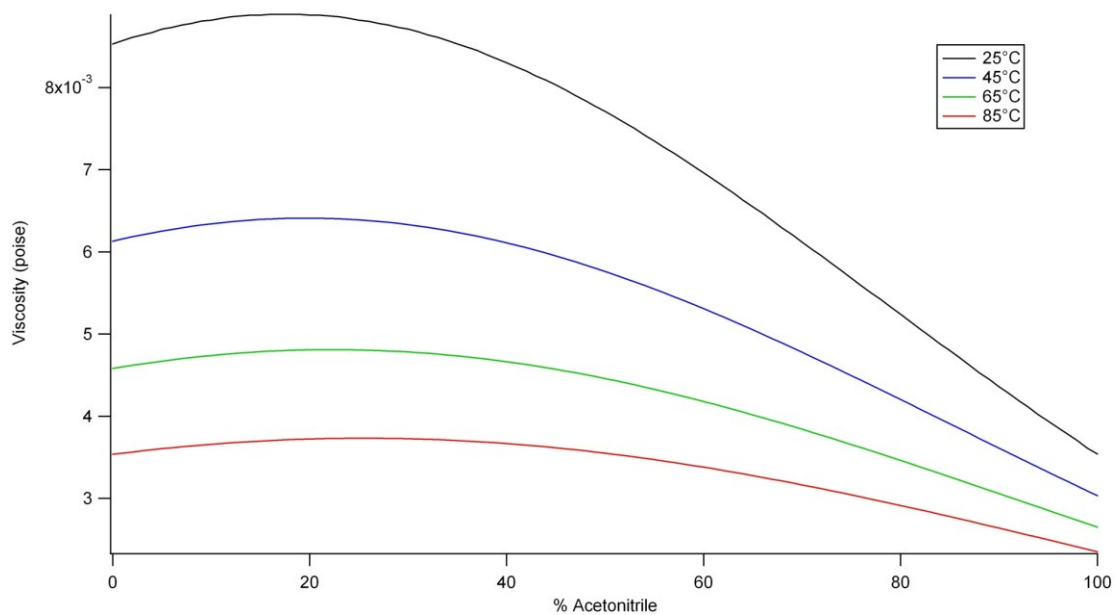


Figure 5-2: Viscosity as a function of acetonitrile/water composition according to the Chen-Horvath equation shown in Equation 5-1 at 25, 45, 65, and 85°C

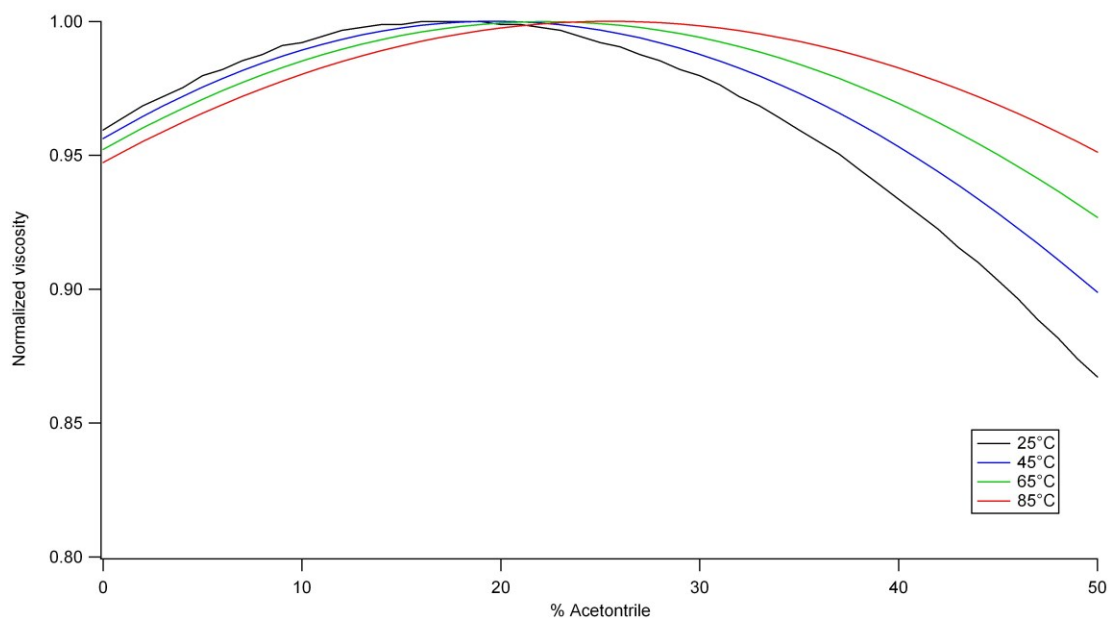


Figure 5-3: Viscosity as a function of acetonitrile/water composition according to the Chen-Horvath equation shown in Equation 5-1 at 25, 45, 65, and 85°C. The data is normalized to the highest viscosity at each temperature to highlight the % change through 0-50% acetonitrile

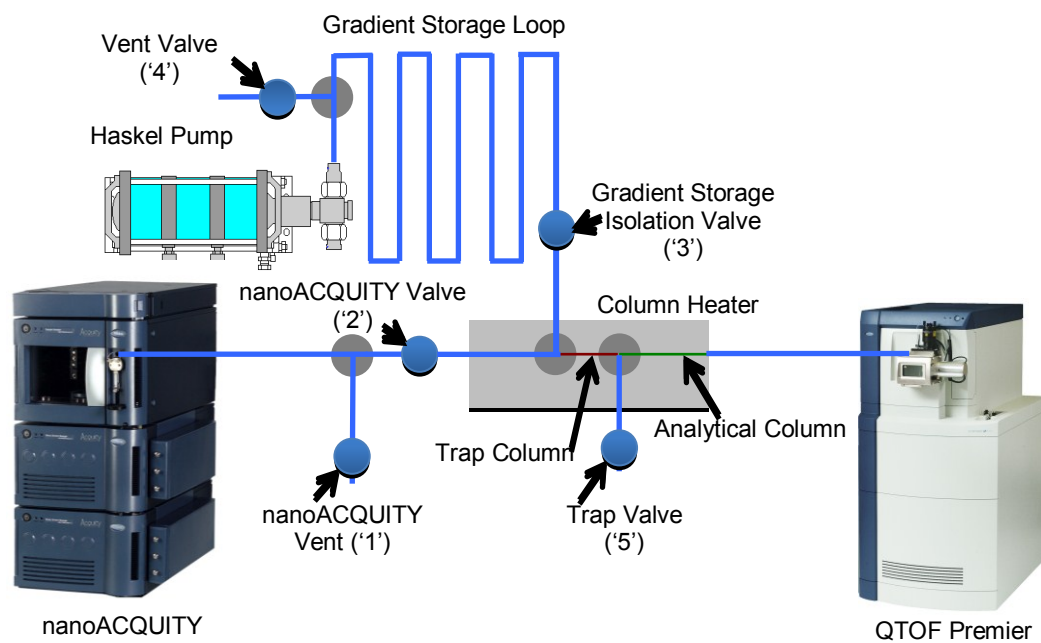


Figure 5-4: Schematic of the modified instrumentation to perform constant pressure gradient UHPLC separations with sample trapping.

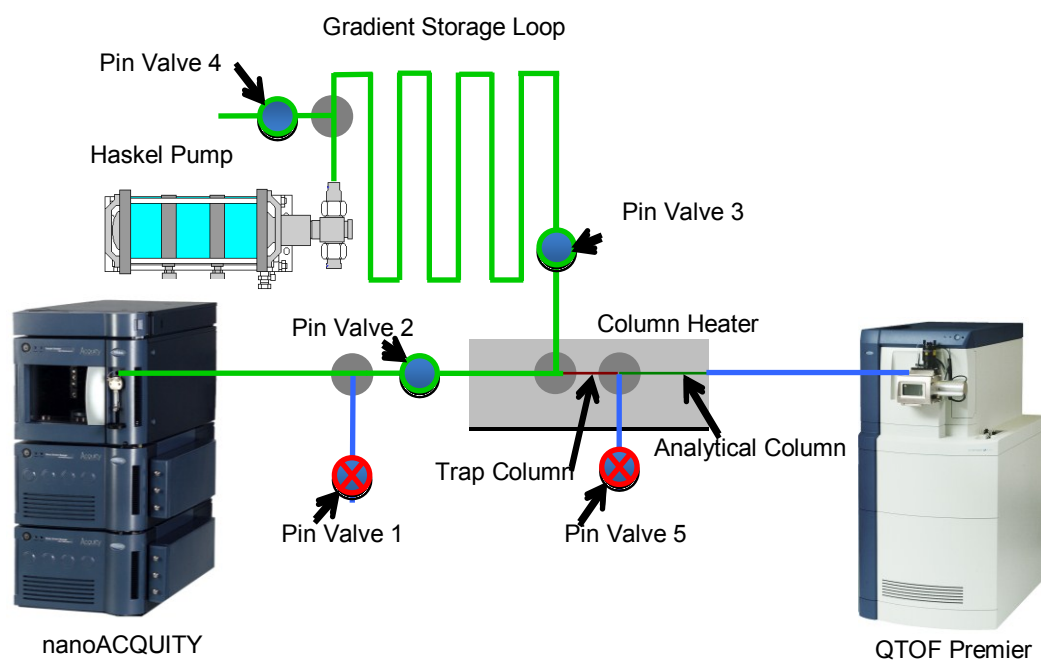


Figure 5-5: Gradient loading scheme: Pin valves 1 and 5 are closed. Pin valves 2, 3, and 4 are open to allow flow from the nanoAcquity to the gradient storage loop.

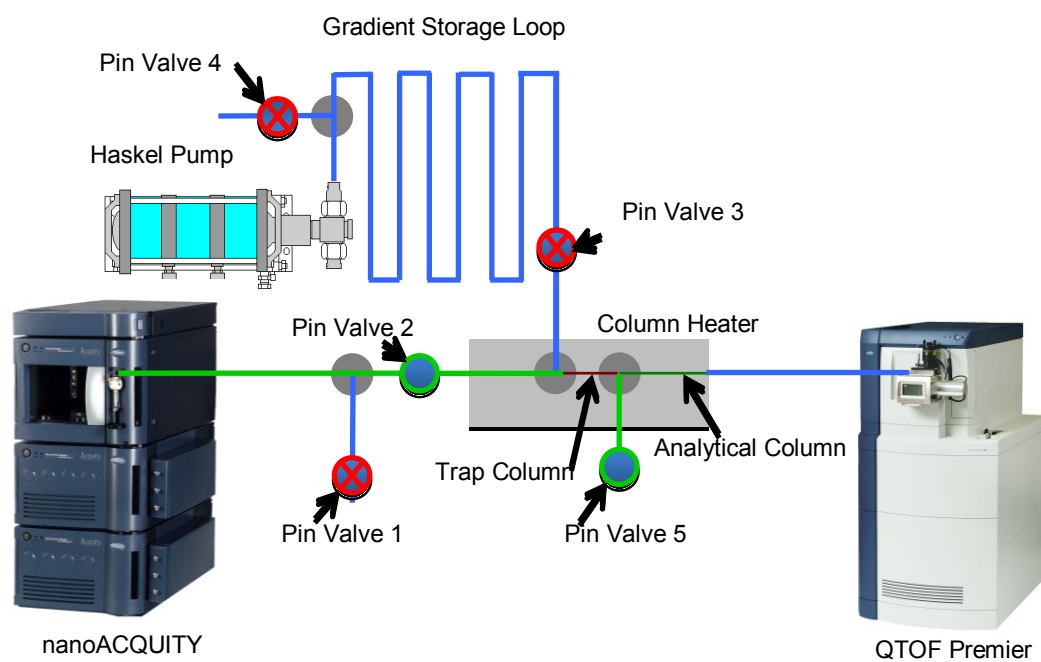


Figure 5-6: Sample trapping scheme: Pin valves 1, 3, and 4 are closed. Pin valves 2 and 5 are open to allow flow from the nanoAcquity through the trap column to waste.

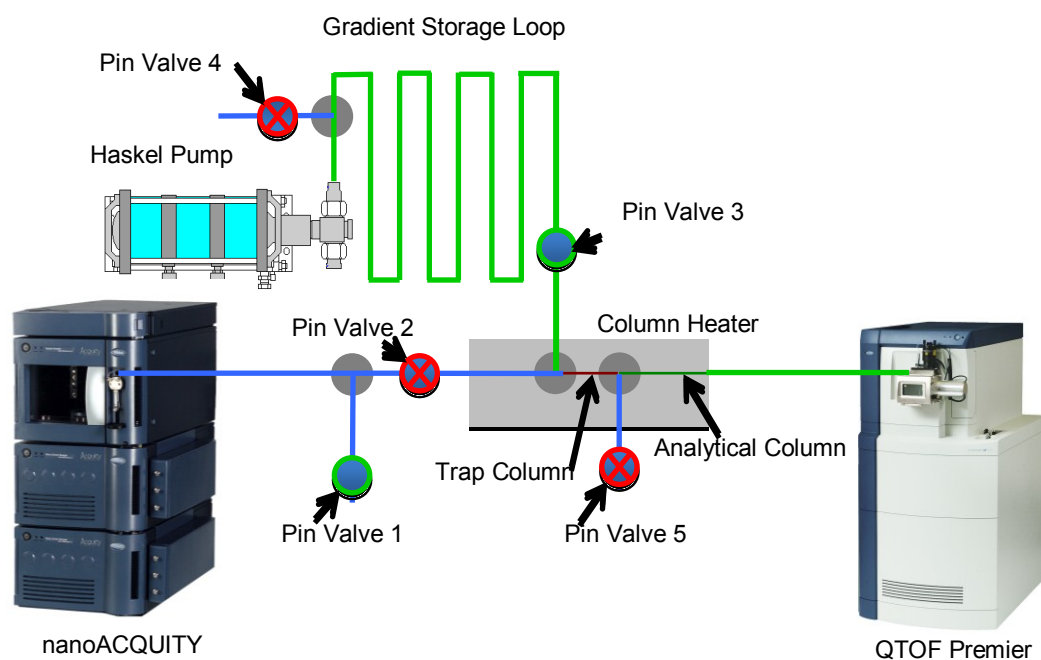


Figure 5-7: Gradient playback at UHPLC pressures: Pin valves 2, 4, and 5 are closed. Pin valve 3 is open, and engagement of the Haskel pump pushes the gradient from the storage loop onto the trap and analytical columns. Pin valve 1 is open to allow flow from the nanoAcquity to ramp down and to divert flow away from the commercial instrument should Pin valve 2 fail during operation.

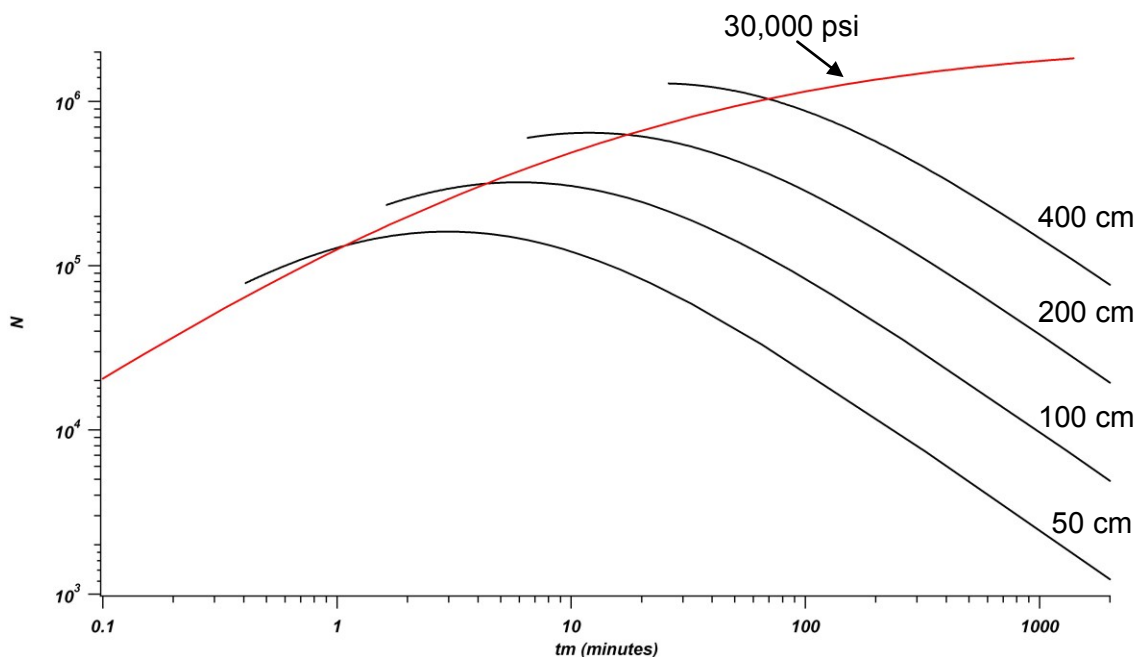


Figure 5-8: Theoretical plates vs. dead times for 50 – 400 cm columns packed with 1.9 μm particles, operated at 65°C. The intersection of the red trace with the curves shows expected performance when operating at 30,000 psi. Curves are constructed using reduced van Deemter coefficients of 1.0, 1.0, and 0.1 for A-, B-, and C-, respectively. Mobile phase viscosities of 0.48 cP and diffusion coefficients of $1.7 \times 10^{-5} \text{ cm}^2/\text{s}$ are assumed.

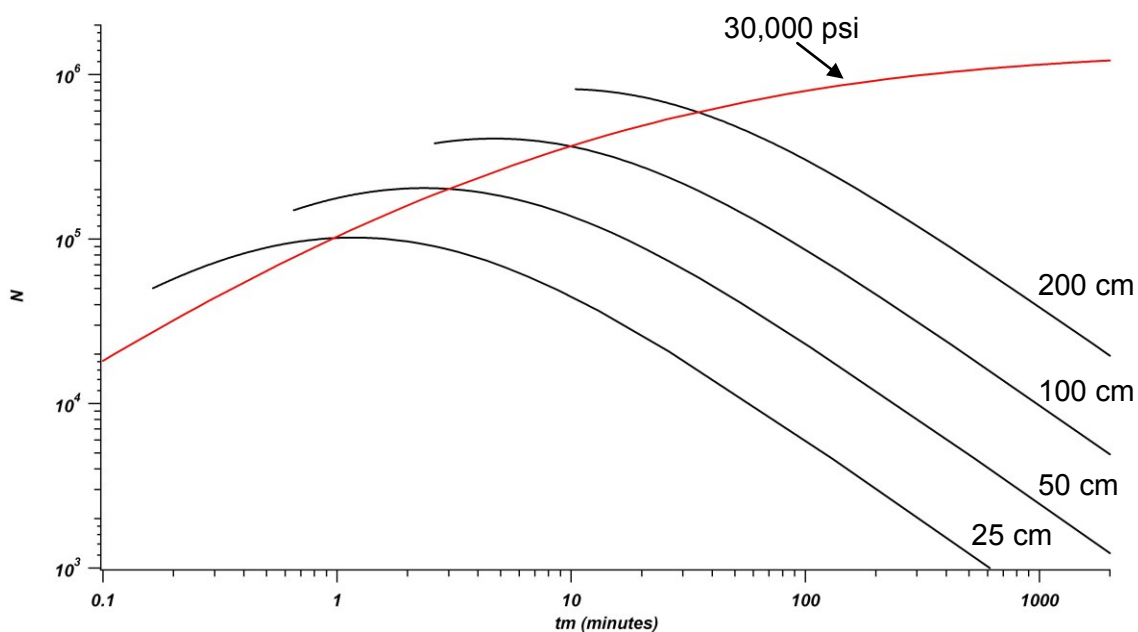


Figure 5-9: Theoretical plates vs. dead times for 25 – 200 cm columns packed with 1.5 μm particles, operated at 65°C. The intersection of the red trace with the curves shows expected performance when operating at 30,000 psi. Curves are constructed using reduced van Deemter coefficients of 1.0, 1.0, and 0.1 for A-, B-, and C-, respectively. Mobile phase viscosities of 0.48 cP and diffusion coefficients of $1.7 \times 10^{-5} \text{ cm}^2/\text{s}$ are assumed.

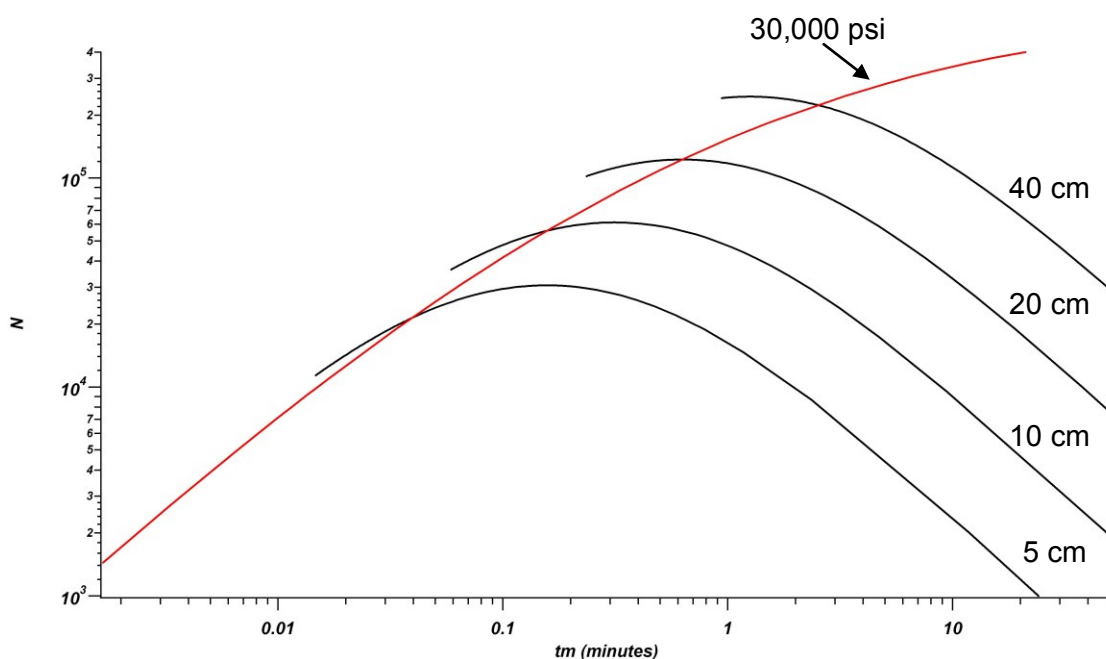


Figure 5-10: Theoretical plates vs. dead times for 25 – 200 cm columns packed with 1.0 μm particles, operated at 65°C. The intersection of the red trace with the curves shows expected performance when operating at 30,000 psi. Curves are constructed using reduced van Deemter coefficients of 1.0, 1.0, and 0.1 for A-, B-, and C-, respectively. Mobile phase viscosities of 0.48 cP and diffusion coefficients of $1.7 \times 10^{-5} \text{ cm}^2/\text{s}$ are assumed.

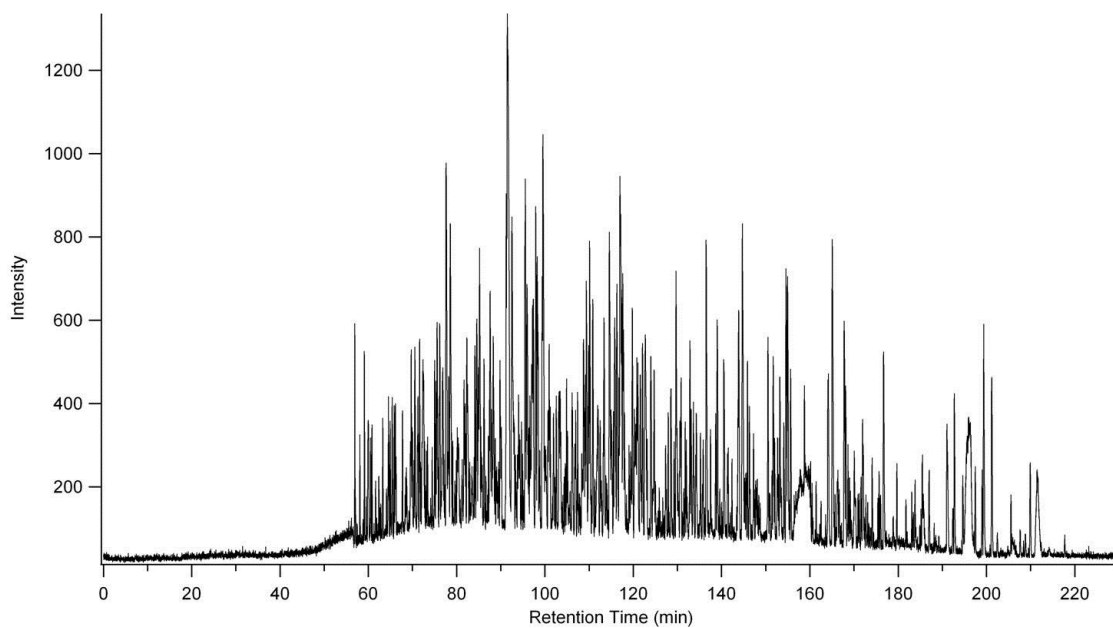


Figure 5-11: Separation of a yeast cell lysate on a 200 cm x 75 μ m ID column packed with 1.9 μ m BEH particles at 30,000 psi and 65°C using a 35 μ L gradient of 4-40% acetonitrile.

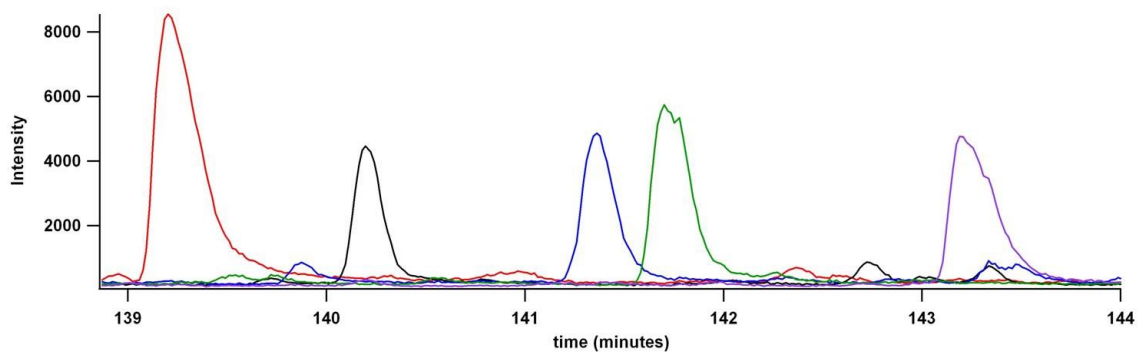


Figure 5-12: Peak tailing as evidenced by five single ion chromatograms from 139-144 minutes for the separation of a yeast cell lysate on a 200 cm x 75 μm ID column packed with 1.9 μm BEH particles at 30,000 psi and 65°C using a 35 μL gradient of 4-40% acetonitrile.

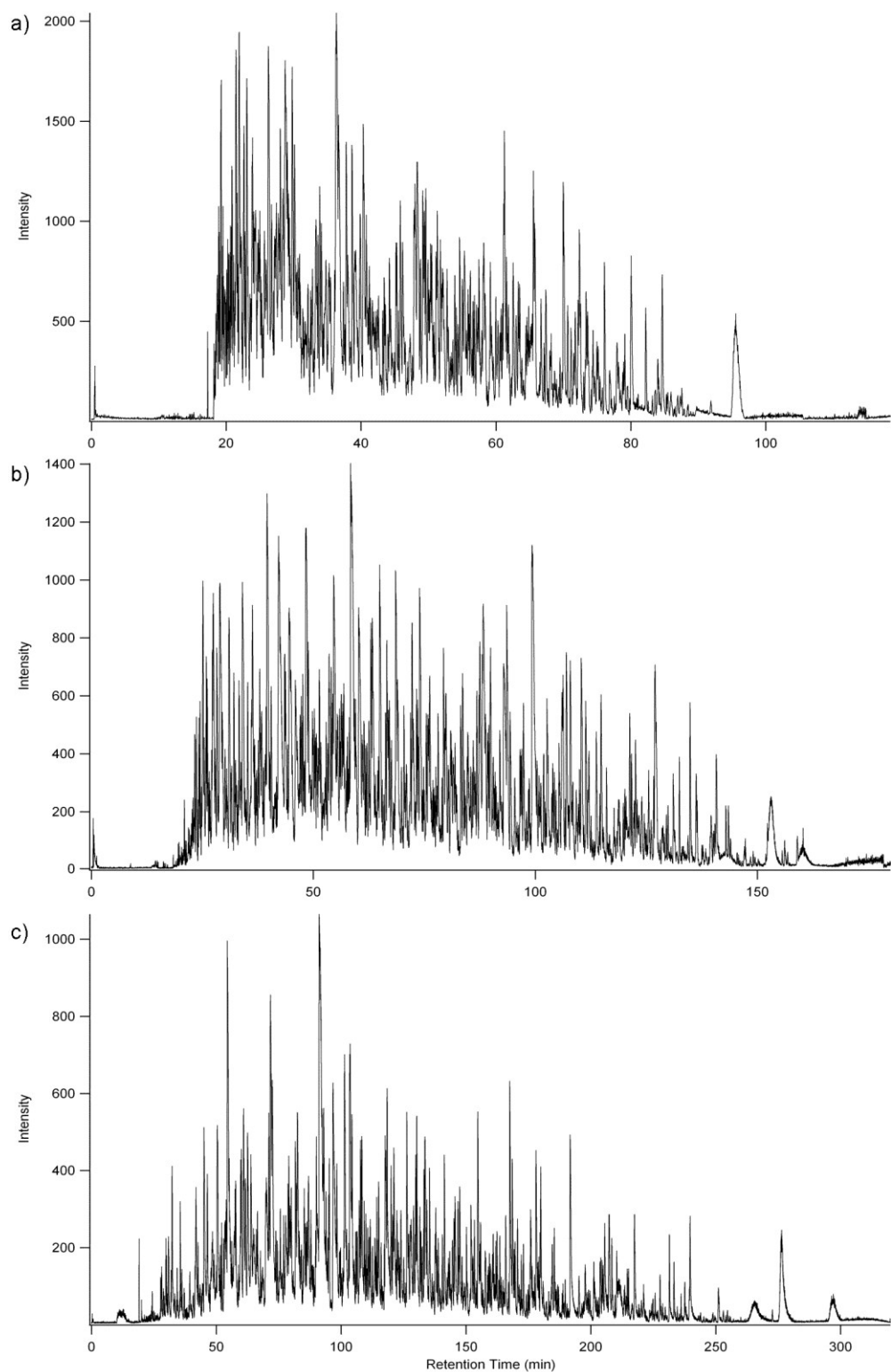


Figure 5-13: Separations of a yeast cell lysate on 75 μm ID columns packed with 1.5 μm BEH particles at 30,000 psi and 65°C. a) 117 cm column, 25 μL gradient of 3-40% acetonitrile; b) 117 cm column, 45 μL gradient of 3-40% acetonitrile; c) 100 cm column, 85 μL gradient of 1-40% acetonitrile.

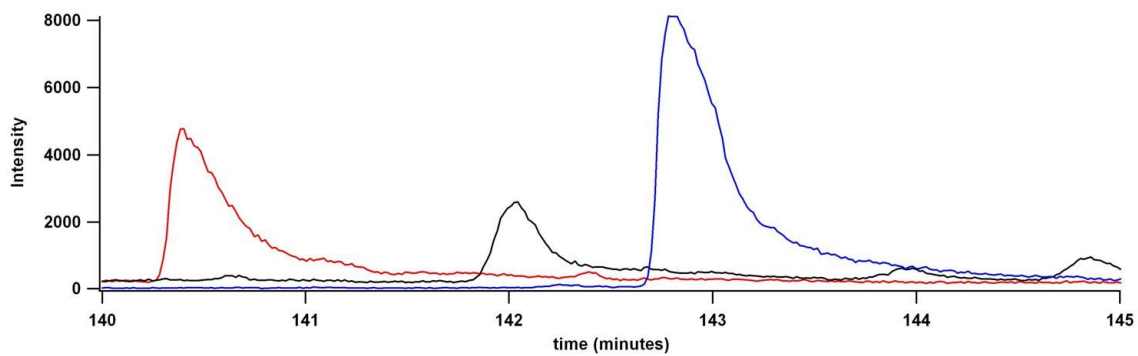


Figure 5-14: Peak tailing as evidenced by three single ion chromatograms from 140-145 minutes for the separation of a yeast cell lysate on a 100 cm x 75 μm ID column packed with 1.5 μm BEH particles at 30,000 psi and 65°C using a 85 μL gradient of 1-40% acetonitrile.

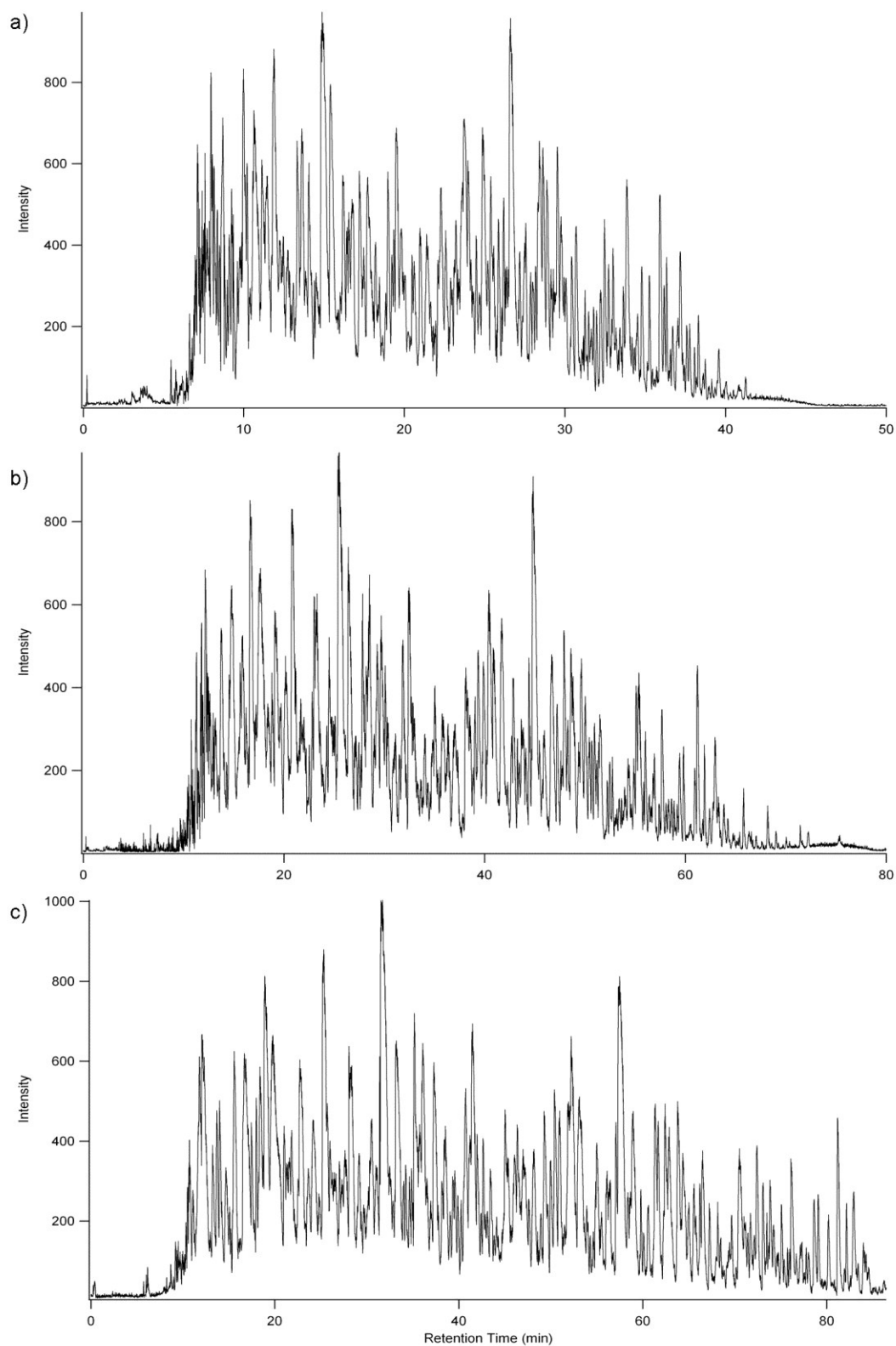


Figure 5-15: Separations of a yeast cell lysate on a 25 cm x 75 μm ID column packed with 1.0 μm BEH particles at 30,000 psi and 65°C using 1-40% acetonitrile gradients. a) 15 μL gradient; b) 25 μL gradient; c) 35 μL gradient

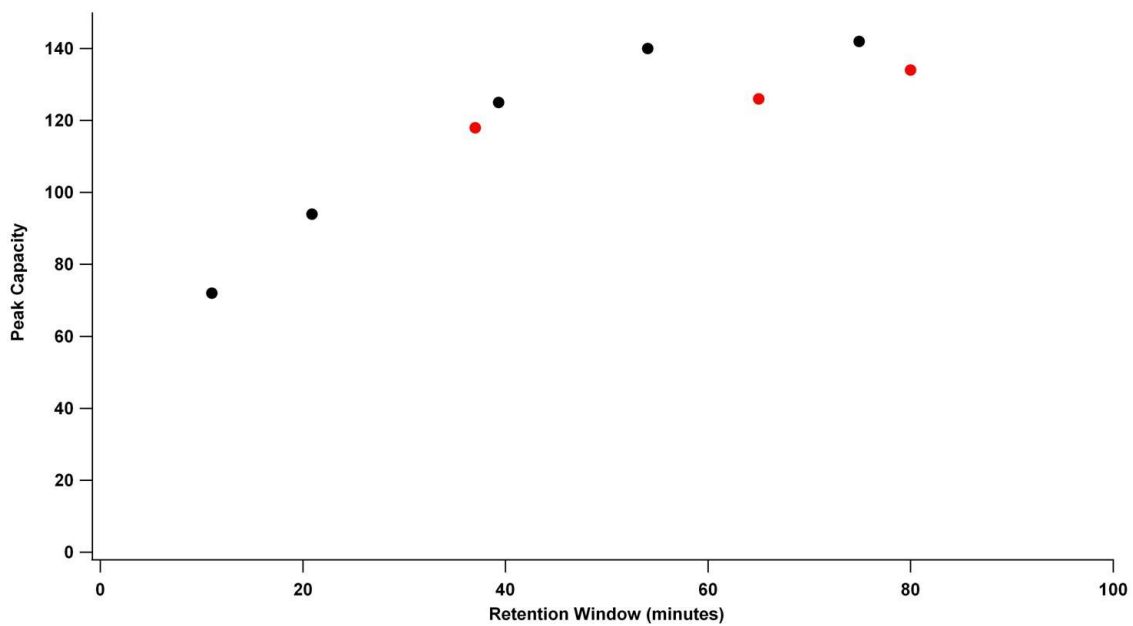


Figure 5-16: Peak capacity vs. retention window plot comparing the performances of a commercial 25 cm x 75 μm ID column packed with 1.9 μm BEH particles (black) and a 25 cm x 75 μm ID column packed with 1.0 μm BEH particles (red).

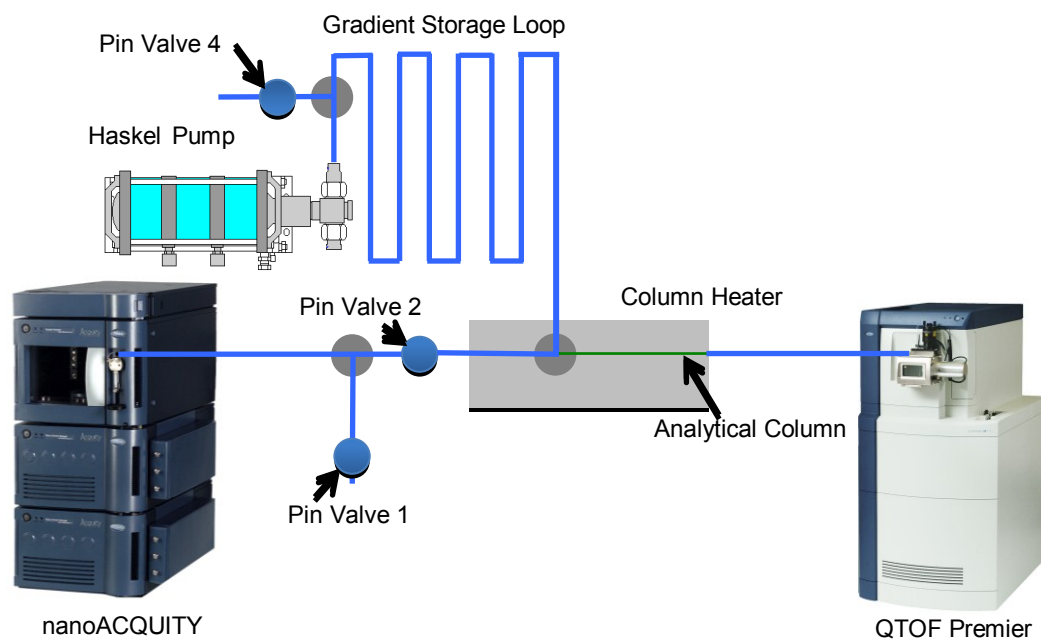


Figure 5-17: Schematic of the modified instrumentation to perform constant pressure gradient UHPLC separations with direct sample injections.

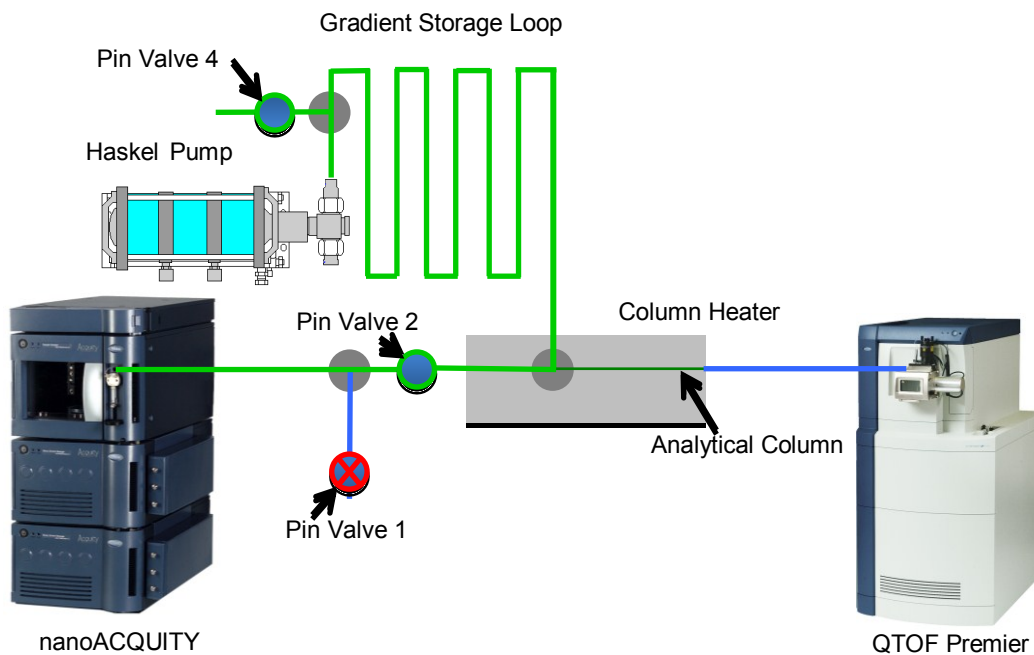


Figure 5-18: Gradient and sample loading scheme in direct injection mode: Pin valve 1 is closed. Pin valves 2 and 4 are open to allow flow from the nanoAcquity to the gradient storage loop.

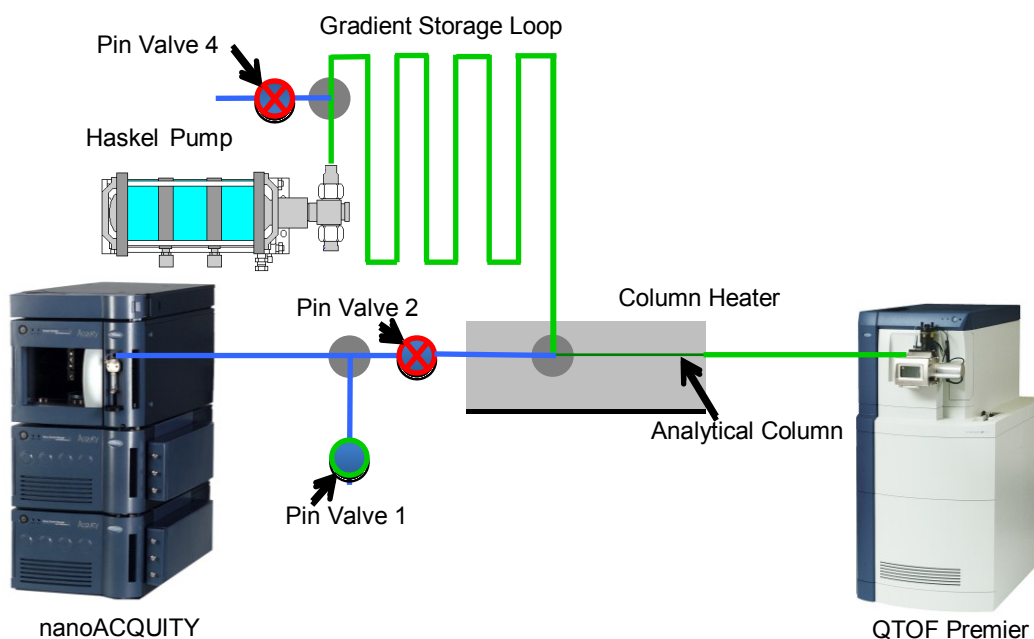


Figure 5-19: Gradient playback at UHPLC pressures in direction mode: Pin valves 2 and 4 are closed. Engagement of the Haskel pump pushes the sample and gradient from the storage loop onto the analytical column. Pin valve 1 is open to allow flow from the nanoAcquity to ramp down and to divert flow away from the commercial instrument should Pin valve 2 fail during operation.

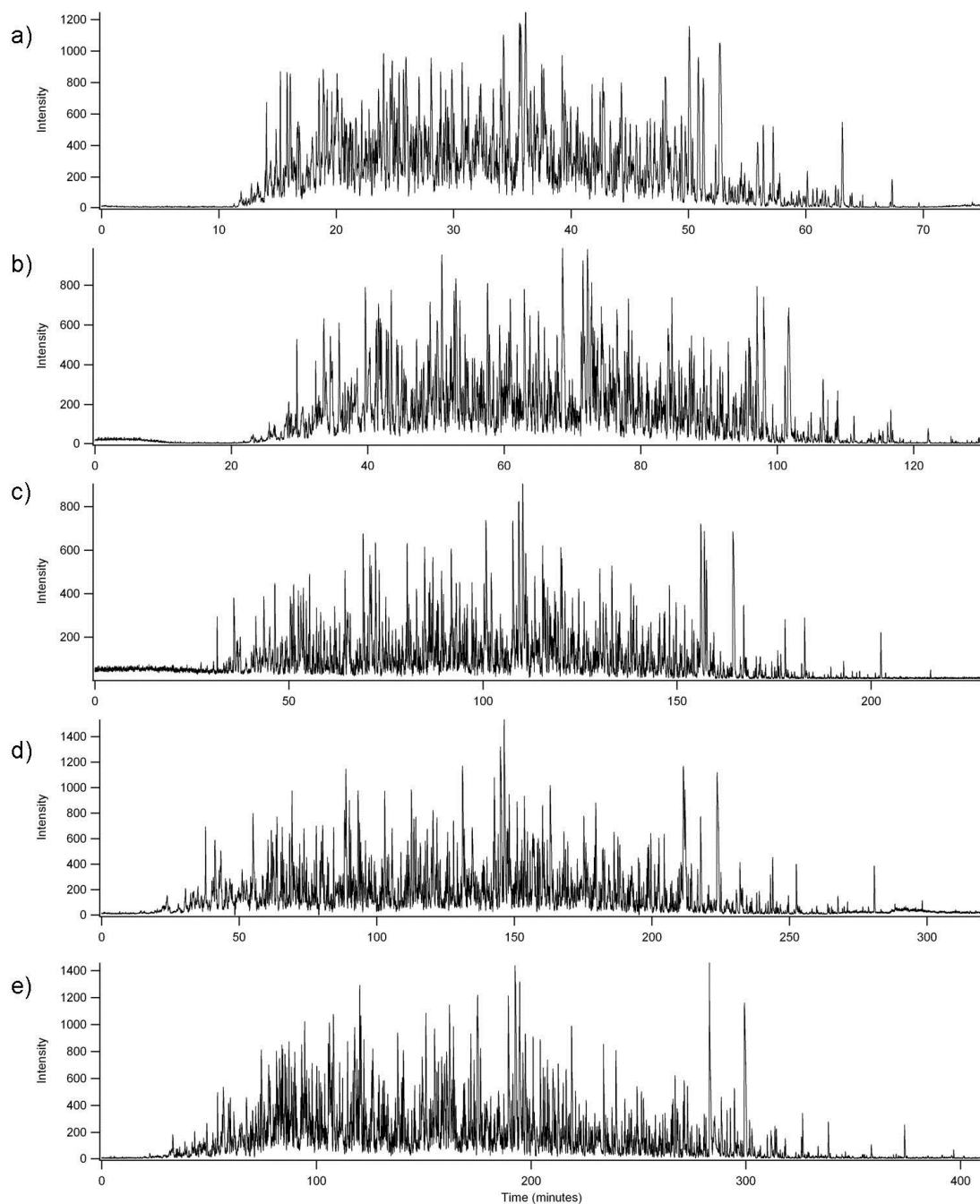


Figure 5-20: Separations of an *E.coli* digestion standard using a 100 cm x 75 μ m ID column packed with 1.5 μ m BEH particles in direct injection mode at 30,000 psi and 65°C with 1-40% acetonitrile gradients with total volumes of: a) 25 μ L; b) 50 μ L; c) 100 μ L; d) 150 μ L; e) 200 μ L.

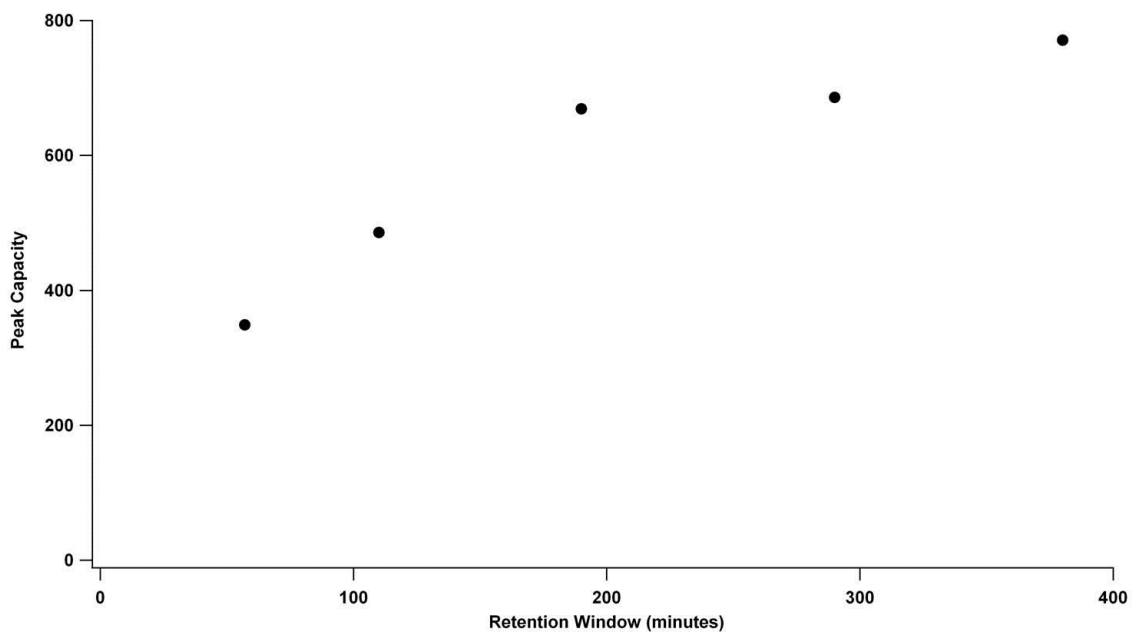


Figure 5-21: Peak capacity vs. retention window plot showing the performance of a 100 cm x 75 μm ID column packed with 1.5 μm BEH particles operated at 30,000 psi and 65°C in direct injection mode.

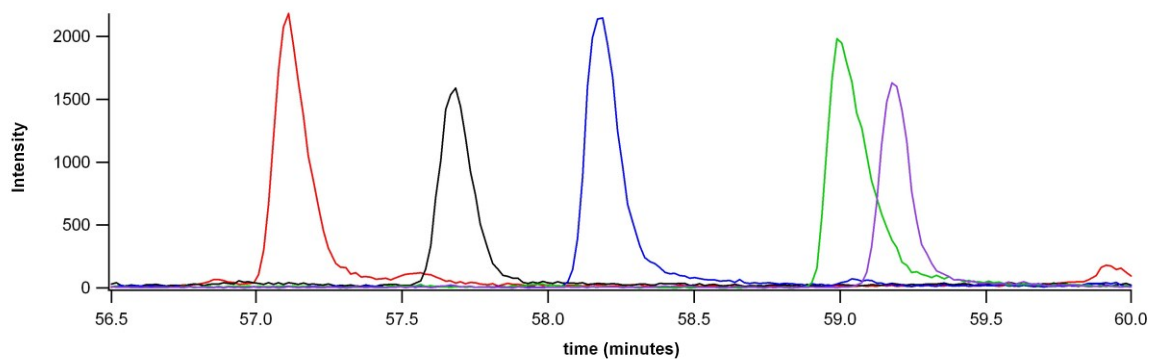


Figure 5-22: Improved peak shape as evidenced by five single ion chromatograms from 57-60 minutes for the separation of an *E.coli* digestion standard on a 100 cm x 75 μ m ID column packed with 1.5 μ m BEH particles at 30,000 psi and 65°C using a 100 μ L gradient of 1-40% acetonitrile in direct injection mode.

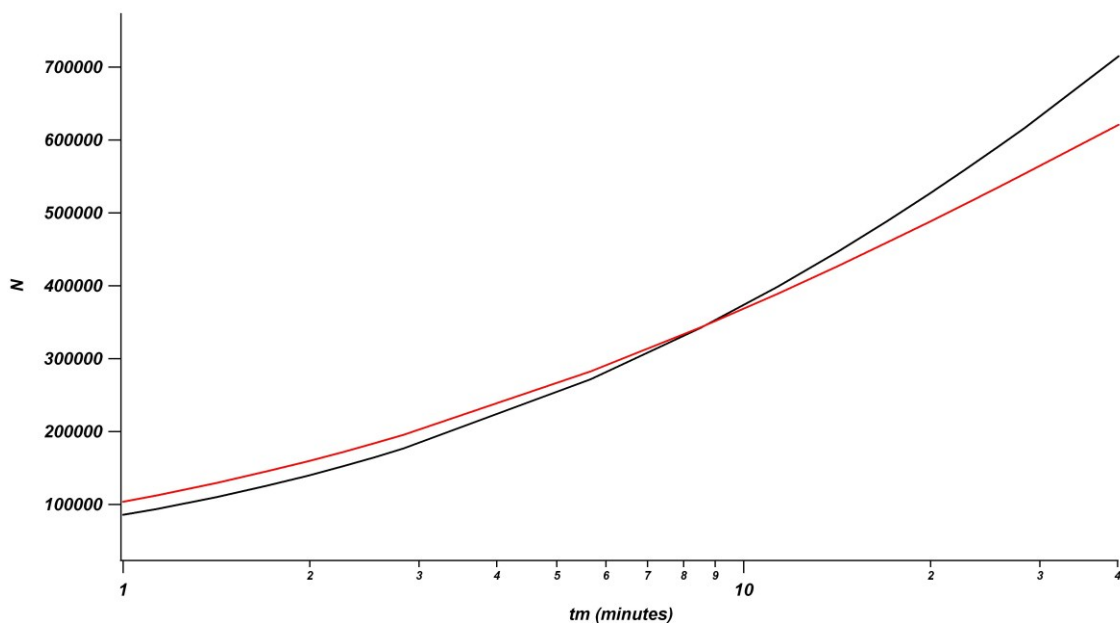


Figure 5-23: Theoretical plates vs. dead time plot highlighting the similarity in performances of columns packed with 1.9 μm (black) and 1.5 μm (red) particles, operated 30,000 psi and 65°C. Curves are constructed using reduced van Deemter coefficients of 1.0, 1.0, and 0.1 for A-, B-, and C-, respectively. Mobile phase viscosities of 0.48 cP and diffusion coefficients of $1.7 \times 10^{-5} \text{ cm}^2/\text{s}$ are assumed.

5.6 References

- ¹ Shen, Y.; Zhang, R.; Moore, R.J.; Kim, J.; Metz, T.O.; Hixson, K.M.; Zhao, R.; Livesay, E.A.; Udseth, E.A.; Smith, R.D. *Analytical Chemistry* **2005**, 77, 3090-3100.
- ² De Malsche, W.; Op De Beeck, J.; De Bruyne, S.; Gardeniers, H.; Desmet, G. *Analytical Chemistry* **2012**, 84, 1214 – 1219.
- ³ Eschelbach, J.W.; Jorgenson, J.W. *Analytical Chemistry* **2006**, 78, 1697-1706.
- ⁴ Chen, H.; Horvath, C. *Analytical Methods and Instrumentation* **1993**, 1, 213-222.
- ⁵ Guillarme, D.; Heinisch, S.; Rocca, J.L. *Journal of Chromatography A* **2004**, 1052, 39-51.
- ⁶ Kaiser, T.J.; Thompson, J.W.; Mellors, J.S.; Jorgenson, J.W. *Analytical Chemistry* **2009**, 81, 2860-2868
- ⁷ Gritti, F.; Guiochon, G. *Journal of Chromatography* **2012**, in press.
<http://dx.doi.org/10.1016/j.chroma.2012.06.092>.
- ⁸ Broeckhoven, K.; Verstraeten, M.; Choikhet, K.; Dittmann, M.; Witt, K.; Desmet, G. *Journal of Chromatography A* **2011**, 1153.